BIOGEOCHEMICAL PROCESSES IN SEDIMENTS ASSOCIATED TO COLD-WATER CORAL ECOSYSTEMS

FROM LIVING REEFS TO ANCIENT MOUNDS

Dissertation
Zur Erlangung des Doktorgrades der Naturwissenschaften (Dr. rer. nat.) im Fachbereich Geowissenschaften der Universität Bremen, Deutschland

vorgelegt von

Laura Mariana Wehrmann

Bremen, Januar 2010

1. Gutachter: Prof. Dr. Bo Barker Jørgensen
2. Gutachter: Priv. Doz. Dr. Matthias Zabel

Weitere Prüfer:
Prof. Dr. Rüdiger Henrich
Dr. Timothy G. Ferdelman

Tag des Promotionskolloquiums: 05.03.2010

PREFACE

This thesis was conducted in the framework of the Euoprean Science Foundation (ESF) EuroDIVERSITY project MiCROSYSTEMS funded by the German Research Foundation (DFG) grant Wi 2677/3-1. The presented work was carried out in the Biogeochemistry Group at the Max Planck Institute for Marine Microbiology in Bremen supervised by Dr. Timothy Ferdelman in close cooperation with the Coral Reef Ecology Work Group (CORE) at the GeoBio-Center, Ludwigs-Maximilians University Munich headed by PD Dr. Christian Wild.

The thesis consists of two parts. Part I presents work concerning biogeochemical processes in living cold-water coral reef associated sediments with focus on microbially-mediated carbon mineralization processes and mechanisms of carbonate preservation. In the first chapter, the manuscript "Carbon mineralization and carbonate preservation in modern cold-water coral reef sediments on the Norwegian shelf", Biogeosciences 6, 663-690, 2009, is presented. Chapter 2 consists of the manuscript "A comparative study on organic matter degradation characteristics in sediments of cold-water coral reef ecosystems" in preparation for submission to Limnology & Oceanography. This study is a follow-up on the work presented in the first chapter and gives insight into the degradation state of sedimentary organic matter in cold-water coral ecosystems. The manuscripts presented in Chapters 1 and 2 are based predominately on my own sample analyses, data evaluation and interpretation. In Chapter 3 the manuscript "Microbial degradation of cold water coral-derived organic matter - potential implication for organic C cycling in the water column above Tisler Reef", Aquatic Biology, 7, 71-80, 2009, is displayed. I contributed during the field sampling, data interpretation and writing processes. Additional collaborative research, to which I contributed analytical and interpretational work and co-authorship, is displayed in Chapters 4 and 5, as abstracts of two manuscripts.

Part II focuses on diagenetic processes in cold-water coral mounds. Cold-water coral mound sites in the Gulf of Cadiz provide a unique environment where organic carbon mineralization and the diagenetic imprint of hydrocarbon-rich deep fluids can be investiagted. The results of this study are presented in the manuscript "The imprint of methane seepage on the geochemical record and early diagenetic processes in cold-water coral mounds on Pen Duick Escarpment, Gulf of Cadiz" presented in Chapter 6 (in revision for Marine Geology). The manuscript is predominantly based on my own sampling, analyses and data interpretation. Additionally, a study on the formation of

gypsum in Mound Perseverance, located in the Porcupine Seabight, is presented in Chapter 7 ("Diagenetic formation of gypsum and dolomite in a cold-water coral mound in the Porcupine Seabight, off Ireland, Sedimentology", in press). I made analytical and interpretational contributions regarding the isotope geochemistry and wrote this section of the manuscript. Chapter 8 presents the abstract of an overview paper of R/V Marion Dufresne cruise MD 169 MiCROSYSTEMS, to which I contributed analytical data and interpretation as co-author.

CONTENT

ABSTRACT

Understanding the role of cold-water coral ecosystems in the marine carbonate cycle and the global carbon budget requires a fundamental knowledge of the complex processes that control organic and inorganic carbon diagenesis, sequestration and long-term storage in the associated siliciclastic sediments. Syn- to post-depositional microbially-mediated diagenetic processes in these sediments are addressed in this thesis with to assess the coupling between sulfur and iron cycles, and carbonate formation and dissolution processes. The main objectives were to examine 1) the effect of living cold-water coral reefs on organic carbon mineralization and carbonate preservation in the reef-associated surface sediments, and 2) biogeochemical processes and the diagenetic history of cold-water coral mound structures influenced by additional (non-steady state) processes such as oxidation events and the migration of hydrocarbon-rich fluids. Using high-resolution pore-water and solid-phase analyses, stable isotope measurements and, pore-water profile modeling, these questions were targeted at two cold-water coral reef systems on the Norwegian margin, Røst Reef and Traenadjupet Reef, Tisler Reef in the Skagerrak, and on a set of cold-water coral mounds located in the Porcupine Basin and the Gulf of Cadiz.

Organic carbon mineralization at the modern cold-water coral reefs on the Norwegian margin occurred in two major zones: a) the reef surface framework consisting of living and dead coral thickets and coral rubble and b) the underlying coral-bearing sediments. Within the reef surface framework benthic reef-associated fauna, mostly inhabiting dead coral branches and coral rubble, as well as the microbial communities living in the adjacent water and associated to the living and dead coral thickets, were responsible for carbon turnover. The cold-water corals *Lophelia pertusa* and *Madrepora oculata* stimulated microbial activity in the reef vicinity by the release of easily degradable dissolved and particulate organic matter. The reef surface framework decoupled the underlying reef sediments from the productive pelagic ecosystem by limiting the influx of organic matter into the sediments. Biogeochemical indicators for the organic matter degradation state, including concentration and composition of total hydrolyzable amino acids and chlorophyll degradation products, showed that the buried organic matter had already undergone strong pre-depositional alteration. Stoichiometric calculations based on modeling of pore-water profiles from Traenadjupet Reef sediments suggested an oxidation state of the organic matter more alkyl-rich than typical carbohydrate stoichiometries. Rates of anaerobic carbon

mineralization in the sediments, predominately driven by organoclastic sulfate reduction and microbial Fe-oxide reduction, were low. Likewise, organic matter mineralization in Gamma Mound, located in the Pen Duick Mound Province, Gulf of Cadiz was driven by dissimilatory iron reduction and organoclastic sulfate reduction coupled to oxidative sulfur cycling at extremely low rates.

Several cold-water coral mounds in Pen Duick Mound Province were influenced by ascending hydrocarbon-rich fluids enriched in lithium and strontium, which presumably originated from deep Mesozoic source rocks. The diagenetic imprint of a sulfate-methane transition zone (SMTZ) present at shallow depth in these mounds was evidenced by the extensive pyritization of reactive Fe-(oxyhydr)oxides and the sulfur isotope signitures of sulfides. At the Pen Duick Alpha Mound, the sulfur isotope composition of pyrite and layers of authigenic high Mg-calcite depleted in ^{13}C were interpreted as signals of a fluctuating depth of the SMTZ.

Carbonate preservation in the cold-water coral reef associated sediments was strongly controlled by the availability of reactive iron. The interplay of low rates of sulfate reduction and the input of terrigenous Fe-rich material led to a buffering of the pore-water carbonate system in the Norwegian reef sediments and the non-methane influenced Gamma Mound (Pen Duick Mound Province). Conversely, processes that led to a strong scavenging of Fe-oxides such as the production of hydrogen sulfide in the SMTZ facilitated carbonate dissolution. This was manifested in Alpha Mound sediments where the upward diffusion of hydrogen sulfide out of the SMTZ caused distinct layers of dissolved corals. At Mound Perseverance in the Porcupine Basin, sediment erosion facilitated the inflow of oxidizing fluids into previously anoxic sediments which resulted in the oxidation of pyrite. The latter process caused a drop in pH that induced coral dissolution and resulted in the oversaturation of pore-water with respect to gypsum and dolomite.

KURZFASSUNG

Um ein Verständnis für die Rolle von Kaltwasserkorallenökosystemen im marinen Karbonatkreislauf und dem globalen Kohlenstoffbudget zu erlangen, benötigen wir tiefgreifende Einsicht in die komplexen Prozesse, welche die Diagenese und langfristige Ablagerung von anorganischem und organischem Kohlenstoff in assoziierten siliziklastischen Sedimenten bedingen. Diese Arbeit befasste sich mit den mikrobiell-gesteuerten frühdiagenetischen Prozessen während und nach der Ablagerung dieser Sedimente mit dem Ziel, die Kopplung zwischen Schwefel- und Eisenkreisläufen und Karbonatbildung und -lösung zu verstehen. Die Hauptziele beinhalteten das Verständnis: 1) des Einflusses von lebenden Kaltwasserkorallenriffen auf den Abbau von organischem Kohlenstoff und Karbonaterhaltung in Riff-assoziierten Sedimenten und 2) der biogeochemischen Prozesse und der diagenetischen Geschichte von Kaltwasserkorallenhügeln („Mounds“) unter dem Einfluss von weiteren (instationären) Prozessen wie Oxidationsereignissen und der Migration von kohlenwasserstoffreichen Fluiden. Unter Verwendung hochauflösender Porenwasser- und Festphasen-bestimmungen und der Analyse von stabilen Isotopen sowie der Modellierung von Porenwasserprofilen wurden diese Fragestellungen an zwei Kaltwasserkorallenriffen am norwegischen Kontinentalhang, Røstriff und Traenadjupetriff, am Tislerriff im Skagerrak, und an Kaltwasserkorallenhügeln im Porcupine-Becken und dem Golf von Cadiz bearbeitet.

Der Abbau organischen Kohlenstoffs in heutigen Kaltwasserkorallenriffen am norwegischen Kontinentalhang fand in zwei Hauptzonen statt: a) dem oberflächlichen Riffgerüst, bestehend aus lebenden Korallen und abgestorbenen Korallenbruchstücken und Korallenschutt, und b) den unterliegenden korallenführenden Sedimenten. Hauptverantwortlich für den Kohlenstoffumsatz im Riffgerüst waren sowohl die benthische Riff-assoziierte Fauna, welche vor allem abgestorbene Korallenfragmente und den Korallenschutt besiedelt, als auch die Mikrobengemeinschaften im umgebenden Wasser und auf lebenden und abgestorbenen Korallen. Die Kaltwasserkorallen *Lophelia pertusa* und *Madrepora oculata* stimulierten die mikrobielle Aktivität in der Riffumgebung durch die Abgabe von leicht abbaubarem gelöstem und partikulärem organischem Material. Das oberflächliche Riffgerüst entkoppelte die unterliegenden Riffsedimente vom produktiven pelagischen Ökosystem, indem es den Eintrag von organischem Material in die Sedimente beschränkte. Biogeochemische Indikatoren für den Abbaugrad von organischem Material,

einschließlich der Konzentration und Zusammensetzung der gesamten hydrolisierbaren Aminosäuren und Chlorophyll-Abbauprodukten zeigten, dass das sedimentäre organische Material bereits vor seiner Ablagerung eine starke Umwandlung erfahren hatte. Eine auf der Modellierung von Porenwasserprofilen von Traenadjupetriff-Sedimenten basierende stöchiometrische Berechnung ergab, dass der Oxidationszustand des organischen Materials alkylreicher war als klassische Kohlenhydrat-zusammensetzungen. Anaerobe Kohlenstoffabbauraten in den Sedimenten, vor allem mediiert durch organoklastische Sulfatreduktion und mikrobielle Eisenoxid-Reduktion, waren niedrig. Gleichermaßen war der Abbau von organischem Material in Gamma Mound (Pen Duick Mound Provinz, Golf von Cadiz) durch niedrige Raten an dissimilatorischer Eisenreduktion, organoklastischer Sulfatreduktion sowie gekoppelt an oxidativen Schwefelkreislauf, charakterisiert.

Mehrere Kaltwasserkorallenhügel in der Pen Duick Mound Provinz wurden durch aufsteigende kohlenwasserstoffreiche Fluide, welche vermutlich aus mesozoischen Muttergesteinen stammten und angereichert an Lithium und Strontium waren, beeinflusst. Der Einfluss einer oberflächennahen Sulfat-Methan-Übergangszone (SMT) auf die Sedimentdiagenese spiegelte sich in einer ausgedehnten Pyritisierung von reaktiven Fe-(oxyhydr)oxiden der Schwefelisotopensignatur von Sulfiden wider. In Alpha Mound, einem der Pen Duick Kaltwasserkorallenhügel, deutete die Schwefelisotopenzusammensetzung von Pyrit und an ^{13}C-abgereicherte autigene Hochmagnesiumkalzit-Lagen auf eine schwankende Tiefe der SMT hin.

Die Karbonaterhaltung in Sedimenten assoziiert mit Kaltwasserkorallenriffen wurde stark reguliert durch die Verfügbarkeit von reaktivem Eisen. Das Zusammenspiel von niedrigen Sulfatreduktionsraten und dem Eintrag von terrigenem Fe-reichem Material, führte zu einer Pufferung des Porenwasserkarbonatsystems in den norwegischen Riffsedimenten und dem Methan-unbeeinflussten Gamma Mound (Pen Duick Mound Provinz). Prozesse, die zu einer vermehrten Reduktion von Eisenoxiden führten, wie die Produktion von Schwefelwasserstoff in der SMT, begünstigten Karbonatlösung. Dies wurde anhand von Alpha Mound Sedimenten gezeigt, wo die Diffusion von Schwefelwasserstoff aus der SMT zu Lagen mit gelösten Korallen führte. In Mound Perseverance (Porcupine-Becken) förderte Sedimenterosion die Zufuhr von oxidierenden Fluiden in zuvor anoxische Sedimente, was Pyritoxidation zur Folge hatte. Dieser Prozess führte zu einer Erniedrigung des pH und induzierte Korallenlösung, was in einer Übersättigung des Porenwassers bezüglich Gips und Dolomit resultierte.

1. INTRODUCTION

1.1 The biogeochemical carbonate cycle

On time scales shorter than ca. 100 ky, the marine carbonate cycle (Emerson and Archer, 1992; Ridgwell and Zeebe, 2005), the terrestrial carbon reservoir (e.g. Myneni et al., 1997; Schimel, 1995; Tans et al., 1990; Walker and Kasting, 1992), and anthropogenic carbon emission (Falkowski et al., 2000; Feely et al., 2004; Goodwin et al., 2008; IPPC, 2007) control atmospheric CO_2 concentrations. Discovered over 250 years ago, cold-water coral ecosystems living in the dark waters of our global ocean remain one of the least understood components of the global carbon cycle. Unique to these ecosystems is their function as short-term source but also long-term sink of CO_2. In this function, they are a valuable player in the marine carbonate cycle and therefore the global carbon budget.

The biogeochemical carbonate cycle has different compartments and transformation processes (Figure 1). Calcium carbonate production (reaction R1) mainly occurs in the marine environment, as carbonate production in the terrestrial system constitutes only a small fraction of global carbonate production.

$$Ca^{2+} + 2HCO_3^- \Leftrightarrow CaCO_3 + CO_{2(aq)} + H_2O \qquad \text{(R1)}$$

Carbonate production and deposition in the ocean occurs in the (1) pelagic (open ocean) and the (2) neritic (shelf) zone. Pelagic carbonate production is much lower than neritic carbonate production but occurs over a much larger area. At present, this results in an approximately equal distribution of carbonate burial into both zones (Milliman, 1993a; Ridgwell et al., 2003; Vecsei, 2004). Studies show that the balance between both reservoirs has a strong effect on the Earth's climate and atmospheric CO_2 concentration (Ridgwell et al., 2003; Volk, 1989).

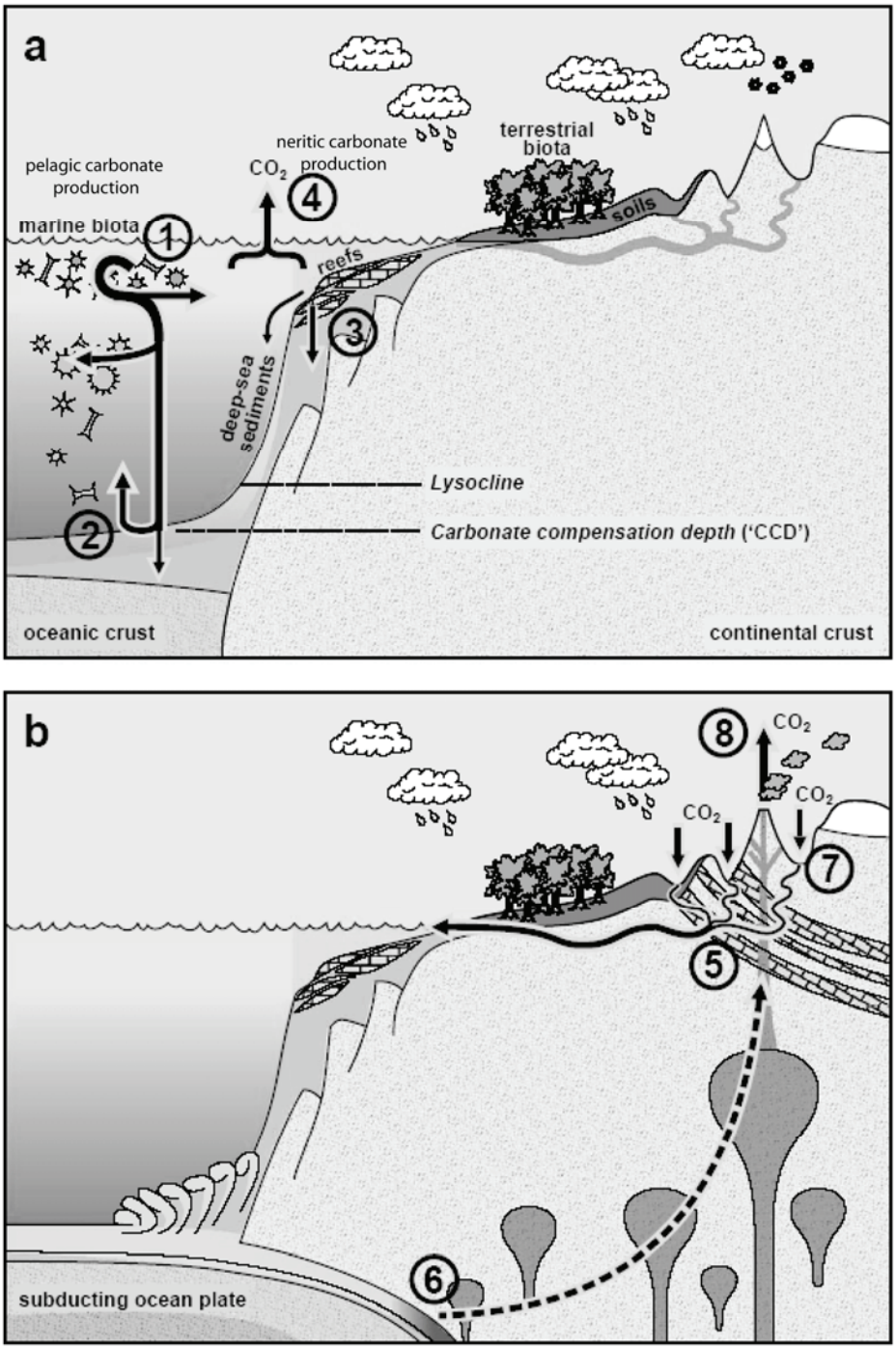

Figure 1: The biogeochemical carbonate cycle (modified from Ridgwell and Zeebe, 2005), **a)** #1) Pelagic carbonate production by coccolithophores and foraminifera. #2) Deposition and recycling of calcium carbonate in deep-sea sediments. #3) Neritic carbonate production by corals, benthic and planktonic animals on the continental shelf and burial and recycling of carbonate in the sediments. #4) Transfer of CO_2 from the ocean to the atmosphere. **b)** #5) Weathering of calcium carbonate deposits uplifted on the continents. #6) Subduction and thermal breakdown (decarbonation) of carbonate in deeply-buried sediments and the mantle. #7) Weathering of silicate rocks. #8) Degassing of CO_2 from metamorphic decarbonation reaction.

The pelagic zone- Biogenic carbonate in surface waters of the open ocean is mainly produced by coccolithophores and planktonic foraminifera as calcite. Surface-produced biogenic carbonate sinks through the water column associated to aggregates or fecal pellets. A fraction of the downward sinking carbonate pool dissolves in the guts of grazing zooplankton (e.g. copepods; Harris, 1994; Jansen and Wolf-Gladrow, 2001; Pond et al., 1995), and in the microenvironments of this "marine snow" where heterotrophic respiration by associated bacteria leads to a pH decrease (Milliman, 1993a; Milliman et al., 1999). These processes result in the release of dissolved inorganic carbon (DIC) into intermediate water masses. Initial estimates suggest that 60-80 % of pelagic produced calcium carbonate is recycled at these depths (Berelson et al., 2007; Feely et al., 2002; Milliman et al., 1999; Sabine et al., 2002). Carbonate preservation in the deep sea strongly depends on the degree of saturation of the water column with respect to biogenic calcite and aragonite. Below the calcite and aragonite saturation horizons carbonate dissolves. Below the calcite and aragonite compensation depths (CCD and ACD), defined as the depth where carbonate settlement is balanced by calcium carbonate dissolution, sediments become almost completely devoid of carbonate particles (Bramlette, 1961).

The neritic zone- The continental shelves are characterized by a wide range of environments which host diverse carbonate production and accumulation regimes. High rates of carbonate production and accumulation are found in shallow coral reefs (e.g. off eastern Australia, the Caribbean Sea and Madagascar), and banks and embayments in tropical and subtropical areas such as Florida Bay and the Persian Gulf (see Milliman, 1993; Milliman and Droxler, 1996; and Wollast, 1998 for review). These sediments are dominated by aragonite and Mg-rich calcite. Carbonate preservation in these environments is thought to be high because only 10-25 % of the produced carbonate dissolves in the sediments, while an equal fraction is exported to deeper water (Wollast, 1998). However, some studies report a carbonate dissolution rate of up to 50 % in Florida platform sediments (Walter et al., 1993; Walter and Burton, 1990). The remaining part of continental shelves is characterized by much lower carbonate production and deposition rates. These environments are often further divided into carbonate-rich and carbonate-poor sediments (Milliman, 1993; Milliman and Droxler, 1996). In this definition, carbonate-rich sediments commonly consist of relict components, such as ooids and dead coral reefs deposited during previous sea level low stands, carbonate sands composed of bryozoan and mollusk remnants, as well as

Halimeda bioherms. Carbonate-poor, primarily siliciclastic sediments dominate at mid and high latitudes. The major source of carbonate in these environments is from benthic organisms but only a small percentage of produced carbonate (~25 %) is preserved in the sediments (Milliman, 1993; Morse et al., 2007). The calculated percentages for the fraction of carbonate that dissolves, is exported or accumulates in different sedimentary environments, however, have uncertainties of greater than 50 % (Milliman and Droxler, 1993).

1.2 The effect of microbial organic carbon oxidation on calcium carbonate preservation and dissolution in marine sediments

The carbonic acid system includes the carbonate ion (CO_3^{2-}), the bicarbonate ion (HCO_3^-), carbonic acid (H_2CO_3), dissolved carbon dioxide ($CO_{2(aq)}$) and in many instances gaseous carbon dioxide ($CO_{2(gas)}$). The relationship between the different species is determined by a sequence of reactions:

$$CO_{2(gas)} \Leftrightarrow CO_{2(aq)} \quad \text{(R2)}$$

$$CO_{2(aq)} + H_2O_{(l)} \Leftrightarrow H_2CO_{3(aq)} \quad \text{(R3)}$$

$$H_2CO_{3(aq)} \Leftrightarrow HCO_3^-{}_{(aq)} + H^+_{(aq)} \quad \text{(R4)}$$

$$HCO_3^-{}_{(aq)} \Leftrightarrow CO_3^{2-}{}_{(aq)} + H^+_{(aq)} \quad \text{(R5)}$$

The precipitation and dissolution of calcium carbonate, respectively depends on the carbonate saturation state Ω of the ambient solution. It is defined as

$$\Omega = \{Ca^{2+}\} \times \{CO_3^{2-}\} / K_{sp} \quad \text{(R6)}$$

where K_{sp} is the solubility constant and $\{Ca^{2+}\}$ and $\{CO_3^{2-}\}$ are the ion activities of the specific ions. At saturation state $\Omega > 1$ calcium carbonate precipitation is thermodynamically favorable, while at $\Omega < 1$ calcium carbonate is undersaturated and tends to dissolve. At a saturation state of $\Omega > 1$ of a solution, however, precipitation of calcium carbonate does not necessarily occur. In ocean surface water, for example, despite a $\Omega = 4.8$ for calcite, no spontaneous precipitation of calcium carbonate is observed (Morse and He, 1993). The saturation state of pore-waters with respect to carbonate minerals is a direct function of the concentration, or ion activity of CO_3^{2-}, which is affected by the concentrations of the other dissolved carbonate species and pH

(reactions R4 and R5). The relationship between the carbonate species is apparent in the definition of total alkalinity (TA; Wolf-Gladrow et al., 2007):

$$TA = [HCO_3^-] + 2\,[CO_3^{2-}] + [B(OH)_4^-] + [OH^-] + [HPO_4^{2-}] + 2\,[PO_4^{3-}] + [H_3SiO_4^-] + [NH3] + [HS^-] - [H^+] - [HSO_4^-] - [HF] - [H_3PO_4] - [HNO_3] \quad (R7)$$

where [x] is the concentration of the species x. The dissolution kinetics of carbonate minerals are controlled by a number of other factors apart from the saturation state of the ambient solution. As carbonate mineral dissolution reactions are strongly surface controlled these factors include carbonate mineralogy, reactive surface area, and the presence of dissolution inhibitors such as phosphate and sulfate (see Morse and Arvidson, 2002; Morse et al., 2007; Morse and Mackenzie, 1990 for review). Aragonite is generally more soluble than calcite, which often leads to a bias towards calcitic bioclasts in marine sediments and in the geological record (e.g. Canfield and Raiswell, 1991; Sanders, 2003).

Numerous studies describe the processes resulting in the dissolution of calcium carbonate in marine surface sediments (above the carbonate saturation horizon) as “organically driven dissolution”, “organic-carbon-driven dissolution”, ”respiration driven dissolution”, or “metabolically induced carbonate dissolution” (e.g. Milliman, 1993; Archer and Maier-Reimer, 1994; Wollast, 1998). These terms refer to the indirect dissolution of calcium carbonate due to organic matter mineralization by the microbial community. It is long known that microbial reactions are a key driver of pore-water pH in marine sediments and thus the pore-water saturation state with respect to calcite and aragonite (e.g. Bathurst, 1975; Milliman, 1974). The mineralization of organic matter in marine sediments follows a sequence of mineralization pathways with different terminal electron acceptors. The order of terminal electron accepting processes is controlled by the free energy yield of the reaction per mole organic carbon oxidized (Emerson et al., 1980; Froelich et al., 1979). This often leads to the establishment of a succession of electron accepting processes with depth in marine sediments. Although this concept is a strong oversimplification of the diagenetic processes it is often used to deduce the effect of the microbial mineralization processes on the pore-water carbonate system.

In the early years of research on the effect of biogeochemical processes on pore-water pH in marine sediments, closed-system models were applied. By definition, these models exclude ion diffusion and exchange with overlying waters as well as between

different confined depth intervals. In several studies the effect of the various carbon mineralization pathways in a constrained sediment layer, as well as of secondary reactions on pH and/or total alkalinity was considered (e.g. Ben-Yaakov, 1973; Canfield and Raiswell, 1991; Emerson et al., 1980; Froelich et al., 1979; Gardner, 1973; Tribble et al., 1990). The initial closed-system models focused on one carbonate species, for examples CO_3^{2-}, and ignored the conversion of carbonate species (reactions R4 and R5; Emerson and Bender, 1981). More elaborate reaction-transport models to determine pH, alkalinity and carbonate saturation state (e.g. Boudreau, 1996; Boudreau and Canfield, 1988; Boudreau and Canfield, 1993; Cai et al., 1995; Jourabchi et al., 2008; Jourabchi et al., 2005; Soetaert et al., 1996) largely overcame these deficiencies by including different diffusion coefficients of dissolved species, exchange with surface waters, dissolution and precipitation of different mineral phases and acid/base reactions. While the complexity of these models is far beyond the scope of this introduction, it is noteworthy that the comparison of closed-system and open-system models revealed that they qualitatively lead to the same behavior with respect to pH and carbonate saturation (Boudreau and Canfield, 1993). On a quantitative level, the closed-system approach mostly represents the extreme upper or lower boundary limits of pore-water pH and carbonate saturation (Boudreau and Canfield, 1993).

A summary of the effects of the terminal electron accepting pathways and the reactions of their bi-products on pore-water pH and TA is shown in Figure 2. Briefly, oxic respiration is considered to induce a decrease of pore-water pH which is eventually buffered by the dissolution of calcium carbonate, while manganese oxide reduction and iron oxide reduction are strong proton consuming processes that increase alkalinity and thus install conditions favorable for carbonate precipitation. In contrast, nitrate reduction neither alters pore-water pH nor saturation state. The effect of organoclastic sulfate reduction in a closed system is dependent on the initial pH, the extent of sulfate reduction (i.e. the amount of sulfate removed from the pore-water) as well as on the availability of iron oxides to form iron-sulfide minerals (Ben-Yaakov, 1973; Gardner, 1973; Morse and Mackenzie, 1990). During the onset of sulfate reduction in a constrained layer, a drop of pore-water pH and carbonate undersaturation is predicted. When approximately 35 % of the pore-water sulfate is reduced (exceeding 3-4 mM sulfate reduced assuming seawater sulfate concentration) the system shifts back to carbonate supersaturation and with further sulfate reduction carbonate precipitation can occur (Ben-Yaakov, 1973; Gardner, 1973; Morse and Mackenzie, 1990). In contrast, if

the sulfate reduction zone in the sediment is characterized by a sufficient pool of reactive iron oxides, the reaction of hydrogen sulfide with iron oxides to form iron sulfide minerals might lead to the inhibition of the initial drop of pH and carbonate undersaturation. Both model types highlight that the interrelation between organoclastic sulfate reduction, hydrogen sulfide oxidation, and iron-sulfide mineral formation exerts a major control on carbonate preservation in marine sediments. In the zone of methanogenesis pore-water saturation state with respect to carbonate is lowered and depending on the initial degree of carbonate oversaturation, carbonate dissolution might occur (Canfield and Raiswell, 1991; Middelburg et al., 1990). Several field studies support the predicted pH effects. For example, Walter and Burton (1990) confirmed the initial sulfate reduction model of Ben-Yaakov (1973), by showing that low rates of sulfate reduction were the main driver for carbonate dissolution in Fe-poor platform carbonate sediments from the Florida Keys. Morse et al. (1992) showed that organoclastic sulfate reduction caused the precipitation of calcium carbonate in a contrasting environment with sufficient amount of reactive iron at Baffin Bay, Texas. In many cases, however, pore-water profiles from marine systems could only be explained by integration of transport and subsequent reaction of the products of the electron accepting pathways. Ku et al. (1999) and Walter et al. (1993) showed that the oxidation of upward diffusing hydrogen sulfide produced during organoclastic sulfate reduction caused strong carbonate dissolution in carbonate sediments of the Bahama and Florida Platforms. Jahnke et al. (1994, 1997) and McNichol et al. (1988) were able to accurately reconcile pore-water profiles from shallow and deep-sea sediments, respectively only when including diffusion and bio-irrigation into their open-system models.

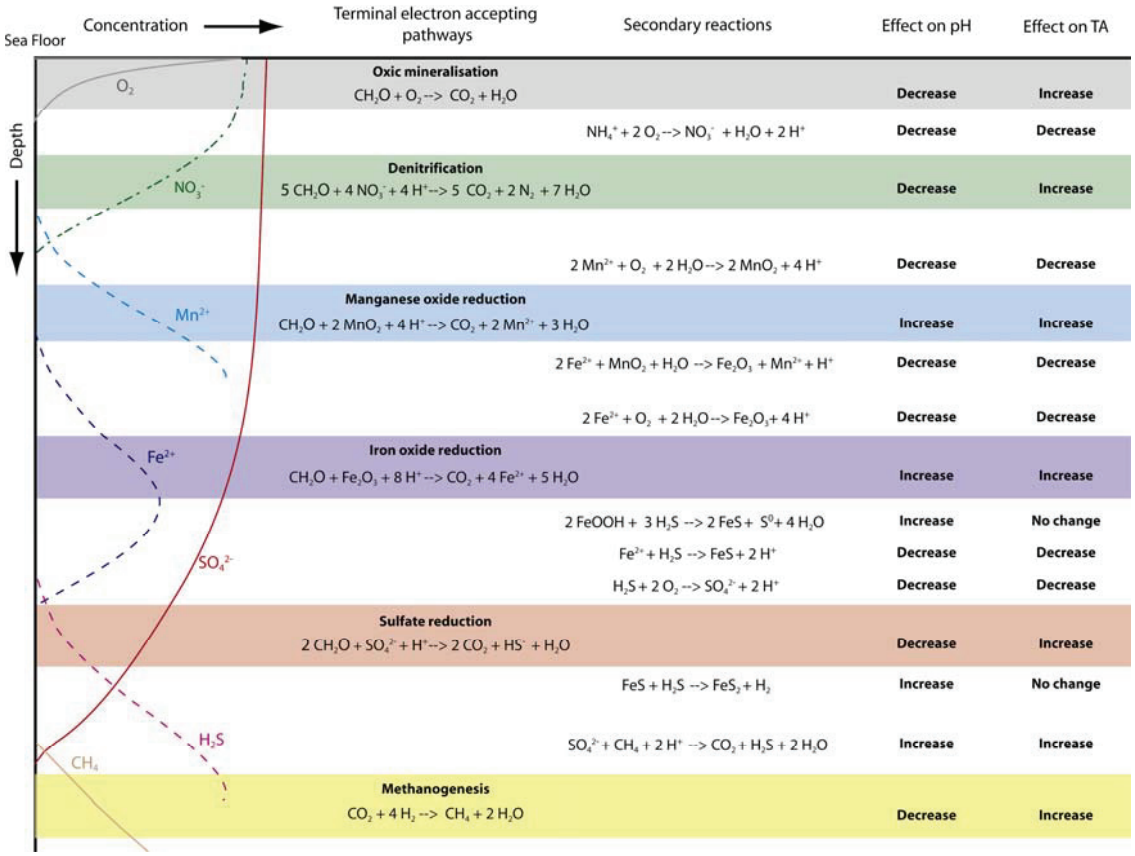

Figure 2: Schematic of the terminal electron accepting pathways in marine sediments following the typical succession with depth (Froehlich et al., 1978). At the overlapping intervals the reactions of the bi-products are shown as well as the most important reactions of these products with solid-phase mineral phases. Also shown is the effect of the individual reactions on pore-water pH and total alkalinity (TA) for an initial pH close to seawater values (pH=8.2) based on Soetaert et al. (2007).

1.3 Cold-water coral ecosystems

Cold-water coral ecosystems formed predominately by the scleractinian corals *Lophelia pertusa* and *Madrepora oculata* commonly occur as patches, well-established reefs systems, but can also build-up enormous cold-water coral mounds (Freiwald, 2002; Roberts et al., 2006; 2009). They are prevalent in a large bathymetric interval and temperature range on continental shelves, seamounts and ridges (Roberts et al., 2006; Wheeler et al., 2007). Surveys on the north-east Atlantic shelf report extensive cold-water coral ecosystems from northern Norway, along the Irish and Scottish margin to the continental slope off Morocco (e.g. Freiwald, 2002; Freiwald and Roberts, 2005; Mortensen et al., 2001; Roberts et al., 2006, 2009; Weaver et al., 2004; Wheeler et al., 2007). Further occurrences include the Mediterranean Sea (Alvarez-Perez et al., 2005; Duineveld et al., 2004; Freiwald et al., 2009; Taviani et al., 2005a; Taviani et al., 2005b; Zibrowius and Taviani, 2005) and Florida Strait (Neumann et al., 1977). Figure 3 shows the global distribution of cold-water corals ecosystems.

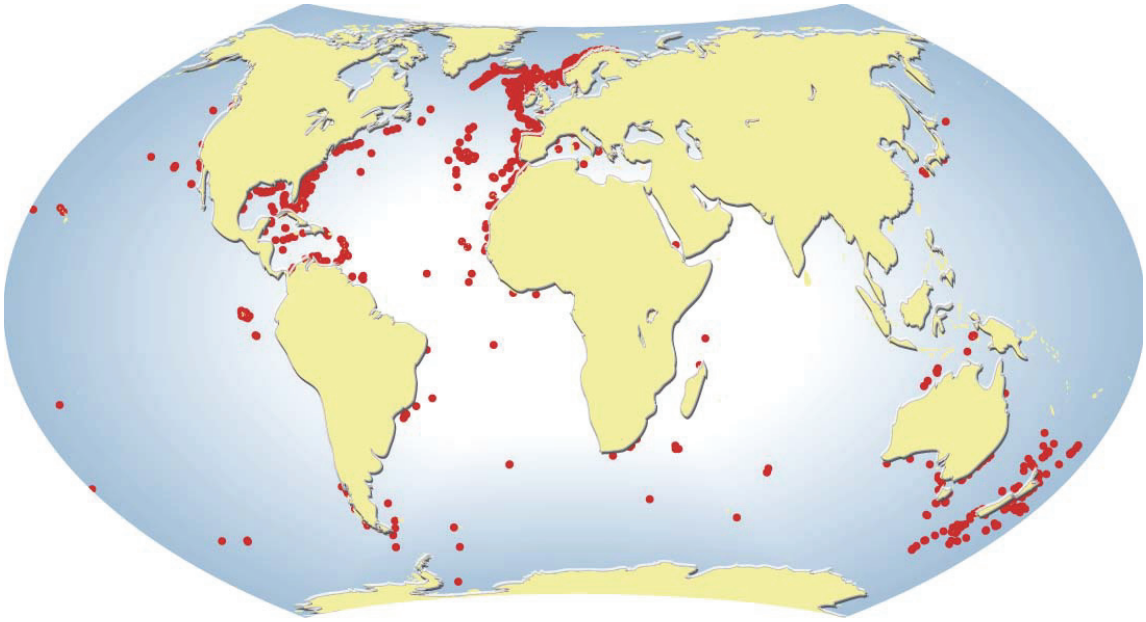

Figure 3: Distribution of cold-water coral ecosystems. UNEP/GRID-Arendal Maps and Graphics Library. 2008. Available at: http://maps.grida.no/go/graphic/coldwater-coral-reefs-distribution. Accessed October 16, 2009.

It is important to note, that a large bias in the presented dataset might exist due to the limited amount of explorations for these ecosystems in regions other than the North Atlantic. Potentially suitable habitats for *L. pertusa* are also assumed to exist in the Indian Ocean, the northern South American shelf, adjacent to Madagascar, on the west coast of Africa and around New Zeeland (Davies et al., 2008). The role of cold-water coral ecosystems in global carbonate budget estimations is not well constrained, but initial estimates indicate that they represent an important sink for inorganic carbon (Dorschel et al., 2007b; Lindberg and Mienert, 2005; Titschack et al., 2009).

1.3.1 Factors governing cold-water coral ecosystem distribution

One requirement for scleractinian cold-water corals, similar to other deep water suspension feeders like gorgonians and cnidarians, is a hard substrate to inhabit (Rogers, 1999; Wilson, 1979). The scleractinian cold-water coral species *L. pertusa* and *M. oculata* are azooxanthellate filter-feeding corals. Thus, in contrast to their warm-water coral counterparts, which host zooxanthellae, endosymbiotic algae transferring photosynthetically fixed carbon to their host (Muscatine et al., 1981), cold-water corals require a food supply from the adjacent water column (Freiwald, 2002).

There are two main hypotheses regarding the factors governing the distribution of cold-water corals. Firstly, the occurrence of cold-water coral reefs has been linked to micro-seepage of thermogenic hydrocarbons (Henriet et al., 1998; Hovland et al., 1998; Hovland and Risk, 2003; Hovland and Thomsen, 1997). In this hypothesis the authors propose a model in which the migration of hydrocarbons into the water column leads to a local fertilization of the ambient water with organic and inorganic compounds which fuel thriving microbial and coral communities. Results from Integrated Ocean Drilling Program (IODP) Expedition 307, which drilled Challenger Mound in the Porcupine Seabight, however, could not corroborate this hypothesis as they report the sulfate-methane transition zone below the mound base and extremely low methane concentrations within the mound sequence (Ferdelman et al., 2006). Another study on the carbon isotope composition of *L. pertusa* from Little Bahama Bank shows that surface-derived material is the dominant carbon source for assimilation and dissolved inorganic carbon (DIC) from ambient seawater is the main carbon source for accretion of the calcareous skeleton (Griffin and Druffel, 1989). In the second hypothesis, a current-controlled and density-controlled mechanism is proposed to govern cold-water coral reef distribution and growth. It is suggested that the occurrence of continuous and adequate current speeds is needed to ensure the supply of food for the filter-feeding corals, and to prevent coral burial by settling of fine-grained sediment particles (Dorschel et al., 2007a; Frederiksen et al., 1992; Mortensen et al., 2001; White et al., 2005; 2007). Accelerated current speeds are triggered by topographic irregularities e.g. seamounts, outcropping rocks, landslide ridges, or created by internal tidal waves (De Mol et al., 2002; Dorschel et al., 2007a; Frederiksen et al., 1992; White, 2007). Dullo et al. (2008) showed preferential coral settlement in water masses of a density of 27.5±0.15 kg/m^3. The apparent strong density control on cold-water coral distribution becomes especially evident in Norwegian fjord systems where corals only occur in those fjords that are characterized by the inflow of Atlantic deep-water (Freiwald et al., 1997; Rogers, 1999). Regional extinction of corals 8000 years ago might have been the result of blocked Atlantic water inflow into several fjord systems (Mikkelsen et al., 1982).

1.3.2 Living cold-water coral ecosystems

Recent studies highlight cold-water coral reefs as hot-spots of biodiversity and biomass production (Roberts et al., 2006; 2009; and reference therein). More than 2600

benthic species are associated with this habitat including sponges, octocorals, echinods, crinoids, bryozoans and crustaceans; its function as a fish refuge, feeding ground and nursery receives increasing attention (Husebø et al., 2002; Jensen and Frederiksen, 1992; Jonsson et al., 2004; Mortensen et al., 1995; Rogers, 1999). Schöttner et al. (2009) have shown that cold-water corals host a specific microbial community different to that of the ambient water and underlying sediment. The authors were able to distinguish between microbial communities living on the coral skeleton, in the tissue and in the mucus, and to illustrate that *L. pertusa* and *M. oculata* facilitate specific, highly diverse microbial habitats. Cold-water coral mucus might furthermore function as an attractive substrate for marine bacteria, archaea, fungi and protozoans, which are described as primary consumers of warm and temperate water coral-derived organic matter (Ducklow and Mitchell, 1979; Herndl and Velimirov, 1986; Wild et al., 2004, 2005, 2008).

Cold-water corals are known to feed on particulate organic matter transported down from productive surface water, re-suspended organic matter in the bottom boundary layer, and on zooplankton prey (e.g. copepods and cumaceans in the coral vicinity; Frederiksen et al., 1992; Freiwald et al., 2002; Kiriakoulakis et al., 2004; 2007; Mienis et al., 2009; Mortensen, 2001; White et al., 2005). This implies a strong coupling of nutrient cycling in the water column to the cold-water coral reef adjacent bottom water. To date, few studies have investigated this relationship. In a recent study on Tisler Reef located in the Skagerrak, Lavaleye et al. (2009) showed the preferential removal of nitrogen-containing labile organic compounds which led to the alteration of the quality of particulate organic matter passing over the reef. The analyses of carbon and nitrogen cycling associated to cold-water coral reefs, especially the role of cold-water coral-derived mucus, was one of the key findings of the studies by Wild et al. (2008, 2009) presented in Chapters 3 and 4.

Cold-water coral reefs are often characterized by a distinct reef facies zonation (Freiwald et al., 1997; Freiwald et al., 2002; Hovland et al., 1998; Mortensen et al., 1995). The different zones represent a habitat for specific reef-associated fauna. Reef zonation is well-described for Sula Reef Complex and Stjernsund Reef off Norway (Freiwald et al., 1997, 2002). Five zones with specific facies patterns were delineated by Freiwald et al. (2002) for the reefs of the Sulfa Reef complex located at 230-300 m water depth (Fig. 4 A): The transition zone between the off-reef sediments and the reef facies is termed *pebbly sand facies* and only covered by scattered, worn coral fragments. The *coral rubble facies* following this zone marks the beginning of the reef slope with

an inclination of 5-25° and is composed of abraded and corroded skeletons of mainly *L. pertusa*. The succeeding zone upslope termed *sediment-clogged framework facies* consists of a Holocene coral framework filled-in by silty clay or sand deposits with a high abundance of shells and bioeroded sponge remains, and has a 20-80° inclination. A gradual change indicates the transition to the *exposed coral framework facies*. This is the steepest section of the slope with an inclination of >90°. Freiwald et al. (2002) describe the main framework as meter-sized slightly displaced parts of recently dead coral colonies with common occurrences of re-colonization of living *L. pertusa* colonies. The uppermost part of the reef is formed by the *living coral framework facies* which consists of hemispherical coral colony clusters.

Stjernsund Reef is an example of a large reef succession hosted on top of a morainic ridge at 235-260 m water depth. Freiwald et al. (1997) denoted four reef facies zones for this reef type (Fig. 4 B): The *distal coral rubble apron* is a >10 cm thick facies composed of coarse coral debris with a diverse preservation state. This zone merges into the *proximal coral debris apron* which is composed of decimeter-sized *L. pertusa* fragments and exhibits the occurrence of large ball-shaped coral aggregates with occasional distribution of living polyps. The reef is topped by the *growing Lophelia-reef mound complex*, which features an outer rim of proliferating white *L. pertusa* satellite colonies canopying a core of dead coral framework. Upslope the *dying reef mound complex* is observed which consists of mostly dead, collapsed coral frameworks undergoing intensive bioerosion.

1.3.3 Cold-water coral mounds

Cold-water coral mounds are enormous structures of up to 300 m in height and several kilometers in diameter (see Roberts et al., 2006; 2009; Wheeler et al., 2007 for review). With more than one thousand known mounds, the Rockall Trough and Porcupine Basin west of Ireland represent major areas of cold-water coral mound occurrences (De Mol et al., 2002; Huvenne et al., 2007; Masson et al., 2003; Mienis et al., 2006; van Weering et al., 2003; Wheeler et al., 2007).

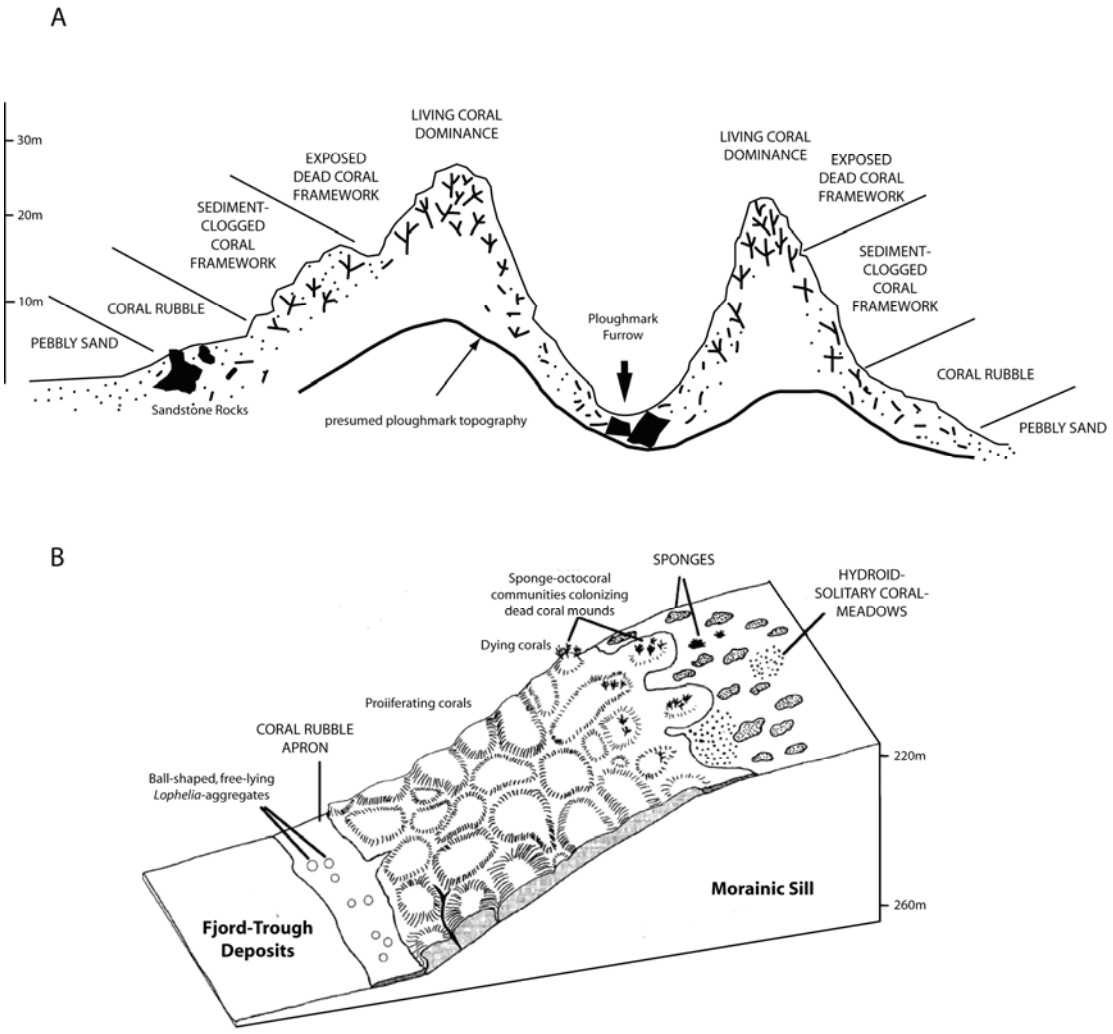

Figure 4: Schematic of the reef facies zonation at A. The Sula Reef Complex (modified from Freiwald et al, 2002) and B. Stjernsund Reef (modified from Freiwald et al, 1997).

Cold-water coral mounds are primarily composed of cold-water coral fragments and shell debris of associated fauna embedded in a loose matrix of hemipelagic sediments (de Haas et al., 2009; Dorschel et al., 2007b; Rüggeberg et al., 2007). Hardground and firmground intervals of several centimeters in thickness are, however, frequently observed and are predominately composed of cemented biogenic carbonate debris, sand and silt (de Haas et al., 2009; Noé et al., 2006). Analyses of the carbonate budget of Challenger Mound showed that background-sediment-derived carbonate represents a significant carbonate source which exceeds the contribution of the embedded corals to the total mound carbonate budget (Titschack et al., 2009). The authors show also that carbonate accumulation rates of the mound surpass the accumulation rates of the adjacent drift deposits by a factor of 3.9 to 11.8 and correspond to about 4 to 12 % of the carbonate accumulation rates of tropical shallow-water reefs.

An elaborate model for mound formation was recently published by de Haas et al. (2009). Briefly, the authors propose that once environmental conditions suitable for coral growth are established and if a hardground for settlement of the planktonic larvae is present, corals can begin to grow and eventually extend into a reef. Baffling of biogenic carbonate debris and allochthonous sediments (foraminifera, lithic grains, etc.) by the corals thereby results in locally enhanced sedimentation rates on the coral reef in comparison to the surrounding seabed. Over time the reef therefore achieves a certain height and develops into a mound structure as for example seen at the Sula Reef complex (Freiwald et al., 2002). At this stage, the mound will start to influence local currents. De Haas et al. (2009) suggest that a positive feedback mechanism evolves which sustains food supply for the corals and further facilitates mound growth. Internal mound growth patterns can be very heterogeneous. This leads to irregular lateral and vertical distributions of sediments (e.g. of varying grain-size). Intriguingly, the present-day overall mound growth rate (± 0.25 mm $year^{-1}$) of a mound at Rockall Trough investigated by de Haas et al. (2009) is only a fraction of the growth rate suggested for *L. pertusa* corallites (up to 25 mm $year^{-1}$; Freiwald et al., 1997; Mortensen and Rapp, 1998).

Cold-water coral mounds usually do not represent continuous sedimentary sequences but show distinct patterns linked to phases of mound growth, stagnation and mound decline. The complex interplay between hydrographical, geological and ecological controlling factors of coral growth driven by environmental changes can lead to large alterations in the growth patterns of individual mounds or mound provinces (Dorschel et al., 2005; 2009; Eisele et al., 2008; Frank et al., 2009; Huvenne et al., 2002; Mienis et al., 2007; Rüggeberg et al., 2007). Changes in the oceanographic conditions have a very strong influence on mound growth because mounds might be affected by different water masses and thus exposed to varying seawater densities. This might expel them from the window of preferred density described by Dullo et al. (2008). A different oceanographic regime might also trigger changes in the supply of organic matter to the mound top, sedimentation rates and current intensities (Dorschel et al., 2005; Huvenne et al., 2003; Rüggeberg et al., 2007). Erosional features are a common phenomenon of cold-water coral mound sequences (Dorschel et al., 2005; Dorschel et al., 2009; Titschack et al., 2009). Changes in the prevailing oceanographic regime are largely

linked to glacial-interglacial oscillations. Therefore periods of favorable or unfavorable mound growth can often be directly correlated to glacial or interglacial time periods (e.g. Kano et al., 2007; Mienis et al., 2009; Frank et al., 2009; Rüggeberg et al., 2007). In turn, cold-water coral mound sediments might serve as a powerful paleoceanographic recorder on continental margins especially during time periods where high current speeds prevent deposition or cause erosion of sediments aside the mounds (Titschak et al., 2009). At present, many discovered mounds are relict cold-water coral build-ups without coverage of living corals. However, individual mounds still host a flourishing coral community, for example Franken Mound on the western Rockall Bank and scores of mounds on the northwest Porcupine Bank (Dorschel et al., 2009; Eisele et al., 2008; Wienberg et al., 2008).

1.3.4 Biogeochemical processes in coral-bearing sediments

Studies of biogeochemical processes in coral-bearing sediments are scarce. Microbially-mediated early diagenetic processes in reef surface sediments play an important role for carbon and nitrogen cycling within the reef system and ultimately control coral skeleton preservation during subsequent burial. Furthermore, biogeochemical processes in cold-water coral mounds might strongly affect syn-depositional mound progression e.g. by causing dissolution of coral skeleton facies or inducing the formation of authigenic carbonate layers.

First insight into biogeochemical processes within a cold-water coral mound was provided by IODP Expedition 307 to Challenger Mound. Initial results indicated that the shape of the pore-water sulfate and alkalinity profiles within the mound sequence were controlled by microbially-mediated organic matter degradation driven by organoclastic sulfate reduction in the top 50 m. The presence of the sulfate-methane transition zone (SMTZ) below the mound base imprinted a diffusion-controlled signal on both profiles (Ferdelman et al., 2006). Hydrogen sulfide concentrations below detection limit suggest sulfide sequestration by ferric-iron containing minerals to form iron-monosulfides and pyrite. Pore-water calcium, magnesium and strontium concentrations showed more intricate behaviors, indicating dissolution of aragonite (presumably from the corals) on the one hand and precipitation of Ca-Mg carbonate minerals on the other. Ferdelman et al. (2006) proposed that organic carbon mineralization by sulfate reduction was the main cause for the apparent aragonite dissolution while re-precipitation of authigenic carbonate phases in other layers was

driven by the subsequent reaction of hydrogen sulfide with reactive Fe-oxide phases to form pyrite. The occurrence of zones of well-preserved coral skeletons alternating with zones of poorly-preserved coral fragments (Ferdelman et al., 2006) and distinct cyclic patterns in content of siliciclastic material (Titschack et al., 2009) point towards a linkage between sediment composition and coral skeleton preservation. A connection between the extent of organic matter degradation, coral dissolution and authigenic carbonate precipitation was also suggested by Foubert et al. (2007) based on variations of magnetic susceptibility and gamma density in cores from mounds located in the Porcupine Seabight.

1.4 Aims and prospectus of this study

This study aims to gain insight into biogeochemical processes in sediments associated with living cold-water coral reef systems as well as to investigate early diagenetic processes in cold-water coral mounds that leave an imprint on the sedimentary record. A major goal for the study of living cold-water coral reef ecosystems is to better understand microbially-mediated diagenetic processes in the sediments from an ecosystem perspective. This is achieved by integrating studies on biogeochemical processes in the reef-associated sediments with observations of microbial carbon turnover in reef adjacent waters and interlinking studies of carbon cycling within the reef. An additional focus is to provide a framework for understanding carbonate preservation patterns in these environments by elucidating the interconnections between the sulfur and iron cycle and carbonate dynamics in the reef sediments. Cold-water coral reef sediments provide the unique opportunity to study carbonate dynamics in a carbonate-rich, siliciclastic environment which receives large input of reactive iron mineral phases. Cold-water coral mounds are investigated with the goal of understanding diagenetic processes at present but also non-steady state diagenetic events that influence these features. The attempt was made to integrate information on the geological and oceanographic setting of the studied cold-water coral mounds.

Investigations were conducted at four study sites. During RV Polarstern Expedition ARK XXII/1a gravity cores were retrieved from two living cold-water coral reefs, Røst Reef and Traenadjupet Reef, located on the Norwegian continental margin. In addition, water column and sediment samples were taken at Tisler Reef, Skagerrak during another field campaign in May 2008. Cores from cold-water coral mounds on

Pen Duick Escarpment in the Gulf of Cadiz were taken during R/V Marion Dufresne Cruise MD 169 MiCROSYSTEMS. Furthermore, sediment samples from a core retrieved at Mound Perseverance in the Porcupine Seabight were analyzed.

Microbially-mediated biogeochemical processes at the living cold-water coral reef sediments on the Norwegian margin were studied to answer the following questions:

1. What are the dominate carbon mineralization pathways in cold-water coral reef associated sediments ?

2. Does methane play a role in the biogeochemical processes of reef sediments ?

3. How are microbially driven geochemical processes and carbonate dynamics linked in coral reef sediments ?

4. What processes govern carbonate preservation in these sediments ?

A major finding of this study is that rates of anaerobic carbon mineralization in the sediments underlying the living reef are extremely low. This is attributed to elevated organic matter turnover by oxic respiration which leaves rather refractory organic carbon for the remaining anaerobic degradation pathways. Based on this hypothesis a second study was conducted on sediments from the Norwegian reefs and Gulf of Cadiz mounds. This study focuses on answering the questions:

1. Can we confirm the hypothesis that organic matter that reaches the anaerobic zone of the sediment has already undergone intensive degradation ?

2. Are there differences in the organic matter quality between different sites within one reef as well as between different reefs and mounds ?

3. What factors control these differences in organic matter quality between the different sites ?

Cold-water coral mounds at Pen Duick Escarpment in the Gulf of Cadiz probably represent unique features, because several of the mounds are affected by the imprint of methane seepage into the mound sequence. Biogeochemical processes in these cold-water coral mounds were studied in the focus of the following questions:

1. How does the presence of methane influence biogeochemical processes in cold-water coral mounds ?

2. How do the unaffected and affected mounds differ in terms of anaerobic carbon mineralization, sulfur and iron cycling, and carbonate preservation and dissolution ?

The investigation of diagenetic processes in cold-water coral mounds was complemented by a collaborative case study on gypsum formation in Mound Perseverance located in the Porcupine Basin. In this study a mechanism for coral dissolution and subsequent formation of gypsum minerals in this mound feature was developed.

References

Archer, D. and Maier-Reimer, E.: Effect of Deep-Sea Sedimentary Calcite Preservation on Atmospheric CO_2 Concentration, Nature, 367, 260-263, 1994.

Alvarez-Perez, G., Busquets, P., De Mol, B., Sandoval, N. G., Canals, M., Casamor, J. L.: Deep-water coral occurrences in the Strait of Gibraltar, in: Cold-water corals and ecosystems, edited by: Freiwald, A. and Roberts, J.M., Springer, Heidelberg, 207-221, 2005.

Bathurst, G.C.: Carbonate sediments and their diagenesis, Developments in Sedimentology, Elservier, Amsterdam, 658 pp, 1975.

Ben-Yaakov, S.: pH Buffering of Pore Water of Recent Anoxic Marine Sediments, Limnol. Oceanogr., 18, 86-94, 1973.

Berelson, W.M., Balch, W. M., Najjar, R., Feely, R. A., Sabine, C. and Lee, K.: Relating estimates of $CaCO_3$ production, export, and dissolution in the water column to measurements of $CaCO_3$ rain into sediment traps and dissolution on the sea floor: A revised global carbonate budget, Global. Biogeochem. Cy., 21, 2007.

Boudreau, B.P.: A method-of-lines code for carbon and nutrient diagenesis in aquatic sediments, Computers & Geosciences, 22, 479-496, 1996.

Boudreau, B.P. and Canfield, D.E.: A Provisional Diagenetic Model for pH in Anoxic Porewaters - Application to the Foam Site, J. Mar. Res., 46, 429-455, 1988.

Boudreau, B.P. and Canfield, D.E.: A comparison of closed-system and open-system models for porewater pH and calcite-saturation state, Geochim. Cosmochim. Ac., 57, 317-334, 1993.

Bramlette, M.N.: Pelagic sediments, in: Oceanography, edited by: Sears, M., American Association for the Advance of Science, Washington, DC, 345-366, 1961.

Cai, W.J., Reimers, C.E. and Shaw, T.: Microelectrode Studies of Organic-Carbon Degradation and Calcite Dissolution at a California Continental Rise Site, Geochim. Cosmochim. Ac., 59, 497-511, 1995.

Canfield, D.E. and Raiswell, R.: Carbonate precipitation and dissolution- Its relevance to fossil preservation, Topics in Geobiology, 9, Plenum Press, New York, 1991.

Davies, A.J., Wisshak, M., Orr, J.C. and Murray Roberts, J.: Predicting suitable habitat for the cold-water coral Lophelia pertusa (Scleractinia), Deep-Sea Res. Pt. I, 55, 1048-1062, 2008.

de Haas, H., Mienis, F., Frank, N., Richter, T. O., Steinacher, R., de Stigter, H., van der Land, C., van Weering, T. C. E.: Morphology and sedimentology of (clustered) cold-water coral mounds at the south Rockall Trough margins, NE Atlantic Ocean, Facies, 55, 1-26, 2009.

De Mol, B., Van Rensbergen, P., Pillen, S., Van Herreweghe, K., Van Rooij, D., McDonnell, A., Huvenne, V., Ivanov, M., Swennen, R. and Henriet, J.-P.: Large deep-water coral banks in the Porcupine Basin, southwest of Ireland, Mar. Geol., 188, 193-231, 2002.

Dorschel, B., Hebbeln, D., Foubert, A., White, M. and Wheeler, A.J.: Hydrodynamics and cold-water coral facies distribution related to recent sedimentary processes at Galway Mound west of Ireland, Mar. Geol., 244, 184-195, 2007a.

Dorschel, B., Hebbeln, D., Rüggeberg, A. and Dullo, C.: Carbonate budget of a cold-water coral carbonate mound: Propeller Mound, Porcupine Seabight, Int. J. Earth Sci., 96, 73-83, 2007b.

Dorschel, B., Hebbeln, D., Rüggeberg, A., Dullo, C. and Freiwald, A.: Growth and erosion of a cold-water coral covered carbonate mound in the Northeast Atlantic during the Late Pleistocene and Holocene, Earth. Planet. Sc. Lett., 233, 33-44, 2005.

Dorschel, B., Wheeler, A.J., Huvenne, V.A.I. and de Haas, H.: Cold-water coral mounds in an erosive environmental setting: TOBI side-scan sonar data and ROV video footage from the northwest Porcupine Bank, NE Atlantic, Mar. Geol., 264, 218-229, 2009.

Ducklow, H.W. and Mitchell, R.: Bacterial-Populations and Adaptations in the Mucus Layers on Living Corals, Limnol. Oceanogr., 24, 715-725, 1979.

Duineveld, G.C.A., Lavaleye, M.S.S. and Berghuis, E.M.: Particle flux and food supply to a seamount cold-water coral community (Galicia Bank, NW Spain), Mar. Ecol. Prog. Ser., 277, 13-23, 2004.

Dullo, C.-W., Flögel, S. and Rüggeberg, A.: Cold-water coral growth in relation to the hydrography of the Celtic and Nordic European continental margin, Mar. Ecol. Prog. Ser., 371, 165-176, 2008.

Emerson, S. and Archer, D.: Glacial carbonate dissolution cycles and atmospheric pCO_2: a view from the ocean bottom, Paleoceanography, 7, 319-31, 1992.

Emerson, S. and Bender, M.: Carbon Fluxes at the Sediment-Water Interface of the Deep-Sea – Calcium Carbonate Preservation, J. Mar. Res., 39, 139-162, 1981.

Emerson, S., Jahnke, R., Bender, M., Froelich, P., Klinkhammer, G., Bowser, C. and Setlock, G.: Early Diagenesis in Sediments from the Eastern Equatorial Pacific, I. Pore Water Nutrient and Carbonate Results, Earth. Planet. Sc. Lett., 49, 57-80, 1980.

Eisele, M., Hebbeln, D. and Wienberg, C.: Growth history of a cold-water coral covered carbonate mound - Galway Mound, Porcupine Seabight, NE-Atlantic, Mar. Geol., 253, 160-169, 2008.

Falkowski, P., Scholes, R. J., Boyle, E., Canadell, J., Canfield, D., Elser, J., Gruber, N., Hibbard, K., Hogberg, P., Linder, S., Mackenzie, F. T., Moore, B., Pedersen, T., Rosenthal, Y., Seitzinger, S., Smetacek, V. and Steffen, W.: The global carbon cycle: A test of our knowledge of earth as a system, Science, 290, 291-296, 2000.

Feely, R.A., Sabine, C. L., Lee, K., Millero, F. J., Lamb, M. F., Greeley, D., Bullister, J. L., Key, R.M., Peng, T. H., Kozyr, A., Ono, T. and Wong, C. S.: In situ calcium carbonate dissolution in the Pacific Ocean, Global. Biogeochem. Cy., 16, 2002.

Feely, R.A., Sabine, C. L., Lee, K., Berelson, W., Kleypas, J., Fabry, V. J. and Millero, F. J.: Impact of anthropogenic CO_2 on the $CaCO_3$ system in the oceans, Science, 305, 362-366, 2004.

Ferdelman, T.G., Kano, A., Williams, T., Henriet, J.-P. and the Expedition 307 Scientists. Proc. IODP, 307: Washington, DC (Integrated Ocean Drilling Program Management International, Inc.). doi:10.2204/iodp.proc.307.102.2006

Foubert, A., Depreiter, D., Beck, T., Maignien, L., Pannemans, B., Frank, N., Blamart, D., Henriet, J.P.: Carbonate mounds in a mud volcano province off north-west Morocco: Key to processes and controls, Mar. Geol., 248, 74-96, 2008.

Frank, N. Ricard, E., Lutringer-Paquet, A., van der Land, C., Colin, C., Blamart, D., Foubert, A., Van Rooij, D., Henriet, J.-P., de Haas, H., van Weering, T.: The Holocene occurrence of cold water corals in the NE Atlantic: Implications for coral carbonate mound evolution, Mar. Geol., 266, 129-142, 2009.

Frederiksen, R., Jensen, A. and Westerberg, H.: The distribution of the scleractinian coral Lophelia pertusa around the Faroe Islands and the relation to internal tidal mixing, Sarsia, 77, 157-171, 1992.

Freiwald, A.: Reef-forming cold-water corals, in: Ocean Margin Systems, edited by: Wefer, G., Billett, D., Hebbeln, D., Jørgensen, B.B., Schlüter, M. and van Weering, T.C.E., Springer, Heidelberg, 365-385, 2002.

Freiwald, A., Beuck, L., Rüggeberg, A., Taviani, M. and Hebbeln, D.: The WHITE CORAL COMMUNITY in the Central Mediterranean Sea Revealed by ROV Surveys, Oceanography, 22, 58-74, 2009.

Freiwald, A., Henrich, R., and Pätzhold, J.: Anatomy of a deep-water coral reef mound from Stjernsund,West Finnmark, Northern Norway, in: Cool-Water Carbonates, edited by: James, N. P. and Clarke, J. A. D., SEPM, Spec. Publ., 56, 141-161, 1997.

Freiwald, A., Huhnerbach, V., Lindberg, B., Wilson, J.B. and Campbell, J.: The Sula Reef Complex, Norwegian shelf, Facies, 47, 179-200, 2002.

Freiwald, A. and Roberts, J.M., Cold-water corals and ecosystems - Preface. Cold-Water Corals and Ecosystems, 7-12, 2005.

Froelich, P.N., Klinkhammer, G. P., Bender, M. L., Luedtke, N. A., Heath, G. R., Cullen, D., Dauphin, P., Hammond, D., Hartman, B. and Maynard, V.: Early oxidation of organic matter in pelagic sediments of the eastern equatorial Atlantic: suboxic diagenesis, Geochim. Cosmochim. Ac., 43, 1075-1090, 1979.

Gardner, L.R.: Chemical models for sulfate reduction in closed anaerobic marine environments, Geochim. Cosmochim. Ac., 37, 53-68, 1973.

Goodwin, P., Follows, M.J. and Williams, R.G.: Analytical relationships between atmospheric carbon dioxide, carbon emissions, and ocean processes, Global. Biogeochem. Cy., 22, 2008.

Griffin, S. and Druffel, E.R.M.: Sources of Carbon to Deep-Sea Corals, Radiocarbon, 31, 533-543, 1989.

Harris, R.P.: Zooplankton Grazing on the Coccolithophore Emiliania-Huxleyi and Its Role in Inorganic Carbon Flux, Mar. Biol., 119, 431-439, 1994.

Henriet, J.-P., De Mol, B., Pillen, S., Vanneste, M., Van Rooij, D., Versteeg, W., Croker, P.F., Shannon, P.M., Unnithan, V., Bouriak, S., Chachkine, P. and The Porcupine-Belgica 97 Shipboard Party: Gas hydrate crystals may help build reefs, Nature, 391, 648-649, 1998.

Herndl, G.J. and Velimirov, B.: Microheterotrophic Utilization of Mucus Released by the Mediterranean Coral Cladocora-Cespitosa, Mar. Biol., 90, 363-369, 1986.

Hovland, M., Mortensen, P.B., Brattegard, T., Strass, P. and Rokoengen, K.: Ahermatypic Coral Banks off Mid-Norway: Evidence for a Link with Seepage of Light Hydrocarbons, Palaios, 13, 189-200, 1998.

Hovland, M. and Risk, M.: Do Norwegian deep-water coral reefs rely on seeping fluids?, Mar. Geol., 198, 83-96, 2003.

Hovland, M. and Thomsen, E.: Cold-water corals - are they hydrocarbon seep related?, Mar. Geol., 137, 159-164, 1997.

Husebø, A., Nottestad, L., Fossa, J.H., Furevik, D.M. and Jørgensen, S.B.: Distribution and abundance of fish in deep-sea coral habitats, Hydrobiologia, 471, 91-99, 2002.

Huvenne, V.A.I., Bailey, W.R., Shannon, P.M., Naeth, J., di Primio, R., Henriet, J.-P., Horsfield, B., de Haas, H., Wheeler, A.J. and Olu-Le Roy, K.: The Magellan mound province in the Porcupine Basin, Int. J. Earth Sci., 96, 85-101, 2007.

Huvenne, V.A.I., Blondel, P. and Henriet, J.-P.: Textural analyses of sidescan sonar imagery from two mound provinces in the Porcupine Seabight, Mar. Geol., 189, 323-341, 2002.

Huvenne, V.A.I., De Mol, B. and Henriet, J.P.: A 3D seismic study of the morphology and spatial distribution of buried coral banks in the Porcupine Basin, SW of Ireland, Mar. Geol., 198, 5-25, 2003.

IPPC (2007): Climate change 2007: The Physical Basis. Contribution of Working Group I to the Fourth Assessment Report of the Intergovernmental Panel on Climate Change, edited by: Solomon, S., Qin, D., Manning, M., Chen, Z., Marquis, M., Averyt, K.B. et al., Cambridge, New York: Cambridge University Press, 131-234, 2007.

Jahnke, R.A., Craven, D.B. and Gaillard, J.F.: The Influence of Organic-Matter Diagenesis on $CaCO_3$ Dissolution at the Deep-Sea Floor, Geochim. Cosmochim. Ac., 58, 2799-2809, 1994.

Jahnke, R.A., Craven, D.B., McCorkle, D.C. and Reimers, C.E.: $CaCO_3$ dissolution in California continental margin sediments: The influence of organic matter remineralization, Geochim. Cosmochim. Ac., 61, 3587-3604, 1997.

Jansen, H. and Wolf-Gladrow, D.A.: Carbonate dissolution in copepod guts: a numerical model, Mar. Ecol. Prog. Ser., 221, 199-207, 2001.

Jensen, A. and Frederiksen, R.: The fauna associated with the bank-forming deep-water coral *Lophelia pertusa* (Scleractinaria) on the Faroe Shelf, Sarsia, 77, 53-69, 1992.

Jonsson, L.G., Nilsson, P.G., Floruta, F. and Lundälv, T.: Distributional patterns of macro- and megafauna associated with a reef of the cold-water coral *Lophelia pertusa* on the Swedish west coast, Mar. Ecol. Prog. Ser., 284, 163-171, 2004.

Jourabchi, P., Van Cappellen, P. and Regnier, P.: Quantitative interpretation of pH distributions in aquatic sediments: A reaction-transport modeling approach, Am. J. Sci., 305, 919-956, 2005.

Jourabchi, P., Meile, C., Pasion, L.R. and Van Cappellen, P.: Quantitative interpretation of pore water O_2 and pH distributions in deep-sea sediments, Geochim. Cosmochim. Ac., 72, 1350-1364, 2008.

Kano, A., Ferdelman, T.G., Williams, T., Henriet, J.P., Ishikawa, T., Kawagoe, N., Takashima, C., Kakizaki, Y., Abe, K., Sakai, S., Browning, E., Li, X. and the IODP Expedition 307 Scientists: Age constraints on the origin and growth history of a deep-water coral mound in northeast Atlantic drilled during Integrated Ocean Drilling Program Expedition 307, Geology, 35, 1051-1054, 2007.

Kiriakoulakis, K., Bett, B.J., White, M. and Wolff, G.A.: Organic biogeochemistry of the Darwin Mounds, a deep-water coral ecosystem, of the NE Atlantic, Deep-Sea Res. Pt. I, 51, 1937-1954, 2004.

Kiriakoulakis, K., Freiwald, A., Fisher, E. and Wolff, G.A.: Organic matter quality and supply to deep-water coral/mound systems of the NW European Continental Margin, Int. J. Earth Sci., 96, 159-170, 2007.

Ku, T.C.W., Walter, L.M., Coleman, M.L., Blake, R.E. and Martini, A.M.: Coupling between sulfur recycling and syndepositional carbonate dissolution: Evidence from oxygen and sulfur isotope composition of pore water sulfate, South Florida Platform, USA, Geochim. Cosmochim. Ac., 63, 2529-2546, 1999.

Lavaleye, M., Duineveld, G., Lundälv, T., White, M., Guihen, D., Kiriakoulakis, K., Wolff, G. A.: Cold-Water Corals on the Tisler Reef Preliminary Observations on the Dynamic Reef Environment, Oceanography, 22, 76-84, 2009.

Lindberg, B. and Mienert, J.: Postglacial carbonate production by cold-water corals on the Norwegian Shelf and their role in the global carbonate budget, Geology, 33, 537-540, 2005.

Masson, D.G., Bett, B. J., Billett, D. S. M., Jacobs, C. L., Wheeler, A. J., Wynn, R. B.: The origin of deep-water, coral-topped mounds in the northern Rockall Trough, Northeast Atlantic. Mar. Geol., 194, 159-180, 2003.

McNichol, A.P., Lee, C. and Druffel, E.R.M.: Carbon Cycling in Coastal Sediments: 1. A Quantitative Estimate of the Remineralization of Organic-Carbon in the Sediments of Buzzards Bay, Ma, Geochim. Cosmochim. Ac., 52, 1531-1543, 1988.

Middelburg, J.J., de Lange, G.J. and Kreulen, R.: Dolomite Formation in Anoxic Sediments of Kau Bay, Indonesia, Geology, 18, 399-402, 1990.

Mienis, F., de Stigter, H.C., de Haas, H. and van Weering, T.C.E.: Near-bed particle deposition and resuspension in a cold-water coral mound area at the Southwest Rockall Trough margin, NE Atlantic, Mar. Geol., 265, 40-50, 2009.

Mienis, F., de Stigter, H.C., White, M., Duineveld, G., de Haas, H. and van Weering, T.C.E.: Hydrodynamic controls on cold-water coral growth and carbonate-mound development at the SW and SE Rockall Trough Margin, NE Atlantic Ocean, Deep-Sea Res. Pt. I, 54, 1655-1674, 2007.

Mienis, F., van Weering, T., de Haas, H., de Stigter, H., Huvenne, V., Wheeler, A.: Carbonate mound development at the SW Rockall Trough margin based on high resolution TOBI and seismic recording, Mar. Geol., 233, 1-19, 2006.

Mikkelsen, N., Erlenkeuser, H., Killingley, J.S. and Berger, W.H.: Norwegian Corals - Radiocarbon and Stable Isotopes in Lophelia-Pertusa, Boreas, 11, 163-171, 1982.

Milliman, J.D.: Recent Sedimentary Carbonates 1, Marine Carbonates. Springer-Verlag, Berlin, 375 pp., 1974.

Milliman, J.D.: Production and accumulation of calcium-carbonate in the ocean - Budget of a nonsteady state, Global. Biogeochem. Cy., 7, 927-957, 1993.

Milliman, J.D. and Droxler, A.W.: Calcium carbonate sedimentation in the global ocean: Linkages between the neritic and pelagic environments, Oceanography, 8, 92-94, 1993.

Milliman, J.D. and Droxler, A.W.: Neritic and pelagic carbonate sedimentation in the marine environment: Ignorance is not bliss, Geol. Rundsch., 85, 496-504, 1996.

Milliman, J.D., Troy, P. J., Balch, W. M., Adams, A. K., Li, Y. H. and Mackenzie, F. T.: Biologically mediated dissolution of calcium carbonate above the chemical lysocline? Deep-Sea Res. Pt. I, 46, 1653-1669, 1999.

Morse, J.W. and Arvidson, R.S.: The dissolution kinetics of major sedimentary carbonate minerals. Earth-Science Reviews, 58, 51-84, 2002.

Morse, J.W., Arvidson, R.S. and Luttge, A.: Calcium Carbonate Formation and Dissolution. Chem. Rev., 107, 342-381, 2007.

Morse, J.W., Cornwell, J.C., Arakaki, T., Lin, S. and Huertadiaz, M.: Iron Sulfide and Carbonate Mineral Diagenesis in Baffin-Bay, Texas, J. Sediment. Petrol., 62, 671-680, 1992.

Morse, J.W. and He, S.L.: Influences of T, S and pCO_2 on the Pseudo-Homogeneous Precipitation of $CaCO_3$ from Seawater - Implications for Whiting Formation, Mar. Chem., 41, 291-297, 1993.

Morse, J.W. and Mackenzie, F.T.: Geochemistry of Sedimentary Carbonates, Developments in Sedimentology. Elservier, Amsterdam, 707 pp., 1990.

Mortensen, P.B.: Aquarium observations on the deep-water coral Lophelia pertusa (L., 1758) (scleractinia) and selected associated invertebrates, Ophelia, 54, 83-104, 2001.

Mortensen, P.B., Hovland, M., Brattegard, T. and Farestveit, R.: Deep-Water bioherms of the Scleractinian Coral *Lophelia pertusa* (L) at 64°N on the Norwegian Shelf: structure and associated megafauna, Sarsia, 80, 145-158, 1995.

Mortensen, P.B., Hovland, M.T., Fossa, J.H. and Furevik, D.M.: Distribution, abundance and size of *Lophelia pertusa* coral reefs in mid-Norway in relation to seabed characteristics, J. Mar. Biol. Assoc. UK, 81, 581-597, 2001.

Mortensen, P.B. and Rapp, H.T.: Oxygen and carbon isotope ratios related to growth line patterns in skeletons of *Lophelia pertusa* (L) (Anthozoa, Scleractinia): Implications for determination of linear extension rates, Sarsia, 83, 433-446, 1998.

Muscatine, L., McCloskey, L.R. and Marian, R.E.: Estimating the Daily Contribution of Carbon from Zooxanthellae to Coral Animal Respiration, Limnol. Oceanogr., 26, 601-611, 1981.

Myneni, R.B., Keeling, C.D., Tucker, C.J., Asrar, G. and Nemani, R.R.: Increased plant growth in the northern high latitudes from 1981 to 1991, Nature, 386, 698-702, 1997.

Neumann, A.C., Kofoed, J.W. and Keller, G.H.: Lithoherms in Straits of Florida, Geology, 5, 4-10, 1977.

Noé, S., Titschack, J., Freiwald, A. and Dullo, W.C.: From sediment to rock: diagenetic processes of hardground formation in deep-water carbonate mounds of the NE Atlantic. Facies, 52, 183-208, 2006.

Pond, D.W., Harris, R.P. and Brownlee, C.: A Microinjection Technique Using a pH-Sensitive Dye to Determine the Gut pH of Calanus-Helgolandicus, Mar. Biol., 123, 75-79, 1995.

Ridgwell, A. and Zeebe, R.E.: The role of the global carbonate cycle in the regulation and evolution of the Earth system, Earth. Planet. Sc. Lett., 234, 299-315, 2005.

Ridgwell, A.J., Kennedy, M.J. and Caldeira, K.: Carbonate deposition, climate stability, and neoproterozoic ice ages, Science, 302, 859-862, 2003.

Roberts, J.M., Wheeler, A. and Freiwald, A.: Cold-Water Corals: The Biology And Geology Of Deep-Sea Coral Habitats. Cambridge University Press, Cambridge, 334 pp, 2009.

Roberts, J.M., Wheeler, A.J. and Freiwald, A.: Reefs of the deep: The biology and geology of cold-water coral ecosystems, Science, 312, 543-547, 2006.

Rogers, A.D.: The biology of *Lophelia pertusa* (LINNAEUS 1758) and other deep-water reef-forming corals and impacts from human activities, Int. Rev. Hydrobiol., 84, 315-406, 1999.

Rüggeberg, A., Dullo, C., Dorschel, B. and Hebbeln, D.: Environmental changes and growth history of a cold-water carbonate mound (Propeller Mound, Porcupine Seabight), Int. J. Earth Sci., 96, 57-72, 2007.

Sabine, C.L., Key, R.M., Feely, R.A. and Greeley, D.: Inorganic carbon in the Indian Ocean: Distribution and dissolution processes, Global. Biogeochem. Cy., 16, 2002.

Sanders, D.: Syndepositional dissolution of calcium carbonate in neritic carbonate environments: geological recognition, processes, potential significance, J. Afr. Earth Sci., 36, 99-134, 2003.

Schimel, D.S.: Terrestrial Ecosystems and the Carbon Cycle, Glob. Change Biol., 1, 77-91, 1995.

Schöttner, S., Hoffmann, F., Wild, C., Rapp, H. T., Boetius, A., Ramette, A.: Inter- and intra-habitat bacterial diversity associated with cold-water corals, ISME Journal, 3, 756-759, 2009.

Soetaert, K., Herman, P.M.J. and Middelburg, J.J.: A model of early diagenetic processes from the shelf to abyssal depths, Geochim. Cosmochim. Ac., 60, 1019-1040, 1996.

Soetaert, K., Hofmann, A.F., Middelburg, J.J., Meysman, F.J.R. and Greenwood, J.: The effect of biogeochemical processes on pH (Reprinted from Marine Chemistry, vol 105, pg 30-51, 2007). Mar. Chem., 106, 380-401, 2007.

Tans, P.P., Fung, I.Y. and Takahashi, T.: Observational Constraints on the Global Atmospheric CO_2 Budget, Science, 247, 1431-1438, 1990.

Taviani, M., Freiwald, A. and Zibrowius, H.: Deep coral growth in the Mediterranean Sea: an overview, in: Cold-water corals and ecosystems, edited by: Freiwald, A. and Roberts, J.M., Springer, Heidelberg, 137-156, 2005a.

Taviani, M., Remia, A., Corselli, C., Freiwald, A., Malinverno, E., Mastrototaro, F., Savini, A., Tursi, A.: First geo-marine survey of living cold-water Lophelia reefs in the Ionian Sea (Mediterranean basin), Facies, 50, 409-417, 2005b.

Titschack, J., Thierens, M., Dorschel, B., Schulbert, C., Freiwald, A., Kano, A., Takashima, C., Kawagoe, N., Li, X. and IODP Expedition 307 scientific party: Carbonate budget of a cold-water coral mound (Challenger Mound, IODP Exp. 307), Mar. Geol., 259, 36-46, 2009.

Tribble, G.W., Sansone, F.J. and Smith, S.V.: Stoichiometric modeling of carbon diagenesis within a coral reef framework, Geochim. Cosmochim. Ac., 54, 2439-2449, 1990.

van Weering, T.C.E., de Haas, H., de Stigter, H.C., Lykke-Andersen, H. and Kouvaev, I.: Structure and development of giant carbonate mounds at the SW and SE Rockall Trough margins, NE Atlantic Ocean, Mar. Geol., 198, 67-81, 2003.

Vecsei, A.: A new estimate of global reefal carbonate production including the fore-reefs, Global Planet. Change, 43, 1-18, 2004.

Volk, T.: Sensitivity of Climate and Atmospheric CO_2 to Deep-Ocean and Shallow-Ocean Carbonate Burial, Nature, 337, 637-640, 1989.

Walker, J.C.G. and Kasting, J.F.: Effects of Fuel and Forest Conservation on Future Levels of Atmospheric Carbon-Dioxide, Global Planet. Change, 97, 151-189, 1992.

Walter, L.M., Bischof, S.A., Patterson, W.P. and Lyons, T.W.: Dissolution and recrystallization in modern shelf carbonates: evidence from pore water and solid phase chemistry, Philos. T. Roy. Soc. Lond. A, 344, 27-36, 1993.

Walter, L.M. and Burton, E.A.: Dissolution of Recent Platform Carbonate Sediments in Marine Pore Fluids, Am. J. Sci., 290, 601-643, 1990.

Weaver, P.P.E., Billett, D. S. M., Boetius, A., Danovaro, R., Freiwald, A., Sibuet, M.: Hot-spot ecosystem research on Europe's deep-ocean margins, Oceanography, 17, 123-143, 2004.

Wheeler, A.J., Beyer, A., Freiwald, A., de Haas, H., Huvenne, V.A.I., Kozachenko, M., Roy, K.O.L. and Opderbecke, J.: Morphology and environment of cold-water coral carbonate mounds on the NW European margin, Int. J. Earth Sci., 96, 37-56, 2007.

White, M., Mohn, C., de Stigter, H. and Mottram, G.: Deep-water coral development as a function of hydrodynamics and surface productivity around the submarine banks of the Rockall Trough, NE Atlantic, in: Cold-water corals and ecosystems, edited by: Freiwald, A. and Roberts, J.M., Springer, Heidelberg, 503-514, 2005.

White, M.: Benthic dynamics at the carbonate mound regions of the Porcupine Sea Bight continental margin, Int. J. Earth Sci., 96, 1-9, 2007.

White, M., Roberts, J.M. and van Weering, T.C.E.: Do bottom-intensified diurnal tidal currents shape the alignment of carbonate mounds in the NE Atlantic?, Geo.-Mar. Lett., 27, 391-397, 2007.

Wienberg, C., Beuck, L., Heidkamp, S., Hebbeln, D., Freiwald, A., Pfannkuche, O., Monteys, X.: Franken Mound: facies and biocoenoses on a newly-discovered "carbonate mound" on the western Rockall Bank, NE Atlantic, Facies, 54, 1-24, 2008.

Wild, C., Mayr, C., Wehrmann, L., Schöttner, S., Naumann, M., Hoffmann, F. and Rapp, H.T.: Organic matter release by cold water corals and its implication for fauna-microbe interaction, Mar. Ecol. Prog. Ser., 372, 67-75, 2008.

Wild, C., Rasheed, M., Jantzen, C., Cook, P., Struck, U., Huettel, M., Boetius, A.: Benthic metabolism and degradation of natural particulate organic matter in carbonate and silicate reef sands of the northern Red Sea, Mar. Ecol. Prog. Ser., 298, 69-78, 2005.

Wild, C., Rasheed, M., Werner, U., Franke, U., Johnstone, R., Huettel, M.: Degradation and mineralization of coral mucus in reef environments, Mar. Ecol. Prog. Ser., 267, 159-171, 2004.

Wild, C., Wehrmann, L.M., Mayr, C., Schöttner, S.I., Allers, E., Lundälv, T.: Microbial degradation of cold-water coral-derived organic matter: potential implication for organic C cycling in the water column above Tisler Reef, Aquat. Biol., 7, 71-80, 2009.

Wilson, J.B: Patch Development of the Deep-Water Coral *Lophelia-Pertusa* (L) on Rockall Bank, J. Mar. Biol. Assoc. UK, 59, 165-177, 1979.

Wolf-Gladrow, D.A., Zeebe, R.E., Klaas, C., Kortzinger, A. and Dickson, A.G.: Total alkalinity: The explicit conservative expression and its application to biogeochemical processes, Mar. Chem., 106, 287-300, 2007.

Wollast, R.: Evaluation and comparison of the global carbon cycle in the coastal zone and in the open ocean, in: The Sea, edited by: Brink K.H. and Robinson A.R., John Wiley & Sons, Inc., pp. 213-252, 1998.

Zibrowius, H. and Taviani, M.: Remarkable sessile fauna associated with deep coral and other calcareous substrates in the Strait of Sicily, Mediterranean Sea, in: Cold-water corals and ecosystems, edited by: Freiwald, A. and Roberts, J.M., Springer, Heidelberg, 807-819, 2005.

PART I:

CARBON CYCLING IN COLD-WATER CORAL REEF ECOSYSTEMS AND BIOGEOCHEMICAL PROCESSES IN REEF-ASSOCIATED SEDIMENTS

CHAPTER 1:

CARBON MINERALIZATION AND CARBONATE PRESERVATION IN MODERN COLD-WATER CORAL REEF SEDIMENTS ON THE NORWEGIAN SHELF

Laura M. Wehrmann[1,2], Nina J. Knab[1], Hans Pirlet[3], Vikram Unnithan[4], Christian Wild[2] and Timothy G. Ferdelman[1]

[1]Biogeochemistry Research Group, Max Planck Institute for Marine Microbiology, Celsiusstrasse 1, D-28359 Bremen, Germany

[2]Coral Reef Ecology Work Group (CORE), GeoBio-Center, Ludwig-Maximilians Universität, Richard-Wagner-Strasse 10, D-80333 München, Germany

[3]Renard Centre of Marine Geology, Department of Geology and Soil Science, Ghent University, Krijgslaan 281 s.8, B-9000 Gent, Belgium

[4] School of Engineering and Science, Jacobs University Bremen, Campus Ring 1, D-28759 Bremen, Germany

Biogeosciences, 6, 663-680, 2009

Abstract

Cold-water coral ecosystems are considered hot-spots of biodiversity and biomass production and may be a regionally important contributor to carbonate production. The impact of these ecosystems on biogeochemical processes and carbonate preservation in associated sediments were studied at Røst Reef and Traenadjupet Reef, two modern (post-glacial) cold-water coral reefs on the Mid-Norwegian shelf. Sulfate and iron reduction as well as carbonate dissolution and precipitation were investigated by combining pore-water geochemical profiles, steady state modeling, as well as solid phase analyses and sulfate reduction rate measurements on gravity cores of up to 3.2 m length. Low extents of sulfate depletion and dissolved inorganic carbon (DIC) production, combined with sulfate reduction rates not exceeding 3 nmol S cm^{-3} d^{-1}, suggested that overall anaerobic carbon mineralization in the sediments was low. These data showed that the coral fragment-bearing siliciclastic sediments were effectively decoupled from the productive pelagic ecosystem by the complex reef surface framework. Organic matter being mineralized by sulfate reduction was calculated to consist of 57 % carbon bound in $-CH_2O-$ groups and 43 % carbon in $-CH_2-$ groups. Methane concentrations were below 1 μM, and failed to support the hypothesis of a linkage between the distribution of cold-water coral reefs and the presence of hydrocarbon seepage. Reductive iron oxide dissolution linked to microbial sulfate reduction buffered the pore-water carbonate system and inhibited acid-driven coral skeleton dissolution. A large pool of reactive iron was available leading to the formation of iron sulfide minerals. Constant pore-water Ca^{2+}, Mg^{2+} and Sr^{2+} concentrations in most cores and decreasing Ca^{2+} and Sr^{2+} concentrations with depth in core 23-18 GC indicated diagenetic carbonate precipitation. This was consistent with the excellent preservation of buried coral fragments.

1. Introduction

Marine surface sediments constitute an important element of the global carbonate cycle. They link carbonate production in the surface ocean with the deep subsurface sedimentary environment (Ridgwell and Zeebe, 2005), but also provide an important record of the ocean's response to changing climate conditions in the past (Broecker and Clark, 2001; Broecker and Clark, 2003; Crowley, 1983). While warm-water coral reefs are considered to contribute substantially to marine carbonate production (Milliman, 1993; Vecsei, 2004), the role of cold-water coral ecosystems remains poorly understood. Initial estimates indicate that cold-water coral reefs can be a regionally important contributor to the $CaCO_3$ budget and account for >1 % of the global $CaCO_3$ production (Lindberg and Mienert, 2005).

Cold-water coral ecosystems, dominated by the azooxanthellate, stony corals *Lophelia pertusa* and *Madrepora oculata*, occur in patches and well-established reef systems, but they can also build up enormous carbonate mounds (Roberts et al., 2006). Cold-water corals are widespread at a range of water depths (30 – 4000 m) along continental margins, seamounts and banks (Wheeler et al., 2007). Recent studies highlight these thriving ecosystems as hot-spots of biodiversity as well as biomass production, revealing a benthic community exceeding 1300 species associated with this habitat (Jensen and Frederiksen, 1992; Mortensen et al., 1995; Roberts et al., 2006; and references therein).

Previous studies have suggested an internal control linking micro-seepage of deep thermogenic hydrocarbons to coral reef occurrence on continental shelves (Hovland et al., 1998; Hovland and Risk, 2003; Hovland and Thomsen, 1997). The authors propose a model in which the migration of hydrocarbons into the water column locally "fertilizes" the ambient seawater with organic and inorganic compounds fueling thriving microbial and coral communities. In an alternative hypothesis, several others suggest that external current- and density-controlled mechanisms govern coral reef distribution and growth (Dorschel et al., 2007; De Mol et al., 2002; Frederiksen et al., 1992; Mienis et al., 2007; Mortensen et al., 2001; White et al., 2005; White, 2007a; White et al., 2007b). This external reef development theory is further supported by the recent study of Dullo et al. (2008), which showed a preferential coral settlement, including Røst Reef and Traenadjupet Reef, in water masses of a density of 27.5 ± 0.15 kg/m^3.

Results from Integrated Ocean Drilling Program (IODP) Expedition 307, which drilled Challenger cold-water coral mound in the Porcupine Seabight, provide the first insight into biogeochemical processes in ancient cold-water coral reef systems (Ferdelman et al., 2006). Decreasing pore-water sulfate and increasing alkalinity concentrations and diagnostic pore-water distributions of Ca^{2+}, Mg^{2+} and Sr^{2+} indicate a coupling between microbially-mediated organic matter degradation and carbonate-mineral diagenesis (Ferdelman et al., 2006). Furthermore, the authors propose that hydrogen sulfide produced during microbially-mediated sulfate reduction reacts with ferric-iron-containing minerals to form iron sulfides, leading to pore-water sulfide depletion. Observations on the occurrence of preferential coral skeleton preservation alternating with zones of poor carbonate preservation (Ferdelman et al., 2006) and distinct recurring cycles exhibiting changes in carbonate content and color reflectance (Titschack et al., 2009) suggest a linkage between sediment composition and coral skeleton preservation. Overall, the findings from IODP expedition 307 indicate a tight coupling between the sulfur, carbon and iron cycles in sediments associated with cold-water coral reef environments.

Several studies (e.g. Boudreau and Canfield, 1993; Ku et al., 1999; Walter et al., 1993; Walter and Burton, 1990) have shown that the relationship between sulfate reduction, hydrogen sulfide oxidation and iron-sulfide mineral formation can drive carbonate dissolution and precipitation in shallow marine sediments. Best et al. (2007) noted that shell preservation of bivalve shells is enhanced in siliciclastic sediments compared to carbonate dominated sediments. A recent comparison of bauxite-contaminated and uncontaminated sites at Discovery Bay, Florida, (Perry and Taylor, 2006) revealed carbonate grain dissolution at the uncontaminated sites compared to the contaminated sites, where carbonates are preserved. The authors attributed the carbonate preservation to the availability of sufficient reactive iron in the bauxite-contaminated sediments. Existing models suggest that the production of hydrogen sulfide and bicarbonate in reactive iron-poor sediments can lead to carbonate dissolution depending on the magnitude of organoclastic sulfate reduction (Ben-Yaakov, 1973; Gardner, 1973; Walter and Burton, 1990). In contrast, if sediments contain a sufficient pool of reactive iron, hydrogen sulfide produced during sulfate reduction reacts with dissolved iron constituents and iron(oxyhydr)oxides to form iron sulfides (Berner, 1970; Berner, 1984) and carbonate undersaturation is prevented (Ben-Yaakov, 1973; Soetaert et al., 2007).

The aim of this study is to investigate how modern cold-water coral reefs influence the adjacent sediment and associated geochemical processes and to provide a framework for understanding carbonate preservation patterns in non-tropical carbonate-rich sediments. The near-shore cold-water coral reefs on the Norwegian shelf serve as an excellent environment to investigate carbonate dynamics in carbonate-rich, siliciclastic sediments receiving a sufficient input of terrigenous material (in particular reactive iron phases). We present data on sulfate reduction rates, diagnostic pore-water profiles (Ca^{2+}, Mg^{2+}, Sr^{2+}, dissolved Mn and Fe, SO_4^{2-} and HS^-, DIC and alkalinity) and solid-phase analyses (TIC, TOC, Fe phases) of seven gravity cores retrieved at Røst Reef and Traenadjupet Reef, located south-west of the Lofoten islands, during R/V Polarstern expedition ARK XXII/1a in June 2007.

2. Study area

2.1 Røst Reef

Røst Reef, discovered in 2002, is regarded as the largest living cold-water coral reef in the world (Nordgulen et al., 2006; Thorsnes et al., 2004). It is located on the northern mid-Norwegian continental slope immediately north-east of the Vøring Plateau at a water depth of 300-400 m (Figs. 1a and 1b). It covers steep ridges originating from the Traenadjupet landslide, one of several submarine landslides that have taken place on the Norwegian continental margin during late Cenozoic times (Damuth, 1978). Deposits from this most recent landslide (approximately 4000 ^{14}C years BP), cover an area of about 9100 km^3 (Laberg and Vorren, 2000). The ridges comprise mostly glaciogenic debris-flow deposits and glaciomarine sediments (Laberg et al., 2002a). They have a maximum length of up to 1 km, reach several tens of meters above the surrounding seafloor, and occur in a very dense spacing (Laberg et al., 2002a). Post-slide hemipelagic sediment deposition varies strongly throughout the Røst Reef region, with the thickest sediment cover found in the small depressions between the ridges immediately inside the slide scar and with minimal sediment deposition occurring along the headwall due to strong currents (Laberg et al., 2002b).

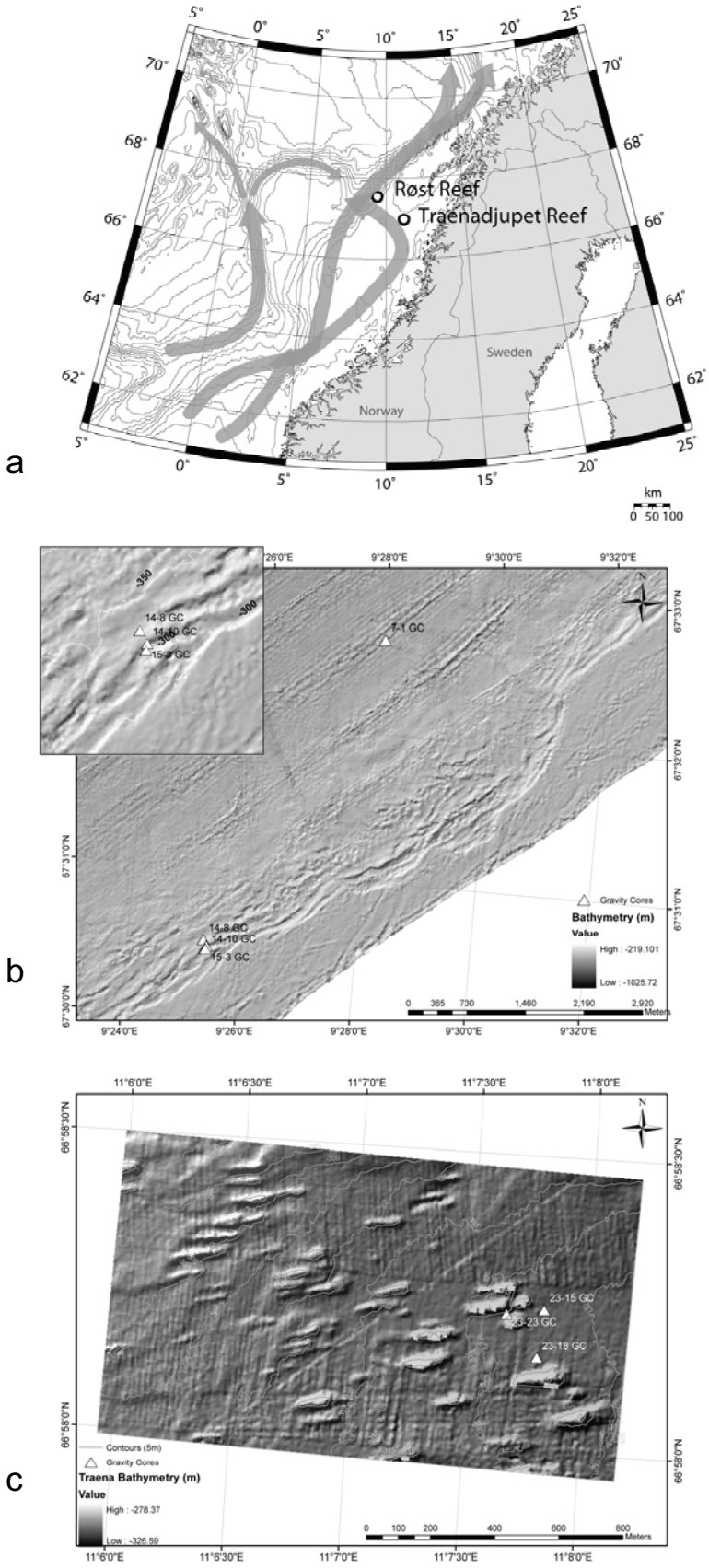

Figure 1: a) Map of the Norwegian Sea with the two investigated reefs (white circles) and the schematic surface water circulation (adapted from Poulain et al., 1996; gray arrows). **b)** Bathymetric map of Røst Reef location. **c)** Bathymetric map of Traenadjupet Reef location. Both maps include the positions of the retrieved gravity cores.

The ridge morphology leads to a distinct habitat zonation of the reef (Fig. 2). Ridge tops are covered by a dense framework of living coral colonies forming terraces towards the lee-side. The upper parts of the slopes consist of glacial clay followed by a coral rubble-dominated facies ("coral rubble zone") on the lower slopes. The depressions between the ridges comprise fine-grained, clay to silt-dominated matrix with embedded coral fragments ("clay zone").

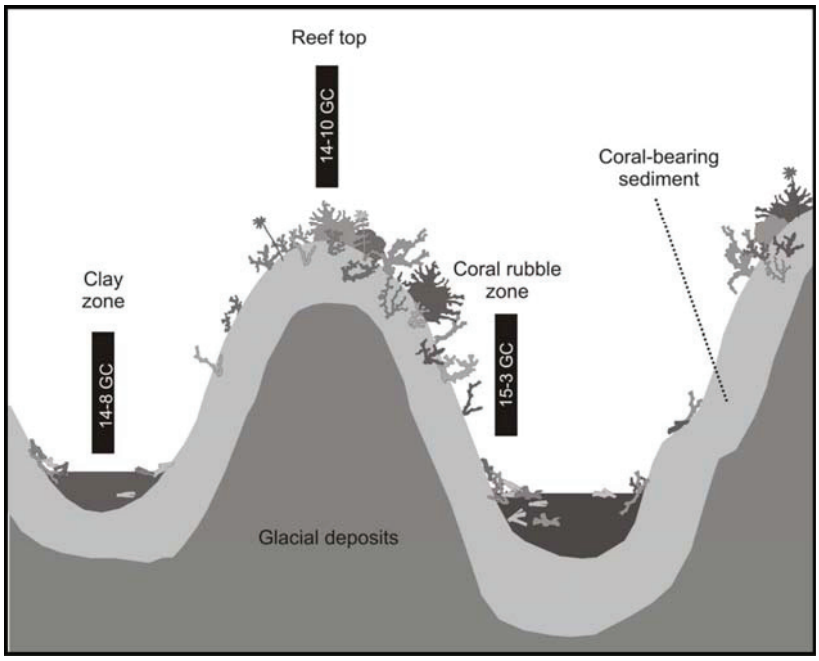

Figure 2: Schematic of Røst Reef zonation.

Surface currents down to 800 m water depth in the Røst Reef region are driven by the confluence of the Norwegian coastal current entering the area from the south. These northeastward-orientated strong currents flow approximately parallel to the Røst Reef (Laberg et al., 2002b; Poulain et al., 1996).

2.2 Traenadjupet Reef

The Traenadjupet Reef area, first described by Hovland and Mortensen (1999), is located in a sheltered embayment on the edge of Traenadjupet, an elongated cross-shelf trough on the mid-Norwegian shelf (Ottesen et al., 2005) (Figs. 1a and c). Studies suggest that the trough formed an important pathway for ice-sheet drainage during Fennoscandian Ice Sheet coverage (Ottesen et al., 2005). The reef is situated on top of Oligocene deltaic sandy fan deposits forming distinct cigar-shaped structures at 300-330 m water depth (Hovland et al., 2005).

Traenadjupet Reef is exposed to a cyclonic circulation predominating in the Lofoten basin (Poulain et al., 1996). It does not feature a distinct habitat zonation comparable to Røst Reef. Instead, living corals only cover a few eastern tips of these structures while most cigar-shaped tops consist of dense coral rubble. The lower parts of the structures are covered by a fine-grained matrix of silt to clay and biogenic debris.

3. Material and methods

3.1 Sample collection

Sediment samples were collected during R/V Polarstern cruise ARK XXII/1a to the mid-Norwegian margin in June 2007. Locations for sediment sampling were selected based on video reconnaissance during the cruise with the research submersible *Jago* (GEOMAR-Kiel). At Røst Reef, cores were taken from the different reef zones (Fig. 2). Cores from Traenadjupet Reef were sampled from the lower parts of the cigar-shaped structures. Sampling locations and water depths of the cores presented in this paper are summarized in Table 1.

Table 1. Sampling location, water depth, core length and core identification.

Reef	Latitude (°N)	Longitude (°E)	Water depth (m)	Core length (cm)	Core identification	Site description
Røst Reef	67°32.64	9°28.05	527	42	7-1 GC	Off-reef
	67°30.52	9°25.34	324	115	14-8 GC	Clay zone
	67°30.48	9°25.40	330	53	14-10 GC	Reef top
	67°30.46	9°25.39	331	163	15-3 GC	Coral rubble zone
Traenadjupet Reef	66°58.24	11°7.82	327	55	23-15 GC	Off-reef
	66°58.16	11°7.80	327	325	23-18 GC	Reef, reactive core
	66°58.23	11°7.66	323	109	23-23 GC	Reef

In total, 7 sediment cores of 0.42-3.25 m length were retrieved at water depths of 323-527 m with a gravity corer (GC; 12 cm ID). They were cut into 1-m sections immediately after core retrieval and the sediment temperature was measured at the top of each section. Sections were stored at 4 °C until further processing. Sub-samples for solid-phase and pore-water analyses, as well as for sulfate reduction rate measurements,

were taken from the cores within a few hours after core retrieval. An overview of measurements applied on the different cores is given in Table 2.

Table 2. Overview of measurements applied on the cores. + indicates conducted measurements. (+) indicates that the measurement has been conducted but values are below detection limit.

Reef	Core identification	TC/TIC/TOC	Sequential Fe-extraction	AVS/CRS	SO_4^{2-}	ICP-OES	DIC/TA	SRR
Røst Reef	7-1 GC	+			+			(+)
	14-8 GC	+			+	+	+	+
	14-10 GC	+			+	+		
	15-3 GC	+	+	+	+	+	+	+
Traenadjupet Reef	23-15 GC	+			+	+		(+)
	23-18 GC	+	+	+	+	+	+	+
	23-23 GC	+			+	+	+	+

3.2 Solid-phase analyses

Samples for solid-phase analyses were taken at 5 cm intervals in the top 2 m and at 10 cm intervals throughout the remaining core. Samples were frozen immediately at -20°C. Frozen samples were freeze-dried, and all coral pieces were removed from the dried samples prior to sample powdering. Total carbon (TC) was determined with a Carlo Erba NA-1500 CNS analyzer using in-house standard (DAN1). Total inorganic carbon (TIC) was measured using a CM 5012 CO_2 Coulometer (UIC) after acidification with phosphoric acid (3 M). Precisions (2σ) were 0.2 wt.% for TC and 0.1 wt.% for TIC. Total organic carbon (TOC) was calculated as the difference between TC and TIC.

A sequential extraction procedure based on Poulton and Canfield (2005) was used to quantify the solid-phase iron pools in cores 15-3 GC and 23-18 GC. The extraction allowed for the determination of carbonate-associated and adsorbed Fe (Fe_{carb}, extraction by sodium acetate), easily reducible Fe-(oxyhydr)oxides (Fe_{ox1}, hydroxylamine-HCl), reducible Fe-(oxyhydr)oxides (Fe_{ox2}, sodium dithionite), magnetite (Fe_{mag}, ammonium oxalate) and poorly reactive silicate Fe (Fe_{PRS}, concentrated HCl). The remaining fraction of unreactive Fe bound as sheet silicates was not quantified during these analyses. Fe analyses were performed by atomic absorption spectrometry (Perkin Elmer). Additionally, acid volatile sulfide (AVS = H_2S + FeS) and

chromium reducible sulfur (CRS = FeS_2 + S^0) were determined on frozen sub-samples of the same cores using a two-step Cr-II method with cold 2M HCl and boiling 0.5M $CrCl_2$ solution (Fossing and Jørgensen, 1989). Fe_{carb} determined during the sequential Fe extraction was corrected for AVS, because sodium acetate treatment results in the complete dissolution of all Fe bound as FeS (Poulton and Canfield, 2005). Fe contents obtained by the sequential extraction procedure, AVS and CRS were corrected for wet-to-dry-weight ratio. Sequential Fe extraction on the sediment samples were conducted in duplicate and generally varied by 5% or less within one extraction sequence and 10% for different sequence runs.

3.3 Pore-water analyses

Pore-water samples were obtained with Rhizones (Rhizosphere Research Products, Wageningen, Netherlands) attached to 5 ml plastic syringes (Seeberg-Elverfeldt et al., 2005). For the determination of SO_4^{2-}, Cl^- and H_2S concentrations aliquots were fixed by adding ZnAc (2%, w/v). SO_4^{2-} and Cl^- concentrations were obtained after 100:1 dilution by non-suppressed anion exchange chromatography as described in Ferdelman et al. (1997). IAPSO standard seawater (Canada) was used as reference standard. Precisions (2σ) for SO_4^{2-} and Cl^- measurements were 0.6 mM and 0.025 M, respectively.

H_2S concentrations were determined from the fixed samples by the diamine complexation method using *N*,*N*-dimethyl-1,4-phenylendiamine-dihydrochloride according to Cline (1969) and subsequent spectrophotometrical measurement at a wavelength of 670 nm. Detection limit of the analyses was 1 μM.

For multi-element pore-water analyses (Fe_{diss} and Mn_{diss}, Ca^{2+}, Mg^{2+} and Sr^{2+}), 1–2 ml aliquots were acidified to 1% HNO_3 (v/v). Samples were analyzed directly from 10-fold diluted samples by inductively coupled plasma optical emission spectroscopy (ICP-OES) using CASS-4 and IAPSO standard seawater (Canada) as reference standards. Precision (2σ) for ICP-OES was < 4% for all elements.

Pore-water aliquots for measurement of dissolved inorganic carbon (DIC) and total alkalinity (TA) were poisoned with $HgCl_2$ (0.25 mM) and sealed headspace-free in 2 ml glass-vials. DIC concentrations were determined by flow-injection (Hall and Aller, 1992). Total alkalinity (TA) was determined by the Gran titration method (Gieskes and Rogers, 1973) on 1:2 (v/v) diluted samples. Precisions (2σ) for DIC and TA determination were 0.4 mM and 0.2 mM, respectively.

The PHREEQC 2.14.3 program (Parkhurst and Appelo, 1999) was used to calculate activities and the saturation index (SI) of aragonite and calcite in core 23-18 GC with SI = 0 representing equilibrium, SI < 0 showing undersaturation and SI > 0 showing oversaturation of the mineral with respect to the pore-water solution.

3.4 Methane concentration measurements

Methane concentrations were determined from 3 cm^3 sediment samples stored upside-down in gas-tight glass bottles containing 6 ml NaOH (2.5%, w/v). Headspace methane concentrations were measured by injection of an aliquot of the gas headspace into a gas chromatograph (Hewlett Packard 5890A) equipped with a packed stainless steel Porapak-Q column (6 ft., 0,125 in., 80/100 mesh Agilent Technologies) and a flame ionization detector. Helium was used as carrier gas at a flow of 2 ml min^{-1}.

3.5 Sulfate reduction rate measurements

Sulfate reduction rates (SRR) were determined in triplicate on-board after subsampling of the GC cores at 5 cm intervals for the upper 2 m and 10 cm intervals in the lower part of the cores. Sediment was sampled in 5-ml glass tubes that were sealed with butyl rubber stoppers. After injection of $^{35}S\text{-}SO_4^{2-}$ (200 kBq) samples were incubated for 20-24h at *in-situ* temperatures in the dark. The incubation period was terminated by transferring the samples into vials containing 20 ml ZnAc (20%, w/v). Reduced radiolabeled sulfur was separated by the cold distillation method described by Kallmeyer et al. (2004) and SRR were calculated after Jørgensen (1978) from the sulfate concentration per cm^{-3} sediment, the total amount of $^{35}S\text{-}SO_4^{2-}$ in the sample and the amount of total reduced inorganic sulfur species.

3.6 Pore-water geochemical modeling

Measured pore-water profiles of SO_4^{2-}, DIC and Ca^{2+} of core 23-18 GC were interpreted using the PROFILE modeling procedure developed by Berg et al. (1998). This numerical modeling procedure fits a series of least-square equations to the concentration profiles. By assuming steady-state conditions and including molecular diffusion, bioturbation and irrigation the net rate of consumption or production of the dissolved species as a function of depth can be calculated using

$$\frac{d}{dz}\left(\varphi D_s \frac{dC}{dz}\right) + \varphi\alpha\left(C_o - C\right) + R = 0 \quad (1)$$

where φ is the porosity, z is the depth, D_s is the molecular diffusivity, C is the pore-water concentration, C_0 is the bottom water concentration, α is the irrigation coefficient and R is the net of production (if R > 0) or consumption (if R < 0). The PROFILE model divides the profiles into a number of zones of constant areal production/consumption rates that can be displayed with the modeled concentration profile. Additionally, it calculates the flux of the dissolved species across the sediment-water interface. In order to successfully reproduce the measured concentration profiles, specific boundary conditions are used at the top and bottom of each profile allowing the input of concentrations or fluxes into the model. In our calculations, pore-water concentrations at the sediment top and at 318 cm depth were used to set boundary conditions. D_s was calculated according to Schulz (2000) as:

$$D_s = \frac{D^0}{\theta^2} \quad (2)$$

where D^0 = temperature-dependent diffusion coefficient of the component in free solution for seawater and θ = tortuosity. Values for θ were calculated based on the relationship (Boudreau, 1997):

$$\theta^2 = 1 - \ln(\varphi^2) \quad (3)$$

Bioirrigation was neglected as we observed no evidence of bioturbation or bioirrigation at depth below 10 cm.

4. Results

4.1 Sediment composition

The three cores taken from the different zones of Røst Reef (Fig. 2) show differences in sediment composition and color. Core 14-10 GC taken at the reef top comprise a mixture of coarse sand, a few cobbles and biogenic debris. The biogenic debris consists of abundant mollusk shells and high numbers of coral skeleton fragments of *L. pertusa* and *M. oculata* in the top 50 cm of the core. Below 50 cm the core consists of sandy sediment with some silt to clay containing minor biogenic debris without coral fragments. Core 15-3 GC, taken in the "coral rubble zone", is topped by a 13 cm thick layer of brown to black coral rubble and biogenic debris with minor mud infill. Below this layer, the sediment is gray and consists of large coral fragments embedded in loose silt, clay and biogenic debris. Beneath 50 cm sponge remains

attached to corals fragments are frequently observed. The sediment in this core becomes more compact with increasing depth but still contains abundant coral fragments. At 158 cm sediment depth, a sharp transition to very compact bluish clay and absence of coral fragments indicate the reef base and underlying glacial ridge deposits. Core 14-8 GC ("clay zone") lacks a coral rubble layer, but is comprised of coral fragments embedded in a matrix of silty clay and bioclasts throughout the core. At 9 cm sediment depth a change in sediment color from brownish-gray to gray occurs. At Røst Reef, sediments are underlain by dark clay indicating that the reef formed directly on top of the ridges of the Traenadjupet landslide. Off-reef core 7-1 GC reveals that sediments away from the reef consist of cohesive, very compact clay with only few biogenic clasts.

Sediment at Traenadjupet Reef is composed of varying amounts of coral fragments and coral rubble of *L. pertusa* and *M. oculata* in a matrix of loose silty clay, biogenic debris and minor cobbles. The sediment color changes from brownish-gray to gray around 7-9 cm in both cores taken from this reef (23-18 GC and 23-23 GC). In core 23-18 GC sponge remains replace the buried corals at 122-130 cm sediment depth. A sharp change in sediment color and composition in the deeper part of both cores from this reef indicates the bottom of the reef. Underlying sediments are comprised of bluish clay that contains stones, probably of glacial origin. Off-reef sediments (23-15 GC) in this area consist of dark silt to clay with a varying sand fraction and sponge spicules.

At both, Røst and Traenadjupet Reef, coral fragments from the top sediment horizons are coated with a brownish crust similar to the coatings of coral fragments retrieved from the surface of other cold-water coral reefs (Freiwald et al., 1997). These crusts are only present within the upper 10-15 cm of the sediments; with the exception of core 14-8 GC, where encrusted corals are found in deeper sediment layers. Sediment directly surrounding corals is often observed to be darker than the adjacent sediment matrix. Microscopic analyses of sediments from both reefs reveal a high content of benthic and planktonic foraminifera, minor percentages of coccolithophores and diatoms and high amounts of sponge spicules. These spicules originate from calcareous as well as siliceous sponges in varying proportions. Bore holes and tubes in the buried coral fragments indicate the colonization of living and dead corals by benthic boring organisms such as sponges, bryozoans and polychaetes. Despite these signs of bioerosion, no visual signs for chemical dissolution of the coral pieces could be observed.

4.2 Solid-phase analyses

A summary of the average TC, TIC and TOC contents of the investigated cores from Røst Reef and Traenadjupet Reef is given in Table 3. Sediments from both reefs are characterized by high TIC contents (Fig. 3) with slightly higher average values of 4.57 (1σ ± 0.97) wt.% at Røst Reef compared to 3.97 (1σ ± 0.87) wt.% at Traenadjupet Reef. Sediments from the surface layer of Røst Reef core 15-3 GC (coral rubble zone) show the highest TIC contents with values of up to 9.05 wt.%. TOC contents (Fig. 3) in sediments from both reefs are low, with most values below 1 wt.%. Sediments from off-reef cores 7-1 GC and 23-15 GC (Fig. 9) are characterized by average TIC contents <0.62 wt.% and average TOC contents <0.40 wt.%.

Table 3. Average TC, TIC and TOC contents and standard deviation (1σ) of cores 14-8 GC, 14-10 GC, 15-3 GC (Røst Reef), 23-18 GC and 23-23 GC (Traenadjupet Reef).

Reef	Core	TC [wt.%]	TIC [wt.%]	TOC [wt.%]
Røst Reef	14-8 GC	4.98 (± 0.22)	4.27 (± 0.35)	0.71 (± 0.26)
	14-10 GC	4.92 (± 1.10)	4.57 (±0.84)	0.35 (± 0.54)
	15-3 GC	5.18 (± 1.43)	4.57 (± 1.44)	0.60 (± 0.34)
Traenadjupet Reef	23-18 GC	4.03 (± 0.90)	3.07 (± 0.62)	0.96 (± 0.46)
	23-23 GC	3.81 (± 0.76)	3.28 (± 0.79)	0.53 (± 0.23)

Table 4 summarizes the average values for the extracted Fe fractions from cores 15-3 GC (Røst Reef) and 23-18 GC (Traenadjupet Reef). Carbonate-associated Fe (Fe_{carb}) content (<0.06 wt.% Fe dry weight) in both investigated cores is low while large fractions of easily reducible and reducible Fe-(oxyhydr)oxides (Fe_{ox1} and Fe_{ox2}; Fig. 4) were found. Magnetite (Fe_{mag}) content in both cores follows trends similar to those of the reactive iron fractions (Fig. 4). Poorly reactive sheet silicate (Fe_{PRS}) constitutes the largest fraction determined with the sequential extraction method with average values above 1.26 wt.% Fe (Fig. 4).

CRS concentrations of cores 15-3 GC and 23-18 GC are presented in Fig. 5. Core 15-3 GC is characterized by very low CRS concentrations (average 0.04 wt.% S) while core 23-18 GC shows larger values for this fraction (CRS average 0.15 wt.% S). AVS concentrations in both cores are below detection limit.

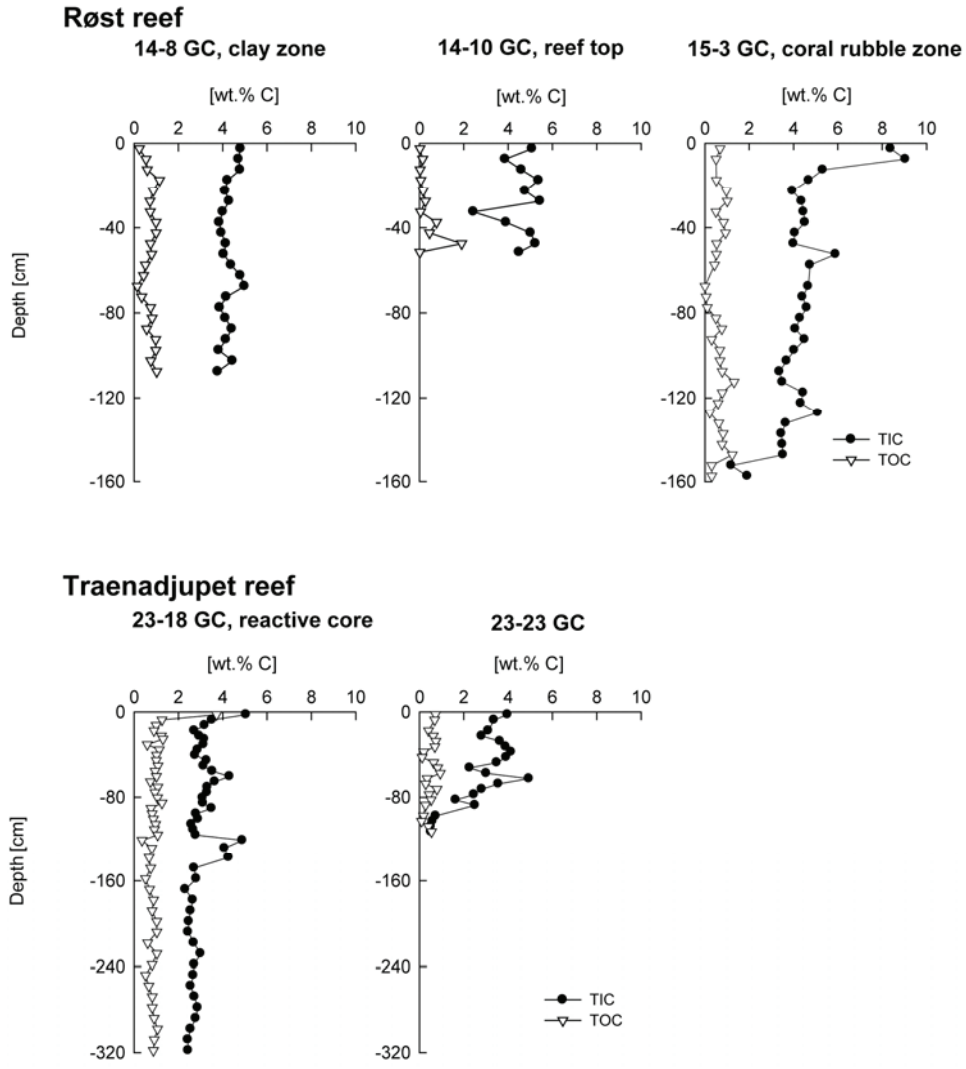

Figure 3: Solid-phase total inorganic carbon (TIC) and total organic carbon (TOC) content in cores 14-8 GC, 14-10 GC and 15-3 GC from Røst Reef and in cores 23-18 GC and 23-23 GC from Traenadjupet Reef.

Table 4. Average values for sequential Fe extractions partitioning between Fe_{carb}, Fe_{ox1}, Fe_{ox2}, Fe_{mag} and Fe_{PRS} contents and standard deviation (1σ) of cores 15-3 GC (Røst Reef) and 23-18 GC (Traenadjupet Reef).

Reef	Core	Fe_{carb} [wt.%]	Fe_{ox1} [wt.%]	Fe_{ox2} [wt.%]	Fe_{mag} [wt.%]	Fe_{PRS} [wt.%]
Røst Reef	15-3 GC	0.03 (± 0.01)	0.22 (± 0.04)	0.30 (± 0.06)	0.15 (± 0.04)	1.26 (± 0.31)
Traenadjupet Reef	23-18 GC	0.04 (± 0.01)	0.29 (± 0.06)	0.23 (± 0.05)	0.16 (± 0.03)	1.39 (± 0.28)

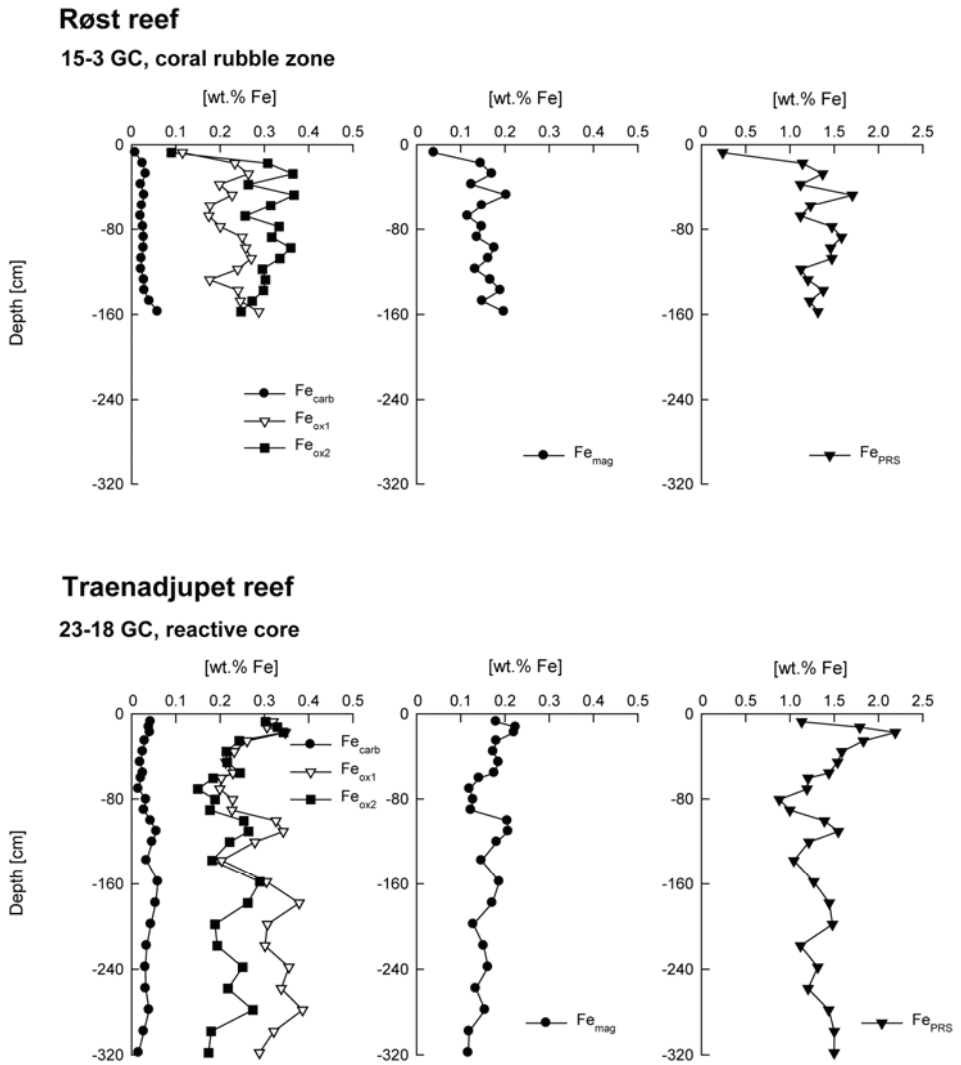

Figure 4: Results of sequential Fe extractions for cores 15-3 GC (Røst Reef) and 23-18 GC (Traenadjupet Reef); Fractions include Fe_{carb}, Fe_{ox1}, Fe_{ox2}, Fe_{mag} and Fe_{PRS}.

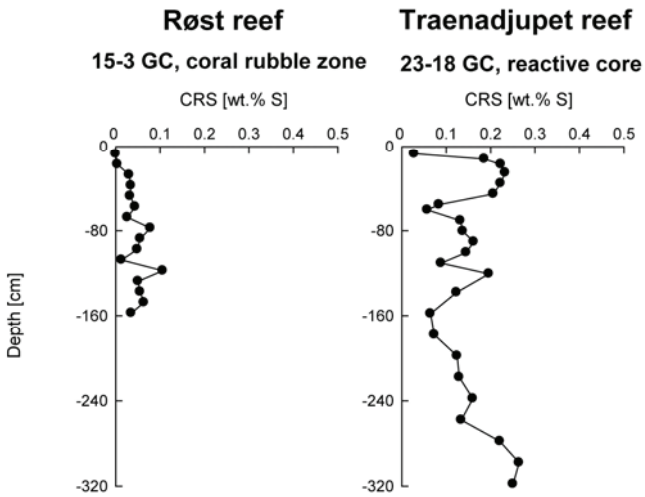

Figure 5: Chromium reducible sulfur (CRS) distribution in cores 15-3 GC (Røst Reef) and 23-18 GC (Traenadjupet Reef).

4.3 Pore-water analyses

Pore-water SO_4^{2-}, Fe_{diss} and Mn_{diss} profiles from cores 14-8 GC, 14-10 GC and 15-3 GC (Røst Reef) are shown in Fig. 6a, and profiles from cores 23-18 GC and 23-23 GC (Traenadjupet Reef) are shown in Fig. 6b. Figure 9 displays the SO_4^{2-} distribution in off-reef core 7-1 GC (Røst Reef) and SO_4^{2-}, Fe_{diss} and Mn_{diss} profiles from off-reef core 23-15 GC (Traenadjupet Reef). The SO_4^{2-} concentrations exhibit small decreases in all reef sites except core 23-18 GC, following a linear trend with a SO_4^{2-} gradient of about 3 mM m^{-1}. In contrast, SO_4^{2-} distribution in core 23-18 GC is characterized by a strong decrease in the top 60 cm of the core to a concentration of around 18 mM followed by a slow decrease in the deeper parts of the core down to minimum value of around 15 mM. Off-reef cores display almost linear SO_4^{2-} profiles. H_2S was not detected (<1 μM) in any of the retrieved pore-water samples.

In the Røst Reef cores 14-8 GC and 15-3 GC, Fe_{diss} concentrations increase from 0 to around 20 μM within the top 30 cm and then decrease gradually with depth to minimum concentrations of <5 μM. Pore-water profiles of the latter core reveal increasing Fe_{diss} concentrations below 120 cm depth with a maximum value of 31 μM at 147.5 cm. Pore-water Mn_{diss} profile of 14-8 GC show a linear increase in the top 60 cm up to values of around 20 μM. Mn_{diss} present in the pore-water of 15-3 GC increase similar to the Fe_{diss} concentration in the top 30 cm reaching values between of 22 and 29 μM. Both Fe_{diss} and Mn_{diss} values decrease again in the clay deposits below the reef base. Core 14-10 GC in contrast is characterized by low Fe_{diss} concentrations (<6 μM) but a strong increase in Mn_{diss} concentrations from 0 to 59 μM in the top 52 cm of the sediment.

At Traenadjupet Reef the Fe_{diss} profile of core 23-18 GC reveals variable concentrations between 2 and 13 μM within the top 148 cm. Between 148 and 178 cm a concentration peak occurs with a maximum value of 17 μM at 168 cm depth. Fe_{diss} concentrations in core 23-23 GC range from 1 μM to a maximum of 47 μM at 72.5 cm. Pore-water Mn_{diss} concentrations in the Traenadjupet Reef cores show maximum values around 14 μM. In core 23-18 GC maximum concentrations are reached at 240 cm, while in core 23-23 GC maximum Mn_{diss} concentrations are reached at 67.5 cm sediment depth. Off-reef core 23-15 GC exhibits increases in Fe_{diss} and Mn_{diss} concentrations in the top 5 cm to average values of 11 μM and 10 μM, respectively.

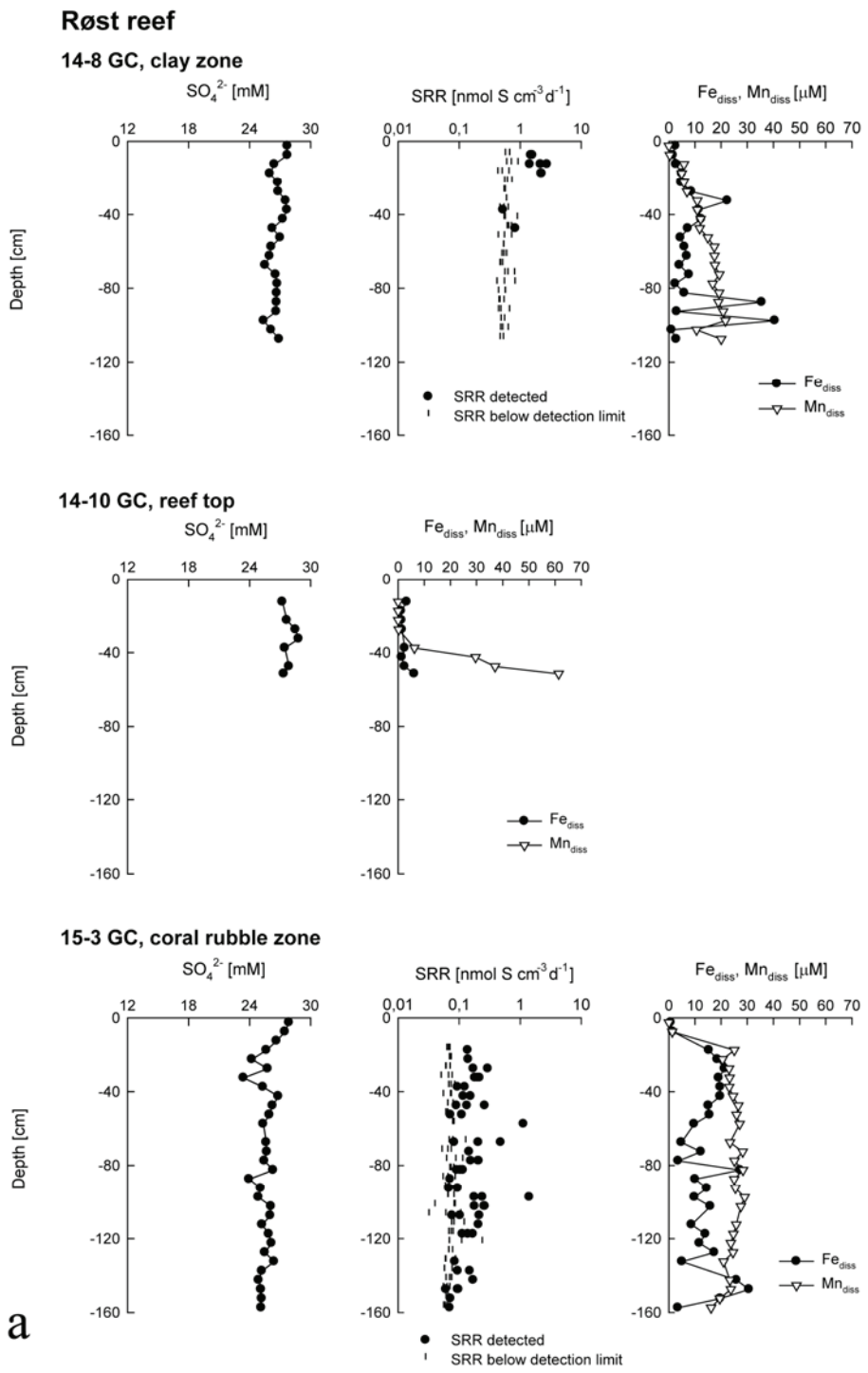

Figure 6a) Pore-water concentration of SO_4^{2-}, SRR, dissolved Fe (Fe_{diss}) and dissolved Mn (Mn_{diss}) in cores 14-8 GC, 14-10 GC and 15-3 GC from Røst Reef.

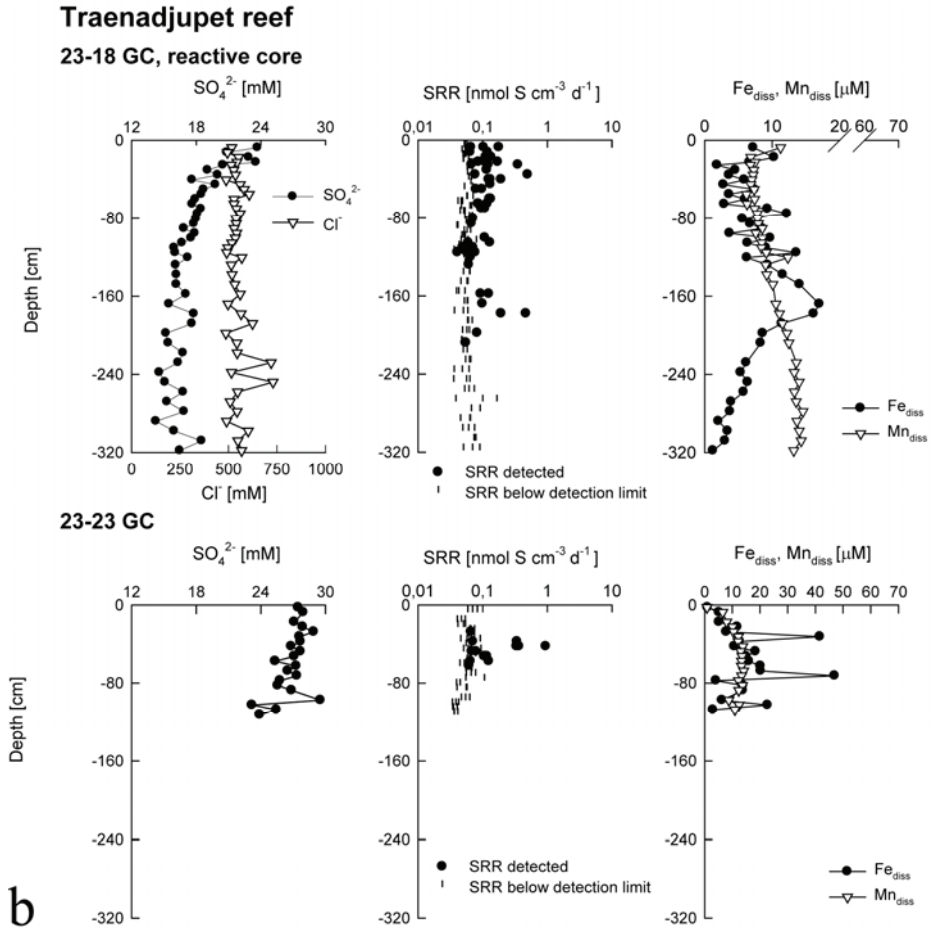

Figure 6b) Pore-water concentration of SO_4^{2-} and Cl^- (23-18 GC), SRR, Fe_{diss} and Mn_{diss} in cores 23-18 GC and 23-23 GC from Traenadjupet Reef; SRR below calculated minimum detection limit are also plotted.

Dissolved Ca^{2+}, Mg^{2+} and Sr^{2+} concentrations are displayed in Figs. 7a (Røst Reef), 7b (Traenadjupet Reef) and Fig. 9 (off-reef core 23-15 GC). Røst Reef cores 14-8 GC, 14-10 GC and 15-3 GC as well as Traenadjupet Reef core 23-23 GC and off-reef core 23-15 GC display constant concentrations for all dissolved constituents close to seawater concentration. In contrast, concentration profiles of core 23-18 GC from Traenadjupet Reef show that Ca^{2+} and Sr^{2+} concentrations in this core decrease in the top 105 cm. Surface Ca^{2+} and Sr^{2+} concentrations start at 10.4 mM and 0.89 mM, respectively, and decrease to values of around 5.4 mM and 0.40 mM at 100 cm sediment depth. Mg^{2+} concentrations remain constant within the top 200 cm of the core (average value of 55.0 mM); below this depth Mg^{2+} concentrations decrease slightly to minimum values of 53.5 mM. In order to exclude salinity changes as the main cause for the decreasing Ca^{2+} and Sr^{2+} profiles, the pore-water concentration of the "conservative" ion Cl^- for this core was determined. Measured concentrations of Cl^- are consistent,

averaging 534 (±27) mM in the top 160 cm and 566 (±71) mM below this sediment depth (Fig. 6b). Sr/Ca and Mg/Ca ratios shown in Figs. 7a and 7b, which can be used to monitor relative changes between different sedimentary carbonate species, are similar in all cores except for core 23-18 GC. Mg/Ca ratios in 23-18 GC increase from 5.8 to 10.7 within the top 110 cm. Furthermore, despite a decrease in both Sr^{2+} and Ca^{2+} in this core, the Sr/Ca ratio steadily decreases from 0.008 to 0.007 with depth.

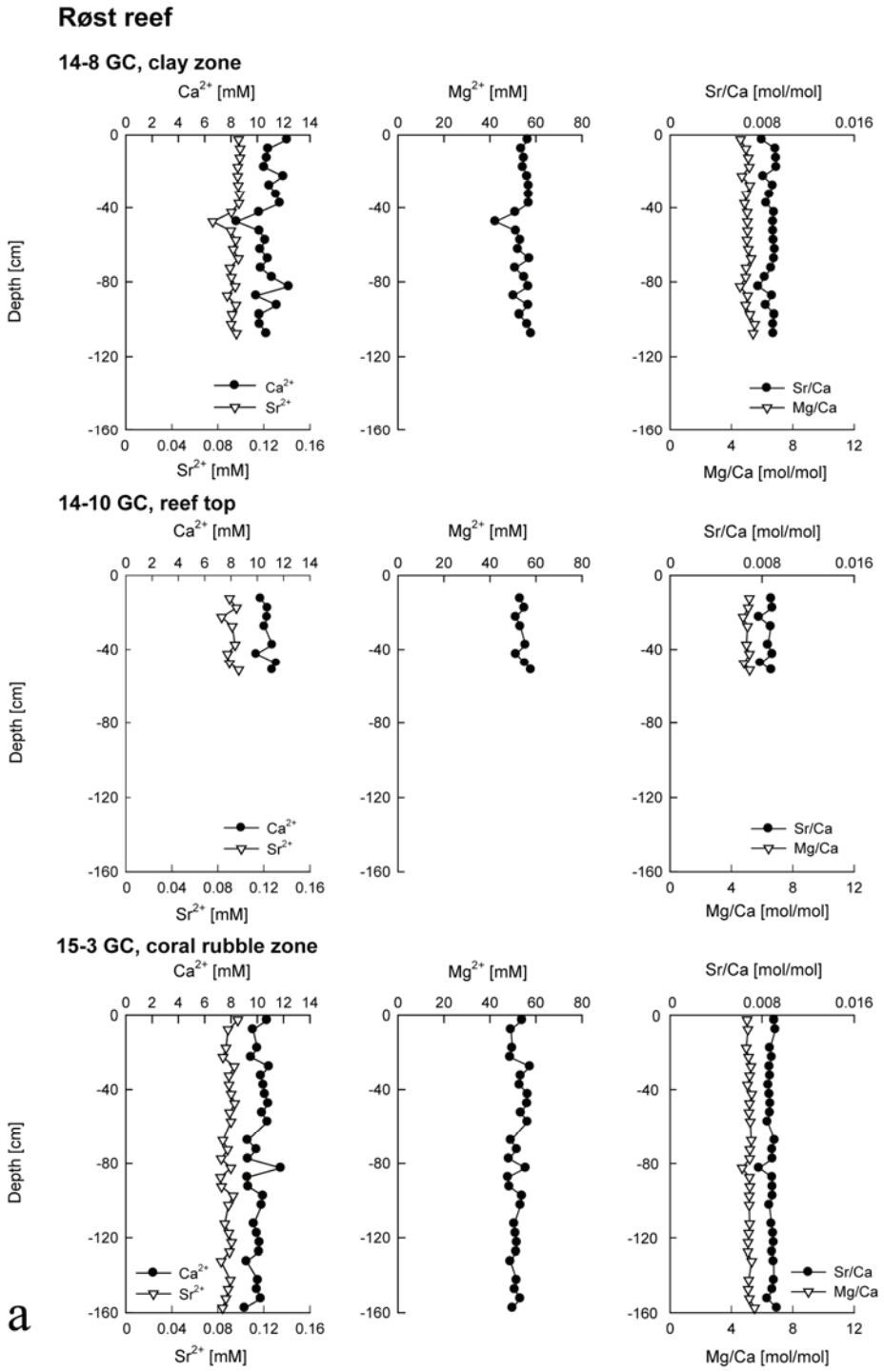

Figure 7a: Pore-water distribution of Ca^{2+}, Sr^{2+} and Mg^{2+}, Sr/Ca ratio and Mg/Ca ratio **a)** in cores 14-8 GC, 14-10 GC and 15-3 GC from Røst Reef.

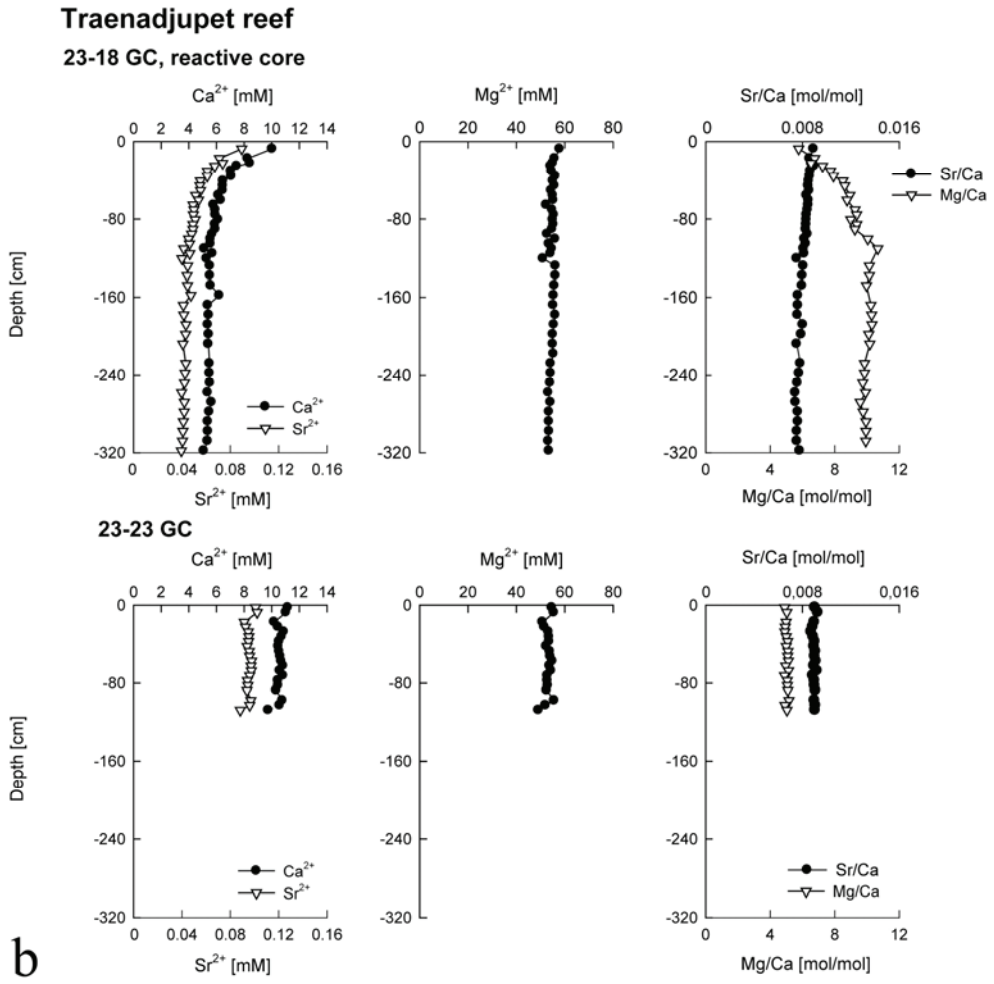

Figure 7b: Pore-water distribution of Ca^{2+}, Sr^{2+} and Mg^{2+}, Sr/Ca ratio and Mg/Ca ratio in cores 23-18 GC and 23-23 GC from Traenadjupet Reef.

Pore-water profiles of DIC and TA (Fig. 8) are inversely correlated with the measured SO_4^{2-} profiles. Pore-water data from Røst Reef reveal only minor increases in the top 40 cm of the cores with average values of 3.6 mM DIC and 3.7 mM TA for 14-8 GC, 2.1 mM DIC and TA for 14-10 GC, 4.2 mM DIC and 4.3 mM TA for 15-3 GC. Core 23-23 GC also follows this trend averaging 3.2 mM DIC and TA. Core 23-18 GC again contrasts strongly. DIC and TA exhibit a concave-up profile in the top 60 cm reaching values around 14 mM and a minor increase in the deeper parts of the sediment to maximum values of 16.7 mM DIC and 16.3 mM TA. Saturation index (SI) values for core 23-18 lie between 0.1 and 1.2 (Fig. 8); calcite is only slightly more saturated than aragonite.

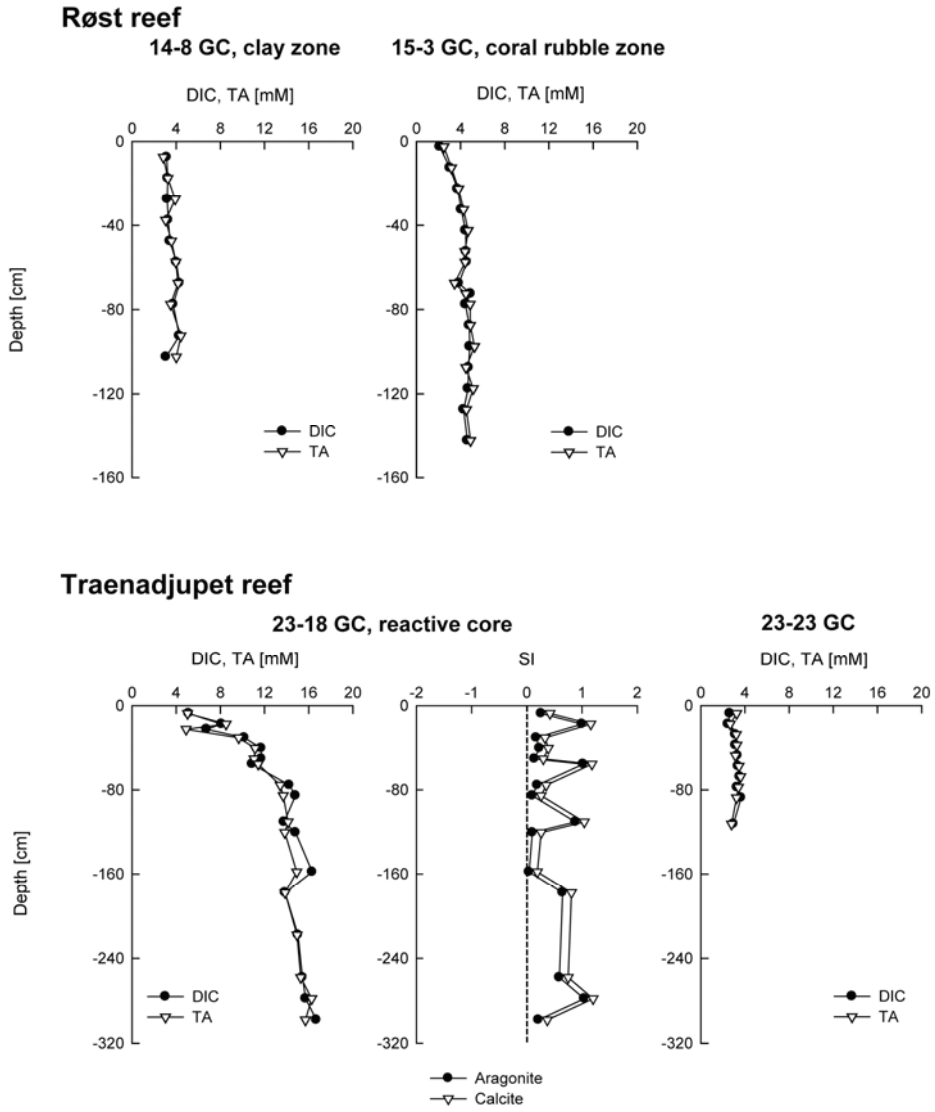

Figure 8: Dissolved inorganic carbon (DIC) concentration and total alkalinity (TA) in the pore-water of cores 14-8 GC and 15-3 GC from Røst Reef and 23-18 GC and 23-23 GC from Traenadjupet Reef. Also shown are calculated saturation indices for aragonite and calcite with respect to the pore-water solution for core 23-18 GC. Values on the left side of the dotted line (SI=0) indicate undersaturation and values on the right side of the line indicate oversaturation of the respective mineral.

4.4 Methane concentration measurements

Methane concentration measurements reveal extremely low methane values below 1 μM at all investigated sediment depths in both coral reefs (data not shown).

4.5 Sulfate reduction rate measurements

SRR data are very low and do not exceed 3 nmol S cm^{-3} d^{-1} (Figs. 6a and 6b). Core 14-8 GC (clay zone) exhibits the highest SRR (averaging 2 nmol S cm^{-3} d^{-1}) of all cores with a peak at 7.5-17.5 cm depth, but with no detectable sulfate reduction below

47.5 cm. However, this core had a higher background signal during the measurement compared to the other cores. In Core 14-10, SRR measurements were not possible due to the extremely high amount of coral fragments. For Røst Reef core 15-3 GC, topped by a layer of coral rubble with only minor sediment infill, SRR measurements were only possible below 15 cm. Here, detected SRR data average 0.22 nmol S cm^{-3} d^{-1} within the top 120 cm. Below this depth rates decrease to less than 0.10 nmol S cm^{-3} d^{-1}. Detected SRR from Traenadjupet Reef core 23-18 GC show average values of 0.13 nmol S cm^{-3} d^{-1} at 5-70 cm sediment depth. Between 70-158 cm SRR drop <0.10 nmol S cm^{-3} d^{-1}. At 158-208 cm a second peak in detected SRR appears, which averages 0.16 nmol S cm^{-3} d^{-1}. At greater depths no sulfate reduction could be detected. In core 23-23 GC SRR data are very low (< 0.15 nmol S cm^{-3} d^{-1}). Elevated values (up to 0.95 nmol S cm^{-3} d^{-1}) only occur at 37.5-42 cm sediment depth. All SRR measurements for the off-reef cores 7-1 GC and 23-15 GC were below detection limit.

4.6 Pore-water profile modeling

Modeled pore-water concentrations, delineated zones of consumption and production for SO_4^{2-}, DIC and Ca^{2+} and the corresponding fluxes of these constituents across the sediment-water interface for core 23-18 GC are shown in Fig. 10. Interpretation of the SO_4^{2-} profile reveals a major zone of sulfate consumption in the top 106 cm of the sediment with a consumption rate of 335 µmol m^{-2} d^{-1} and a zone of minor consumption in the deeper part of the core (25 µmol m^{-2} d^{-1}). The DIC profile is characterized by a production zone with a production rate of 412 µmol m^{-2} d^{-1} at 0-149 cm sediment depth and a consumption zone of approximately equal area below this depth with a consumption rate of 163 µmol m^{-2} d^{-1}. Modeling of the Ca^{2+} concentration reveals a major zone of consumption in the upper 103 cm of this core with a consumption rate of 101 µmol m^{-2} d^{-1}. At greater depths, only small changes in the profile are evident as indicated by a production rate of 0.2 µmol m^{-2} d^{-1}.

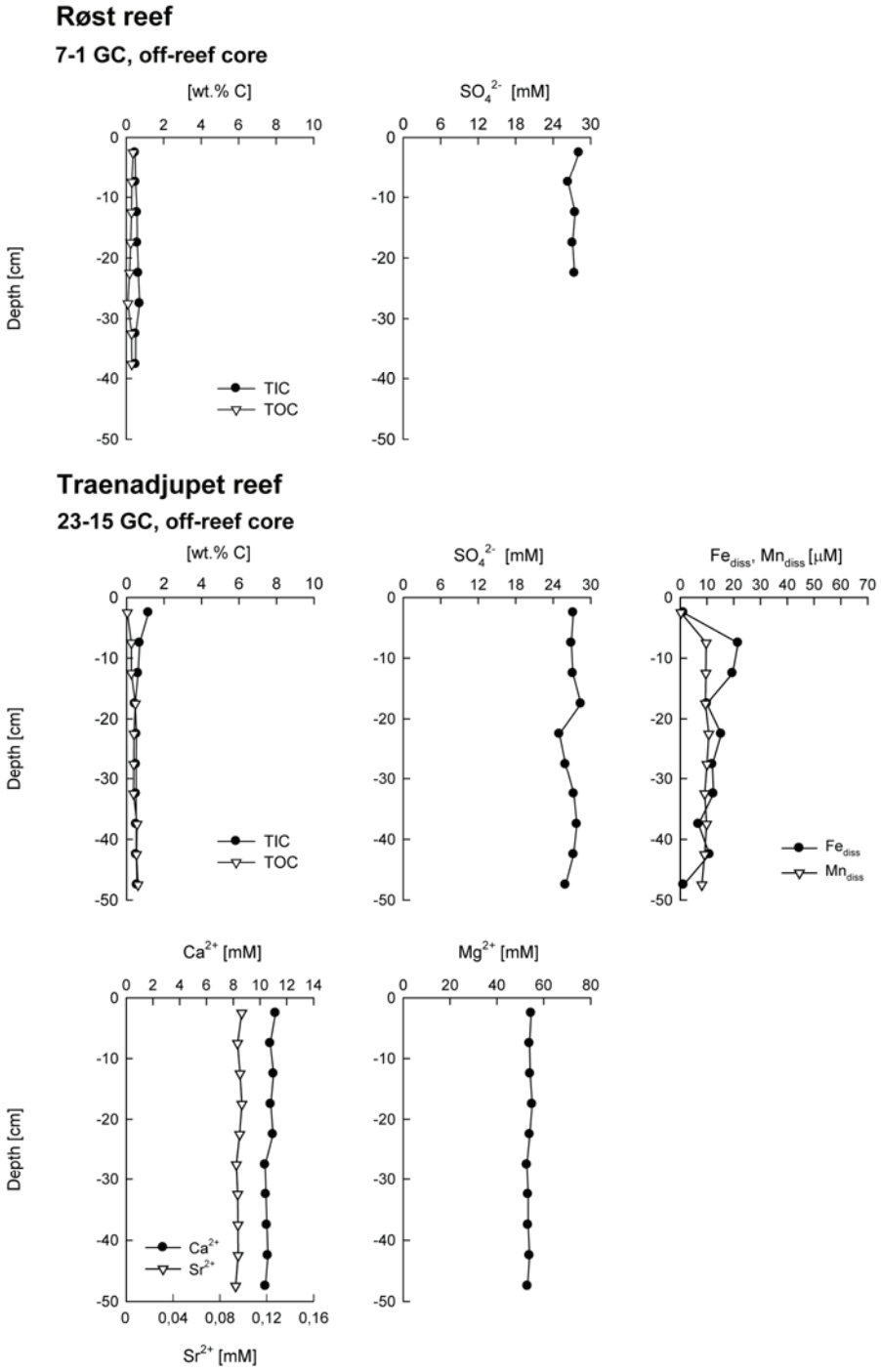

Figure 9: Solid-phase total inorganic carbon (TIC) and total organic carbon (TOC) content and pore-water SO_4^{2-} concentration in off-reef cores 7-1 GC and 23-15 GC. Also shown are pore-water distributions of Ca^{2+}, Sr^{2+} and Mg^{2+} as well as Fe_{diss} and Mn_{diss} in core 23-15 GC.

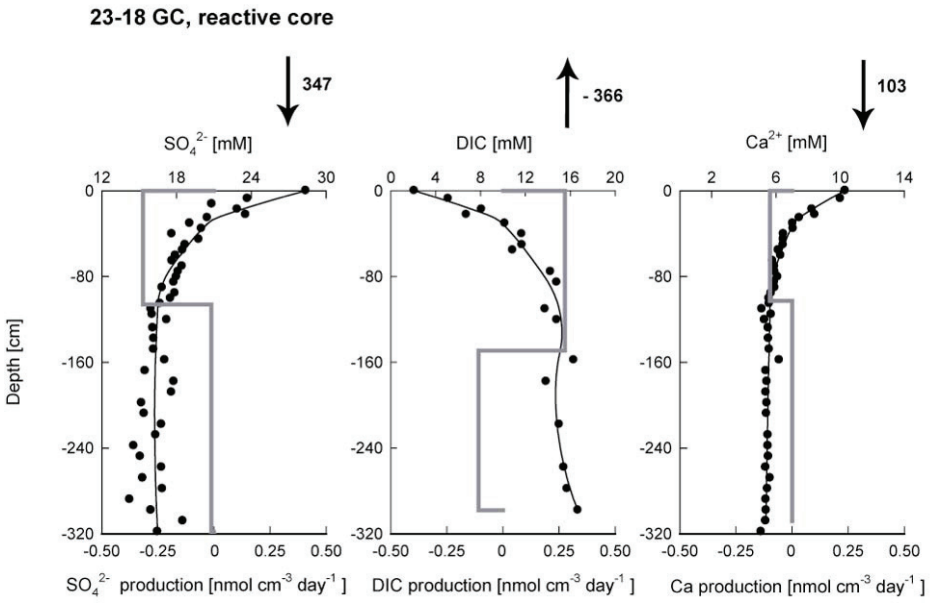

Figure 10: Measured concentration of DIC, SO_4^{2-} and Ca^{2+} (dots), calculated least-square fit concentration profiles (black lines) and modeled rates of production (positive values) and consumption (negative values; grey lines). Calculated fluxes across the sediment-water interface are shown in µmol m^{-2} day^{-1}; negative values indicate flux out of the sediment.

5. Discussion

5.1 Microbially-mediated organic carbon mineralization

Distributions of pore-water metabolites such as SO_4^{2-}, DIC, and Fe_{diss} and Mn_{diss}, combined with direct rate measurements reveal extremely low rates of anaerobic carbon mineralization in the investigated cold-water coral reef sediments. Organoclastic sulfate reduction appears to be the dominant electron donating process in these sediments. Rates of sulfate reduction shown in Figs. 6a and 6b, however, do not exceed detected rates of 3 nmol S cm^{-3} d^{-1} at any site. These values are clearly higher than at the reference sites outside the coral reefs where no sulfate reduction was detected, but rates are very low in comparison to other high-latitude shelf areas, where sulfate reduction generally dominates microbially-mediated organic carbon mineralization (Jørgensen, 1982; Thamdrup and Canfield, 1996). For instance, Kostka et al. (1999) detected SRR of up to 100 nmol S cm^{-3} d^{-1} in surface sediments located north of the Lofoten Islands and warm-water carbonate reef sediments exhibit an order of magnitude higher SRR (Werner et al., 2006) than those detected for the Norwegian cold-water coral reef sediments. By comparison, these rates are in the range of rates reported in a study of carbon mineralization at Central Kvitøya Trench, Spitzbergen where long periods of ice coverage restrict primary production and limit the supply of organic carbon to the sediment (Vandieken et al. 2006).

Sulfate-reducing activities at all sites exhibit distinct, and often multiple zonations throughout the entire core. Such variability has been observed in other deep sediment profiles e.g. the Kattegatt (Iversen and Jørgensen, 1985), the Namibian upwelling area (Fossing et al., 2000), and the equatorial Pacific (Parkes et al., 2005). This zonation can be attributed to variable sedimentation and organic matter input. Only in the younger, top 70.5 cm of Traenadjupet core 23-18 GC (Fig. 6b), sulfate reduction activities are constantly above the detection limit, thus we designated 23-18 GC as the "reactive core". The SO_4^{2-} profile of core 23-18 GC shown in Fig. 6b displays the steepest gradient compared to the other cores where only small decreases in SO_4^{2-} concentration are evident. Elevated CRS values (Fig. 5) are also consistent with higher sulfate reduction activities in core 23-18 GC than at other sites.

Dissimilatory NO_3^- reduction is limited to a narrow zone close to the sediment surface, as indicated by NO_3^- detection only in the top 10 cm of the sediment (data not shown). Only at the top of Røst Reef (14-10 GC) NO_3^- was detected down to 32.5 cm sediment depth. Elevated Mn_{diss} and Fe_{diss} concentrations in the pore-water displayed in Figs. 6a and 6b, suggest the occurrence of dissimilatory Fe- and Mn-oxide reduction as described by Lovley (1987, 1991). More likely, these elevated concentrations result from hydrogen sulfide reacting with the available reactive iron pool and iron/manganese-containing minerals to form Fe-sulfide and dissolved metal species (Afonso and Stumm, 1992; Canfield et al., 1992; Yao and Millero, 1996). In Figures 6a and 6b, distinct zones of Mn and Fe release into the pore-waters that directly correspond with zones of enhanced sulfate-reducing activity in cores at Traenadjupet (23-23 GC at 40 cm depth; 23-18 GC at 160 cm depth) and Røst Reef (15-3 GC throughout the core) are evident. Pore-water DIC concentrations shown in Fig. 8, which reflect the remineralization of organic carbon to CO_2 in marine sediments, display values below 4.2 mM and thus confirm low organic carbon mineralization in most reef sediments. Only in the top 140 cm of the "reactive core" 23-18 GC, does sulfate reduction drive the DIC concentrations higher (up to 16.7 mM).

At Røst Reef differences in pore-water profiles of SO_4^{2-}, Fe_{diss}, Mn_{diss} and SRR (Fig. 6a) as well as NO_3^- distribution between the investigated sites suggest that the reef zonation is not only evident in the type of facies coverage but to a certain extent also reflected in microbial-driven diagenesis. The reef top core 14-10 GC shows a deep penetration of NO_3^- and a steep increase in Mn_{diss} (Fig. 6a) at the bottom of the core. A layer of coarse rubble lacking a fine-grained fraction probably allowed the advective

transport of NO_3^- into the surface rubble and the extension of the suboxic zone to greater depth at the top of Røst Reef. Core 15-3 GC retrieved at the coral rubble zone displays a steeper decrease in SO_4^{2-} concentration and detectable SRR almost throughout the entire core compared to core 14-8 GC from the clay zone where only scattered SRR data occur in the top 17.5 cm. This indicates that despite the fact that TOC content does not differ significantly between the two sites, microbial activity in the coral rubble zone in closer proximity to the living part of the reef is slightly elevated compared to the clay zone. It remains to be further investigated which factors control these differences e.g. higher sedimentation rates or enhanced burial of reef-associated fauna, for example gorgonians or sponge remains which were found in the coral rubble zone core.

When comparing the on-reef cores with results from analyses of the off-reef cores (Fig. 9) it becomes evident that microbially-mediated processes in the reef sediments do exceed activity in the off-reef cores where pore-water constituents show only minor changes in concentration. Off-reef cores 7-1 GC (Røst Reef) and 23-15 GC (Traenadjupet Reef) display almost linear SO_4^{2-} profiles and no detectable sulfate reduction. Elevated Fe_{diss} and Mn_{diss} concentrations in core 23-15 GC indicate that dissimilatory Fe- and Mn-reduction might proceed at low rates. Low average TOC contents <0.4 wt.% detected in both cores suggest that organic matter supply to the sediments is very limited at these sites.

The low rates of anaerobic carbon mineralization observed in the investigated cold-water coral reef sediments may to a great extent be controlled by an extremely low flux of (labile) organic carbon to the sediments. We suggest that the coral framework structure overlaying the coral-bearing sediments decouples the biogeochemical processes in the underlying reef sediments from the productive pelagic ecosystem (Fig. 11). The reefs are characterized by a large number of reef-framework-associated benthic suspension feeders (e.g. cnidarians, poriferans, mollusks) that can directly filter and remove organic particles from the water column (Jensen and Frederiksen, 1992; Jonsson et al., 2004), thereby acting as a sink for organic matter and reducing its supply to the reef sediments. This contrasts with the situation observed in the Darwin Mounds in the Rockall Trough where deep-water coral communities have colonized sandy surfaces. There, Kiriakoulakis et al. (2004) observed that echiuran worms effectively transport organic matter through conveyer-belt feeding into the sandy surface sediments. Within

the clay-rich surfaces of the Norwegian reefs, bioturbation into deeper sediment layers appears to be minimal.

Carbon turnover by microbial respiration within interior coral frameworks is an important process during organic carbon diagenesis in warm-water coral reefs (Sansone et al., 1988; Tribble et al., 1990). Similarly, oxygen sensor measurements conducted at Røst Reef indicate low oxygen concentrations in the water column close to the reef surface (A. Purser, personal communication). Microbial oxygen consumption rates in the water column are also elevated close to the reef surface (Wild et al., 2008). Oxic microbial respiration may therefore be of greater importance in cold-water coral reef environments than in other high-latitude shelf areas, where it is generally regarded as a minor mineralization pathway (3.6-17.4% of the total organic carbon oxidation, Canfield et al., 1993). Aerobic respiration in the overlying water column and living coral framework limits the amount of organic carbon reaching the sediment due to a rapid recycling of labile "fresh" material. Moreover, this process also alters the quality of the organic material reaching the sediment, leaving a large fraction of refractory "old" material that is inefficiently degraded under anoxic conditions (Hulthe et al., 1998).

Low methane concentrations (<1 μM) at all investigated sediment depths in both coral reefs (data not shown) do not provide evidence for a coupling of cold-water coral reef distribution and the appearance of hydrocarbon seepage at the Mid-Norwegian cold-water coral reefs as previously suggested (Henriet et al., 1998; Hovland et al., 1998; Hovland and Risk, 2003 and Hovland and Thomsen, 1997). The reefs are also underlain by very compact glacial clays, which inhibit the flux of deeper seated hydrocarbons into the post-glacial deposits. The glacial deposits furthermore represent a hard substrate, which the corals need for colonization (Frederiksen et al., 1992). Both reefs are located on elevated positions exposed to high current velocities that deliver nutrients and organic matter to the corals and inhibit sediment burial. Several studies have shown that these conditions promote the settlement and growth of cold-water corals (De Mol et al., 2002; Frederiksen et al., 1992; Freiwald, 2002; Mortensen et al., 2001; Roberts et al., 2006; Wheeler et al., 2007; White, 2007a). Furthermore, Dullo et al. (2008) showed that both reefs are located in water masses of a density of 27.5 ± 0.15 kg/m^3 which seems to be a prerequisite for coral development and growth. We conclude that these external current- and density-controlled mechanisms control coral reef distribution and growth at the investigated reefs.

5.2 Sulfate, metal and carbonate dynamics

Sulfate reduction is an ongoing process in the coral reef-associated sediments, although hydrogen sulfide could not be detected in the pore-water. Hydrogen sulfide produced during sulfate reduction readily reacts with reactive iron minerals as well as with dissolved Fe constituents to form iron sulfide minerals that principally occur in these sediments as pyrite (CRS fraction). The sequential iron extractions reveal a large pool of reactive Fe-(oxyhydr)oxides (Fe_{ox1} and Fe_{ox2}; Fig. 4) such as ferrihydrite, lepidocrocite and goethite, which are characterized by very short half-lives with respect to their reaction with hydrogen sulfide (Canfield et al., 1992; Poulton et al., 2004).

The removal of hydrogen sulfide from the pore-water by reactive iron minerals has consequences for the coupling between dissimilatory sulfate reduction and pore-water carbonate dynamics. Depending on the magnitude of sulfate reduction and the initial value of pore-water pH, the accumulation of sulfide and DIC in the pore-water may decrease the pH below carbonate saturation, which may lead to carbonate dissolution (Ben-Yaakov, 1973; Gardner, 1973). The oxidation of hydrogen sulfide strongly enhances this process (Walter and Burton, 1990; Walter et al., 1993). Sulfate reduction linked to carbonate dissolution accounts for significant carbonate losses at modern platform carbonate sediments off Florida and at Tahitian warm-water coral reefs (Ku et al., 1999; Tribble, 1993; Walter et al., 1993; Walter and Burton, 1990). However, if a sufficient pool of reactive iron minerals is present in the sediment, dissolved sulfide reduces ferric iron and precipitates as iron-monosulfides (FeS), intermediate ironsulfide species, and pyrite (Afonso and Stumm, 1992; Berner, 1984; Morse et al., 1992; Pyzik and Sommer, 1981; Rickard and Luther, 2007; Wilkin and Barnes, 1996). The reductive dissolution of iron oxides is a strong proton consuming process. This buffers the carbonic acid system above carbonate undersaturation and carbonate dissolution is inhibited. The described mechanism depends on the amount of produced sulfide as well as on the availability of reactive Fe-(oxyhydr)oxides. At the investigated reefs both factors seem to contribute to a well-buffered pore-water system and may explain the excellent preservation of cold-water coral fragments. A similar mechanism has been proposed to enhance coral preservation in cold-water coral mound systems drilled in IODP Expedition 307 (Ferdelman et al., 2006).

Linear pore-water Mg^{2+}, Ca^{2+} and Sr^{2+} profiles and constant Mg/Ca and Sr/Ca ratios in the sediment cores investigated in the present study (Figs. 7a and 7b) further suggest the absence of extensive net carbonate dissolution. Moreover, in core 23-18 GC,

decreasing Ca^{2+} and Sr^{2+} concentrations in the sulfate reduction zone indicate ongoing syn-depositional carbonate precipitation commonly expressed in the form:

$$Ca^{2+} + 2\ HCO_3^- \rightarrow CaCO_3 + H_2O + CO_2 \quad \text{(R1)}$$

This process is the result of carbonate supersaturation caused by the production of bicarbonate via sulfate reduction. Similar trends in DIC and total alkalinity profiles of core 23-18 GC suggest that the production of bicarbonate (the dominant DIC species at the pore-water pH modeled with the PHREEQC program) entirely accounts for the rise in total alkalinity. The decreasing Sr^{2+} concentration associated with the decrease in Ca^{2+} was probably either the result of the incorporation of Sr^{2+} into the precipitating calcium carbonate species or due to an adsorption of Sr^{2+} onto freshly formed carbonate minerals. Changes in the Sr/Ca ratio may suggest that the mineralogy of the precipitating mineral changed with depth, and an increasing amount of Sr^{2+} was incorporated into the crystal structure or adsorption was enhanced in deeper sediment layers. Calculations of the pore-water carbonate saturation index for aragonite and calcite shown in Fig. 8 reveal that conditions were favorable for the precipitation of both minerals. Decreasing pore-water Sr^{2+} concentration and a constant Mg^{2+} profile in the upper part of core 23-18 GC suggest that authigenic precipitation of aragonite may be occurring. Sr^{2+} is more frequently substituted in the aragonite structure while Mg^{2+} is more frequently incorporated in the calcite structure (Morse et al., 2007).

5.3 Stoichiometry of the diagenetic processes

Attempts are often made to deduce an overall net reaction stoichiometry of the main biogeochemical processes in sediments during early diagenesis. The mineralization of organic matter via sulfate reduction coupled to iron reduction in marine sediments can be expressed as follows:

$$\begin{aligned} 6\ SO_4^{2-} + {}^{12}/_{106}(CH_2O)_{106}(NH_3)_{16}(H_3PO_4) + 3\ Ca^{2+} + 4\ FeOOH \\ \rightarrow 6\ HCO_3^- + 3\ CO_2 + 3\ CaCO_3 + 2\ FeS_2 + 2\ FeS \\ + {}^{192}/_{106}NH_3 + {}^{12}/_{106}H_3PO_4 + 11\ H_2O \end{aligned} \quad \text{(R2)}$$

With some assumptions, this stoichiometry can be assessed by comparing calculated fluxes across the sediment-water interface for SO_4^{2-}, DIC and Ca^{2+} (Fig. 10) obtained

through steady-state diagenetic modeling of the pore-water profiles using the PROFILE program (Berg et al., 1998). We selected the "reactive core" 23-18 GC to conduct this comparison because it displays the largest variations in the measured pore-water constituents.

The stoichiometry given in Eq. (R2) implies a 2:1 ratio of SO_4^{2-} versus Ca^{2+} consumption and a 2:3 ratio for SO_4^{2-} consumption versus DIC production (HCO_3^- + CO_2). Because ¼ of produced HCO_3^- is consumed by $CaCO_3$ precipitation (Eq. R1), correction for the Ca^{2+} precipitated leads to a 1:2 ratio for sulfate consumption versus total DIC production. At the site where core 23-18 GC was taken, the fluxes of SO_4^{2-} and Ca^{2+} across the sediment-water interface are calculated to be 347 µmol cm^{-2} d^{-1} and 103 µmol cm^{-2} d^{-1}, respectively, which gives a ratio of 3.4:1. This ratio exceeds by far the 2:1 ratio expressed in Eq. (R2) and suggests that less Ca^{2+} than expected is removed. The PROFILE program furthermore calculated a DIC flux across the sediment-water interface of 366 µmol cm^{-2} d^{-1}, which gives a total DIC flux (DIC in the pore-water + Ca^{2+} precipitated) of 469 µmol cm^{-2} d^{-1}. In conclusion, the ratio of SO_4^{2-} flux versus total DIC flux calculated for this core is 1:1.4 instead of 1:2, which seems to indicate a decreased DIC flux. Assuming that all DIC production originates from sulfate reduction and is consumed by $CaCO_3$ precipitation, a calculation of the expected DIC flux, using the carbon stoichiometry in Eq. (R2), would give a value of 591 µmol cm^{-2} d^{-1}. Note that in Eq. (R2) all organic matter turnover proceeds via sulfate reduction, and dissimilatory metal oxide reduction is assumed to be minimal. However, even if microbial iron reduction is considered as a major pathway for organic matter mineralization, metal oxide reduction would also lead to enhanced, not less, DIC production.

Overall, the stoichiometry derived simply from the combination of the different single reaction equations may oversimplify the occurring processes. The representation of organic matter degraded within the sediment surface layer by Redfield stoichiometry as -CH_2O- may not in all cases be correct (Hammond et al., 1996; Jahnke et al., 1994; Martin et al., 1987; Takahashi et al., 1985). These studies suggest that organic matter reaching the sediment may be, on average, more reduced than represented by the Redfield stoichiometry because it contains a large fraction of its carbon in -CH_2- groups. This leads to a shift of the overall organic matter composition towards a more complex mixture and reduces the ratio of oxidant (e.g. O_2 or SO_4^{2-}) to produced DIC from a 1:2

ratio towards a 1:1 ratio because for each mole SO_4^{2-} consumed an amount <1 mole of DIC is produced.

Based on the calculated fluxes the following stoichiometric equation describes the biogeochemical processes within core 23-18 GC:

$$6\ SO_4^{2-} + {}^{12}/_{106}(CH_2O)_{42.5}(CH_2)_{31.8}(NH_3)_{16}(H_3PO_4) + 1.76\ Ca^{2+} + 4\ FeOOH$$
$$\rightarrow 4.88\ HCO_3^- + 1.76\ CO_2 + 1.76\ CaCO_3 + 2\ FeS_2 + 2\ FeS$$
$$+ {}^{192}/_{106}NH_3 + {}^{12}/_{106}H_3PO_4 + 9.76\ H_2O \qquad \text{(R3)}$$

The stoichiometry used for the organic material in Eq. (R3), therefore represents the average composition of the organic matter degraded during sulfate reduction in the cold-water coral reefs off Norway. This indicates that ~ 57 % of the degraded organic carbon was bound in the form of $-CH_2O-$ groups while ~ 43 % was bound as $-CH_2-$ groups.

We cannot rule out that other processes are involved that would lead to an additional DIC consumption, and therefore, explain the lack in produced DIC. First, the precipitation of other carbonate minerals e.g. magnesium carbonates could occur. The conservative magnesium profile in the top 200 cm, however, belies this possibility. Second, although we attributed all sulfate consumption to microbial sulfate reduction, other processes could lead to the observed decrease in pore-water sulfate concentration without producing DIC, such as the co-precipitation of sulfate with carbonate to form carbonate-associated sulfate (Staudt and Schoonen, 1995). However, the presence of sulfate reducing activity throughout the core as measured experimentally, suggests that dissimilatory sulfate reduction is the major process removing sulfate. Attributing the DIC deficit to a shift in the metabolized organic matter from carbohydrate-dominated to a more reduced alkyl stoichiometry is the most parsimonious explanation.

6. Conclusions

Highly productive cold-water coral reef ecosystems strongly influence biogeochemical processes in adjacent coral-bearing sediments, although surprisingly, the influence acts as a negative feedback. This first biogeochemical study on recently deposited cold-water coral reef sediments allows the following conclusions:

1. Organic carbon turnover in the investigated cold-water coral reefs occurs in two major zones (Fig. 11): (A) the complex reef surface framework consisting of living and dead coral thickets and coral rubble and (B) the underlying carbonate-rich, coral

fragment-bearing sediments. A rich benthic community of suspension feeders and a high organic matter turnover by oxic microbial respiration reduces the influx of organic matter into the underlying sediments. Therefore, the underlying sediments are characterized by extremely low rates of anaerobic carbon mineralization. The coral framework effectively decouples the reef sediments from the productive pelagic ecosystem.

2. Cold-water coral distribution at both reefs is not linked to hydrocarbon seepage. The underlying compact glacial deposits served as the initial hard substrate for coral settlement.

3. Stoichiometric calculations indicate the oxidation of organic matter with an average oxidation state below that of classic carbohydrate stoichiometries in these sediments. Thus, the limited amount of organic matter that reaches the sediment and that can be anaerobically metabolized appears to be rich in alkyl carbon.

4. Three tightly coupled diagenetic processes occur in these recent sediments: Microbially-mediated organic carbon mineralization by organoclastic sulfate reduction and by Fe-oxide reduction, reaction of produced hydrogen sulfide with dissolved Fe species and Fe-(oxyhydr)oxides to form Fe-sulfides, and authigenic carbonate precipitation instead of carbonate dissolution. The interplay of low rates of sulfate reduction and the availability of a sufficiently reactive iron pool in the siliciclastic sediments leads to a buffering of the pore-water carbonate system. This coupling ultimately prevents carbonate dissolution and favors authigenic carbonate precipitation. Overall, the sediments represent an excellent environment for cold-water coral skeleton preservation and provide a model for initial or surface diagenetic processes that may have occurred in cold-water carbonate mounds such as Challenger Mound.

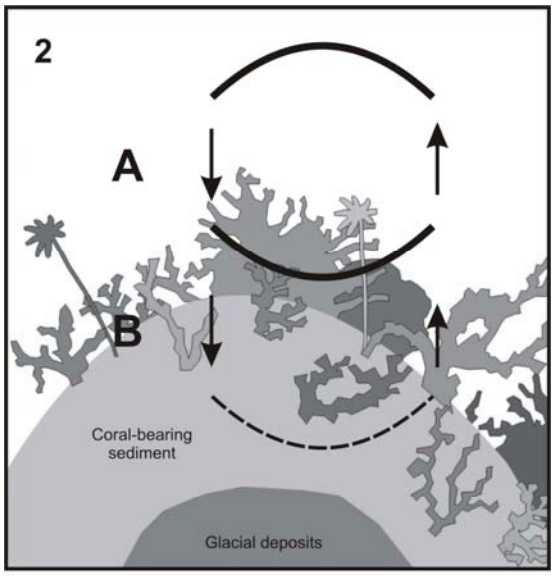

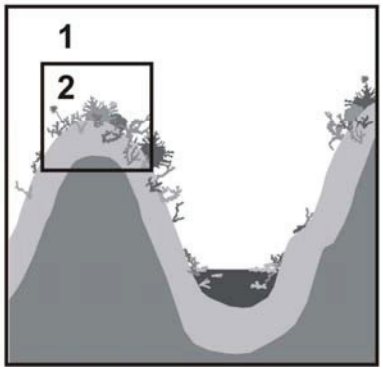

Figure 11: Model of the two major zones of organic matter mineralization in Norwegian cold-water coral reefs: (A) the complex reef surface-framework and (B) the underlying carbonate-rich, coral fragment-bearing sediments.

References

Afonso, M.D. and Stumm, W.: Reductive Dissolution of Iron(III) (Hydr)oxides by Hydrogen Sulfide, Langmuir, 8, 1671-1675, 1992.

Ben-Yaakov, S.: pH Buffering of Pore Water of Recent Anoxic Marine Sediments, Limnol. Oceanogr., 18, 86-94, 1973.

Berg, P., Risgaard-Petersen, N. and Rysgaard, S.: Interpretation of measured concentration profiles in sediment pore water, Limnol. Oceanogr. , 43, 1500-1510, 1998.

Berner, R.A.: Sedimentary Pyrite Formation, Am. J. Sci., 268, 1-23, 1970.

Berner, R.A.: Sedimentary Pyrite Formation - an Update, Geochim. Cosmochim. Ac., 48, 605-615, 1984.

Best, M.M.R., Ku, T.C.W., Kidwell, S.M. and Walter, L.M.: Carbonate Preservation in Shallow Marine Environments: Unexpected Role of Tropical Siliciclastics, J. Geol., 115, 437-456, 2007.

Boudreau, B.P.: Diagenetic Models and their Implementation: Modelling Transport and Reactions in Aquatic Sediments, Springer, Berlin, 1997.

Boudreau, B.P. and Canfield, D.E.: A comparison of closed-system and open-system models for porewater pH and calcite-saturation state, Geochim. Cosmochim. Ac., 57, 317-334, 1993.

Broecker, W.S. and Clark, E.: Glacial-to-Holocene Redistribution of Carbonate Ion in the Deep Sea, Science, 294, 2152-2155, 2001.

Broecker, W.S. and Clark, E.: $CaCO_3$ dissolution in the deep sea: Paced by insolation cycles, Geochem. Geophy. Geosy., 4, 1-13, 2003.

Canfield, D.E., Jørgensen, B.B., Fossing, H., Glud, R., Gundersen J., Ramsing, N.B., Thamdrup, B., Hansen, J.W., Nielsen, L.P. and Hall, P.O.J.: Pathways of organic carbon oxidation in three continental margin sediments, Mar. Geol., 113, 27-40, 1993.

Canfield, D.E., Raiswell, R. and Bottrell, S.: The Reactivity of Sedimentary Iron Minerals toward Sulfide, Am. J. Sci., 292, 659-683, 1992.

Cline, J.D.: Spectrophotometric Determination of Hydrogen Sulfide in Natural Waters, Limnol. Oceanogr., 14, 454-458, 1969.

Crowley, T.J.: Calcium-Carbonate Preservation Patterns in the Central North-Atlantic During the Last 150,000 Years, Mar. Geol., 51, 1-14, 1983.

Damuth, J.E.: Echo Character of Norwegian-Greenland Sea: Relationship to Quaternary Sedimentation, Mar Geol., 28, 1-36, 1978.

De Mol, B., Van Rensbergen, P., Pillen, S., Van Herreweghe, K., Van Rooij, D., McDonnell, A., Huvenne, V., Ivanov, M., Swennen, R. and Henriet, J.P..: Large deep-water coral banks in the Porcupine Basin, southwest of Ireland, Mar. Geol., 188, 193-231, 2002.

Dorschel, B., Hebbeln, D., Foubert, A., White, M. and Wheeler, A.J.: Hydrodynamics and cold-water coral facies distribution related to recent sedimentary processes at Galway Mound west of Ireland, Mar. Geol., 244, 184-195, 2007.

Dullo, C.-W., Flögel, S. and Rüggeberg, A.: Cold-water coral growth in relation to the hydrography of the Celtic and Nordic European continental margin, Mar. Ecol. Prog. Ser., 371, 165-176, 2008.

Ferdelman, T.G., Kano, A., Williams, T., Henriet, J.-P. and the Expedition 307 Scientists. Proc. IODP, 307: Washington, DC (Integrated Ocean Drilling Program Management International, Inc.). doi:10.2204/iodp.proc.307.102.2006

Ferdelman, T.G., Lee, C., Pantoja, S., Harder, J., Bebout, B.M. and Fossing, H.: Sulfate reduction and methanogenesis in a Thioploca-dominated sediment off the coast of Chile, Geochim. Cosmochim. Ac., 61, 3065-3079, 1997.

Fossing, H., Ferdelman, T.G. and Berg, P.: Sulfate reduction and methane oxidation in continental margin sediments influenced by irrigation (South-East Atlantic off Namibia), Geochim. Cosmochim. Ac., 64, 897-910, 2000.

Fossing, H. and Jørgensen, B.B.: Measurement of bacterial sulfate reduction in sediments: Evaluation of a single-step chromium reduction method, Biogeochemistry, 8, 205-222, 1989.

Frederiksen, R., Jensen, A. and Westerberg, H.: The distribution of the scleractinian coral Lophelia pertusa around the Faroe Islands and the relation to internal tidal mixing, Sarsia, 77, 157-171, 1992.

Freiwald, A., Henrich, R., and Pätzhold, J.: Anatomy of a deep-water coral reef mound from Stjernsund,West Finnmark, Northern Norway, in: Cool-Water Carbonates, edited by: James, N. P. and Clarke, J. A. D., SEPM, Spec. Publ., 56, 141-161, 1997.

Freiwald, A.: Reef-forming cold-water corals, in: Ocean Margin Systems, edited by: Wefer, G., Billett, D., Hebbeln, D., Jørgensen, B.B., Schlüter, M. and van Weering, T.C.E., Springer, Heidelberg, 365-385, 2002.

Gardner, L.R.: Chemical models for sulfate reduction in closed anaerobic marine environments, Geochim. Cosmochim. Ac., 37, 53-68, 1973.

Gieskes, J.M. and Rogers, W.C.: Alkalinity Determination in Interstitial Waters of Marine Sediments, J. Sediment. Petrol., 43, 272-277, 1973.

Hall, P.O. and Aller, R.C.: Rapid, small-volume, flow injection analysis for ΣCO_2 and NH_4^+ in marine and freshwaters, Limnol. Oceanogr., 37, 1113–1119, 1992.

Hammond, D.E., McManus, J., Berelson, W.M., Kilgore, T.E. and Pope, R.H.: Early diagenesis of organic material in equatorial Pacific sediments: stoichiometry and kinetics, Deep-Sea Res. Pt. II, 43, 1365-1412, 1996.

Henriet, J.-P., De Mol, B., Pillen, S., Vanneste, M., Van Rooij, D., Versteeg, W., Croker, P.F., Shannon, P.M., Unnithan, V., Bouriak, S., Chachkine, P.: Gas hydrate crystals may help build reefs, Nature, 391, 647-649, 1998.

Hovland, M. and Mortensen, P.B.: Norske korallrev og prosesser i havbunnen. John Grieg Forlag, Bergen, Norway, 1999.

Hovland, M., Mortensen, P.B., Brattegard, T., Strass, P. and Rokoengen, K.: Ahermatypic Coral Banks off Mid-Norway: Evidence for a Link with Seepage of Light Hydrocarbons, Palaios, 13, 189-200, 1998.

Hovland, M., Ottesen, D., Thorsnes, T., Fossa, J.H. and Bryn, P.: Occurrence and implications of large Lophelia-reefs offshore Mid Norway, in: Onshore - offshore relationships on the North Atlantic margin, edited by: Wandas, B., Nystuen, J.P., Eide, E. and Gradstein G., Norwegian Petroleum Society (NPF), Special Publications. Elsevier B.V., Amsterdam, 265-270, 2005.

Hovland, M. and Risk, M.: Do Norwegian deep-water coral reefs rely on seeping fluids?, Mar. Geol., 198, 83-96, 2003.

Hovland, M. and Thomsen, E.: Cold-water corals - are they hydrocarbon seep related?, Mar. Geol., 137, 159-164, 1997.

Hulthe, G., Hulth, S. and Hall, P.O.J.: Effect of oxygen on degradation rate of refractory and labile organic matter in continental margin sediments, Geochim. Cosmochim. Ac., 62, 1319-1328, 1998.

Iversen, N. and Jørgensen, B.B.: Anaerobic methane oxidation rates at the sulfate methane transition in marine sediments from Kattegat and Skagerrak (Denmark), Limnol. Oceanogr., 30, 944-955, 1985.

Jahnke, R.A., Craven, D.B. and Gaillard, J.F.: The influence of organic matter diagenesis on $CaCO_3$ dissolution at the deep-sea floor, Geochim. Cosmochim. Ac., 58, 2799-2809, 1994.

Jensen, A. and Frederiksen, R.: The fauna associated with the bank-forming deep-water coral Lophelia pertusa (Scleractinaria) on the Faroe Shelf, Sarsia, 77, 53-69, 1992.

Jonsson, L.G., Nilsson, P.G., Floruta, F. and Lundälv, T.: Distributional patterns of macro- and megafauna associated with a reef of the cold-water coral Lophelia pertusa on the Swedish west coast, Mar. Ecol. Prog. Ser., 284, 163-171, 2004.

Jørgensen, B.B.: A comparison of methods for the quantification of bacterial sulfate reduction in coastal marine sediments. 1. Measurements with radiotracer techniques, Geomicrobiol. J., 1, 11-27, 1978.

Jørgensen, B.B.: Mineralization of organic matter in the sea bed - the role of sulphate reduction, Nature, 296, 643-645, 1982.

Kallmeyer, J., Ferdelman, T.G., Weber, A., Fossing, H. and Jørgensen, B.B.: A cold chromium distillation procedure for radiolabeled sulfide applied to sulfate reduction measurements, Limnol. Oceanogr.-Meth., 2, 171-180, 2004.

Kiriakoulakis, K., Bett B.J., White M., and Wolff G.A.: Organic biogeochemistry of the Darwin Mounds, a deep-water coral ecosystem, of the NE Atlantic, Deep-Sea Res. Pt. I, 51, 1937-1954, 2004.

Kostka, J.E., Thamdrup, B., Glud, R.N. and Canfield, D.E.: Rates and pathways of carbon oxidation in permanently cold Arctic sediments, Mar. Ecol. Prog. Ser., 180, 7-21, 1999.

Ku, T.C.W., Walter, L.M., Coleman, M.L., Blake, R.E. and Martini, A.M.: Coupling between sulfur recycling and syndepositional carbonate dissolution: Evidence from oxygen and sulfur isotope composition of pore water sulfate, South Florida Platform, USA, Geochim. Cosmochim. Ac., 63, 2529-2546, 1999.

Laberg, J.S. and Vorren, T.O.: The Traenadjupet Slide, offshore Norway - morphology, evacuation and triggering mechanisms, Mar. Geol., 171, 95-114, 2000.

Laberg, J.S., Vorren, T.O., Mienert, J., Evans, D., Lindberg, B., Ottesen, D., Kenyon, N.H. and Henriksen, S.: Late Quaternary palaeoenvironment and chronology in the Traenadjupet Slide area offshore Norway, Mar. Geol., 188, 35-60, 2002a.

Laberg, J.S., Vorren, T.O., Mienert, J., Bryn, P. and Lien, R.: The Traenadjupet Slide: a large slope failure affecting the continental margin of Norway 4,000 years ago, Geo.-Mar. Lett., 22, 19-24, 2002b.

Lindberg, B. and Mienert, J.: Postglacial carbonate production by cold-water corals on the Norwegian Shelf and their role in the global carbonate budget, Geology, 33, 537-540, 2005.

Lovley, D.R.: Organic matter mineralization with the reduction of ferric iron - A review, Geomicrobiol. J., 5, 375-399, 1987.

Lovley, D.R.: Dissimilatory Fe(III) and Mn(IV) Reduction, Microbiol. Rev., 55, 259-287, 1991.

Martin, J.H., Knauer, G.A., Karl, D.M. and Broenkow, W.W.: Vertex: carbon cycling in the northeast Pacific, Deep-Sea Res., 34, 267-285, 1987.

Mienis, F., de Stigter, H.C., White, M., Duineveld, G., de Haas, H. and van Weering, T.C.E.: Hydrodynamic controls on cold-water coral growth and carbonate-mound development at the SW and SE Rockall Trough Margin, NE Atlantic Ocean, Deep-Sea Res. Pt. I, 54, 1655-1674, 2007.

Milliman, J.D.: Production and accumulation of calcium carbonate in the ocean: Budget of a nonsteady state, Global. Biogeochem. Cy., 7, 927-957, 1993.

Morse, J.W., Arvidson, R.S. and Luttge, A.: Calcium Carbonate Formation and Dissolution, Chem. Rev., 107, 342-381, 2007.

Morse, J.W., Cornwell, J.C., Arakaki, T., Lin, S. and Huerta-Diaz, M.: Iron Sulfide and Carbonate Mineral Diagenesis in Baffin Bay, Texas, J. Sediment. Petrol., 62, 671-680, 1992.

Mortensen, P.B., Hovland, M., Brattegard, T. and Farestveit, R.: Deep-Water bioherms of the Scleractinian Coral Lophelia pertusa (L) at 64°N on the Norwegian Shelf: structure and associated megafauna, Sarsia, 80, 145-158, 1995.

Mortensen, P.B., Hovland, M.T., Fossa, J.H. and Furevik, D.M.: Distribution, abundance and size of Lophelia pertusa coral reefs in mid-Norway in relation to seabed characteristics, J. Mar. Biol. Assoc. UK, 81, 581-597, 2001.

Nordgulen, O., Bargel, T.H., Longva, O. and Ottesen, D.: A preliminary study of Lofoten as a potential World Heritage Site based on natural criteria, Geological Survey of Norway, 2006.

Ottesen, D., Rise, L., Knies, J., Olsen, L. and Henriksen, S.: The Vestfjorden-Traenadjupet palaeo-ice stream drainage system, mid-Norwegian continental shelf, Mar. Geol., 218, 175-189, 2005.

Parkes, R.J., Webster, G., Cragg, B.A., Weightman, A.J., Newburry, C.J., Ferdelman, T.G., Kallmeyer, J., Jørgensen, B.B., Aiello, I.W. and Fry, J.C.: Deep sub-seafloor prokaryotes stimulated at interfaces over geological time, Nature, 436, 390-394, 2005.

Parkhurst, D.L. and Appelo, C.A.J.: User's guide to PHREEQC (Version 2): A computer program for speciation, batch-reaction, one-dimensional transport, and inverse geochemical calculations, U.S. Geological Survey Water-Resources Investigations Report, 99-4259, 310 pp., 1999.

Perry, C.T. and Taylor, K.G.: Inhibition of dissolution within shallow water carbonate sediments: impacts of terrigenous sediment input on syn-depositional carbonate diagenesis, Sedimentology, 53, 495-513, 2006.

Poulain, P.M., Warn-Varnas, A. and Niiler, P.P.: Near-surface circulation of the Nordic seas as measured by Lagrangian drifters, J. Geophys. Res.-Oceans., 101, 18237-18258, 1996.

Poulton, S.W. and Canfield, D.E.: Development of a sequential extraction procedure for iron: implications for iron partitioning in continentally derived particulates, Chem. Geol., 214, 209-221, 2005.

Poulton, S.W., Krom, M.D. and Raiswell, R.: A revised scheme for the reactivity of iron (oxyhydr)oxide minerals towards dissolved sulfide, Geochim. Cosmochim. Ac., 68, 3703-3715, 2004.

Pyzik, A.J. and Sommer, S.E.: Sedimentary iron monosulfides: kinetics and mechanism of formation, Geochim. Cosmochim. Ac., 45, 687-698, 1981.

Rickard, D. and Luther III, G.W.: Chemistry of Iron Sulfides, Chem. Rev., 107, 514-562, 2007.

Ridgwell, A. and Zeebe, R.E.: The role of the global carbonate cycle in the regulation and evolution of the Earth system, Earth. Planet. Sc. Lett., 234, 299-315, 2005.

Roberts, J.M., Wheeler, A.J. and Freiwald, A.: Reefs of the Deep: The Biology and Geology of Cold-Water Coral Ecosystems, Science, 312, 543-547, 2006.

Sansone, F.J., Andrews, C.C., Buddemeier, R.W. and Tribble, G.W.: Well-point sampling of reef interstitial water, Coral Reefs, 7, 19-22, 1988.

Schulz, H.D.: Quantification of early diagensis: Dissolved constituents in marine pore water, in: Marine Geochemistry, edited by: Schulz, H.D. and Zabel, M., Springer, Heidelberg, 85-128, 2000.

Seeberg-Elverfeldt, J., Schlüter, M., Feseker, T. and Kölling, M.: Rhizon sampling of porewaters near the sediment-water interface of aquatic systems, Limnol. Oceanogr.-Meth., 3, 361-371, 2005.

Soetaert, K., Hofmann, A.F., Middelburg, J.J., Meysman, F.J.R. and Greenwood, J.: The effect of biogeochemical processes on pH, Mar. Chem., 106, 380-401, 2007.

Staudt, W.J. and Schoonen, M.A.A.: Sulfate incorporation into sedimentary carbonates, in: Geochemical Transformations of Sedimentary Sulfur, edited by: Vairavamurthy M.A.,

Schoonen, M.A.A., Eglinton, T.I., Luther III, G.W. and Manowitz, B., Acs Symposium Series, American Chemical Society, Washington D.C., 332-345, 1995.

Takahashi, T., Broecker, W.S. and Langer, S.: Redfield Ratio Based on Chemical Data from Isopycnal Surfaces, J. Geophys. Res.-Oceans., 90, 6907-6924, 1985.

Thamdrup, B. and Canfield, D.E.: Pathways of carbon oxidation in continental margin sediments off central Chile, Limnol. Oceanogr., 41, 1629-1650, 1996.

Thorsnes, T., Fossa, J.H. and Christensen, O.: Deep-water coral reefs. Acoustic recognition and geological setting, Hydro International, 8, 26-29, 2004.

Titschack, J., Thierens, M., Dorschel, B., Schulbert, C., Freiwald, A., Kano, A., Takashima, C., Kawagoe, N., Li, X. and IODP Expedition 307 scientific party: Carbonate budget of a cold-water coral mound (Challenger Mound, IODP Exp. 307), Mar. Geol., 259, 36-46, 2009.

Tribble, G.W.: Organic Matter Oxidation and Aragonite Diagenesis in a Coral Reef, J. Sediment. Petrol., 63, 523-527, 1993.

Tribble, G.W., Sansone, F.J. and Smith, S.V.: Stoichiometric modeling of carbon diagenesis within a coral reef framework, Geochim. Cosmochim. Ac., 54, 2439-2449, 1990.

Vandieken V., Nickel, M. and Jørgensen, B.B.: Carbon mineralization in Artic sediments northeast of Svalbard: Mn(IV) and Fe(III) reduction as principal anaerobic respiratory pathways, Mar. Ecol. Prog. Ser., 322, 15-27, 2006.

Vecsei, A.: A new estimate of global reefal carbonate production including the fore-reefs, Global Planet. Change, 43, 1-18, 2004.

Walter, L.M., Bischof, S.A., Patterson, W.P. and Lyons, T.W.: Dissolution and recrystallization in modern shelf carbonates: evidence from pore water and solid phase chemistry, Philos. T. Roy. Soc. Lond. A, 344, 27-36, 1993.

Walter, L.M. and Burton, E.A.: Dissolution of Recent Platform Carbonate Sediments in Marine Pore Fluids, Am. J. Sci., 290, 601-643, 1990.

Wheeler, A.J., Beyer, A., Freiwald, A., de Haas, H., Huvenne, V.A.I., Kozachenko, M., Roy, K.O.L. and Opderbecke, J.: Morphology and environment of cold-water coral carbonate mounds on the NW European margin, Int. J. Earth Sci., 96, 37-56, 2007.

Werner, U., Bird, P., Wild, C., Ferdelman, T., Polerecky, L., Eickert, G., Jonstone R., Hoegh-Guldberg, O. and de Beer, D.: Spatial patterns of aerobic and anaerobic mineralization rates and oxygen penetration dynamics in coral reef sediments, Mar. Ecol. Prog. Ser., 309, 93-105, 2006.

White, M., Mohn, C., de Stigter, H. and Mottram, G.: Deep-water coral development as a function of hydrodynamics and surface productivity around the submarine banks of the Rockall Trough, NE Atlantic, in: Cold-water corals and ecosystems, edited by: Freiwald, A. and Roberts, J.M., Springer, Heidelberg, 503-514, 2005.

White, M.: Benthic dynamics at the carbonate mound regions of the Porcupine Sea Bight continental margin, Int. J. Earth Sci., 96, 1-9, 2007a.

White, M., Roberts, J.M. and van Weering, T.C.E.: Do bottom-intensified dirunal tidal currents shape the alignment of carbonate mounds in the NE Atlantic?, Geo.-Mar. Lett., 27, 391-397, 2007b.

Wild, C., Mayr, C., Wehrmann, L., Schöttner, S., Naumann, M., Hoffmann, F. and Rapp, H.T.: Organic matter release by cold water corals and its implication for fauna-microbe interaction, Mar. Ecol. Prog. Ser., 372, 67-75, 2008.

Wilkin, R.T. and Barnes, H.L.: Pyrite formation by reactions of iron monosulfides with dissolved inorganic and organic sulfur species, Geochim. Cosmochim. Ac., 60, 4167-4179, 1996.

Yao, W.S. and Millero, F.J.: Oxidation of hydrogen sulfide by hydrous Fe(III) oxides in seawater, Mar. Chem., 52, 1-16, 1996.

CHAPTER 2:
A COMPARATIVE STUDY ON ORGANIC MATTER DEGRADATION CHARACTERISTICS IN SEDIMENTS OF COLD-WATER CORAL REEF ECOSYSTEMS

Laura M. Wehrmann[1,2], Sandra I. Schöttner[1,2], Birgit Kürzel[3], Timothy G. Ferdelman[1] and Michael J. Formolo[1]

[1] Biogeochemistry Research Group, Max Planck Institute for Marine Microbiology, Celsiusstrasse 1, 26129 Bremen, Germany

[2] Coral Reef Ecology Work Group (CORE), GeoBio-Center, Ludwig-Maximilans Universität, Richard-Wagner-Strasse 10, D-80333 München, Germany

[3] Institute for Chemistry and Biology of the Marine Environment (ICBM), Faculty of Mathematics and Science, University Oldenburg, Carl-von-Ossietzky-Str. 9-11, D-26111 Oldenburg, Germany

In preparation for *Limnology & Oceanography*

Abstract

The degradation state of sedimentary organic matter was investigated at two cold-water coral reefs, Røst Reef and Traenadjupet Reef, on the Norwegian margin and at two cold-water coral mounds, Beta and Gamma Mound, from Pen Duick Mound Province in the Gulf of Cadiz. A set of indicators based on different components of the bulk organic matter pool suggested highly degraded material throughout depth at the mound sites. These indicators included the chlorin index based on chlorophyll degradation products and the amino acid-based Degradation Index developed by [Dauwe, B., Middelburg, J.J., 1998, Amino acids and hexosamines as indicators of organic matter degradation state in North Sea sediments. Limnol. Oceanogr. 43, pp. 782-798]. Concentrations of total hydrolysable amino acids (THAA) at the reef sites were twice as high as at the mound sites but low compared to other ocean margin sites. The relative contribution of amino acids to total organic carbon (%T_{aa}C) in surface sediments ranged from 5 to 7 % at the Norwegian reefs to 3 to 5 % at the mound sites, and the amino acid contribution to total nitrogen (%T_{aa}N) was 17 to 25 % at the reef and ~11 % at the mound sediments. We attributed the low percentages of %T_{aa}C and %T_{aa}N to extensive pre-depositional degradation of the organic matter. In conjunction, the coral-bearing sediments were characterized by extremely low mole-% contributions of aspartic acid (< 4 %) and glutamic acid (< 8%) and elevated fractions of the non-protein degradation products β-alanine and γ-amino butyric acid. At the Norwegian cold-water coral reefs, the relative composition of the remaining THAA pool remained largely unchanged with sediment depth, while the cold-water coral mounds exhibited distinct compositional changes with depth indicating selective amino acid degradation and/or uptake. The contribution of amino acid nitrogen from living bacteria to the sedimentary THAA nitrogen yield for Beta Mound revealed that <3.5 % of the total amino acid nitrogen pool can be explained by the living bacterial community.

1. Introduction

Continental margins play an important role in the global carbon and nitrogen cycle (Walsh, 1991), and they represent major zones of organic carbon production, mineralization and burial (Hedges and Keil, 1995; Walsh, 1991). Cold-water coral reef ecosystems are distributed worldwide on continental margins at mid- and high-latitudes as patches, well-established reef systems and large cold-water coral mounds (Roberts et al., 2006; Rogers, 1999). These ecosystems are considered to be unique hot-spots of biodiversity, biomass production and carbon cycling (Roberts et al., 2009; Roberts et al., 2006; Van Oevelen et al., 2009).

Cold-water coral ecosystems differ from warm-water coral systems due to the fundamentally different feeding strategies of their main framework-building coral inhabitants. While warm-water corals host zooxanthellae-endosymbiotic algae which provide photosynthetically fixed carbon (Muscatine et al., 1981), the reef-dominating cold-water corals *Lophelia pertusa* and *Madrepora oculata* are heterotrophic filter-feeders (Freiwald, 2002). It is hypothesized that the latter feeding strategy serves as one of the main controlling factors for cold-water coral distribution. Consequently, cold-water coral ecosystems are preferentially distributed atop elevated topographic structures in areas of high currents speeds, where the combination of the relief and the hydrodynamic regime assures sufficient organic matter supply (Freiwald, 2002; Kiriakoulakis et al., 2007; Mienis et al., 2007; Mortensen et al., 2001; Thiem et al., 2006; White et al., 2005). Hydrodynamically driven organic matter supply mechanisms include internal waves, tidal currents, deep-water bottom currents and rapid downwelling events (Davies et al., 2009; Frederiksen et al., 1992; Mienis et al., 2007; Mienis et al., 2009; Thiem et al., 2006; White, 2007; White et al., 2005). Cold-water corals feed on a mixed diet which includes particulate organic matter transported down from productive surface waters, re-suspended organic matter in the bottom boundary layer and zooplankton prey, e.g. copepods (Duineveld et al., 2004; Freiwald, 2002; Rogers, 1999). Studies on the quality and composition of particulate organic matter reaching cold-water coral mounds in the Rockall Trough show that it is characterized by both “fresh”, presumably labile organic matter and “aged”, reworked material (Kiriakoulakis et al., 2004; 2007; Mienis et al., 2007; 2009). Little is known about the processes that control the delivery and reactivity of organic matter to the associated coral-bearing sediments. However, these unknown processes are integral to the carbon remineralization and diagenetic processes in these sediments.

The carbon flow between the different food-web compartments of a cold-water coral ecosystem was investigated by Van Oevelen et al. (2009) on coral-covered mounds at Rockall Bank. The authors showed that the coral community is only responsible for 9 % of carbon ingestion while a high percentage of carbon flux is consumed by associated suspension- and filter-feeding macrofauna. This macrofauna predominately inhabits dead coral fragments and is accompanied by mobile epifauna such as gastropods and smaller sessile organisms including sponges and hydroids as well as bacteria (Van Oevelen et al., 2009). The activity of the dense assemblage of reef-associated organisms presumably facilitates enhanced carbon cycling and intercepts organic matter, preventing it from reaching the underlying sediments (Van Oevelen et al., 2009). A similar hypothesis was proposed by Wehrmann et al. (2009) who showed that rates of anaerobic carbon mineralization in reef-associated sediments are extremely low. The authors attributed this finding to enhanced carbon mineralization within the overlying coral framework and coral rubble by both the benthic macrofaunal community and aerobic and anaerobic microbial respiration. These processes not only limit the amount of organic material reaching the sediments but they also alter its degradation state. The underlying reef sediments are thus effectively decoupled from the productive pelagic ecosystem because the coral reef surface layer functions as a barrier to the transfer of organic matter to the sediments (Wehrmann et al., 2009). This distinguishes cold-water coral ecosystems from many modern continental shelf habitats where overlying water column processes are often a first order control on the delivery and degradation state of organic matter reaching the sediments.

Despite these initial results, the magnitude of organic carbon mineralization, the degradation processes that transform labile organic carbon to less bioreactive forms, and the burial of organic matter in these environments are poorly understood. Two distinct habitats were chosen to gain further insight into these processes, living cold-water coral reefs on the Norwegian margin, Traenadjupet Reef and Røst Reef, and cold-water coral mounds in the Gulf of Cadiz, Beta and Gamma Mound. While the cold-water coral reefs on the Norwegian slope are post-glacial, the cold-water coral mounds have developed prior to the Younger Drays and might only be covered by little Holocene sediment. These depositional environments allow for the investigation of early-diagenetic OM degradation characteristics during initial reef coverage but also allow giving a perspective on the long-term development of OM degradation at the mound sites. By integrating a variety of proven indicators for the organic matter degradation state,

including chlorin indices, amino acid compositions, and calculated Degradation Indices we address the efficiency of carbon mineralization within cold-water coral reef and mound ecosystems. Insights into these processes provide information regarding the long-term carbon burial and remineralization in similar ecosystems throughout the geological record.

2. Study area

2.1 Lofoten cold-water coral reefs

Røst Reef and Traenadjupet Reef are located on the mid-Norwegian margin in close proximity to the Lofoten Islands (Fig. 1). Røst Reef is regarded as the largest living cold-water coral reef in the world (Thorsnes et al., 2004). It covers steep ridges originating from the Traenadjupet landslide which occurred approximately 4000 ^{14}C years BP north-east of the Vøring Plateau (Laberg and Vorren, 2000). The ridges, located at 300-400 m water depth, are densely packed and reach several tens of meters above the surrounding seafloor (Laberg et al., 2002). Wehrmann et al. (2009) described a distinct facies zonation at this reef. The ridge tops are covered by a complex framework of living coral colonies forming terraces towards the lee-side, ridge slopes host a coral rubble-dominated facies and the depressions comprise coral fragments embedded in clay to silt-dominated sediments. Traenadjupet Reef is located south-east of Røst Reef in a sheltered embayment on the edge of a cross-shelf trough on the mid-Norwegian shelf which presumably formed an important pathway for ice-sheet drainage during the Fennoscandian Ice sheet coverage (Ottesen et al., 2005). The reef is located at 300-330 m water depth on top of Oligocene deltaic sandy fan deposits (Hovland et al., 2005). These cigar-shaped structures are covered with living cold-water corals at a few eastern tips and dense coral rubble on the top.

2.2 Pen Duick Mound Province

The investigated cold-water coral mounds, Beta and Gamma Mound, are part of a series of mounds located on Pen Duick Escarpment in the Gulf of Cadiz west of the Gibraltar Arc between the Iberian Peninsula and the Moroccan margin (Fig. 1). The Pen Duick Escarpment represents a fault-bounded cliff of 6 km length and 80-125 m height situated on the southeastern leg of Renard Ridge (Foubert et al., 2008; Van Rooij et al. in review). Beta Mound is characterized by two summits; it has a height of approximately 20 m and a maximum diameter of 450 m (Van Rooij et al., in review).

Gamma Mound, located 2.5 km NNW of Beta Mound, has a conical shape with a height of approximately 15 m and a diameter of 300 m at the mound foot (Van Rooij et al. in review). At present, living cold-water coral coverage in the Gulf of Cadiz is scarce and coral reef decline is estimated to have occurred at the end of the Younger Dryas (Wienberg et al., 2009).

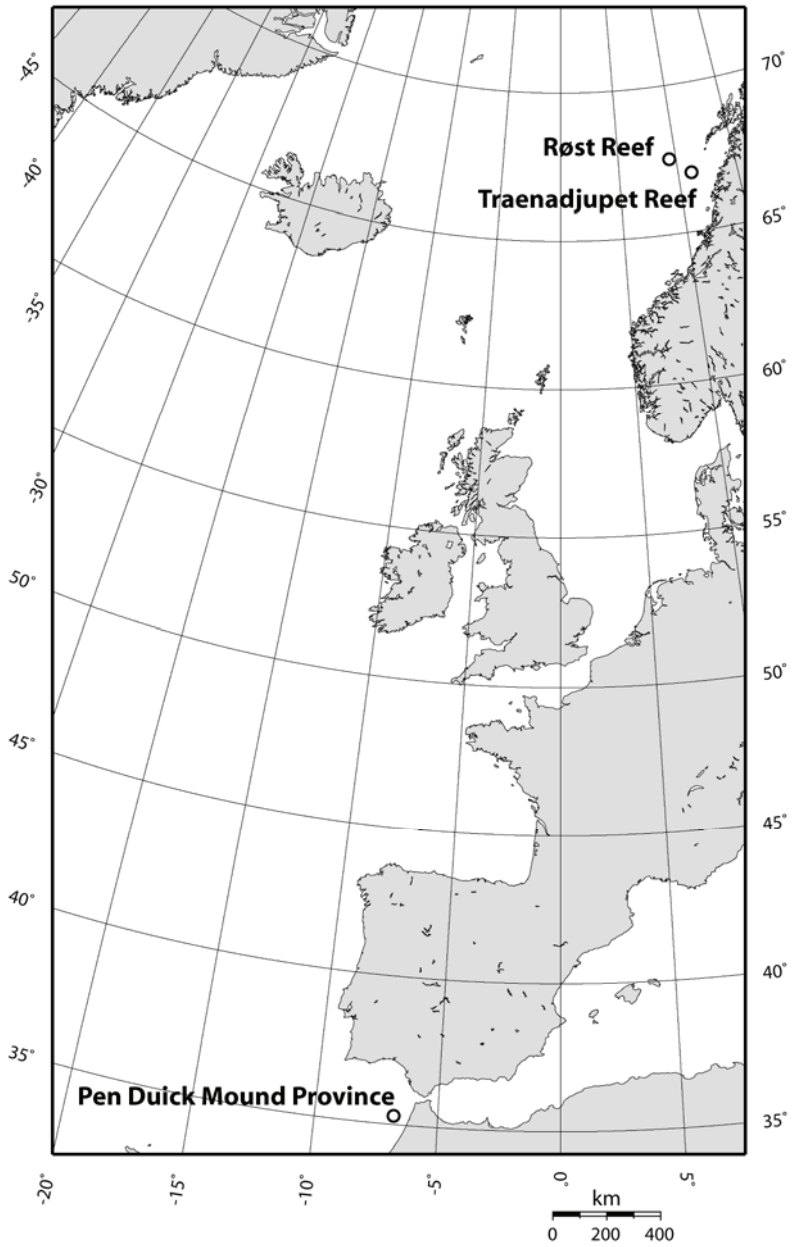

Figure 1: Map of the North Atlantic including the study areas on the Norwegian margin and in the Gulf of Cadiz.

3. Material and methods

3.1 Sample collection

Sediment samples were collected during R/V Polarstern Cruise ARK XXII/1a to the mid-Norwegian margin in June 2007 and R/V Marion Dufresne Cruise MD169 MiCROSYSTEMS to the Gulf of Cadiz in June 2008. During both cruises, sediment cores were taken with a gravity corer, cut into 1-m sections immediately after retrieval, and stored at 4°C. Within a few hours after core retrieval sub-samples for solid-phase analyses were taken and frozen at –20°C. In the home laboratory, frozen sediment samples were freeze-dried, and all visible coral and shell pieces were removed. Samples were kept in the dark until further processing. For the present study, a core from the coral rubble zone at Røst Reef (15-3 GC) and a core from the lower part of the cigar-shaped structures at Traenadjupet Reef (23-18 GC) were analyzed. The core from Beta Mound (MD08-3214) was retrieved at the mound top, the core from Gamma Mound slightly to the mound flank (MD08-3221; Table 1).

Table 1. Sampling location, water depth and core recovery of the cores investigated for this study.

Location	Core	Latitude (°North)	Longitude (°East/West)	Water depth [m]	Core recovery [cm]
Røst Reef	15-3 GC	67°30.46’	09°25.39’(E)	331	163
Traenadjupet Reef	23-18 GC	67°58.16’	11°07.80’(E)	327	325
Beta Mound	MD08-3214	35°17.74’	06°47.26’(W)	506	252
Gamma Mound	MD08-3221	35°18.87’	06°48.08’(W)	543	510

3.2 Total organic carbon and C/N-ratio

All cores have been previously analyzed for total organic carbon (TOC) content (Wehrmann et al., 2009; Wehrmann et al., in revision). Based on these results, sample intervals for the mound cores were chosen for this study. Total carbon (TC) and total nitrogen (TN) were determined with a CarboErba NA-1500 CNS and total inorganic carbon was measured using a CM 5012 CO_2 Coulometer (UIC) after acidification with phosphoric acid (3 mol l^{-1}). Total organic carbon (TOC) was calculated as the difference between TC and TIC. The C/N-ratio was calculated as the molar ratio of TOC to TN.

3.3 Chlorin extractions and Chlorin Index

For the determination of chlorins, 30-60 mg of freeze-dried sediment was extracted three times with 5 ml acetone (HPLC-grade; Roth, Germany) on ice according to Schubert et al. (2005). Immediately after extraction the fluorescence intensity (FI) of sediment extracts was measured with a Hitachi F-2000 fluorometer at λ_{ex}= 428 nm and λ_{em}= 671 nm. The chlorophyll α (Fluka, Germany) acidification-product pheophytin α was used as calibration standard. Extracts were then acidified and FI was re-measured. The Chlorin Index (CI) was calculated as the ratio of FI of un-acidified to acidified sediment extract (Schubert et al., 2005):

$$\text{Chlorin Index (CI)} = \frac{\text{Fl. intensity}_{\text{acidified extract}}}{\text{Fl. intensity}_{\text{original extract}}} \quad (1)$$

Chlorin Index ranges from 0.2 for fresh chlorophyll α, which can be used as a proxy for fresh organic matter, to values approaching 1 for refractory organic material (Schubert et al., 2005).

3.4 Amino acid extraction and analyses

Hydrolysable amino acids aspartic acid (Asp), glutamic acid (Glu), histidine (His), serine (Ser), araginine (Arg), glycine (Gly), threonine (Thr), ß-alanine (ß-Ala), alanine (Ala), γ-amino butyric acid (γ-Aba), valine (Val), phenylalanine (Phe), isoleucine (Ile), leucine (Leu) and lysine (Lys) were extracted from 0.15-0.25 g freeze-dried sediment samples with α-amino-n-butyric acid (α-Aba, Sigma-Aldrich) as an internal reference standard. Hydrolysis was performed with 5 ml of 6 mol l^{-1} hydrochloric acid (HCl) at 155°C for 1 h under nitrogen in combusted glass ampoules. The hydrolysis step was terminated by placing samples into an ice bath. The hydrolyzate was transferred into combusted glass vials and the HCl was removed by gentle heating (50°C) to dryness. The residue was re-dissolved in Milli-Q water and the evaporation step was repeated. The samples were filtered (0.25 µm, Acrodisc) and adjusted to neutral pH with sodium hydroxide (NaOH). Extracts were filtered again and adjusted to final pH of 9.4-9.5 with 0.1 mol l^{-1} boric acid buffer. Amino acid concentrations in the dissolved hydrolyzate were determined by reverse-phase high performance liquid chromatography (HPLC) of fluorescent *o*-phtaldialdehyde-derived products according to Lindroth and Mopper (1979). Concentrations of the individual

amino acids were calculated based on three-point standard calibration curves using an amino acid standard solution (Standard H, Pierce) to which Asp, ß-Ala, γ-Aba, α-Aba and Lys (Sigma) were added. Method blanks were processed similar to the samples and showed negligible concentrations of amino acids.

The contribution of amino-acid derived carbon (% $T_{aa}C$) and nitrogen (% $T_{aa}N$) to the total organic carbon and nitrogen pool was calculated based on the 15 identified amino acids. Most likely this calculation leads to a small underestimation of these variables due to our inability to determine the concentration of Tyrosine (Tyr), Ornithine (Orn), Taurine (Tau) and Methionine (Met). These amino acids, however, usually constitute a minor fraction (< 4 mole-%) of the total hydrolysable amino acid concentration in sediments (Lomstein et al., 2006; Lomstein et al., 2009; Vandewiele et al., 2009).

3.5 Principal component analysis

To evaluate changes in the amino acid composition both down-core and between the four sites, a principal component analysis (PCA) was performed in R v2.10.0 (The R Project for Statistical Computing) using the 'stats' package. Amino acid data from Dauwe and Middelburg (1998) were included to compare our dataset with previously published Degradation Indicies across a wide range of organic matter quality. For the combination of both datasets it was necessary to exclude Lys from our dataset and Met and Tyr from the Dauwe and Middelburg (1998) dataset. The first axis of the PCA (Fig. 10), which explained 54 % of the total variance in the combined dataset, was used to calculate the Degradation Index (DI):

$$\text{Degradation Index (DI)} = \sum_i \left[\frac{\text{var}_i - \text{AVG var}_i}{\text{STD var}_i} \right] \text{x fac.coef.}_i \qquad (2)$$

where var_i, AVG_i, STD var_i, and $fac.coef._i$ are the mole-%, mean, standard deviation and factor score coefficient of $amino\ acid_i$, respectively (Dauwe et al., 1999). A second PCA was performed excluding the dataset of Dauwe and Middelburg (1998) to emphasize the compositional changes in the amino acid contributions among the cold-water coral ecosystem sites. The first axis of the latter PCA, which was again used to calculate the DI, explained 66 % of the total variance in this dataset. Factor coefficients for the second PCA are listed in Table 2.

Table 2. Results of comprehensive PCA analysis combining the data from this study and Dauwe & Middelburg (1998). Shown are the factor coefficients for the individual amino acids and the calculated degradation indicies (DI).

Comprehensive PCA analysis					
Factor coefficient		Degradation Index			
		Dauwe & Middelburg (1998)		Cold-water coral ecosystem sites	
Asp	0.678	SK	3.1	15-3 GC/1 (0-5 cm)	0.6
Glu	0.459	BG-2	3.2	15-3 GC/5 (20-25 cm)	-1.1
His	-0.077	BG-1	3.1	15-3 GC/9 (40-45 cm)	-1.3
Ser	0.193	BG-A	3.1	15-3 GC/14 (65-70 cm)	-1.5
Arg	-0.257	FF	2.8	15-3 GC/18 (85-90 cm)	-1.0
Gly	-0.024	BF	3.5	15-3 GC/22 (105-110 cm)	-1.0
Thr	0.067	BG-B	3.1	15-3 GC/26 (125-130 cm)	-1.3
β-Ala	-0.208	Phy-B	3.0	15-3 GC/30 (145-150 cm)	-1.0
Ala	-0.327	Phy-C	3.2	23-18 GC/2 (5-10 cm)	-0.4
γ-Aba	-0.159	Bac	3.0	23-18 GC/9 (40-45 cm)	-0.5
Val	-0.168	Zoo	3.3	23-18 GC/13 (58-63 cm)	-0.5
Phe	-0.038	Saan-T	2.5	23-18 GC/17 (78-83 cm)	-0.1
Ile	-0.035	Dab-T	2.8	23-18 GC/21 (98-103 cm)	-1.0
Leu	-0.097	Saan-S1	3.5	23-18 GC/25 (118-123 cm)	-1.1
		Dab-S1	3.0	23-18 GC/28 (143-153 cm)	-0.6
		Saan-S2	2.6	23-18 GC/30 (163-173 cm)	-0.5
		Dab-S2	2.8	23-18 GC/34 (203-213 cm)	-1.0
		Tur-red	1.8	23-18 GC/38 (243-253 cm)	-1.9
		Tur-ox	1.7	23-18 GC/44 (303-313 cm)	-0.2
				MD08-3221/1 (0-5 cm)	0.2
				MD08-3221/3 (10-15 cm)	-2.1
				MD08-3221/5 (20-25 cm)	-2.0
				MD08-3221/9 (40-45 cm)	-1.0
				MD08-3221/19 (90-95 cm)	-2.6
				MD08-3221/27 (130-135 cm)	-2.0
				MD08-3221/35 (170-175 cm)	-1.5
				MD08-3221/43 (210-215 cm)	-1.9
				MD08-3221/51 (250-255 cm)	-2.1
				MD08-3221/59 (290-295 cm)	-2.4
				MD08-3221/67 (330-335 cm)	-2.2
				MD08-3221/83 (410-415 cm)	-2.4
				MD08-3221/99 (490-495 cm)	-1.5
				MD08-3214/1 (0-5 cm)	-1.2
				MD08-3214/2 (5-10 cm)	0.0
				MD08-3214/4 (15-20 cm)	-0.5
				MD08-3214/8 (35-40 cm)	-2.0
				MD08-3214/16 (75-80 cm)	-2.4
				MD08-3214/24 (115-120 cm)	-3.3
				MD08-3214/32 (150-155 cm)	-1.1
				MD08-3214/38 (180-185 cm)	-2.5
				MD08-3214/43 (210-215 cm)	-1.2
				MD08-3214/49 (240-245 cm)	-1.4

Abbreviations for samples from Dauwe & Middelburg (1998) stand for Skagerrak (SK), German Bight 0-1 cm (GB-1), German Bight 1-15 cm (GB-2), Brouwershavensche Gat A and B (BG-A and GB-B), Frisian Front (FF), Broad Fourteens (BF), algae (Phy-B), phytoplankton (Phy-C), bacteria (Bac), zooplankton (Zoo), Saanich Inlet trap material (Saan-T), 0-1 cm sediment (Saan-S1), 1-15 cm sediment (Saan-S2), Dabob Bay trap material (Dab-T), 0-1 cm sediment (Dab-1), 1-15 cm sediment (Dab-2), unoxidized turbidite (Tur-red) and oxidized turbidite (Tur-ox).

4. Results

4.1 Total organic carbon analyses and C/N-ratio

The total organic carbon (TOC) content of core 15-3 GC from Røst Reef and core 23-18 GC from Traenadjupet Reef was previously determined to average 0.6 (± 0.4) wt. % and 1.0 (± 0.5) wt. %, respectively, with no down-core trends (Wehrmann et al., 2009). The average TOC concentrations in core MD08-3214 from Beta Mound and MD08-3221 from Gamma Mound are 0.5 (± 0.3) wt. % and 0.4 (± 0.2) wt. % (Fig. 2), respectively. C/N-ratio values were scattered but higher in the cores from Røst Reef (8.5 ± 3.8) and Traenadjupet Reef (8.4 ± 2.4) compared to the cores from Beta Mound (6.6 ± 2.3) and Gamma Mound (7.9 ± 2.4) (Fig. 2).

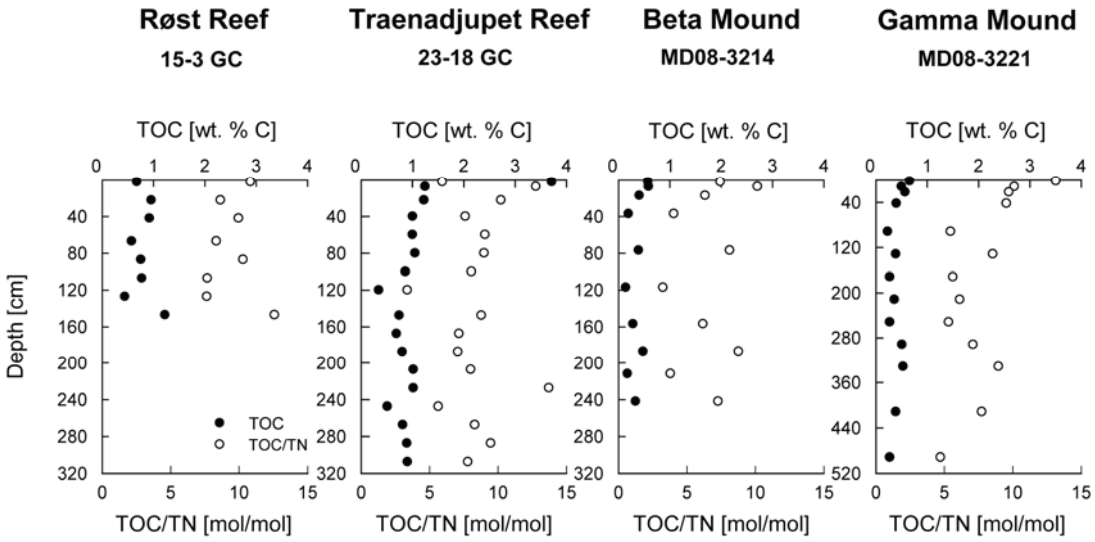

Figure 2: Total organic carbon (TOC) content and total organic carbon to total nitrogen (TOC/TN) ratio with depth.

4.2 Chlorin extractions and Chlorin Index

Chlorin concentrations and calculated chlorin indices varied between the sample locations. The highest chlorin concentrations were determined for Traenadjupet Reef core 23-18 GC with average values of 343 (± 114) ng g^{-1}. Core 15-3 GC from Røst Reef showed average values of 232 (± 109) ng g^{-1}. Both cores displayed variable concentrations with depth (Fig. 3). In contrast, the cores MD08-3214 from Beta Mound and MD08-3221 from Gamma Mound showed a higher consistency in chlorin concentrations with depth averaging 288 (± 27) ng g^{-1} and 209 (± 35) ng g^{-1}, respectively (Fig. 3). Calculated chlorin indices at the reef and the mound sites ranged

between 0.69 and 0.93; except at the surface of core 15-3 GC from Røst Reef, where a lower value of 0.52 was determined.

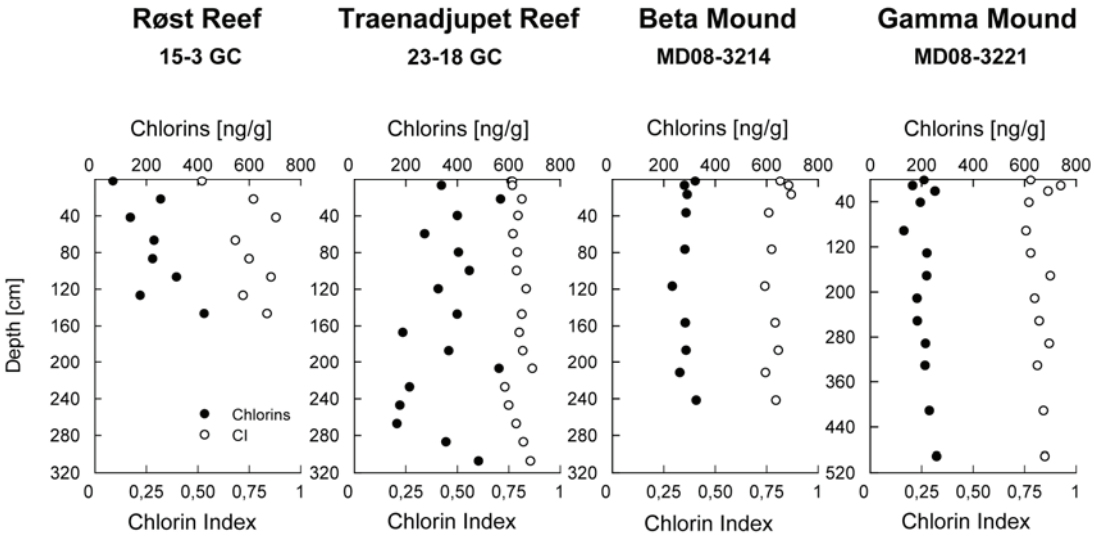

Figure 3: Chlorin concentrations and chlorin indicies (CI) with depth.

4.3 Amino acid distributions

All four cores showed the highest total hydrolysable amino acid (THAA) concentrations in the core top and decreasing values with depth (Fig. 4a). Core 15-3 GC (Røst Reef) and 23-18 GC (Traenadjupet Reef) showed slightly scattered distributions with surface values of 10.2 µmol g^{-1} and 8.3 µmol g^{-1}, respectively. Decreases in THAA concentrations in core MD08-3214 (Beta Mound) and core MD08-3221 (Gamma Mound) from surface values of 3.7 and 5.5 µmol g^{-1}, respectively to values of < 2 µmol g^{-1} were measured. Correspondingly, $\%T_{aa}C$ and $\%T_{aa}N$ showed a general decrease at all stations (Fig. 4b), although these decreases were within the analytical uncertainties of the measurement for the Traenadjupet Reef core. At the coral reef sites, $\%T_{aa}C$ decreased from maximum values of 7.4 % (Røst Reef) and 5.3 % (Traenadjupet Reef) to values around 4 %. At the coral mound sites, surface $\%T_{aa}C$ were 4.8 % and 2.8 % for Beta Mound and Gamma Mound, respectively, and quickly dropped to values < 2 %. The percentage of total nitrogen present as amino acid nitrogen ($\%T_{aa}N$) ranged from 25.3 % at the sediment surface to 11.5 % at 65-70 cm in core 15-3 GC (Røst Reef) and from 16.8 % at 58-62 cm to 7.5 % at 163-173 cm in core 23-18 GC (Traenadjupet Reef). $\%T_{aa}N$ values in the cores from the cold-water coral mounds were lower, with values of 11.5 % and 11.7 % at the surface and values of 3 % and 2 % for Beta and Gamma Mound, respectively at greater depth.

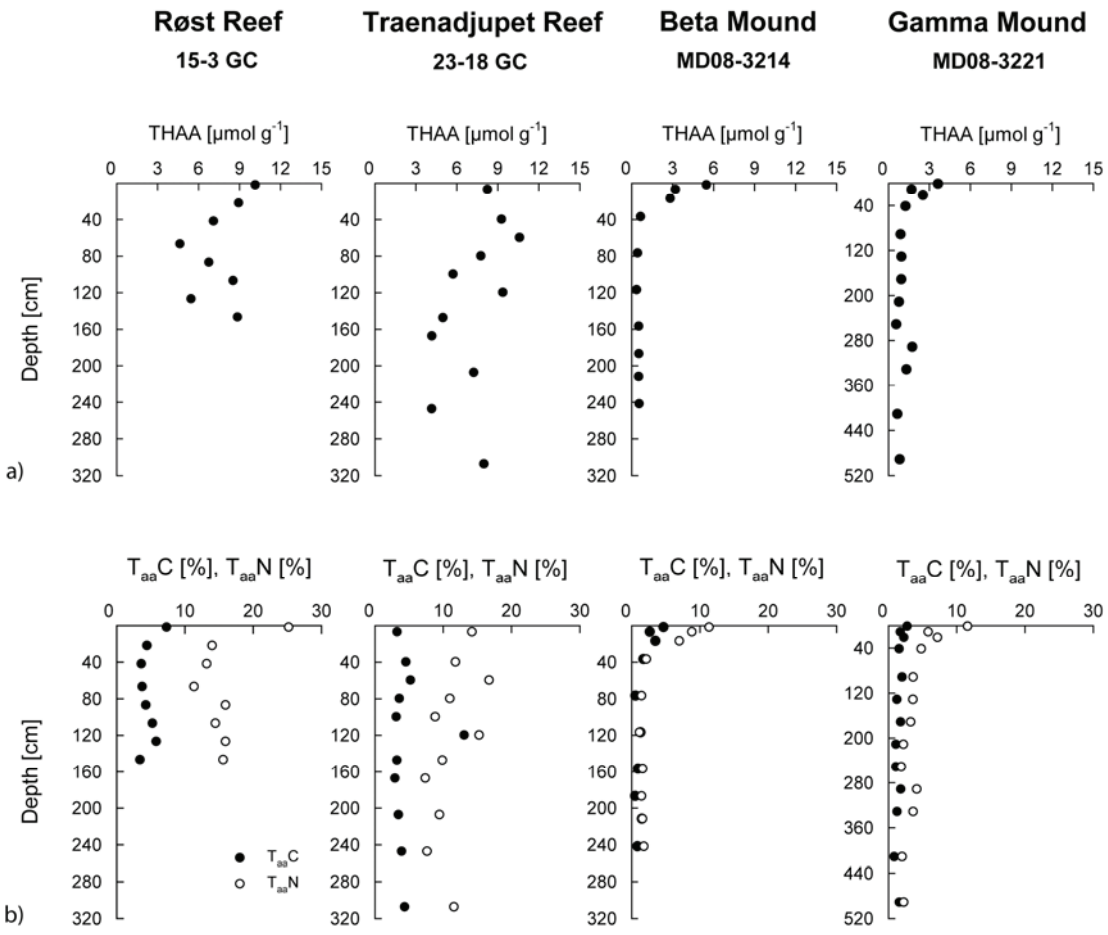

Figure 4: a) Total hydrolysable amino acid (THAA) concentrations with depth and **b)** contribution of amino acid-derived carbon ($T_{aa}C$) and nitrogen ($T_{aa}N$) to the total organic carbon and nitrogen pools with depth.

The mole-% contributions of the individual amino acids to the THAA pool in the surface sediments for the cores retrieved at the four stations are displayed in Figure 5. The surface sediments at the coral reef sites (15-3 GC and 23-18 GC) are dominated by Gly (~ 21 %) followed by Ala (~13.5 %) and Ser, Arg, Thr and Val at a similar range of 7.5-9.8 %. The mound core MD08-3214 showed highest surface contribution for Ala (19.2 %) followed by Gly (18 %) while the surface sediment of core MD08-3221 was dominated by Gly (17.5 %) followed by Ala (14.5 %). Ser, Arg, Thr and Val were in a similar range as described for the coral reef sites. Asp and Glu were less abundant at all sites with mole-% contribution of ≤ 5 % except for an elevated Glu contribution of 7.4 % for the top of the core from Gamma Mound. The non-protein amino acids β-Ala and γ-Aba contributed < 3 % to the THAA in the surface sediments from all locations.

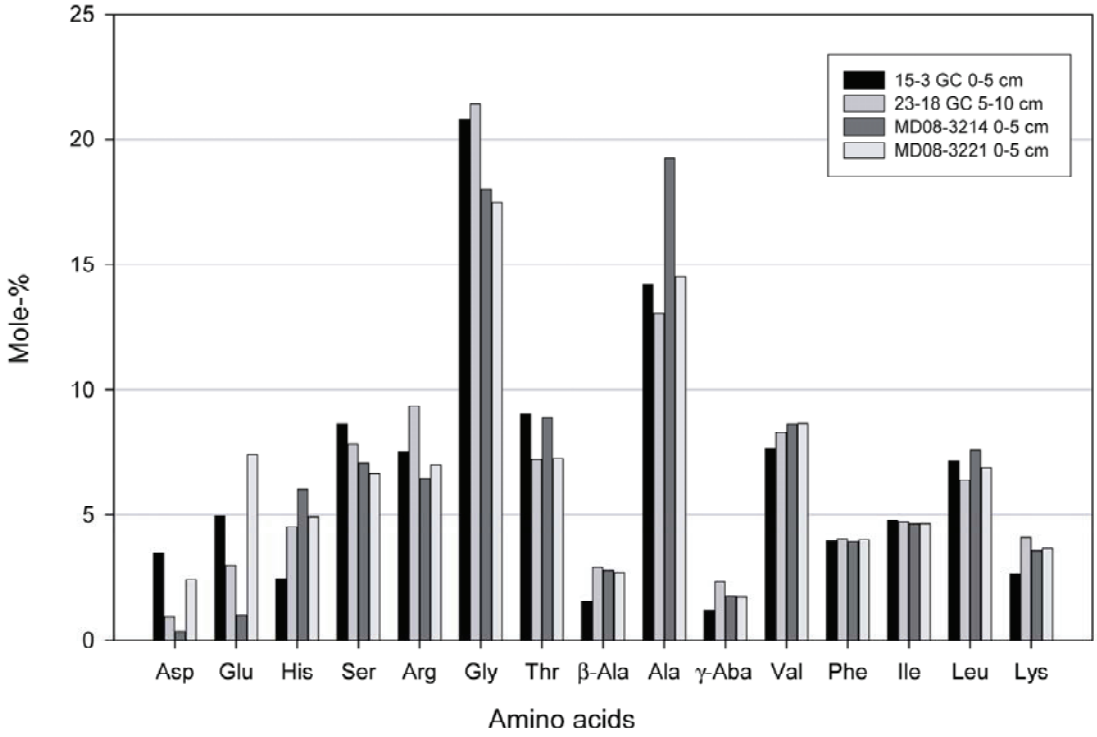

Figure 5: Mole-% contribution of the individual amino acids to the THAA pool in the surface sediments. Abbreviations stand for aspartic acid (Asp), glutamic acid (Glu), histidine (His), serine (Ser), arginine (Arg), glycine (Gly), threonine (Thr), β-alanine (β-Ala), alanine (Ala), γ-amino butyric acid (γ-Aba), valine (Val), isoleucine (Ile), leucine (Leu) and lysine (Lys).

The mole-% contributions of the acidic amino acids Asp and Glu to the THAA with depth are shown in Figure 6a. Down-core the contribution of Asp remained low and close to the detection limit with values of < 3.5 %. Glutamic acid mole-% contents were highly variable with depth with values between 1-7.5 % at all sites and showed no distinct pattern with depth. A general increase with depth was noticed for the mole-% of the non-protein amino acids β-Ala and γ-Aba which was least pronounced in core 23-18 GC from Traenadjupet Reef (Fig. 6b). At the mound sites, the non-protein amino acids contributed > 10 % to the sedimentary THAA yield. Apart from a small decrease at the surface of core 15-3 GC, the percent contribution of the basic amino acids His, Arg and Lys to the THAA at the coral reef sites remained unchanged with depth (Fig. 7a). Similarly, the mole-% contribution of the hydroxylic amino acids Ser and Thr remained largely constant with depth, indicating a loss of these amino acids at the same rate as the THAA pool in the coral-reef associated sediments.

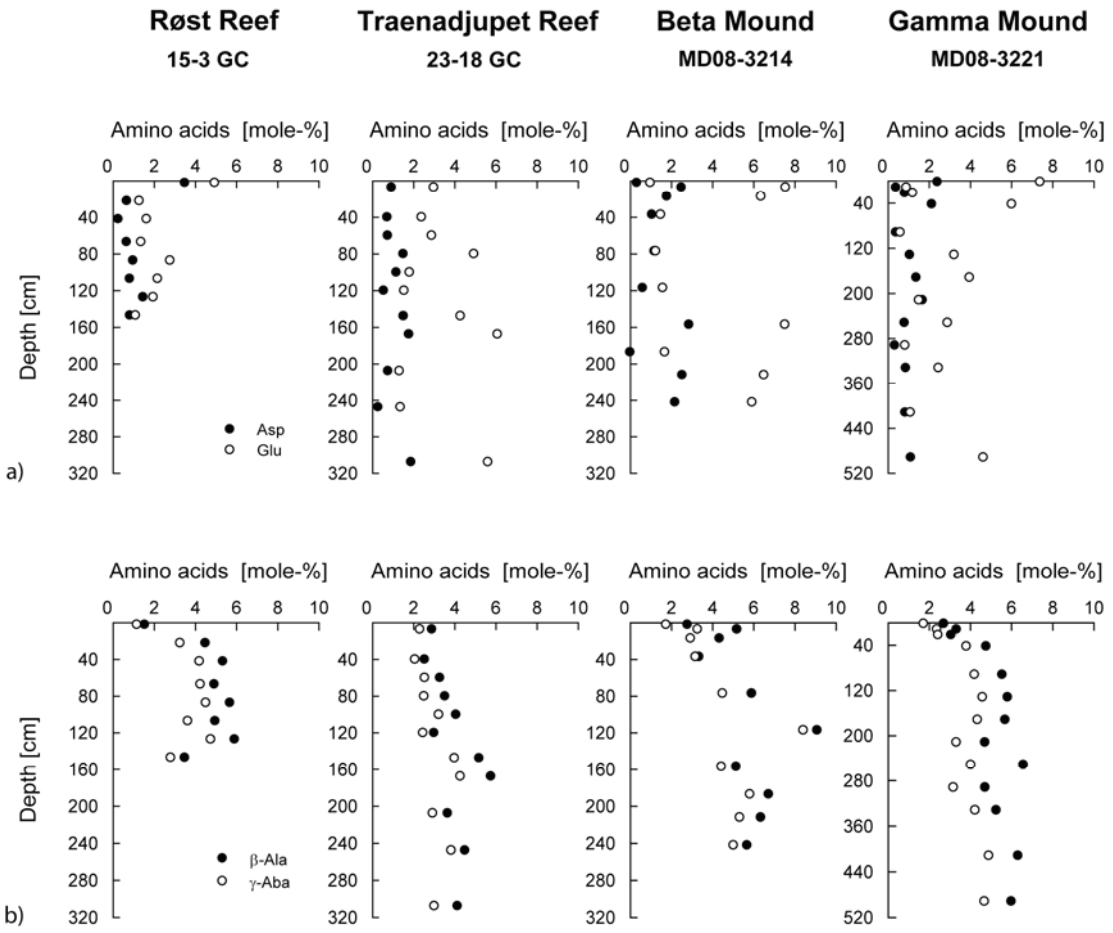

Figure 6: Mole-% contributions of **a)** the acidic amino acids aspartic acid (Asp) and glutamic acid (Glu) and **b)** the non-protein amino acids β-alanine (β-Ala) and γ-amino butyric acid (γ-Aba) with depth.

At the mound sites, a decrease in the mole-% of His was evident which reached concentrations below detection limit at depths below 75 cm at Beta Mound and ≤ 3 % mole-% at Gamma Mound. Higher mole-% values for Arg at both mounds were observed in the surface sediment compared to greater depth. Changes in the relative contribution of Lys to the THAA with depth at these sites were minor. The mole-% contribution of the hydroxylic amino acids Ser and Thr at both mounds decreased with depth which was more pronounced at Beta Mound than at Gamma Mound (Fig. 7b). The overall contribution of the dominating neutral amino acids Gly, Ala and Val showed only minor changes for core 15-3 GC (Rost Reef) and MD08-3221 (Gamma Mound) and core 23-18 GC (Traenadjupet Reef) (Fig. 8a). Core MD08-3214 (Beta Mound) showed an increase in the mole-% contribution of Val accompanied by a subtle decrease in the mole-% contribution of Gly. The less abundant neutral amino acids Leu, Ile and Phe showed minor changes in their mole-% values at the coral reef sites (Fig. 8b). At the coral mound sites, a tendency to a higher relative contribution of Leu with

depth was observed, as well as slight increases in the contribution of Ile and Phe in the top 40 cm of the Beta Mound core (Fig. 8b).

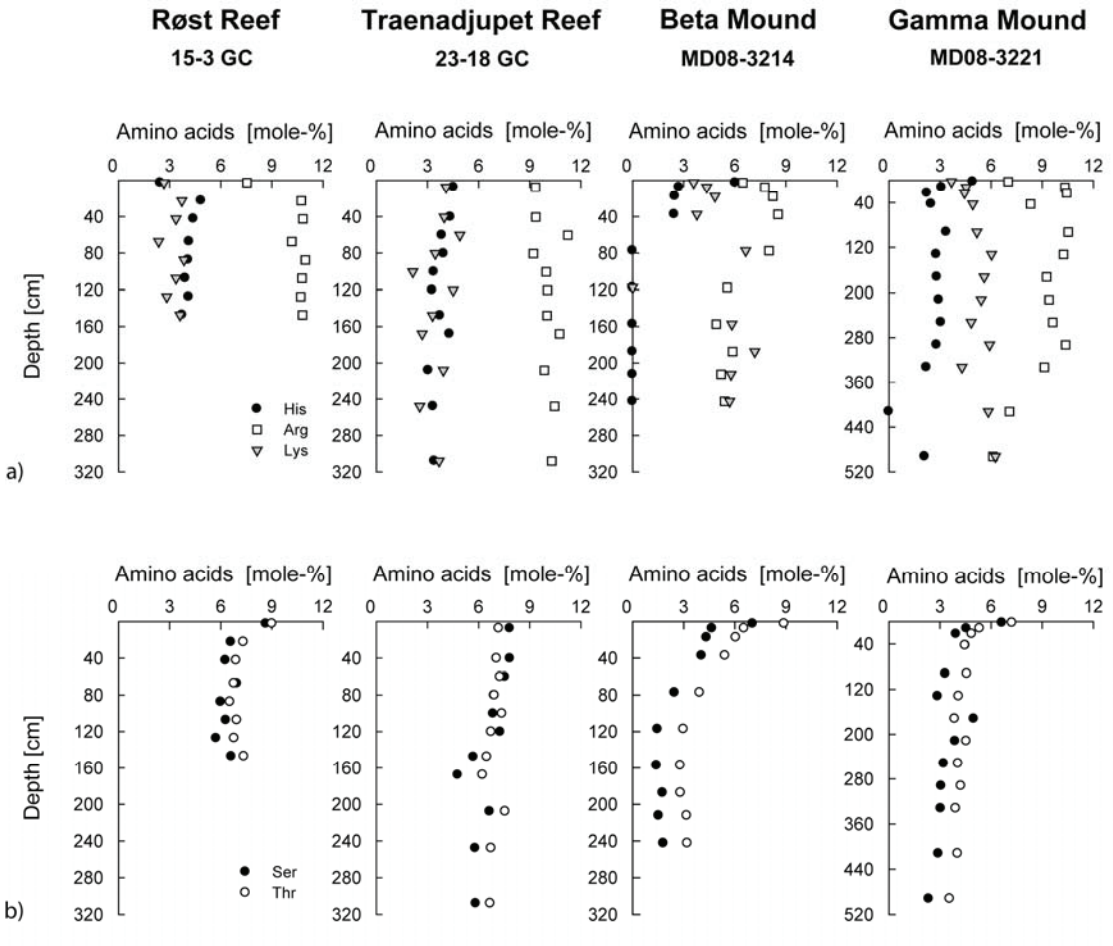

Figure 7: Mole-% contributions of **a)** the basic amino acids histidine (His), arginine (Arg) and lysine (Lys) and **b)** the hydroxylic amino acids serine (Ser) and threonine (Thr) with depth.

4.4 Degradation Index

The Degradation Index (DI) highlights systematic compositional changes in the THAA pool related to organic matter degradation. The Degradation Indices calculated for the cold-water coral reef and mound sites based on the comprehensive PCA including the Dauwe and Middelburg (1998) dataset clearly reflected the high state of degradation of these sediments (Tab. 2). The DI values calculated for the present cold-water coral ecosystem dataset were always lower than DI values calculated for the Dauwe and Middelburg (1998) sites (Tab. 2). The DI for two turbidite samples (Tur-ox and Tur-red) were the most similar to the DI values calculated for the cold-water coral reef surface sediments. These differences can be largely attributed to deviances in the contributions of Asp and Glu, which are positively correlated with the Dauwe and

Middelburg (1998) dataset, and of Arg, Ala and the non-protein amino acids, which were more abundant in the samples from our dataset (PC1; Fig. 10). Values for the DI based on the comprehensive PCA for the modern cold-water coral reef sediments ranged from 0.6 for the top sediment of core 15-3 GC to -1.9 at 293-303 cm depth in core 23-18 GC. The cold-water coral mound sediments showed lower DI values in the range of 0.2 (top of core MD08-3221) to -3.3 (115-120 cm in core MD08-3214) with most values < -1.5 reflecting a higher state of degradation at the mound sites (Tab. 2). The second axis (PC2) of the PCA gives additional information that the higher DI of the mound sediments can be attributed to deviances in Gly and Arg which are positively correlated with the reef sediments and Val and Leu which showed a higher mole-% contribution at the mound sites (Fig. 10).

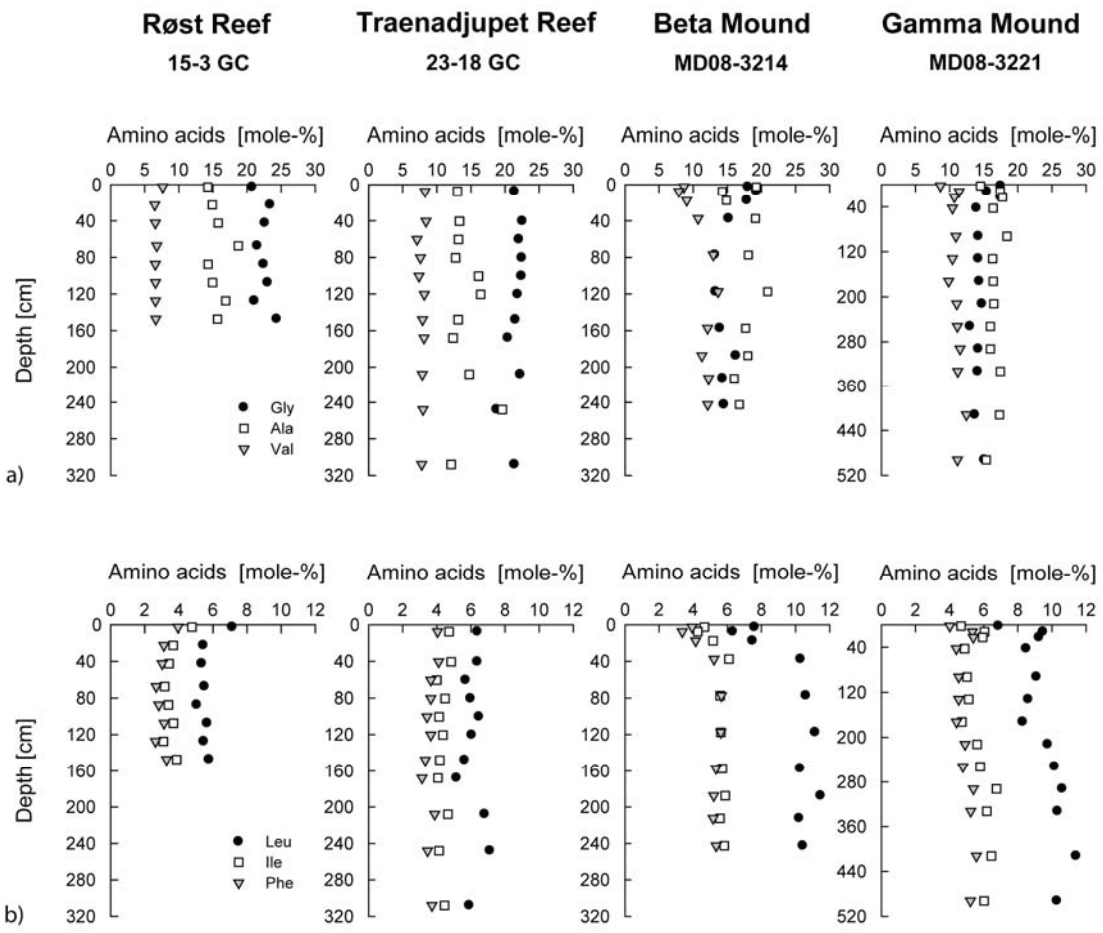

Figure 8: Mole-% contributions of **a)** the neutral amino acids glycine (Gly), alanine (Ala) and valine (Val) as well as **b)** the less abundant neutral amino acids leucine (Leu), isoleucine (Ile) and phenylalanine (Phe) with depth.

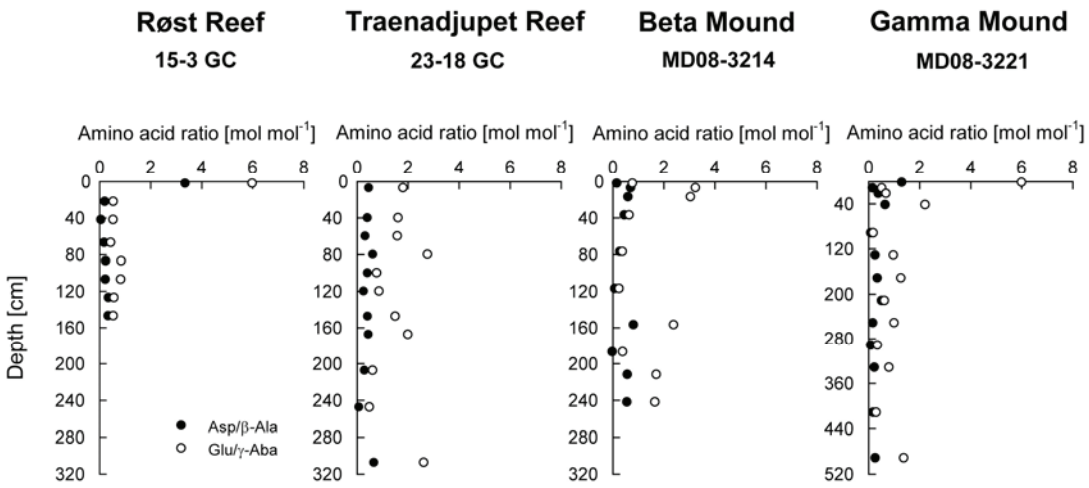

Figure 9: Ratios of the amino acids aspartic acid (Asp) to β-alanine (β-Ala) and glutamic acid (Glu) to γ-amino butyric acid (γ-Aba) with depth.

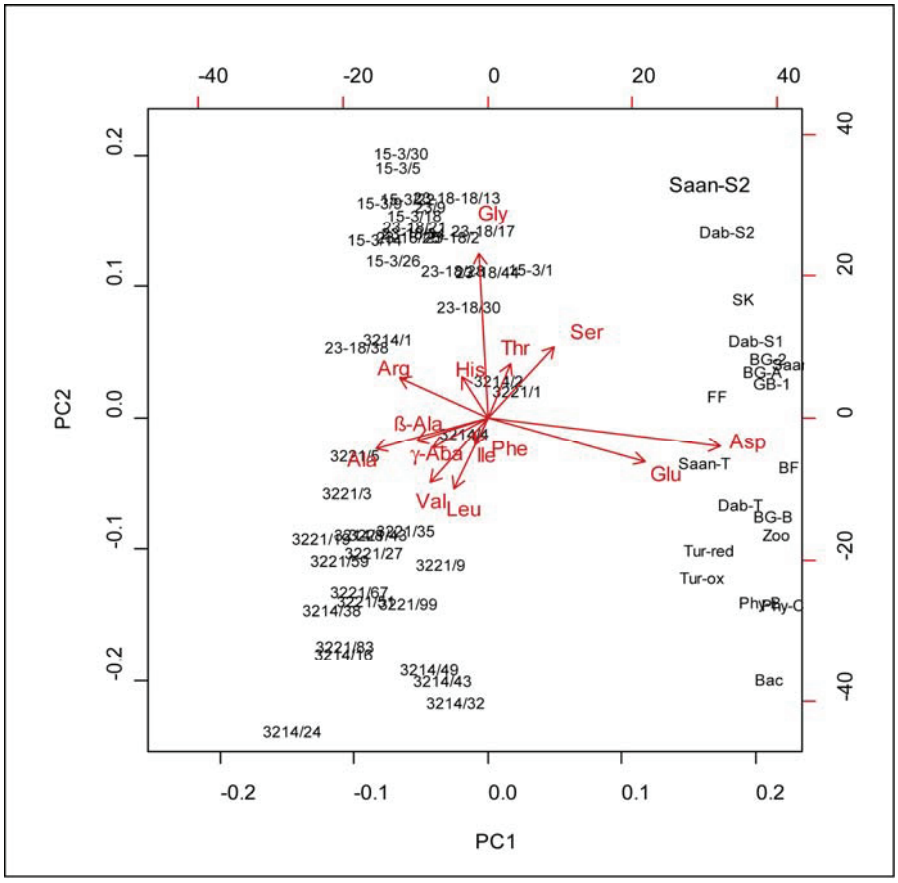

Figure 10: Results of PCA applied to the mole-% amino acid contributions for the comprehensive dataset.

Degradation Index values calculated from the PCA based solely on our dataset for the cold-water coral ecosystem sites with depth are displayed in Figure 11. They provide additional information on the differences in organic matter degradation state between the reef and mound sites. Values based on this PCA are in the range of 1.1 to

3.3 for the Lofoten coral reef cores 15-3 GC and 23-18 GC and show no pronounced down-core trends. Degradation Index values are in the range of -5 to 1.3 for the Pen Duick coral mound cores MD08-3214 and MD08-3221. Core MD08-3214 showed a strong drop in DI values in the top 120 cm and core MD08-3221 showed decreases in DI with depth.

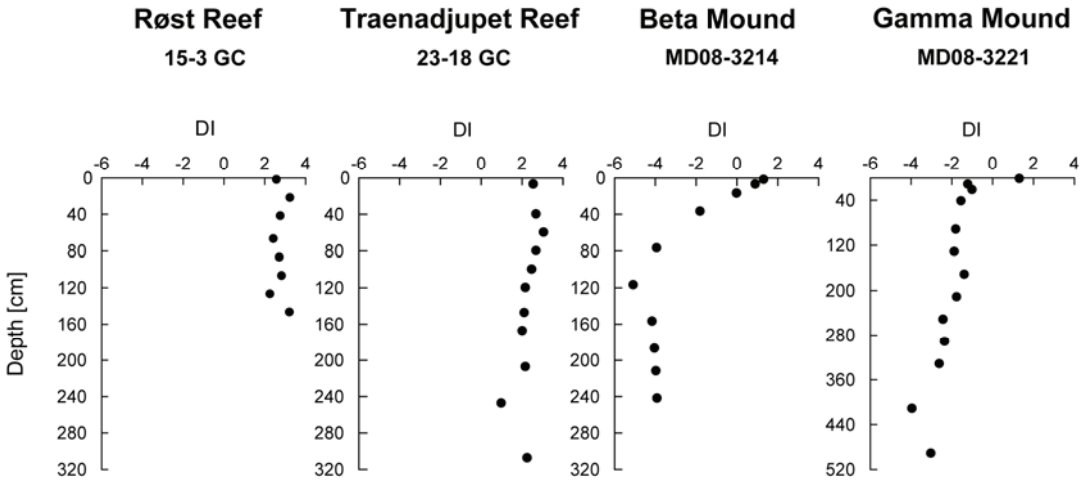

Figure 11: Degradation indicies (DI) with depth based on PCA of the cold-water coral ecosystem dataset.

5. Discussion

5.1 The overall degradability of organic matter

The low total organic carbon concentrations (TOC) at the investigated coral-reef and cold-water coral mound associated sediments may result from the combination of a low input of particulate organic carbon from the overlying reef and a dilution effect due to the large input of particulate inorganic carbon. All sites are characterized by high TIC concentrations of in average 4.6 and 3.1 wt.% for Røst Reef and Traenadjupet Reef (Wehrmann et al., 2009) and 4.8 % and 5.1 % for Beta and Gamma Mound (Wehrmann et al., in revision). The C/N-ratios (6.6 to 8.5) indicate that the sedimentary organic carbon is mainly of marine origin at both locations. Modern planktonic organic matter (OM) has typical C/N-ratios of 5-7 which can increase to values up to 12 during later stages of degradation in the sediment (Emery and Uchupy, 1984). The C/N-ratios close to values of fresh phytoplankton might, at first, suggest that the organic material buried in the coral-bearing sediments is relatively fresh and undegraded OM available for microbial degradation. However, these values need to be taken with caution because the adsorption of ammonium to clay minerals, especially illite, can strongly lower the C/N-

ratio (Müller, 1977; Schubert and Calvert, 2001). The coral-bearing sediments at the investigated sites comprise mostly of loose silt, clay and biogenic debris (Wehrmann et al., 2009) and thus might facilitate the adsorption of ammonium. Furthermore, in low organic matter environments such as the investigated cold-water coral reef sediments, the contribution of inorganic nitrogen to the total nitrogen can be significant and thus artificially depress the C/N-ratio (Meyers, 1997).

A more direct and reliable indicator of the freshness of organic matter is the Chlorin Index (CI) introduced by Schubert et al. (2005). Chlorins comprise degradation products of chlorophyll that are ubiquitous in marine surface sediments. The CI is a measure of the ratio of chlorophyll and its degradation products released during acidification in the sediments (Schubert et al., 2005). Chlorin index is in the range of 0.2 for chlorophyll α, a proxy for recent and fresh OM, to values approaching 1 for highly degraded sediments. The CI overcomes the dilution effect caused by the strong input of background carbonate in the cold-water coral bearing sediments by giving a relative ratio of the fluorescent intensities of original and acidified extract. In the present study, CI values range from 0.52 for the surface sediment at the Røst Reef coral rubble zone to values > 0.75 throughout the entire lengths of the other cores including values > 0.85 for large sediment intervals (Fig. 3). These findings suggest a rapid alteration of the deposited chlorophyll-containing OM within the surface layer of the living cold-water coral reefs, thus leading to the presence of altered OM in deeper sediment layers. This is in agreement with CI values from the reef top of Røst Reef (0.34) and from a second coral rubble station in proximity to core 15-3 GC (0.51; data not shown), which indicate that relatively fresh OM reaches the surface of the reef, but then undergoes efficient remineralization before reaching the anaerobic zone of the sediments. Most likely, the overlying coral rubble habitat serves as a major filter for the chlorophyll-containing compounds. The comparison of the two cold-water coral reef sites reveals that although chlorin concentrations of core 23-18 GC from Traenadjupet Reef are up to three times the concentrations of chlorins determined for Røst Reef core 15-3 GC, the CI of core 23-18 GC ranges from 0.77 at the surface to 0.87 at depth, indicating a higher degradation state for the surface sediment than at depth. The difference in CI values for both cores might be controlled by their location. Core 15-3 GC from the coral rubble zone at Røst Reef is located in closer proximity to the living reef top which is presumably more exposed to incoming fresh OM compared to 23-18 GC, which is located at some distance from the living coral zone at Traenadjupet Reef. The CI of the

mound sediments is high with values of in average 0.80 and 0.83 for Beta and Gamma Mound, respectively, and indicate an elevated degradation state of this material. Intriguingly, CI values at the depth interval of 5-25 cm at both mound sites are higher than for the rest of the cores. This might indicate that this zone is affected by additional processes that facilitate the degradation of OM. These processes might include the influx of oxygen due to bioirrigation and bioturbation which was suggested to cause elevated CI values at an intensively-bioturbated site in the Chilean coastal upwelling region (Niggemann, 2005).

Amino acids constitute an important fraction of OM deposited into marine sediments since they are found in all living organisms (Lee, 1988). It has been shown, that amino acids are degraded at a faster rate than the bulk OM pool, which makes their detection another powerful tool for the investigation of the degradation state of sedimentary OM (e.g. Cowie and Hedges, 1994; Henrichs 1993; Wakeham and Lee 1993). In the present study, the amount of total hydrolysable amino acids (THAA) shows surface values of ~10 μmol g^{-1} for the Norwegian cold-water coral reef sediments (corresponding to ~1100 μg g^{-1}) and values of 5.5 and 3.7 μmol g^{-1} (corresponding to 620 and 430 μg g^{-1}) for Beta and Gamma Mound (Fig. 4). Comparison with other sites reveals that these values are in the range of values reported from other continental margin sediments. For example, Boski et al. (1998) showed surface values of 140-860 μg g^{-1} for sediments from the NW European Continental Margin and Steinberg et al. (1987) report a total amino acid concentration of ~11 μmol g^{-1} for sediments from 1300 m water depth on the continental margin off Southern New England. These THAA concentrations are one order of magnitude lower than values reported for coastal sediments (e.g. the Washington coast; Keil and Fogel, 2001; Keil et al., 1998) but are remarkably similar to total amino acid yields from surface sediments in the deep ocean (e.g. the Porcupine Abyssal Plain; Horsfall and Wolff, 1997). As the THAA content is strongly correlated with the bulk TOC concentration (Keil et al., 2000), it reflects to a certain extent the low TOC values of the coral-bearing sediments and underlines the finding that the amount of degradable OM reaching these sediments is limited and probably diluted. However, while the TOC content does not show a down-core pattern with depth at any of the investigated sites (Fig. 2), THAA concentrations show distinct decreases especially at the mound sites. Correspondingly, the percentages of amino acid-derived carbon and nitrogen to TOC and TN ($\%T_{aa}C$, $\%T_{aa}N$; Fig. 4b) which are more robust measures of amino acid dynamics with respect to the bulk OM pool (Keil et

al., 2000), show strong decreases at all sites. Whereas surface $\%T_{aa}C$ and $\%T_{aa}N$ values for the Norwegian reefs are within the typical range reported for continental margin sediments (12±10 % for carbon and 30±12 % for nitrogen; Keil et al., 2000), the surface percentages for the mounds are at the lower end of the range. The strong depletion of amino-acid derived carbon and nitrogen with depth can be explained by the in-situ degradation of the amino acids by an active microbial community in the sediments. Thus, while the CI only illustrates the overall elevated degradation state of the buried OM, the application of the amino acids allows for a more definitive analysis of the relative changes of this OM with depth.

The calculated values for the Degradation Index (DI) based on Dauwe and Middelburg (1998) and Dauwe et al. (1999) complete our set of indicators for the degradation state of the cold-water coral ecosystem associated sediments. The DI based on the first comprehensive principal component analysis (PCA) combining the original Dauwe and Middelburg (1998) and our datasets gives strong evidence that the investigated cold-water coral reef and mound sediments are characterized by OM with a high degradation state (Tab. 2). In this respect they might be comparable to turbidite sediments which are characterized by highly refractory OM (Dauwe and Middelburg, 1998). The DI values based on both PCAs additionally support the hypothesis that the organic matter in the cold-water coral mound sediments are more degraded than the organic matter buried in the Lofoten reef sediments (Fig. 10 and 11). This indicates a continued degradation of OM during the gradual transition of a cold-water coral reef to a mound.

5.2 Individual amino acid trends with depth and between sites

A common tool used to assess the degradation state of OM in marine sediment is the ratio of the acidic amino acids aspartic acid (Asp) and glutamic acid (Glu) to the non-protein amino acids β-alanine (β-Ala) and γ-amino butyric acid (γ-Aba) (Cowie and Hedges 1994; Lee and Cronin 1982). This approach is based on the observation that the mole-% contributions of Asp and Glu decrease with depth in the water column and sediment, and thus ongoing degradation, while the relative contributions of their decarboxylation products β-Ala and γ-Aba increase. In the present study, the sediments were characterized by extremely low concentrations of Asp and Glu which did not show clear trends with depth. β-Ala and γ-Aba showed low mole-% contributions in the surface sediment of core 15-3 GC (Røst Reef) and MD08-3221 (Gamma Mound) but

otherwise elevated values of 2.5-8 % with subtle down-core trends to higher relative contributions (Fig. 6). The low concentrations of acidic amino acids resulted in very low ratios of the acidic to non-protein amino acids and little variation with depth (Fig. 9). Only at Røst Reef and Gamma Mound were distinct decreases of the ratios below the surface layer observed, which indicate that the surface layers are characterized by less degraded OM. Overall, these findings indicate a highly progressed state of OM degradation at the coral reef-associated sediments. At this degradation state, the spatial distribution of the Asp/β-Ala and Glu/γ-Aba does not seem to offer information on the progression of the degradation state.

Aspartic acid and glutamic acid are highly abundant in organic matter sources of marine sediments like phyto- and zooplankton (Cowie et al., 1992), and generally constitute a large fraction of the total amino acid pool in marine sediments. Aspartic acid, for example, was reported to be the dominant amino acid in sediments from the NW European Continental Margin (Boski et al., 1998) and the inner Oslorfjord, Norway (Haugen and Lichtentaler, 1991) and Asp and Glu are among the most abundant amino acids in sediments from the Chilean upwelling region (Lomstein et al., 2006). The cold-water coral ecosystems investigated in this study are characterized by extremely low concentrations of acidic amino acids strongly contrast continental margin sediments. It can be suggested that Asp and Glu are effectively removed from the bulk organic matter pool prior to sediment deposition at the cold-water coral reef ecosystems. This preferential removal is most likely due to enhanced microbial degradation in the reef-adjacent water column and overlying coral rubble zone. Similarly, the discovery of elevated mole-% contributions of the degradation products β-Ala and γ-Aba to the total amino acid yield in the surface sediments indicates that highly degraded OM reaches the sediments. The preferential removal of acidic amino acids by microbial degradation has been previously suggested by Steinberg et al. (1987) for sediments on the continental margin off southern New England. The authors inferred a correlation between the concentration of acidic amino acids in surface sediments and water depth. Increased water depth allows for an increased oxygen exposure time of the sinking OM and enhanced microbial degradation of the sinking OM during passage through the water column.

The selective degradation of Glu, along with tyrosine (Tyr) and phenylalanine (Phe) in marine sediments has been previously reported by several studies (see Cowie et al. 1992; Dauwe et al., 1999; for review). It is attributed to the primary occurrence of

these amino acids in the diatom cell plasma which might be lost during early stages of degradation (Hecky et al., 1973). In contrast, the amino acids glycine (Gly), threonine (Thr) and serine (Ser) are more abundant in (diatom) cell-walls and thus are less prone to degradation which often leads to an increase in the relative contribution of these amino acids to the THAA pool with increasing degradation state of the OM (Cowie et al., 1992; Dauwe and Middelburg, 1998; Lee and Cronin, 1982). In the investigated coral-reef associated sediments, however, the cell wall-associated amino acids show distinct decreases in their relative abundance with depth, especially at the coral mound sites (Figs. 7b and 8a), while the intracellular Phe remains relatively unchanged down-core (Fig. 8b). This might indicate that at later stages of degradation and with progressive depletion of labile substrates, microbial OM mineralization might be less selective and also degrade refractory amino acids (e.g. from cell-wall material).

Apart from their use as carbon substrates for microbial degradation, amino acids in the sediment are also assimilated by the infaunal benthic community. This might be the case for the essential amino acids arginine (Arg) and histidine (His) which show strong depletion with depth at the coral mound sites. A similar finding has been made by Dauwe and Middelburg (1998) who suggested that the deficiency of these amino acids in North Sea sediments can be attributed to their preferential uptake to fulfill animal nutrition, for example of sediment-ingesting animals.

The microbial remineralization of OM not only leads to the removal of amino acids, but the active microbial community also facilitates the in-situ production of new amino acids, and might therefore constitute an important fraction of the total amino acid content of sediments (Benner and Kaiser, 2003; Grutters et al., 2002; Kaiser and Benner, 2008; Keil and Fogel, 2001; Lomstein et al., 2006; Lomstein et al., 2009). During OM diagenesis, prokaryotic remains such as D-amino acids and muramic acid, which are building blocks of the cell wall polymer peptidoglycan, accumulate in the sediment (Lomstein et al., 2009; Pedersen et al., 2001). It is assumed that with increasing sediment depth, the importance of bacteria as contributors of THAA increases and that they might even dominate the THAA pool at great sediment depth (Pedersen et al., 2001). To test if bacteria contribute a significant fraction of amino acid nitrogen to the sedimentary THAA nitrogen yield, we estimated the contribution of amino acids from bacteria for Beta Mound using an approach similar to Lomstein et al. (2006). This approach utilizes bacterial cell numbers from Beta Mound. Bacterial cell numbers based on acridine orange direct counts (AODC) from core MD08-3214 from Beta Mound

were around 1 x 10^9 cells cm^{-3} in the top 140 cm, 1 x 10^8 cells cm^{-3} at 145-200 cm, and between 1.6 x 10^8 and 1 x 10^9 cells cm^{-3} below 200 cm (Templer et al., in review). Using a dry weight of bacterial cells of 2.8 x 10^{-13} g, a protein dry weight content of 55% (Brock and Madigan, 1991) and a nitrogen to protein conversion factor of 6.25 (Jones, 1931), this gives a contribution of nitrogen to the THAA nitrogen yield of the sediment of < 3.5 %. This estimate indicates that the living microbial community only contributes a small fraction to the amino acid-derived nitrogen at Beta Mound. Conversely, this might suggest that the fraction of amino acids from other sources (e.g. cell wall remains of phytoplankton) still constitute the largest pool of amino acids in these sediments. The relative changes of individual amino acids compared to the bulk THAA pool with depth are therefore primarily controlled by preferential microbial degradation and uptake by benthic fauna rather than variability of microbial-derived amino acids.

6. Conclusions

Cold-water coral reef ecosystem are hot-spots of carbon mineralization driven by the activity of the reef-associated macro-fauna and the microbial communities hosted in the biofilm of the coral rubble facies overlying the reef sediments (Wehrmann et al., 2009; Van Oevelen et al., 2009). Enhanced OM turnover in this zone reduces the influx of OM into the sediments and alters its degradation state. Thus, carbon mineralization at cold-water coral ecosystems might be much more efficient than at other continental margin habitats. Sediments underlying cold-water coral ecosystems are characterized by a highly elevated degradation state of the buried OM. The CI index and the amino acid-based diagenetic indicators, including the Degradation Index, derived from the Norwegian coral reef surface sediments, emphasize that the elevated degradation state is not merely driven by anaerobic mineralization processes in the sediment but that the low concentrations of OM that reach the reef sediments has already undergone strong pre-depositional diagenetic alteration. Our study thus supports the hypothesis by Wehrmann et al. (2009) that the reef-associated sediments are effectively decoupled from the overlying flourishing reef.

Distinct decreases in the contribution of amino acid-derived carbon and nitrogen to the total organic carbon and nitrogen pool suggest in-situ mineralization of the sedimentary amino acids, while the contribution of the active microbial community to the total amino acid pool remains small. At the coral mound sites, systematic

compositional changes in the amino acid pool reveal that the degradation of the THAA is not uniform but rather that individual amino acids are more prone to degradation and/or be taken up by other processes (e.g. as nutritional supply for the infaunal benthic community).

Comparison between the Norwegian reef sediments and the Gulf of Cadiz mounds generates a window into long-term degradation patterns of cold-water coral-bearing sediments. Decreases in the relative contribution of (diatom) cell wall-associated amino acids to the THAA yield indicate the remineralization of more refractory OM at later stages of degradation. Also, the degradation index suggests the progressive degradation of OM during reef-mound transition.

References

Benner, R. and Kaiser, K.: Abundance of amino sugars and peptidoglycan in marine particulate and dissolved organic matter, Limnol. Oceanogr., 48, 118-128, 2003.

Boski, T., Pessoa, J., Pedro, P., Thorez, J., Dias, J. M. A. and I. R. Hall: Factors governing abundance of hydrolyzable amino acids in the sediments from the NW European Continental Margin (47-50 degrees N), Prog. Oceano., 42, 145-164, 1998.

Brock, T. D. and Madigan, M. T.: Biology of Microorganisms, 6 ed. Prentice-Hall International (UK), 1993.

Brown, F. S., Baedecker, M. J., Nissenbaum A. and Kaplan, I. R.: Early Diagenesis in a Reducing Fjord, Saanich Inlet, British-Columbia - III. Changes in organic constituents of sediment, Geochim. Cosmochim. Ac., 36, 1185-1203, 1972.

Cowie, G. L. and Hedges, J. I.: Biochemical Indicators of Diagenetic Alteration in Natural Organic-Matter Mixtures, Nature 369: 304-307, 1994.

Cowie, G. L., Hedges, J. I. and Calvert, S. E.: Sources and Relative Reactivities of Amino-Acids, Neutral Sugars, and Lignin in an Intermittently Anoxic Marine-Environment, Geochim. Cosmochim. Ac., 56, 1963-1978, 1992.

Dauwe, B. and Middelburg, J. J.: Amino acids and hexosamines as indicators of organic matter degradation state in North Sea sediments, Limnol. Oceanogr., 43, 782-798, 1998.

Dauwe, B., Middelburg, J. J., Herman, P. M. J. and Heip, C. H. R.: Linking diagenetic alteration of amino acids and bulk organic matter reactivity, Limnol. Oceanogr., 44, 1809-1814, 1999.

Davies, A. J., Duineveld, G. C. A., Lavaleye, M. S. S., Bergman, M. J. N., van Haren, H. and Roberts, J. M: Downwelling and deep-water bottom currents as food supply mechanisms to the cold-water coral Lophelia pertusa (Scleractinia) at the Mingulay Reef complex, Limnol. Oceanogr., 54, 620-629, 2009.

Duineveld, G. C. A., Lavaleye, M. S. S. and Berghuis, E. M.: Particle flux and food supply to a seamount cold-water coral community (Galicia Bank, NW Spain), Mar. Ecol. Prog. Ser., 277, 13-23, 2004.

Emery, K. O. and Uchupy, E.: The Geology of the Atlantic Ocean. Springer-Verlag, 1984.

Foubert, A., Depreiter, D., Beck, T., Maignien, L., Pannemans, B., Frank, N., Blamart, D., Henriet, J.P.: Carbonate mounds in a mud volcano province off north-west Morocco: Key to processes and controls, Mar. Geol., 248, 74-96, 2008.

Frederiksen, R., Jensen, A. and Westerberg, H.: The distribution of the scleractinian coral Lophelia pertusa around the Faroe Islands and the relation to internal tidal mixing, Sarsia, 77, 157-171, 1992.

Freiwald, A.: Reef-forming cold-water corals, in: Ocean Margin Systems, edited by: Wefer, G., Billett, D., Hebbeln, D., Jørgensen, B.B., Schlüter, M. and van Weering, T.C.E., Springer, Heidelberg, 365-385, 2002.

Grutters, M., van Raaphorst, W., Epping, E., Helder, W., de Leeuw, J. W., Glavin, D. P. and Bada, J. Preservation of amino acids from in situ-produced bacterial cell wall peptidoglycans in northeastern Atlantic continental margin sediments, Limnol. Oceanogr., 47, 1521-1524, 2002.

Grutters, M., van Raaphorst, W. and Helder, W.: Total hydrolysable amino acid mineralisation in sediments across the northeastern Atlantic continental slope (Goban Spur), Deep-Sea Res. Pt. I, 48, 811-832, 2001.

Haugen, J. E. and Lichtentaler, R.: Amino acid diagenesis, organic carbon and nitrogen mineralization in surface sediments from the Inner Oslofjord, Norway, Geochim. Cosmochim. Ac., 55, 1649-1661, 1991.

Hecky, R. E., Mopper, K., Kilham, P. and Degens, E.T.: Amino-Acid and Sugar Composition of Diatom Cell-Walls, Mar. Biol., 19, 323-331, 1973.

Hedges, J. I., and Keil, R. G.: Sedimentary Organic-Matter Preservation - an Assessment and Speculative Synthesis, Mar. Chem., 49, 81-115, 1995.

Henrichs, S. M.: Early diagenesis of organic matter: the dynamics (rates) of cycling of organic compounds, in: Organic Geochemistry, editied by Engel, M. H. and Macko, S. A., Plenum Press, 101-117, 1993.

Horsfall, I. M. and Wolff, G. A.: Hydrolysable amino acids in sediments from the Porcupine Abyssal Plain, northeast Atlantic Ocean, Org. Geochem., 26, 311-320, 1997.

Hovland, M., Ottesen, D., Thorsnes, T., Fossa, J.H. and Bryn, P.: Occurrence and implications of large Lophelia-reefs offshore Mid Norway, in: Onshore - offshore relationships on the North Atlantic margin, edited by: Wandas, B., Nystuen, J.P., Eide, E. and Gradstein G., Norwegian Petroleum Society (NPF), Special Publications. Elsevier B.V., Amsterdam, 265-270, 2005.

Husebo, A., Nottestad, L., Fossa, J.H., Furevik, D.M. and Jorgensen, S.B.: Distribution and abundance of fish in deep-sea coral habitats, Hydrobiologia, 471, 91-99, 2002.

Jensen, A. and Frederiksen, R.: The fauna associated with the bank-forming deep-water coral *Lophelia pertusa* (Scleractinaria) on the Faroe Shelf, Sarsia, 77, 53-69, 1992.

Jonsson, L.G., Nilsson, P.G., Floruta, F. and Lundälv, T.: Distributional patterns of macro- and megafauna associated with a reef of the cold-water coral *Lophelia pertusa* on the Swedish west coast, Mar. Ecol. Prog. Ser., 284, 163-171, 2004.

Kaiser, K. and Benner, R.: Major bacterial contribution to the ocean reservoir of detrital organic carbon and nitrogen, Limnol. Oceanogr., 53, 99-112, 2008.

Keil, R. G. and Fogel, M. L.: Reworking of Amino Acid in Marine Sediments: Stable Carbon Isotopic Composition of Amino Acids in Sediments along the Washington Coast, Limnol. Oceanogr., 46, 14-23, 2001.

Keil, R. G., Tsamakis, E., Giddings, J. C. and Hedges, J. I.: Biochemical distributions (amino acids, neutral sugars, and lignin phenols) among size-classes of modern marine sediments from the Washington coast, Geochim. Cosmochim. Ac., 62, 1347-1364, 1998.

Keil, R. G., Tsamakis, E. and Hedges, J. I.: Early diagenesis of particulate amino acids in marine systems, in: Perspectives in Amino Acid and Protein Geochemistry, editied by Goodfriend, C. A., Collins, M. J., Fogel, M. L., Macko, S. A. and Wehmiller, J. F., Oxford University Press, 66-82, 2000.

Kiriakoulakis, K., Bett, B.J., White, M. and Wolff, G.A.: Organic biogeochemistry of the Darwin Mounds, a deep-water coral ecosystem, of the NE Atlantic, Deep-Sea Res. Pt. I, 51, 1937-1954, 2004.

Kiriakoulakis, K., Freiwald, A., Fisher, E. and Wolff, G.A.: Organic matter quality and supply to deep-water coral/mound systems of the NW European Continental Margin, Int. J. Earth Sci., 96, 159-170, 2007.

Laberg, J.S. and Vorren, T.O.: The Traenadjupet Slide, offshore Norway - morphology, evacuation and triggering mechanisms, Mar. Geol., 171, 95-114, 2000.

Laberg, J.S., Vorren, T.O., Mienert, J., Evans, D., Lindberg, B., Ottesen, D., Kenyon, N.H. and Henriksen, S.: Late Quaternary palaeoenvironment and chronology in the Traenadjupet Slide area offshore Norway, Mar. Geol., 188, 35-60, 2002.

Lee, C.: Amino acid chemistry and amine biogeochemistry in particulate material and sediments, in: Nitrogen Cycling in Coastal Marine Environments, editied by: Blackburn, T.H. and Sorensen, J., Wiley, 126-141, 1988.

Lee, C. and Cronin, C.: The Vertical Flux of Particulate Organic Nitrogen in the Sea - Decomposition of Amino-Acids in the Peru Upwelling Area and the Equatorial Atlantic, J. Mar. Res., 40, 227-251, 1982.

Lindroth, P. and Mopper, K.: High-Performance Liquid-Chromatographic Determination of Subpicomole Amounts of Amino-Acids by Precolumn Fluorescence Derivatization with Ortho-Phthaldialdehyde, Anal. Chem., 51, 1667-1674, 1979.

Lomstein, B. A., Jørgensen, B. B., Schubert, C. J. and Niggemann, J.: Amino acid biogeo- and stereochemistry in coastal Chilean sediments, Geochim. Cosmochim. Ac., 70, 2970-2989, 2006.

Lomstein, B. A., Niggemann, J., Jørgensen, B. B. and Langerhuus, A. T.: Accumulation of prokaryotic remains during organic matter diagenesis in surface sediments off Peru, Limnol. Oceanogr., 54, 1139-1151, 2009.

Meyers, P. A.: Preservation of Elemental and Isotopic Source Identification of Sedimentary Organic-Matter, Chem. Geol., 114, 289-302, 1994.

Meyers, P. A.: Organic geochemical proxies of paleoceanographic, paleolimnologic, and paleoclimatic processes, Org. Geochem., 27, 213-250, 1997.

Mienis, F., de Stigter, H.C., White, M., Duineveld, G., de Haas, H. and van Weering, T.C.E.: Hydrodynamic controls on cold-water coral growth and carbonate-mound development at the SW and SE Rockall Trough Margin, NE Atlantic Ocean, Deep-Sea Res. Pt. I, 54, 1655-1674, 2007.

Mienis, F., de Stigter, H.C., de Haas, H. and van Weering, T.C.E.: Near-bed particle deposition and resuspension in a cold-water coral mound area at the Southwest Rockall Trough margin, NE Atlantic, Mar. Geol., 265, 40-50, 2009.

Mortensen, P.B., Hovland, M., Brattegard, T. and Farestveit, R.: Deep-Water bioherms of the Scleractinian Coral *Lophelia pertusa* (L) at 64°N on the Norwegian Shelf: structure and associated megafauna, Sarsia, 80, 145-158, 1995.

Mortensen, P.B., Hovland, M.T., Fossa, J.H. and Furevik, D.M.: Distribution, abundance and size of *Lophelia pertusa* coral reefs in mid-Norway in relation to seabed characteristics, J. Mar. Biol. Assoc. UK, 81, 581-597, 2001.

Müller, P. J.: C/N Ratios in Pacific Deep-Sea Sediments - Effect of inorganic ammonium and organic nitrogen-compounds sorbed by clays, Geochim. Cosmochim. Ac., 41, 765-776, 1977.

Muscatine, L., McCloskey, L. R. and Marian, R. E.: Estimating the daily contribution of carbon from zooxanthellae to coral animal respiration, Limnol. Oceanogr., 26, 601-611, 1981.

Niggemann, J.: Composition and degradation of organic matter in sediments from the Peru-Chile upwelling region, PhD thesis, Department of Geosciences, University Bremen, 2005.

Ottesen, D., Rise, L., Knies, J., Olsen, L. and Henriksen, S.: The Vestfjorden-Traenadjupet palaeo-ice stream drainage system, mid-Norwegian continental shelf, Mar. Geol., 218, 175-189, 2005.

Pedersen, A. G. U., Thomsen, T. R., Lomstein, B. A. and Jørgensen, N. O. G.: Bacterial influence on amino acid enantiomerization in a coastal marine sediment, Limnol. Oceanogr., 46, 1358-1369, 2001.

Reed, J. K., Weaver, D. C. and Pomponi, S. A.: Habitat and fauna of deep-water *Lophelia pertusa* coral reefs off the southeastern US: Blake Plateau, Straits of Florida, and Gulf of Mexico, B. Mar. Sci., 78, 343-375, 2006.

Roberts, J.M., Wheeler, A. and Freiwald, A.: Cold-Water Corals: The Biology And Geology Of Deep-Sea Coral Habitats. Cambridge University Press, Cambridge, 334 pp, 2009.

Roberts, J.M., Wheeler, A.J. and Freiwald, A.: Reefs of the Deep: The Biology and Geology of Cold-Water Coral Ecosystems, Science, 312, 543-547, 2006.

Rogers, A.D.: The biology of Lophelia pertusa (LINNAEUS 1758) and other deep-water reef-forming corals and impacts from human activities, Int. Rev. Hydrobiol., 84, 315-406, 1999.

Schubert, C. J. and Calvert, S. E.: Nitrogen and carbon isotopic composition of marine and terrestrial organic matter in Arctic Ocean sediments: implications for nutrient utilization and organic matter composition, Deep-Sea Res. Pt. I, 48, 789-810, 2001.

Schubert, C. J., Niggemann, J., Klockgether, G. and Ferdelman, T. G.: Chlorin Index: A new parameter for organic matter freshness in sediments, Geochem. Geophy. Geosy., 6, 2005.

Steinberg, S. M., Venkatesan, M. I. and Kaplan, I. R.: Organic Geochemistry of Sediments from the Continental-Margin Off Southern New-England, USA –Part I. Amino-Acids, Carbohydrates and Lignin, Mar. Chem., 21, 249-265, 1987.

Templer, S.P., Vasconcelos, C. and McKenzie, J.A.: Microbial community composition and biogeochemical processes in cold-water-coral carbonate mounds in the Gulf of Cadiz, on the Moroccan margin, Mar. Geol., in review.

Thiem, O., Ravagnan, E., Fossa, J. H. and Berntsen, J.: Food supply mechanisms for cold-water corals along a continental shelf edge, Journal of Marine Systems, 60, 207-219, 2006.

Thorsnes, T., Fossa, J.H. and Christensen, O.: Deep-water coral reefs. Acoustic recognition and geological setting, Hydro International, 8, 26-29, 2004.

van Oevelen, D., Duineveld, G., Lavaleye, M., Mienis, F., Soetaert, K. and Heip, C. H. R.: The cold-water coral community as a hot spot for carbon cycling on continental margins: A food-web analysis from Rockall Bank (northeast Atlantic), Limnol. Oceanogr., 54, 1829-1844, 2009.

Vandewiele, S., Cowie, G., Soetaert, K. and Middelburg, J. J.: Amino acid biogeochemistry and organic matter degradation state across the Pakistan margin oxygen minimum zone, Deep-Sea Res. Pt. II, 56, 376-392, 2009.

Wakeham, S. G. and Lee, C.: Production, transport, and alteration of particulate organic matter in the marine water column, in Organic Geochemistry, editied by Engel, M. H. and Macko, S. A., Plenum Press, 145-169, 1993.

Walsh, J. J.: Importance of Continental Margins in the Marine Biogeochemical Cycling of Carbon and Nitrogen, Nature, 350, 53-55, 1991.

Wehrmann, L.M., Knab, N.J., Pirlet, H., Unnithan, V., Wild, C., Ferdelman, T.G.: Carbon mineralization and carbonate preservation in modern cold-water coral reef sediments on the Norwegian shelf, Biogeosciences, 6, 663-680, 2009.

Whelan, J. K.: Amino acids in a surface sediment core of Atlantic Abyssal Plain, Geochim. Cosmochim. Ac., 41, 803-810, 1977.

White, M.: Benthic dynamics at the carbonate mound regions of the Porcupine Sea Bight continental margin, Int. J. Earth Sci., 96, 1-9, 2007.

White, M., Mohn, C., de Stigter, H. and Mottram, G.: Deep-water coral development as a function of hydrodynamics and surface productivity around the submarine banks of the Rockall Trough, NE Atlantic, in: Cold-water corals and ecosystems, edited by: Freiwald, A. and Roberts, J.M., Springer, Heidelberg, 503-514, 2005.

Wienberg, C., Hebbeln, D., Fink, H.G., Mienis, F., Dorschel, B., Vertino, A., López Correa, M., Freiwald, A.: Scleractinian cold-water corals in the Gulf of Cádiz-First clues about their spatial and temporal distribution, Deep-Sea Res. Pt. I, 56, 1873-1893, 2009.

CHAPTER 3:
MICROBIAL DEGRADATION OF COLD WATER CORAL-DERIVED ORGANIC MATTER - POTENTIAL IMPLICATION FOR ORGANIC C CYCLING IN THE WATER COLUMN ABOVE TISLER REEF

Christian Wild[1], Laura M. Wehrmann[1,2], Sandra S. Schöttner[1,2], Christoph Mayr[3], Elke Allers[2], and Thomas Lundälv[4]

[1]Coral Reef Ecology Work Group (CORE), GeoBio-Center and Department of Earth & Environmental Science, Ludwig-Maximilians Universität, Richard Wagner Str. 10, 80333 Munich, Germany

[2]Max Planck Institute for Marine Microbiology, Celsiusstr. 1, 28359 Bremen, Germany

[3]GeoBio-Center and Department of Earth & Environmental Science, Ludwig-Maximilians Universität, Richard Wagner Str. 10, 80333 Munich, Germany

[4]Sven Loven Centre for Marine Sciences, Tjärnö University of Gothenburg, SE-452 96 Strömstad, Sweden

Aquatic Biology, 7, 71-80, 2009

Abstract

Cold water corals release organic matter, in particular mucus, but its role in the ecological functioning of reef ecosystems is still poorly understood. This study investigates planktonic microbial degradation of mucus released by *Lophelia pertusa* colonies from Tisler Reef, Skagerrak. Results are compared to the degradation of dissolved and particulate organic substrates including the carbohydrates glucose and starch as well as gum xanthan and the cyanobacterium *Spirulina* as model organism for phytoplankton. Resulting microbial organic C degradation rates for the dissolved fraction of *Lophelia* mucus showed nearly linear progression over time and revealed similar degradation rates compared to glucose and starch. Degradation of the particulate mucus fraction displayed rather exponential progression and was much faster than degradation of the dissolved fraction. In addition, particulate mucus degradation showed a 4-fold increase compared to those of the added *Spirulina* suspension. Mucus associated microbial communities apparently play a key role in organic matter recycling, as degradation rates more than doubled in untreated compared to sterile coral mucus over 3 d incubation. Quantification of O_2 consumption in the water column above Tisler Reef showed significantly increased values in direct reef vicinity. C stable isotope signatures of suspended POM close to Tisler were close to that of *Lophelia*-derived mucus, and high dissolved organic carbon (DOC) concentrations were detected above Tisler Reef. These findings support the stimulating effect of cold water coral reefs on microbial activity in the adjacent water column and may indicate some control over organic C cycling.

1. Introduction

Cold water coral ecosystems are hotspots of biodiversity hosting a benthic community of more than 1300 reef-associated species (Jensen and Frederiksen, 1992; Mortensen et al., 1995; Freiwald et al., 2004; Roberts and Hirshfield, 2004). The main framework-building, scleractinian corals *Lophelia pertusa* and *Madrepora oculata* rely on food supply transported down from productive surface waters or by redistribution of suspended particulate organic matter in the bottom boundary layer as well as on zooplankton prey in the coral vicinity (Freiwald, 2002; Duineveld et al., 2004; Kiriakoulakis et al., 2004; 2005; White et al., 2005; Roberts et al., 2006). This filter-feeding lifestyle contrasts the main lifestyle of hermatypic warm water corals, which host zooxanthellae, endosymbiotic algae transferring photosynthetically fixed carbon to their host (Muscatine et al., 1981). Carbon and nutrient cycling as well as ecosystem functioning (Goreau et al., 1979; Romaine et al., 1997; Wild et al., 2004) are well studied in tropical coral reef systems. These ecological and biochemical processes are however far less understood in cold water coral reefs, and studies investigating the interrelations between corals and reef-associated organisms, particularly planktonic microbial assemblages, are scarce.

Recent research at Norwegian cold water coral reefs showed that cold water corals release high quantities of particulate and dissolved organic matter, in particular mucus (Wild et al., 2008). The cold water coral-derived mucus represents an attractive organic substrate for planktonic microbial assemblages and stimulates microbial activity in the adjacent water column as evident by high microbial organic matter turnover rates (Wild et al. 2008). The establishment of fauna-microbe interaction may play an important role for ecosystem functioning, e.g. as a vector for carbon and nutrient cycling in the reef system. It also facilitates the generation of specific microbial habitats showing distinct patterns of microbial diversity (Schöttner et al., 2009). Lavaleye et al. (2009) furthermore described a “reef effect” leading to the preferential removal of labile N-rich compounds and, thus, altering the quality of particulate organic matter passing over a cold water coral reef and suggest that cold water coral reef ecosystems do play an important role in C mineralization. High aerobic microbial mineralization of organic matter in the overlying water column and coral framework (Wild et al., 2008) may in addition limit the amount of labile organic material reaching the reef-associated sediments, where extremely low rates of anaerobic C mineralization were detected (Wehrmann et al., 2009).

This pilot study aims to extend the understanding of the interplay between cold water corals and associated planktonic microbial assemblages. It targets the microbial degradability of cold water coral-derived organic material in comparison to other dissolved and particulate organic substrates. Supplementary in-situ studies investigating O2 consumption rates as a proxy for microbial activity and dissolved organic carbon (DOC) as well as particulate organic matter (POM) concentrations and C isotope signatures in the water column above Tisler Reef, Skagerrak, are presented. Studies were conducted in May 2008 by the combined deployment of line attached Niskin bottles and a remotely operated vehicle (ROV), thereby allowing exact tracking of sampling locations in close vicinity to the cold water coral reef.

2. Material and methods

2.1 Study site

Experiments presented in this study were conducted between 20 and 27 May 2008 at Sven Loven Centre for Marine Sciences, Skagerrak, Sweden. In-situ sampling was carried out at 3 neighbouring stations above the central part of the nearby Tisler Reef, Skagerrak (Station 1: 58° 59.902 N, 10° 57.736 E, Station 2: 58° 59.806 N, 10° 57.979 E, Station 3: 58° 59.796, 10° 58.001 E; water depth at all stations ca. 108 - 114 m), close to the border between Sweden and Norway. The Tisler Reef is a relatively large inshore reef (ca. 1200 x 200 m live reef over a depth range of 70 – 160 m), dominated by the hermatypic scleractinian *Lophelia pertusa*.

2.2 Microbial degradation of *Lophelia* mucus and reference substrates

To study the microbial degradation of *Lophelia*-derived mucus in comparison with reference substrates, two independent experiments were conducted, a dissolved and a particulate substrate experiment. In these experiments microbial DOC and POC degradation of *Lophelia*-derived mucus were separately investigated in comparison with different organic substrates, because coral mucus comprises both a dissolved and a particulate fraction (Wild et al., 2004; 2008). Both fractions were separated by filtration through sterile 0.2 µm syringe filters (Millipore). An overview of both experiments with the respective substrates added is given in Table 1. Immediately before each experiment, mucus was freshly collected from 10 to 20 small (lengths: 3 - 10 cm) *Lophelia pertusa* fragments. The fragments were originally sampled from Tisler Reef and kept in 40 l glass aquaria with deep water flow-through (in-situ water pumped from ca. 50 m water

depth and pre-filtered over coarse sand) for between 2 and 60 d prior to the mucus sampling. Mucus was collected by exposing the coral fragments to air for 3 to 5 min. Mucus released during the first minute was discarded, and the subsequent production was collected in glass Petri dishes. When necessary, sterile-filtered seawater (0.2 µm, Millipore) was used to detach mucus from the coral fragments. In total, 200 to 400 ml of diluted mucus (approximately 1:5, mucus:seawater) was retrieved from all coral fragments during the two samplings. *Lophelia* mucus was added to 30 ml Winkler glass bottles in volumes of 5 ml (particulate substrate experiment) and 10 ml (dissolved substrate experiment) with n = 4 replicate volumes for each experiment. Glucose (monohydrate; 2g l^{-1} deep water) and starch (2 g l^{-1} deep water) suspensions were used for the dissolved substrate experiment. For the particulate substrate experiment, in addition to the untreated mucus, also 5 ml sterile *Lophelia*-mucus (heated to ca. 100 °C in a glass vial) were used. As reference substrates, gum xanthan (model mucus without any N components, FLUKA; 1g l^{-1} deep water) and *Spirulina* (phytoplankton model organism) suspensions (Sigma; 1g l^{-1} deep water) were used. For each experiment, the respective reference substrate suspensions (Table 1) were added to Winkler glass bottles (volume: 30 - 120 ml) in replicates of 4. All bottles were subsequently filled with the deep water containing natural microbial assemblages and incubated at in-situ temperature (5 - 6 °C) in a cool room in the dark for an incubation period of 95 h (dissolved substrate experiment) or 69 h (particulate substrate experiment). Deep water without the addition of further substrates was also incubated in replicates of 4 for each experiment as control. O_2 water concentrations in all treatments were measured in time series using Winkler titration (Winkler, 1888), and O_2 consumption rates were calculated by linear regression of all 4 data points. Microbial organic carbon degradation was calculated by relating the resulting O_2 consumption rates to the respective total organic C content of each type of organic matter (measured as described below in replicates of n = 3 – 4, sample volumes: 5 - 10 ml) assuming that 1 mol of organic C is mineralized by 1 mol of O_2.

Table 1. Overview of substrate incubation experiments and respective organic matter addition (n.d. = not determined). All incubation experiments with *Lophelia* mucus, glucose and starch addition took place in 30 ml, gum xanthan incubations in 60 ml, and *Spirulina* as well as control incubations in 120 ml glass bottles.

Experiment	Start date	Incubation duration (h)	Substrate solutions used	DOC concentration (mM)	POC concentration (mM)	Added volumes (ml)	Added DOC (µmol)	Added POC (µmol)
dissolved substrate	20.05.2008	95	*Lophelia* mucus (untreated)	60	n.d.	10	603	
			glucose (monohydrate; 2 g/l deep water)	60	n.d.	10	600	
			starch (2g/l deep water)	74	n.d.	5	370	
			deep water control	3	n.d.			
particulate substrate	24.05.2008	69	*Lophelia* mucus (untreated)	n.d.	2	5		11
			Lophelia mucus (sterile)	n.d.	2	5		11
			gum xanthan (FLUKA; 1g/l deep water)	n.d.	12	10		123
			Spirulina (SIGMA; 1g/l deep water)	n.d.	26	10		259
			deep water control	n.d.	0,003			

2.2 Microbial planktonic activity and organic matter concentrations above Tisler Reef

For this sampling, three 3 l Niskin bottles mounted on a steel cable were deployed from the research vessel R/V Lophelia to collect water samples from various water depths (108 to 114 m) above the central part of Tisler Reef. The lowest Niskin bottle was descended from the research vessel down to the reef. Exact positioning of this bottle was visually verified using simultaneous video survey by the contemporaneously deployed ROV of type Sperre SUB-fighter 7500 DC. With this method it was possible to collect water samples from directly within or shortly above Tisler Reef. During 3 independent deployments, water samples were retrieved from ≤ 1.0 m, 5.0 m and 50.0 m above the reef at each time. In-situ samplings took place during calm days. Parallel ADCP Acoustic Doppler Current Profiler) measurements revealed that the NW-component (the main current direction at Tisler) of the water currents above Tisler reef for the days of our sampling (May 21 and 22) were similar and always less than 10 cm s^{-1} at all stations in the three respective water depths (T. Lundälv, unpublished data).

Within 30 min after retrieval of each water sample, 10 ml aliquots were taken for later measurement of DOC as described below. Within 12 h after sample retrieval (samples were kept at in-situ temperature of 4 - 6 °C in the meantime), 500 ml aliquots were taken for later measurements of POM as described below. In addition, two aliquots from each water sample were filled into two ca. 60 ml Winkler glass bottles for

determination of O_2 concentration at present and after incubation for 106 to 108 h in the dark at *in-situ* temperature in a cold-room using Winkler titration. After this period, O_2 concentration of the incubated water samples was measured as described above and subtracted from the start values to calculate planktonic microbial O_2 consumption as a proxy for microbial activity.

2.3 DOC, POM and isotope analyses

For measurement of dissolved organic carbon (DOC) concentrations, circa 10 ml of the sample solutions were filtered through 0.2 µm sterile syringe filters (polyethersulfone membrane, *VWR Collection*). The first 4 ml of the filtrate were discarded and the following 6 ml were collected in new, pre-combusted glass ampoules, which were instantly frozen at -20 °C and kept frozen until analysis. Samples for DOC measurements retrieved from the water column above Tisler Reef were shock-frozen on the vessel using liquid nitrogen stored in a dry shipper. DOC concentrations were determined by high temperature catalytic oxidation (HTCO) using a Rosemount Dohrmann DC-190 total organic carbon (TOC) analyser. After defrosting, each sample was treated by adding 100 µl of 20 % phosphoric acid and purged with O_2 (using an injection needle) for 5 min to remove dissolved inorganic carbon. DOC concentration of each sample was measured five times. An outlier test was conducted, and the DOC concentrations of the remaining samples were averaged. Potassium hydrogenphtalate was used as standard for calibrating the TOC analyser.

POC and PON concentrations were measured by filtering particulate substrate suspensions and collected water samples onto pre-combusted GF/F filters (Whatman, 25 mm diameter), which were dried for at least 48 h at 40 °C and kept dry until analysis. Respective concentration and isotope measurements were performed with a Carlo Erba NC 2500 elemental analyzer, coupled via a THERMO/Finnigan Conflo II- interface with a THERMO/Finnigan MAT Delta plus isotope ratio mass spectrometer. Elemental concentrations were calculated from certified elemental standards (Atropine, Cyclohexanone-2,4-dinitrophenylhydra-zone; Thermo Quest, Italy) and typically showed standard deviations < 5 %. Carbon stable isotope ratios ($R = {}^{13}C/{}^{12}C$) are given in the conventional delta notation [$\delta^{13}C = (R_{sample}/R_{VPDB} - 1) \cdot 1000$] relative to Vienna PeeDee Belemnite (VPDB) standard (Craig, 1957; Coplen, 1995) and atmospheric nitrogen (Mariotti 1984), respectively. Standard deviations for repeated stable isotope measurements of lab standard (Peptone) were better than 0.15 ‰.

3. Results

3.1 Microbial degradation of Lophelia mucus and reference substrates

The dissolved substrate experiment showed that in all incubations with substrate addition, the O_2 concentration decreased significantly linearly (ANOVA, $p < 0.02$), whereas this was not the case in the seawater control ($p = 0.257$). *Lophelia* mucus was degraded by the microbial assemblage with an O_2 consumption rate of 12.7 μM O_2 d^{-1}, which was similar to rates measured for the glucose (15.4 μM O_2 d^{-1}) and starch (11.3 μM O_2 d^{-1}) incubations (Fig. 1). All three kinds of substrate were 15- to 20-fold faster degraded than the deep-water controls (0.8 μM O_2 d^{-1}). Resulting microbial DOC degradation revealed similar rates for all incubations with added substrates (Table 2).

Statistical analyses of results from the particulate substrate experiment showed that only in the incubation with gum xanthan, the O_2 concentrations decreased significantly linearly (ANOVA, $p < 0.05$). Both the addition of *Spirulina* cells and untreated coral mucus resulted in high microbial O_2 consumption rates of 81.9 and 60.1 μM O_2 d^{-1} if calculated over the total duration of this experiment (Fig. 2). O_2 consumption in the sterile mucus incubation (13.1 μM O_2 d^{-1}) was more than 4-fold lower than that in the untreated mucus incubation and very similar to that in the gum xanthan solution (14.7 μM O_2 d^{-1}). All substrate-amended incubations showed higher microbial O_2 consumption than the controls with natural suspended organic matter (1.9 μM O_2 d^{-1}). The decrease in O_2 concentration was however not linear over the entire incubation period (ANOVA, $p = 0.075$), but showed initially (first day) comparably low microbial O_2 consumption for both, untreated and filtered mucus, with similar rates of 6.4 and 4.3 μM O_2 d^{-1}. The *Spirulina* suspension was degraded very slowly during first day (rate: 0.4 μM O_2 d^{-1}), which was even lower than that of the seawater control (1.0 μM O_2 d^{-1}). After the first day, microbial O_2 consumption rates showed an approximately exponential progression ($R^2 > 0.65$ for both treatments) with maximum values of 120.3 and 225.9 μM O_2 d^{-1} for the third day in the untreated mucus and *Spirulina* incubation, respectively. O_2 concentrations in the other three treatments decreased almost linearly ($R^2 > 0.89$ for sterile mucus, gum xanthan and seawater control). Overall, resulting planktonic microbial organic matter degradation rates were much higher for the particulate compared to the dissolved substrates. Highest rates were determined for the untreated *Lophelia* mucus with an about 4-fold higher value compared to the *Spirulina* solution. Gum xanthan represents an unfavourable organic substrate for microbial respiration as indicated by the low degradation rates (Table 2).

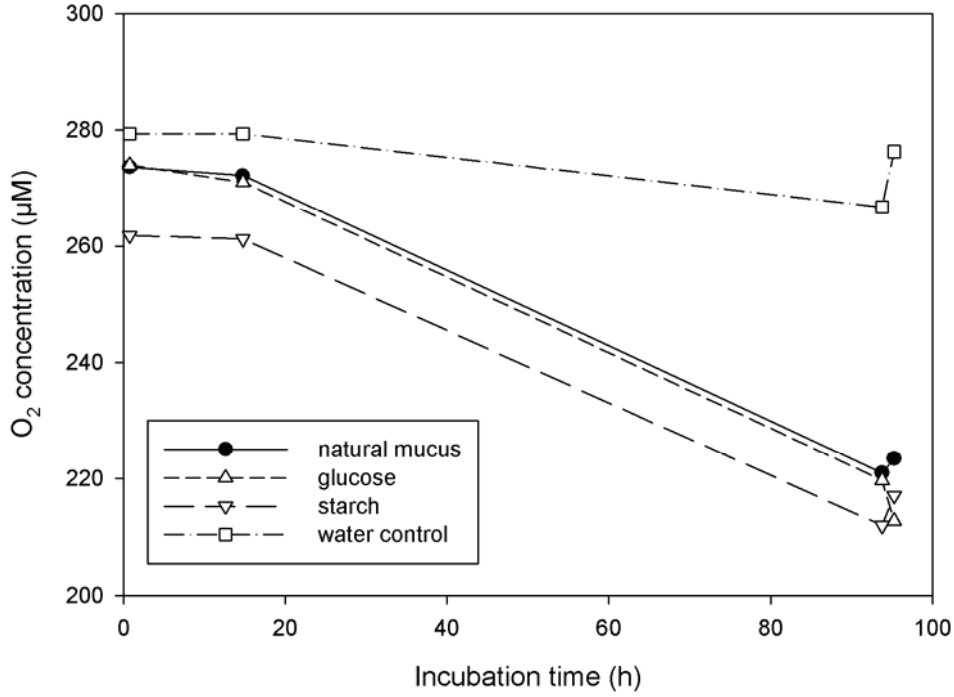

Figure 1: O_2 concentration decrease during dissolved substrate incubation experiment. Mucus was collected from Lophelia pertusa fragments.

Table 2. Summary of microbial carbon degradation rates for the substrates used in both experiments. O_2 consumption values are corrected for the respective background respiration in the controls and the volumes in the incubation bottles.

Experiment	Substrate suspensions used	Added DOC (µmol)	Added POC (µmol)	O_2 consumption (µmol d^{-1})	Organic matter degradation (% d^{-1})
Dissolved substrate	*Lophelia* mucus	603		0.33	0.05
	Glucose	600		0.42	0.07
	Starch	370		0.29	0.08
Particulate substrate	*Lophelia* mucus		11	1.58	15.0
	Gum xanthan		123	0.66	0.5
	Spirulina		259	9.61	3.7

3.2 Microbial planktonic activity above Tisler Reef

Analysis of microbial activity in water samples collected from three different stations at three depths above Tisler Reef revealed that microbial O_2 consumption was very similar and not significantly different between ≤ 1 m (11.9 ± 2.0 µM O_2 d^{-1}) and 5 m above the reef (12.1 ± 2.8 µM d^{-1}), but significantly higher ($p < 0.02$, two tailed U-test after Wilcoxon, Mann and Whitney) compared to 50 m above the reef (8.2 ± 0.4 µM d^{-1}), i.e. in the middle of the water column (Fig. 3a).

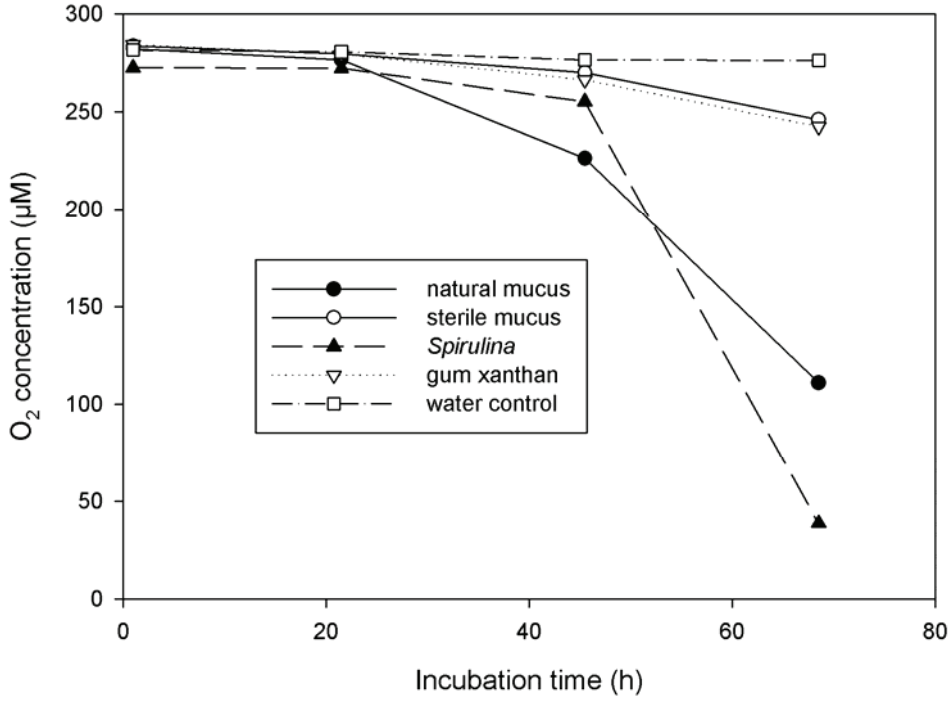

Figure 2: O_2 concentration decrease during particulate substrate incubation experiment. Both kinds of mucus were collected from Lophelia pertusa fragments. For the phytoplankton treatment a suspension containing the cyanobacterium Spirulina was used.

3.3 POM, DOC and $\delta^{13}C$ distribution above Tisler Reef

POC and PON concentrations in the water column above Tisler Reef showed high variability and no significant differences ($p > 0.05$, two tailed U-test after Wilcoxon, Mann and Whitney) between the three investigated water depths (Fig. 3b). DOC water concentrations above Tisler Reef were very high with maximum values of 55 ± 32 mM in direct reef vicinity. However, similar to POM, DOC concentrations were highly variable and therefore not significantly different between the two stations directly above Tisler Reef and the mid-water column station at 50 m water depth, which showed a DOC concentration of 15 ± 12 mM (Fig. 3c).

The C:N ratio of POM suspended in the water column above Tisler Reef was highly variable at the deepest station (Table 3) and not significantly different from the other stations.

$\delta^{13}C$ signatures of suspended POM revealed significantly more positive values at the two stations close to Tisler Reef compared to the mid-water column station ($p < 0.02$, two tailed U-test after Wilcoxon, Mann and Whitney). The $\delta^{13}C$ values of suspended POM at the deep stations were close to those measured in the *Lophelia* mucus suspensions used in the laboratory incubation experiments (Table 3).

4. Discussion

4.1 Degradability of *Lophelia*-derived mucus and associated microbial activity

The present study broadens our understanding of the microbial degradability of cold water coral-derived organic material, particularly mucus. The dissolved substrate experiment showed that *Lophelia* mucus was degraded at similar rates as the standard carbohydrate components glucose and starch commonly used as main carbon source in culture media in the field of microbiology. Furthermore, the particulate substrate experiment showed that *Lophelia* mucus was degraded at a similar rate as the added *Spirulina* suspension, which represents a model organism for phytoplankton. These findings emphasize the attractiveness of *Lophelia* mucus as substrate for marine bacteria and potentially other microbes, including archaea, fungi and protozoans, which are described as primary consumers of warm and temperate water coral-derived organic matter (Ducklow and Mitchell, 1979; Ducklow, 1990; Wild et al., 2004a; 2004b; 2005). The microbial community inhabiting *Lophelia* mucus apparently plays a key role in the degradation of this organic material as revealed by the pronounced differences in microbial degradation rates between the untreated and sterile mucus incubations. This can be explained by mucus-specific microbial communities as described for warm water corals (Ritchie and Smith, 2004; Ritchie, 2006; Koopermann et al., 2007; Allers et al., 2008). Such an explanation is also supported for cold water corals by the studies of Neulinger et al. (2008) and Kellogg et al. (in press), which indicate that *Lophelia*-specific microbial communities exist. Furthermore, the study of Schöttner et al. (2009) showed that different *Lophelia*- and *Madrepora*-generated habitats, including the coral mucus surface layer, offer niches for specific microbial communities.

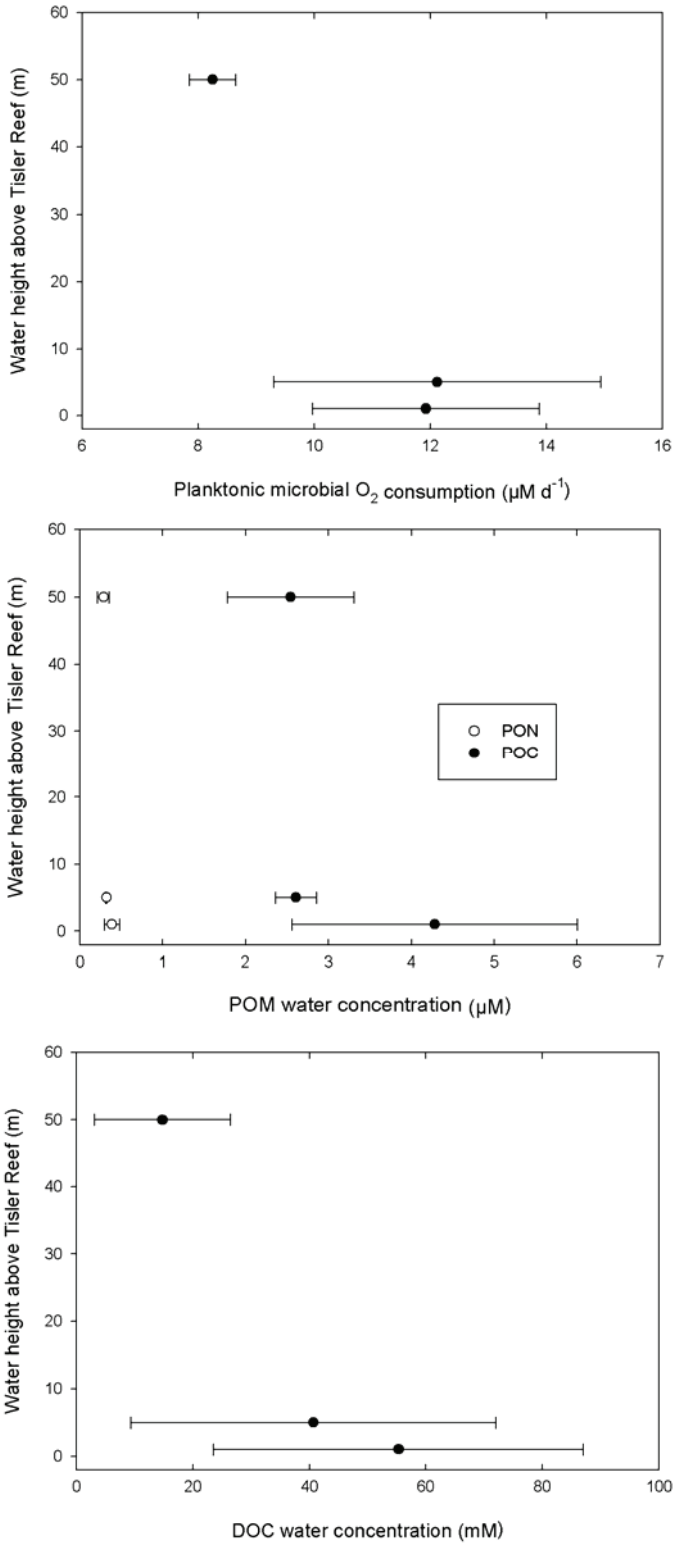

Figure 3: Microbial O_2 consumption (upper panel) along with POM (middle panel) and DOC (lower panel) concentrations above Tisler Reef. Values are means ± SD of 3 replicate in-situ samplings at three different Tisler Reef locations over a total period of ca. 5 h on 22 May 2008.

The finding that *Lophelia*-derived mucus is much faster degraded by microbes than gum xanthan as model for mucus and organic reference substrate for coral mucus may be explained by the missing N-components in gum xanthan. Bacterial production in the degradation of fresh marine POM was reported to correlate best with PON (Grossart and Ploug, 2001), and the low C:N ratios observed in cold-water coral derived mucus hint to high PON contents (Wild et al., 2008).

Table 3, C:N ratios and C stable isotope signature of suspended POM in the water column above Tisler Reef in comparison to particulate substrates used in the laboratory incubation experiments. Values are averages ± SD of n = 3-4 replicate measurements each (n.a. = not applicable).

	C:N ratio	$\delta^{13}C$
In-situ water sampling		
≤ 1m above reef	12 ,0 ± 3,7	-23,7± 0,3
5 m above reef	9,0 ± 1,0	-23,8 ± 0,3
50 m above reef	8,6 ± 0,6	-25,2 ± 0,5
Laboratory substrates		
Lophelia mucus	5,7 ± 0,3	-23,1± 1,0
Spirulina	4,4 ± 0,1	-20,9 ± 0,1
gum xanthan	n.a.	-24,8± 0,5

Microbial activity measured as O_2 consumption was very similar in the mucus incubation of the dissolved substrate experiment (12.7 µM O_2 d^{-1}) compared to all water samples collected from within and less than 5 m above Tisler Reef (11.9 - 12.1 µM O_2 d^{-1}). This may indicate that *Lophelia* mucus was a main component of the organic matter suspended in waters neighbouring Tisler Reef and controlled microbial activity. Such an assumption is further supported by the $\delta^{13}C$ values of POM suspended in the water column close to the reef showing similar values as *Lophelia*-derived mucus used in the laboratory incubation experiments of the present study. In addition, Wild et al. (2008) demonstrated that both dissolved (47 ± 19 mg DOC m^{-2} d^{-1}) and particulate (1.4 ± 1.2 mg POC m^{-2} d^{-1}) organic carbon can be released in high quantities into the surrounding water column by *Lophelia pertusa*.

Microbial O_2 consumption in the water column above Tisler Reef revealed a similar gradient as described by Wild et al. (2008) for Røst Reef, but with more than doubled maximum values in direct vicinity of Tisler (12.5 – 14.3 µM O_2 d^{-1}) compared

to Røst Reef (5.4 µM O_2 d^{-1}). This indicates that planktonic microbial activity is generally stimulated by the influence of cold water coral reefs and suggests that microbial assemblages in the immediate reef vicinity contribute to the turnover of organic carbon in the reef ecosystem. The higher microbial activity at directly above the reef observed in the present study may not be explained by the closer proximity of the water sample origin relative to the respective coral reef (< 1m above Tisler Reef compared to 4-5 m above Røst Reef), which was attained through video-assisted sampling, because also the microbial activity at 5 m above Tisler Reef was clearly higher than at the same height above Røst Reef. Differences in bottom water temperature (5 - 6 °C at both reef locations), which could potentially also have an effect on microbial activity, are obviously also not the reason for the observed differences. Thus, organic matter availability may be the key factor in controlling microbial activity close to cold water coral reefs.

The present study on Tisler Reef thus confirms some of the main findings of the study conducted by Wild et al. (2008) on reefs off Northern Norway, in particular that a) cold water coral-derived mucus represents an attractive substrate for the associated microbial assemblages, and b) that microbial activity in the water column in close proximity to a cold water coral reef is elevated. The results of the present study thereby extend the spatial validity of those previous findings and further support the hypothesis that cold water coral-derived organic matter may have an important ecological function as carrier of energy from the corals to a range of (primarily microbial) consumers. Although the stimulation of microbial activity above Tisler Reef was less pronounced than described for Røst Reef (Wild et al., 2008), it was detectable despite the more eutrophic character of the Skagerrak (especially during the study period in spring with phytoplankton blooms) compared to the more oligotrophic Norwegian Sea (Freiwald et al., 2004).

4.2 Carbon cycling in the reef and the potential role of coral mucus in ecosystem functioning

The present study showed that both particulate and dissolved organic matter concentrations are high in direct reef vicinity. Concentrations of POC (22 to 80 µg l^{-1}) and PON (3 to 6 µg l^{-1}) in the water column above Tisler Reef were in the range of values reported from the water column above Røst Reef in the Norwegian Sea (Wild et al., 2008). DOC concentrations in the water column above Tisler Reef were very high

with values of 55 ± 32 mM. These values exceed reported DOC concentrations of the deep ocean by three orders of magnitude (Hansell and Carlson, 1998) and concentrations reported from estuaries (Guo and Santschi, 1997; Guo and Santschi 2000; Klinkhammer et al., 2000; Lobbes et al., 2000) or warm water coral reefs (van Duyl and Gast, 2001; De Goeij and Van Duyl, 2007) by more than one order of magnitude. The data of the present study are furthermore supported by high DOC concentrations of 0.5 to 1.8 mM measured in water samples collected from the high-latitude Røst Reef during RV Polarstern cruise ARKXXII/1a in June 2007 (Wild et al., unpublished data). Contamination of samples can be largely excluded, as new pre-combusted ampoules were used for sample collection, and samples were immediately frozen onboard after collection.

The reported DOC values indicate the presence of a high pool of easily degradable labile DOC available to the associated planktonic microbial community. DOC concentrations in the upper part of the water column can be attributed to exudates of the declining spring phytoplankton bloom (Dafner and Wangersky, 2002). The increase of DOC concentrations close to the reef surface however indicates that further sources contribute to the DOC pool at the reef sites. The most likely source is organic matter production and release by the reef biota, particularly corals, which occur in high abundances at Tisler Reef (Roberts and Hirshfield, 2004; Fossaa et al., 2005).

Ferrier-Pages et al. (1998; 2000) showed that the uptake of heterotrophic nutrition serves warm water corals as a source for nutrients, e.g. nitrogen and phosphorous, while the surplus of carbon taken up is subsequently released again as DOC. Lavaleye et al. (2009) suggested that cold water coral reefs in contrast serve as a filter for high quality particulate organic matter as evident by the preferential removal of labile N-rich components during the passage over Tisler Reef and also indicated by the particulate substrate experiment of the present study. Contemporaneously, Wild et al. (2008) showed that cold water coral-derived mucus is characterized by C:N ratios close to or even below the Redfield ratio (= ca. 6.6), which describes the typical molar C:N:P ratio for phytoplankton as 106:16:1. These findings suggest a transfer of N from the particulate to the dissolved fraction and argue against a comparable mechanism of nitrogen retention in cold-water coral ecosystems as previously described for warm water coral reefs. Instead, findings of the present study may indicate that cold-water corals actively release labile organic matter and stimulate heterotrophic bacteria in the adjacent water column. This is also supported by the fast degradation of coral mucus in

comparison to other labile compounds, e.g. glucose and starch, during the dissolved substrate experiment presented in this study.

Reef associated fauna, particularly corals, consume POC that is transported down from the productive surface layer (Kiriakoulakis et al., 2005), and in turn can release organic carbon with a high DOC:POC ratio (Wild et al., 2008). While POC concentrations do not seem to change greatly between the beginning and end of the passage over Tisler Reef (Lavaleye et al., 2009), obviously high amounts of DOC are released, which accumulate in reef adjacent waters. This may indicate that C transferred down from primary production in the surface layers may undergo several cycles by the DOC-microbial food chain before storage or loss from the system by deposition, current transport or transformation into refractory DOC that cannot be mineralised on short time scales. Such a theoretical concept termed "network virtual amplification" (Higashi et al., 1993) has been previously suggested in relation to DOC-food web dynamics. It implies that no new energy is created, but the amount of available energy is increased due to recycling. Via the release of labile components such as mucus, corals may act as main drivers of this recycling mechanism and assure a fast re-entrance into the food web via recycling by heterotrophic bacteria, which in turn are consumed by e.g. protozoa so that loss into the overlying water column is prevented. The chemical composition of cold water coral-derived organic matter with its low C:N ratio (Wild et al., 2008) may facilitate this process. It results in longer C retention in the coral reef system, thus effectively sustaining C availability during times of low input from outside, e.g. during winter times when phytoplankton activity and thus supply of "fresh material" is limited (Roberts et al., 2006). Scleractinian corals themselves are known to feed on pico- and nanoplankton including bacteria and protozoa (Houlbreque et al. 2004, Houlbrèque et al., 2006). Low $\delta^{15}N$ values of *Lophelia*- and *Madrepora*-derived mucus (Wild et al., 2008) are in agreement to these explanations as they indicate the input of N from autochthonous microbial sources.

The retention of essential nutrients such as N is likely of less importance in cold compared to warm water corals reefs, while the supply of C is of higher importance due to the high need of heterotrophic feeding for cold water corals. The present study may therefore indicate that cold water corals assure their long-term C supply by the actual release of C, which may represent a new mechanism of C storage in the reef system. Planktonic heterotrophic bacteria fulfil an important function in trophodynamics, because they can convert coral-derived DOC to POC, thereby making it available for

higher trophic levels again. But also sponges, which occur in high abundances in cold-water coral reef ecosystems, may benefit from the release of high amounts of DOC, because it is known that sponge-microbe consortia can fix DOC in cold water coral reef ecosystems (van Duyl et al., 2008).

The release of organic matter by cold water corals and its subsequent microbial consumption therefore potentially depicts a newly described combined assimilatory-dissimilatory process (Jones et al., 2006), while the trapping of suspended particles and formation of aggregates induced by coral-derived organic material in warm water coral reef ecosystems (Wild et al., 2004) represents true ecosystem engineering (Jones et al., 1997), because it involves several modifications on the physical properties of particles (e.g. aggregation, sedimentation rate) suspended in reef waters.

References

Allers, E., Niesner, C., Wild, C. and Pernthaler, J.: Microbes enriched in seawater after the addition of coral mucus, Appl. Environ. Microbiol., 74, 10, 3274-3278, 2008.

Coplen, T.B.: Reporting of stable hydrogen, carbon, and oxygen isotopic abundances (Technical Report), Geothermics, 24, 707-712, 1995

Craig, H.: Isotopic standards for carbon and oxygen and correction factors for mass-spectrometric analysis of carbon dioxide, Geochim. Cosmochim. Ac., 12,133-149, 1957.

Dafner, E.V. and Wangersky, P.J.: A brief overview of modern directions in marine DOC studies Part II - Recent progress in marine DOC studies, J. Environ. Monit., 4, 55-69, 2002.

De Goeij, J.M. and Van Duyl, F.C.: Coral cavities are sinks for dissolved organic carbon (DOC), Limnol. Oceanogr., 52, 2608-2617, 2007.

Ducklow, H. and Mitchell, R.: Bacterial populations and adaptations in the mucus layers on living corals, Limnol. Oceanogr., 24, 715-725, 1979.

Ducklow, H.W.: The biomass, production and fate of bacteria in coral reefs, in: Coral reefs, ecosystems of the world, editied by: Dubinsky, Z., Vol 25. Elsevier, Amsterdam, 265-289, 1990.

Duineveld, G.C.A., Lavaleye, M.S.S. and Berghuis, E.M.: Particle flux and food supply to a seamount cold-water coral community (Galicia Bank, NW Spain), Mar. Ecol. Prog. Ser., 277, 13-23, 2004.

Ferrier-Pages, C., Gattuso, J.P., Cauwet, G., Jaubert, J. and Allemand, D.: Release of dissolved organic carbon and nitrogen by the zooxanthellate coral *Galaxea fascicularis*, Mar. Ecol. Prog. Ser., 172, 265-274, 1998.

Ferrier-Pages, C., Leclercq, N., Jaubert, J. and Pelegri, S.P.: Enhancement of pico- and nanoplankton growth by coral exudates, Aquat. Micr. Ecol., 21, 203-209, 2002.

Fossa, J.H., Lindberg, B., Christensen, O., Lundälv, T., Svellingen, I., Mortensen, P.B. and Alvsvaag, J.: Mapping of *Lophelia* reefs in Norway: experiences and survey methods, in: Cold-water corals and ecosystems, edited by Freiwald, A., Roberts, J.M., Springer, Berlin Heidelberg, 359-391, 2005.

Freiwald, A.: Reef-forming cold-water corals, in: Ocean Margin Systems, edited by: Wefer, G., Billett, D., Hebbeln, D., Jørgensen, B.B., Schlüter, M. and van Weering, T.C.E., Springer, Heidelberg, 365-385, 2002.

Freiwald, A., Fossa, J.H., Grehan, A., Koslow, T. and Roberts, J.M.: Cold-water coral reefs, Vol 1. UNEP-WCMC, Cambridge, UK, 2004.

Goreau, T.F., Goreau, N.I. and Goreau, T.J.: Corals and coral reefs. Sci. Am., 241, 124-135, 1979.

Grossart, H.P. and Ploug, H.: Microbial degradation of organic carbon and nitrogen on diatom aggregates, Limnol. Oceanogr., 46, 267-277, 2001.

Guo, L. and Santschi, P.H.: Isotopic and elemental characterization of colloidal organic matter from the Chesapeake Bay and Galveston Bay, Mar. Chem., 59, 1-15, 1979.

Guo, L.D. and Santschi, P.H.: Sedimentary sources of old high molecular weight dissolved organic carbon from the ocean margin benthic nepheloid layer, Geochim. Cosmochim. Ac., 64, 651-660, 2000.

Hansell, D.A. and Carlson, C.A.: Deep ocean gradients in dissolved organic carbon concentrations, Nature 395:263-266, 1998.

Henry, L.A. and Roberts, J.M.: Biodiversity and ecological composition of macrobenthos on cold-water coral mounds and adjacent off-mound habitat in the bathyal Porcupine Seabight, NE Atlantic, Deep-Sea Res. Pt. I, 54, 654-672, 2007.

Higashi, M., Patten, B.C. and Burns, T.P.: Network trophic dynamics—the modes of energy-utilization in ecosystems, Ecol. Model., 66, 1-42, 1993.

Houlbrèque, F., Delesalle, B., Blanchot, J., Montel, Y. and Ferrier-Pagès, C.: Picoplankton removal by the coral reef community of La Prévoyante, Mayotte Island, Aquat. Microb. Ecol., 44, 59-70, 2006.

Houlbreque, F., Tambutte, E., Richard, C. and Ferrier-Pages, C.: Importance of micro-diet for scleractinian corals, Mar. Ecol. Prog. Ser., 282, 151-160, 2004.

Jensen, A. and Frederiksen, R.: The fauna associated with the bank-forming deep-water coral *Lophelia pertusa* (Scleractinaria) on the Faroe Shelf, Sarsia, 77, 53-69, 1992.

Jones, C.G., Lawton, J.H. and Shachak, M.: Positive and negative effects of organisms as physical ecosystem engineers, Ecology, 78, 1946-1957, 1997.

Jones, C.G., Gutiérrez, J.L., Groffmana, P.M. and Shachaka, M.: Linking ecosystem engineers to soil processes: a framework using the Jenny State Factor Equation, Europ. J. Soil. Biol., 42, 39-53, 2006.

Kellogg, C.A., Lisle, J.T. and Galkiewicz, J.P.: Culture-independent characterization of bacterial communities associated with the cold-water coral *Lophelia pertusa* in the Northeastern Gulf of Mexico, Appl. Environ. Microbiol., 75, 8, 2294-2303, 2009.

Kiriakoulakis, K., Bett, B.J., White, M. and Wolff, G.A.: Organic biogeochemistry of the Darwin Mounds, a deep-water coral ecosystem, of the NE Atlantic, Deep-Sea Res. Pt. I, 51, 1937-1954, 2004.

Kiriakoulakis, K., Fisher, E., Wolff, G.A., Freiwald, A., Grehan, A. and Roberts, J.M.: Lipids and nitrogen isotopes of two deep-water corals from the North-East Atlantic: initial results and implications for their nutrition, in: Cold water corals and ecosystems, editied by: Freiwald, A. and Roberts, J.M., Springer, Berlin Heidelberg, 715-729, 2005.

Klinkhammer, G.P., McManus, J., Colbert, D. and Rudnicki, M.D.: Behavior of terrestrial dissolved organic matter at the continent-ocean boundary from high-resolution distributions, Geochim. Cosmochim. Ac., 64, 2765-2774, 2000.

Koopermann, N., Ben-Dov, E., Kramarsky-Winter, E., Barak, Z. and Kushmaro, A.: Coral mucus-associated bacterial communities from natural and aquarium environments, FEMS Microbiol. Let., 276, 106-113, 2007.

Lavaleye, M., Duineveld, G., Lundälv, T., White, M., Guihen, D., Kiriakoulakis, K. and Wolff, G.A.: Cold-water corals on the Tisler Reef, Oceanogr., 22, 54-62, 2009.

Lobbes, J.M., Fitznar, H.P. and Kattner, G.: Biogeochemical characteristics of dissolved and particulate organic matter in Russian rivers entering the Arctic Ocean, Geochim. Cosmochim. Ac., 64, 2973-2983, 2000.

Mariotti, A.: Atmospheric nitrogen is a reliable standard for natural ^{15}N abundance measurements, Nature, 303, 685-687, 1984.

Mortensen, P.B., Hovland, M., Brattegard, T. and Farestveit, R.: Deep water bioherms of the scleractinian coral *Lophelia pertusa* at 64° on the Norwegian Shelf - structure and associated megafauna, Sarsia, 80, 145-158, 1995.

Muscatine, L., McCloskey, L.R. and Marian, R.E.: Estimating the daily contribution of carbon from zooxanthellae to coral animal respiration, Limnol. Oceanogr., 26, 601-611, 1981.

Neulinger, S.C., Järnegren, J., Ludvigsen, M., Lochte, K., Dullo, W.C.: Phenotype-specific bacterial communities in the cold-water coral *Lophelia pertusa* (Scleractinia) and their implications for the coral's nutrition, health, and distribution, Appl. Environ. Microbiol., 74, 7272-7285, 2008.

Ritchie, K.B.: Regulation of microbial populations by coral surface mucus-associated bacteria, Mar. Ecol. Prog. Ser., 322, 1-14, 2006.

Ritchie, K.B. and Smith, G.W.: Microbial communities of coral surface mucopolysaccharide layers, Springer, Berlin, Germany, 2004.

Roberts, J.M., Wheeler, A.J. and Freiwald. A.: Reefs of the deep: The biology and geology of cold-water coral ecosystems, Science, 312, 543-547, 2006.

Roberts, S. and Hirshfield, M.: Deep-sea corals: out of sight, but no longer out of mind, Front. Ecol. Environ., 2, 123-130, 2004.

Romaine, S., Tambutte, E., Allemand, D. and Gattuso, J.P.: Photosynthesis, respiration and calcification of a zooxanthellate scleractinian coral under submerged and exposed conditions, Mar. Biol., 129, 175-182, 1997.

Schöttner, S., Hoffmann, F., Wild, C., Rapp, H. T., Boetius, A., Ramette, A.: Inter- and intra-habitat bacterial diversity associated with cold-water corals, ISME Journal, 3, 756-759, 2009.

van Duyl, F.C. and Gast, G.J.: Linkage of small-scale spatial variations in DOC, inorganic nutrients and bacterioplankton growth with different coral reef water types, Aquat. Micro. Ecol, 24, 17-26, 2001.

van Duyl, F.C., Hegeman, J.A.H., Maier, C.: Dissolved carbon fixation by sponge-microbe consortia of deep water coral mounds in the northeastern Atlantic Ocean, Mar. Ecol. Prog. Ser., 358, 137-150, 2008.

Wehrmann, L.M., Knab, N.J., Pirlet, H., Unnithan, V., Wild, C. and Ferdelman, T.G.: Carbon mineralization and carbonate preservation in modern cold-water coral reef sediments on the Norwegian shelf, Biogeosciences, 6, 663-680, 2009.

White, M., Mohn, C., de Stigter, H. and Mottram, G.: Deep-water coral development as a function of hydrodynamics and surface productivity around the submarine banks of the Rockall Trough, NE Atlantic, in: Cold-water corals and ecosystems, edited by: Freiwald, A. and Roberts, J.M., Springer, Heidelberg, 503-514, 2005.

Wild, C., Huettel, M., Klueter, A., Kremb, S.G., Rasheed, M. and Jørgensen, B.B.: Coral mucus functions as an energy carrier and particle trap in the reef ecosystem, Nature, 428, 66-70, 2004.

Wild, C., Mayr, C., Wehrmann, L., Schöttner, S., Naumann, M., Hoffmann, F. and Rapp, H.T.: Organic matter release by cold water corals and its implication for fauna-microbe interaction, Mar. Ecol. Prog. Ser., 372, 67-75, 2008.

Wild, C., Rasheed, M., Jantzen, C., Cook, P., Struck, U., Huettel, M., Boetius, A.: Benthic metabolism and degradation of natural particulate organic matter in carbonate and silicate reef sands of the northern Red Sea, Mar. Ecol. Prog. Ser., 298, 69-78, 2005.

Winkler, L.W.: The determination of dissolved oxygen in water, Ber. Deutsch. Chem. Ges., 21, 2843-2857, 1988.

CHAPTER 4:

ORGANIC MATTER RELEASE BY COLD WATER CORALS AND ITS IMPLICATION FOR FAUNA–MICROBE INTERACTION

Christian Wild[1], Christoph Mayr[2], Laura Wehrmann[1,3], Sandra Schöttner[1,3], Malik Naumann[1], Friederike Hoffmann[3], Hans Tore Rapp[4]

[1]Coral Reef Ecology Work Group (CORE), GeoBio-Center and Department of Earth & Environmental Science, Ludwig-Maximilians Universität, Richard Wagner Str. 10, 80333 Munich, Germany

[2]GeoBio-Center and Department of Earth & Environmental Science, Ludwig-Maximilians Universität, Richard Wagner Str. 10, 80333 Munich, Germany

[3]Max Planck Institute for Marine Microbiology, Celsiusstr. 1, 28359 Bremen, Germany

[4]University of Bergen, Centre for Geobiology and Department of Biology, PO Box 7800, Bergen, Norway

Marine Ecology Progress Series, 372, 67-75, 2008

Abstract

Particulate (POM) and dissolved organic matter (DOM) released by the cold water corals *Lophelia pertusa* (L.) and *Madrepora oculata* (L.) was collected, analysed and quantitatively compared to that released by warm water reef-building corals. Particulate nitrogen (PN) and particulate organic carbon (POC) release rates of *L. pertusa* were 0.14 ± 0.07 mg N m^{-2} h^{-1} and 1.43 ± 1.22 mg C m^{-2} h^{-1}, respectively, which is in the lower range of POM release rates measured for warm water corals, while dissolved organic carbon (DOC) release was 47 ± 19 mg C m^{-2} h^{-1}. The resulting high DOC:POC ratio indicates that most cold water coral-derived organic matter immediately dissolved in the water column. Cold water corals, similar to their warm water counterparts, produced large amounts of nitrogen-rich coral mucus with C:N ratios of 5 to 7 for *Lophelia*- and 7 to 9 for *Madrepora*-derived mucus. A 7-fold increase in the oxygen consumption rates in cold water coral mucus-amended seawater containing the natural microbial assemblage indicates that this organic matter provided an attractive food source for pelagic microbes. *In situ* investigations at Røst Reef, Norway, showed that microbial activity in the seawater closest to the reef was 10 times higher than in the overlying water column. This suggests that cold water corals can stimulate microbial activity in the direct reef vicinity by the release of easily degradable and nutrient-rich organic matter, which may thereby function as a vector for carbon and nutrient cycling via the microbial loop in cold water coral reef systems.

CHAPTER 5:

EFFECTS OF SEDIMENTATION LOAD AND SEDIMENT TYPE ON THE COLD-WATER CORAL *LOPHELIA PERTUSA*

Elke Allers[1*], Raeid M. M. Abed[1,2], Laura M. Wehrmann[1,3], Tao Wang[1], Ann I. Larsson[4], Autun Purser[5], Dirk de Beer[1]

[1] Max Planck Institute for Marine Microbiology, Celsiusstr. 1, 28359 Bremen, Germany

[2] Current affiliation: Sultan Qaboos University, College of Science, Biology Department, P.O. Box: 36, Postal Code 123, Al Khoud, Sultanate of Oman

[3] Coral Reef Ecology Group (CORE), GeoBio-Center & Department of Earth and Environmental Science, Ludwig-Maximilians Universität, Richard Wagner Str. 10, 80333 München, Germany

[4] Department of Marine Ecology, Tjärnö, University of Gothenburg, 452 96 Strömstad, Sweden

[5] Jacobs University Bremen, Campus Ring 1, 28759 Bremen, Germany

Submitted to *Coral reefs*

Abstract

The present study investigated by experiments whether or not sedimentation events can negatively affect the cold-water coral *Lophelia pertusa.* Fragments of live corals were collected from the Tisler Reef in the Norwegian Skagerrak and were in the laboratory exposed to various concentrations of fine particulate material collected from the vicinity of the reef or drill cuttings from oil drilling projects. Due to their branching morphology and mucus release, sedimentation of resuspended material on *L. pertusa* resulted only in low coverage rates. Microsensor measurements showed that on coral surfaces where sediments were not wholly cleared following exposure, anoxia at the coral-sediment interface developed within 7-11 days. However, *L. pertusa* did not display visible signs of damage. Only complete burial of coral branches for > 24 h in anoxic sediment resulted in coral death. H_2S production was only indicated in a few of the experimental samples, and consequently the risk of exposure of the coral tissue to sulfide during sediment coverage events appears to be low. Sulfate reduction rates in *L. pertusa* reef sediment slurries were also low. In conclusion, *L. pertusa* is likely to survive short-term sedimentation events provided they do not lead to complete burial.

PART II:

DIAGENETIC PROCESSES IN COLD-WATER CORAL MOUNDS

CHAPTER 6:

THE IMPRINT OF METHANE SEEPAGE ON THE GEOCHEMICAL RECORD AND EARLY DIAGENETIC PROCESSES IN COLD-WATER CORAL MOUNDS ON PEN DUICK ESCARPMENT, GULF OF CADIZ

Laura M. Wehrmann[a,b], Stefanie P. Templer[c,1], Benjamin Brunner[a], Stefano M. Bernasconi[c], Lois Maignien[d] and Timothy G. Ferdelman[a]

[a] Biogeochemistry Research Group, Max Planck Institute for Marine Microbiology, Celsiusstrasse 1, 26129 Bremen, Germany

[b] Coral Reef Ecology Work Group (CORE), GeoBio-Center, Ludwig-Maximilans Universität, Richard-Wagner-Strasse 10, D-80333 München, Germany

[c] Swiss Federal Institute of Technology (ETH) Zurich, Geological Institute, Universitätstrasse 16, 8092 Zürich, Switzerland

[d] Laboratory of Microbial Ecology and Technology, Faculty of Bioengineering, Ghent University, Coupure Links 653, 9000 Gent, Belgium

[1] Present address: Earth, Atmospheric and Planetary Sciences, Massachusetts Institute of Technology, 77 Mass Avenue, E25-625, Cambridge, MA 02139, USA

***Marine Geology,* in revision**

Abstract

The diagenetic history and biogeochemical processes in three cold-water coral mounds located in close proximity to each other on Pen Duick Escarpment in the Gulf of Cadiz were examined. The influence of ascending methane-rich fluids from underlying sediment strata delineated two mound groups: Alpha and Beta Mound showed evidence for the presence of a sulfate-methane transition zone (SMTZ) at shallow depth, whereas Gamma Mound appeared to lack a shallow SMTZ. In the methane-influenced Alpha and Beta Mound, upward diffusion of hydrogen sulfide from the shallow SMTZ caused extensive pyritization of reactive iron phases as indicated by values for the degree of pyritization >0.7. This secondary pyritization overprinted the sulfur isotope composition of sulfides formed during organoclastic sulfate reduction. The almost complete consumption of reactive iron phases by upward diffusing sulfide limited dissimilatory iron reduction to the top layer in these mounds while organic matter in the pyritized zones below was primarily degraded by organoclastic sulfate reduction. Hydrogen sulfide produced during sulfate reduction coupled to the anaerobic oxidation of methane (AOM) diffused upward and induced aragonite dissolution as evidenced in strongly corroded corals in Alpha Mound. This mound has been affected by strong fluctuations in the depth of the SMTZ, as observed by distinct layers with abundant diagenetic high-Mg calcite with a ^{13}C-enriched carbon isotope composition. In the non-methane influenced Gamma Mound low sulfate reduction rates, elevated concentrations of dissolved iron, and solid-phase iron speciation indicated that organic matter mineralization was driven by dissimilatory iron reduction and organoclastic sulfate reduction coupled to oxidative sulfur cycling. The latter process led to ^{34}S-depletion in pyrite of up to 70 ‰ relative to pore-water sulfate.

1. Introduction

Cold-water coral ecosystems occur worldwide within a large bathymetric and temperature range on continental shelves, seamounts and ridge systems (Roberts et al., 2006; Wheeler et al., 2007). They represent a sink for inorganic carbon that has so far not been fully considered in global carbonate budget estimations (Lindberg and Mienert, 2005; Titschack et al., 2009). These ecosystems, formed predominately by the scleractinian corals *Lophelia pertusa* and *Madrepora oculata* occur as patches, reefs systems as well as cold-water coral mounds (Freiwald, 2002; Roberts et al., 2006). Mounds composed of cold-water coral fragments embedded in a loose matrix of hemipelagic sediments (Dorschel et al., 2007; Rüggeberg et al., 2007; Titschack et al., 2009) can form enormous carbonate build-ups of up to 300 m in height and of several kilometers in diameter (Mienis et al., 2007; Wheeler et al., 2007). Surveys on the NE Atlantic margin report their distribution from northern Norway to the continental slope off Morocco (e.g. Freiwald, 2002; Roberts et al., 2006; Weaver et al., 2004; Wheeler et al., 2007, De Mol et al., 2009). While morphology, growth history and environmental setting of individual mounds or mound provinces are often well-constrained (De Mol et al., 2007; Eisele et al., 2008; Huvenne et al., 2003; Mienis et al., 2007; van Weering et al., 2003; Wheeler et al., 2007), less is known about microbially-mediated early diagenetic processes in these large carbonate fabrics. Biogeochemical processes, however, might play an important role in syn-depositional mound stabilization and ultimately control coral skeleton preservation. A tight coupling between microbially-mediated organic matter degradation and carbonate-mineral diagenesis was proposed for the sediments of Challenger Mound, which was drilled during the Integrated Ocean Drilling Program (IODP) Expedition 307 (Ferdelman et al., 2006). A detailed microbiological survey of mound sediments suggests the presence of a significant and active prokaryotic community in this mound (Webster et al., 2009). The influence of cold-water coral ecosystems on biogeochemical processes and carbonate preservation in associated sediments at post-glacial reefs on the Norwegian shelf has been elucidated by Wehrmann et al. (2009).

In 2002, cold-water coral mounds were discovered in the Gulf of Cadiz, a tectonically active area characterized by gas seepage, fluid venting, and the occurrence of numerous mud volcanoes (e.g. Baraza and Ercilla, 1996; Gardner, 2001; Pinheiro et al., 2003; Somoza et al., 2003; Van Rensbergen et al., 2005). The discovery of cold-water coral mounds in an area of gas seepage is very intriguing as biogeochemical

processes associated with the oxidation of methane can leave a fundamental diagenetic imprint in the sedimentary record, pore-water composition and isotopic signatures of pore-water and solid-phase constituents in marine sediments. Sulfate reduction coupled to the anaerobic oxidation of methane (AOM) proceeds according to the following net reaction (Valentine and Reeburgh, 2000, Nauhaus et al., 2002, Treude et al., 2003, and reference therein):

$$CH_4 + SO_4^{2-} \rightarrow HCO_3^- + HS^- + H_2O \quad (1)$$

This process, apparently mediated by a consortium of anaerobic methane-oxidizing archaea and sulfate-reducing bacteria (Boetius et al., 2000; Hinrichs et al., 1999; Knittel et al., 2003, 2005; Michaelis et al., 2002; Niemann et al., 2006b; Orphan et al., 2001; Valentine and Reeburgh, 2000), can lead to a strong modification of the primary sediment composition by dissolution and precipitation of iron and sulfur bearing mineral phases, e.g. iron oxides, barite, and pyrite (Jørgensen et al., 2004; Neretin, 2004, Passier, 1998, Riedinger et al., 2005). The prominent role of these minerals as paleoceanographic and palaeoclimatologic proxies demands a careful assessment of the mechanisms and extents of diagenetic alteration in the sedimentary record (Jørgensen and Kasten, 2006; März et al., 2008; Riedinger et al., 2005).

So far, little is known about the imprint of AOM coupled to sulfate reduction on the sedimentary record within a cold-water coral mound and how it affects modes of early diagenesis. Initial studies by Foubert et al. (2008) and Maignien et al. (in press) described the presence of a shallow sulfate-methane transition zone (3.0-3.5 m sediment depth) at Alpha Mound on Pen Duick Escarpment and suggest a possible link between methane-driven diagenetic processes and coral dissolution as well as carbonate production.

In the present study, we provide evidence that deep fluids and methane ascend to near surface sediments of three cold-water coral mounds, Alpha, Beta and Gamma Mound on the Pen Duick Escarpment. These mounds thus represent a model system for exploring the impact of fluid flow and methane seepage on coral-bearing, carbonate-rich siliciclastic sediments. The comparison of a non-methane influenced coral-framework mound, i.e. Gamma Mound and methane influenced structures such as Alpha and Beta Mound allows us to evaluate the imprint of methane cycling on recent early diagenetic processes and the geological record.

2. Regional setting

The study area Pen Duick Escarpment is located in the Gulf of Cadiz west of the Gibraltar Arc between the Iberian Peninsula and the Moroccan margin (Fig. 1a). The complex structural development of the Gulf of Cadiz is controlled by subduction associated to the westward motion of the Betic-Rifean orogenic arc, dextral strike-slip movement along the Azores-Gibraltar Plate Boundary, and the Africa-Eurasia plate convergence motion (Gutscher et al., 2002; Maldonado and Nelson, 1999; Medialdea et al., 2004, 2008; Zitellini et al., 2009). These processes led to the formation of a large allochthonous unit which is covered by an undeformed Late Miocene to Plio-Quarternary sedimentary pile (Maldonado et al., 1999; Meldialdea et al., 2004; Zitellini et al., 2009). Along the Moroccan margin, several sub-parallel ridges are located that represent large rotated blocks confined by lystric faults that formed Plio-Pleistocene centers of deposition including Renard Ridge and Vernadsky Ridge (Van Rensbergen et al., 2005). The Pen Duick Escarpment represents a NE-SW oriented fault-bounded cliff of 6 km length and 80 to 125 m height situated on the southeastern leg of Renard Ridge (Van Rooij et al., in review). The nature of the substratum below Pen Duick Escarpment is largely unknown. On the northeastern site, the escarpment is underlain by a small subbasin which is suggested to host a discontinuous stratigraphic record with interference from adjacent mud volcanoes (Van Rooij et al., in review). To the southwest, the escarpment flank descends into a depression with a maximal depth of 10-20 m (Van Rooij et al., in review). Average slope gradients of the cliff are about 15 to 20° at the south-west facing part and up to 25° at the eastern edge (Foubert et al., 2008). Seismic profiles across Pen Duick Escarpment provide evidence for gas accumulation and features related to hydrocarbon (gas) seepage (Van Rooij et al., in review). Renard and Vernadsky Ridges are located in the El Arraiche mud volcano field which consists of eight mud volcanoes that are situated around the ridges on top of normal faults which constrain the rotated blocks (Van Rensbergen et al., 2005). The onset of mud volcano activity in the El Arraiche mud volcano field is estimated at 2.5 Ma before present (Van Rensbergen et al., 2005). Pen Duick Escarpment is separated from its closest neighboring mud volcano, Gemini Mud Volcano, by an only 1 km wide moat feature (Fig. 1b; Van Rooij et al., in review).

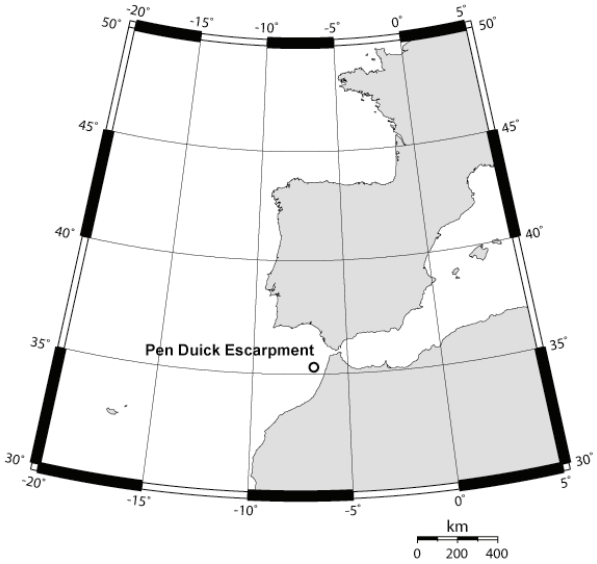

a)

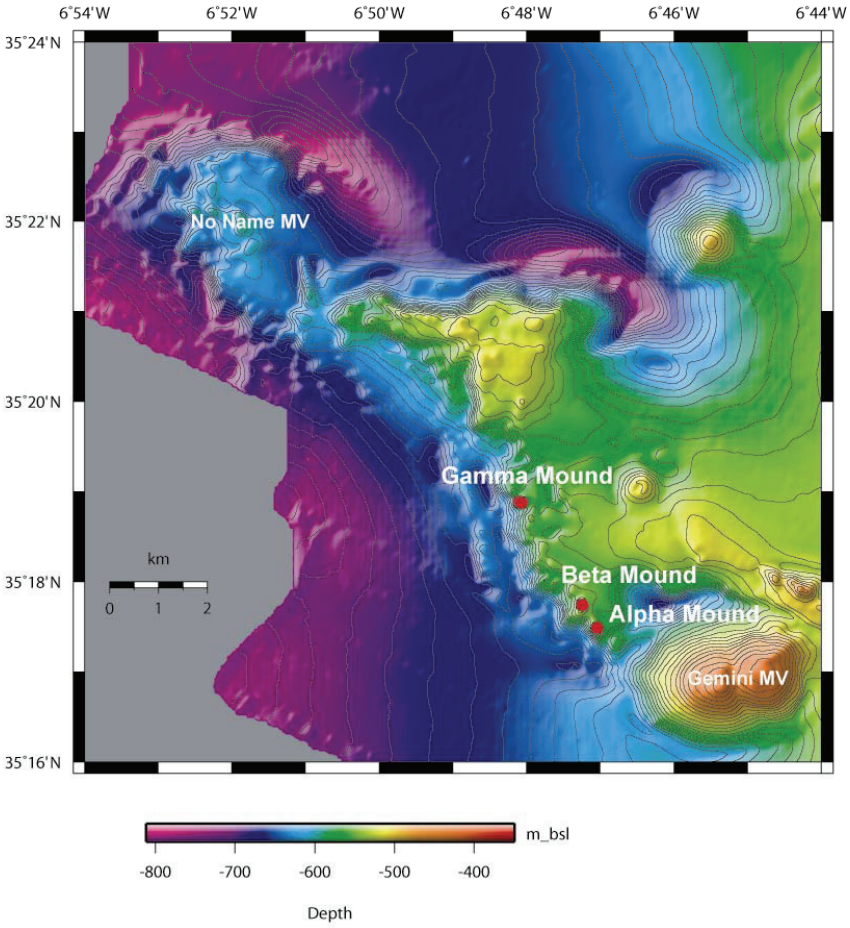

b)

Figure 1: a) Location of the study area Pen Duick Escarpment in the Gulf of Cadiz. **b)** Location of Alpha, Beta and Gamma Mound on the escarpment. Also shown are No Name Mud Volcano (MV) and Gemini MV.

Fluid escape structures such as mud volcanoes, pockmarks and carbonate chimneys are widely distributed in the Gulf of Cadiz (e.g. Baraza and Ercilla, 1996; Díaz-del-Río et al., 2003; León et al., 2006; Medialdea et al., 2008; Niemann et al., 2006a; Pinheiro et al., 2003; Somoza et al., 2003; Stadnitskaia et al., 2008; Van Rensbergen et al., 2005; Van Rooij et al., 2005). The source of fluids migrating into the mud volcano systems on the Betic-Rifean margin is inferred to be the allochtonous unit. For mud volcanoes located on the lower continental slope it is suggested that they might be related to sources below this unit, probably of Mesozoic age (Fernández-Puga et al., 2007; Medialdea et al., 2008). Analyses of venting hydrocarbon gas composition at active mud volcanoes suggest a large thermogenic component (Stadnitskaia et al., 2006; Nuzzo et al., 2009). The extensional faulting of the ridges in the El Arraiche mud volcano field facilitates migration of overpressured fluid and mud-breccia flow, expressed in the formation of the mud volcanoes.

The Pen Duick Mound Province hosts a series of 15 identified cold-water coral mounds covering the cliff top and several smaller mounds at the base. Further small mound-like features have been discovered in the sedimentary sequences surrounding the escarpment and have been interpreted as buried mounds (Foubert et al., 2008). The 15 cold-water coral mounds are distributed in a water depth of 500-600 m and reach up to 60 m in height and about 500 m in diameter at the mound base (Foubert et al., 2008; Van Rooij et al., in review). Seismic profiles suggest that the mound base is an erosional surface, interpreted as the outcropping basement that is forming Renard Ridge (Foubert et al., 2008).

In this study, three cold-water coral mounds were investigated, Alpha, Beta and Gamma Mound, which reside next to each other on the cliff top (Fig. 1b). Alpha Mound is located on the southeastern side of Pen Duick Escarpment close to Gemini Mud Volcano. The mound has an elongated shape parallel to the escarpment with a maximum diameter of 350 m and a minimal height of 15 m (Van Rooij et al, in review). At 300 m distance from Alpha Mound to the NNW, Beta Mound is located. The mound is characterized by two summits and has a maximum diameter of 450 m and a height of approximately 20 m (Van Rooij et al., in review). Gamma Mound is located at 2.5 km NNW of Beta Mound. It has a conical shape with a width of 300 m and a height of approximately 15 m (Van Rooij et al., in review). The hydrographic setting affecting cold-water coral mounds in the El Arraiche mud volcano field in the Gulf of Cadiz has been reviewed by Foubert et al. (2008), Wienberg et al. (2009) and Van Rooij et al. (in

review). It is mainly influenced by North Atlantic Central Water (NACW) with temperatures of 10.7 to 11.8°C and a salinity of 35.55 to 35.65 psu (Foubert et al., 2008; Van Rooij et al., in review).

3. Material and methods

3.1 Sample collection

During R/V Marion Dufresne Cruise MD 169 MiCROSYSTEMS to the Gulf of Cadiz in July 2008, sediments were recovered by gravity coring from Alpha Mound (MD08-3218), Beta Mound (MD08-3214) and Gamma Mound (MD08-3221 and MD08-3231) for pore-water and solid-phase geochemical analyses. Cores from Alpha and Beta Mound were taken from the mound summits, the cores from Gamma Mound were taken slightly to the western flank. Sampling location, water depth and core recovery of the four cores are listed in Table 1. All cores were cut into 1 m sections immediately after retrieval and stored at 4°C prior to opening. The cores were opened within a few hours after retrieval and subsampled for solid-phase and pore-water analyses and sulfate reduction rate measurements. The sampling interval for all parameters was 10 to 20 cm for cores from Alpha Mound, Beta Mound and Gamma Mound core MD08-3231, and 40 cm for Gamma Mound core MD08-3221 below 100 cm.

Table 1. Sampling location, water depth and core recovery of the presented cores.

Location	Core	Latitude (°North)	Longitude (°West)	Water depth [m]	Core recovery [cm]
Alpha Mound	MD08-3218	35°17.47’	06°47.05’	528	427
Beta Mound	MD08-3214	35°17.74’	06°47.26’	506	252
Gamma Mound	MD08-3221	35°18.87’	06°48.08’	543	510
Gamma Mound	MD08-3231	35°18.90’	06°48.19’	550	378

3.2 Methane concentration measurements

Methane concentrations were determined from 3 cm^3 sediment samples stored upside-down in gas-tight glass vials containing 10 ml NaOH (2.5%, w/v) using a gas chromatograph (5890A, Hewlett Packard). Samples from all cores were taken at a vertical resolution of 20 cm. To minimize possible effects of depressurization and warming of the cores, holes were pre-drilled into the core liner and sealed with tape prior to coring which allowed fast sampling immediately after core retrieval.

3.3 Solid-phase composition

Total carbon (TC) and total inorganic carbon (TIC) were measured coulometrically with an UIC, Inc. system on freeze-dried samples after removal of all coral pieces. For coulometric TC-measurement, the samples were combusted at 950ºC to completely oxidise all TC. Samples for TIC analysis were treated with 2N $HClO_3$ at room temperature to release carbonate carbon. Total organic carbon content (TOC) was determined as the difference between TC and TIC. Carbonate content was calculated from TIC assuming $CaCO_3$ as the main mineral form.

X-ray diffraction (XRD analysis) was carried out to quantify the relative amounts of different carbonate mineralogies on freeze-dried subsamples according to Hardy and Tucker (1988). Measurements were performed on smear mounts with $\leq 0.01°2\theta$ steps and 1-2 sec of scanning time using an XDS 2000 Scintag Inc.™, with a ø/ø 'Goniometer and Peltier Detector'. The relative proportions of different carbonate minerals were quantified on the basis of the (104) peak areas of calcite, high Mg-calcite and dolomite, and the (111) peak area of aragonite using the software "DiffracPlus". The position of the peak was used to determine the Mg content of carbonate minerals (Lumsden, 1979). The peak areas were measured for the main peaks of the carbonate minerals aragonite (3.4 Å), high-Mg calcite with more than 5 mol% $MgCO_3$ (2.9 to 3.0 Å), calcite (3.035 Å), and dolomite (2.888 Å) (Naehr et al., 2007).

Samples for determination of acid volatile sulfide (AVS = H_2S + FeS) and chromium reducible sulfur (CRS = FeS_2 + S^0) were frozen immediately after core sampling. A two-step Cr-II method with cold 2M HCl and boiling 0.5M $CrCl_2$ solution (Fossing and Jørgensen, 1989) was conducted on subsamples and the concentration of trapped sulfide from both steps was measured by the diamine complexation method (Cline, 1969). Determination of carbonate-associated and adsorbed iron ($Fe_{ads+carb}$, sodium acetate extraction), easily reducible Fe-(oxyhydr)oxides (Fe_{ox1}, hydroxylamine-

HCl extraction), reducible Fe-(oxyhydr)oxides (Fe_{ox2}, sodium dithionite extraction), and poorly reactive silicate Fe (Fe_{PRS}, concentrated HCl extraction) was performed by sequential extraction after Poulton and Canfield (2004). For dissolved Fe-analysis of the extract a Ferrozine/HEPES/hydroxylamine hydrochloride solution was prepared (Stokey, 1970). Iron content and CRS were corrected for wet-to-dry-weight ratio. The degree-of-pyritization (DOP) introduced by Berner (1970) and refined by Raiswell and Canfield (1996, 1998) was calculated as follows:

$$DOP = \frac{\left(Fe_{Pyrite}\right)}{\left(Fe_{Pyrite}\right)+\left(Fe_{ox1}+Fe_{ox2}\right)} \quad (2)$$

Pyrite-Fe corresponds to the amount of Fe associated with CRS, presuming that CRS consists mostly of FeS_2. Dithionite-extractable-Fe refers to the fraction of solid-phase iron that is extracted from sediment during treatment with a buffered citrate-dithionite solution. It includes Fe-(oxyhydr)oxides such as ferrihydrite, lepidocrocite, goethite and hematite corresponding to the fractions Fe_{ox1} and Fe_{ox2}, respectively extracted during the sequential extraction procedure.

3.4 Pore-water geochemistry

For pore-water analyses, samples were obtained by Rhizones (Rhizosphere Research Products, Wageningen, Netherlands) attached to 2 ml and 5 ml plastic syringes (Seeberg-Elverfeldt et al., 2005). Aliquots for sulfate (SO_4^{2-}), including sulfur and oxygen isotope analyses, hydrogen sulfide (H_2S) and chloride (Cl^-) were fixed by ZnAc addition (2 %, w/v). SO_4^{2-} and Cl^- were measured by ion chromatography with IAPSO standard seawater as external reference standard. H_2S was measured after appropriate dilution by the diamine complexation method (Cline, 1969). Multi-element pore-water analyses (Fe_{diss}, Li^+, Na^+, Ca^{2+}, Mg^{2+} and Sr^{2+}) were conducted on acidified pore-water aliquots (1 % HNO_3, v/v) by inductively coupled plasma optical emission spectroscopy (ICP-OES). Dissolved inorganic carbon (DIC) and total alkalinity (TA) were determined on pore-water subsamples poisoned with $HgCl_2$ (0.25 mM) and sealed headspace-free in 2 ml glass vials. Dissolved inorganic carbon (DIC) concentrations were determined by flow-injection (Hall and Aller, 1992) using a conductivity detector (VWR scientific, model 1054). The Gran titration method (Gieskes and Rogers, 1973)

was used to determine total alkalinity (TA). A more detailed description of the methods can be found in Wehrmann et al. (2009).

3.5 Sulfate reduction rate measurements

Sediments for the determination of sulfate reduction rates (SRR) were sampled in triplicates into 5 ml glass tubes and sealed headspace-free with butyl rubber stoppers. Sediment samples were incubated with trace amounts of $^{35}S\text{-}SO_4^{2-}$ (20 µL, 200 kBq) at in situ temperature in the dark for 36 h. The incubation step was terminated by transferring the samples into vials containing 20 ml ZnAc (20 %, w/v). The activities of $^{35}S\text{-}SO_4^{2-}$ and total reduced inorganic sulfur species ($TRI^{35}S$) produced via sulfate reduction in the sample were measured by wet scintillation counting (Kallmeyer et al. 2004). Turnover rates were calculated according to Jørgensen (1978).

3.6 Stable isotope analyses

Stable sulfur isotope analyses were performed on the solid phase CRS fraction and on pore-water sulfate. CRS was converted to Ag_2S by treatment with $AgNO_3$ and subsequent washing with NH_4OH to remove any colloidal silver. For the determination of SO_4^{2-} isotopes, ZnAc-fixed aliquots were sonicated and filtered (0.45 µm) to remove H_2S trapped as ZnS. Filtered samples were acidified and subjected to a $BaCl_2$-solution to induce the precipitation of $BaSO_4$. Precipitates were washed several times with deionized water and dried. Sulfur isotope ratios were measured by weighing 0.4-0.6 mg of $BaSO_4$ or 0.2-0.4 mg Ag_2S with 1 mg of V_2O_5 into a tin capsule and combustion at 1060ºC in an elemental analyzer (EURO EA Elemental Analyzer) to produce SO_2. The evolved SO_2 was carried by a helium stream through a GC column, Finnigan Conflo III, and into a Finnigan Delta V stable isotope ratio mass spectrometer to determine $\delta^{34}S$. The sulfur isotope measurements were calibrated with reference materials NBS 127 ($\delta^{34}S$ = +20.3 ‰) and IAEA-SO-6 ($\delta^{34}S$ = –34.1 ‰). The standard error (1σ) of the measurement was less than 0.2 ‰ for $\delta^{34}S$. For oxygen isotope analyses, 0.3-0.4 mg of $BaSO_4$ was weighed into a silver capsule. The sample was carbothermically reduced at 1450ºC in a TC/EA (Thermo-Fisher) to yield carbon monoxide gas which was analyzed in continuous flow mode with a Finnigan Delta V stable isotope mass spectrometer.

Samples for the analyses of carbon and oxygen isotope compositions of the bulk sedimentary carbonate were freeze-dried for 24 h and 0.1-0.2 mg of powdered bulk samples were analyzed with a Kiel IV Inc. Carbonate Device connected to a Delta V

Plus Dual Inlet MS. The analytical reproducibility (1σ) of the isotope data based on repeated measurements of laboratory standards was ±0.02 ‰ for $\delta^{13}C$ and ±0.08 ‰ for $\delta^{18}O$. All $\delta^{18}O$ values were corrected for dolomite–phosphoric acid fractionation at 70°C using a fractionation factor of 1.0093 (Rosenbaum and Sheppard, 1986). Carbon isotope analyses of dissolved inorganic carbon ($\delta^{13}C$-DIC) were conducted on a gas bench coupled to a Finnigan MAT 252 after sample acidification. The carbon isotope composition was calibrated against NBS 19 ($\delta^{13}C$= 1.95 ‰). The standard error (1σ) of the measurement was less than 0.1‰ for $\delta^{13}C$. Sulfur isotopic composition is reported with respect to Vienna Canyon Diablo Troilite (VCDT), oxygen isotopic composition is reported with respect to Vienna Standard Mean Oceanic Water (VSMOW) and carbon isotopic composition with respect to Vienna Pee Dee Belemnite Standard (VPDB) in common δ-notation.

4. Results

4.1 Sediment description

Core MD08-3218 from Alpha Mound is characterized by a top zone of 20 cm consisting of brownish-yellow to brown compact clay followed by alternating layers of light gray to dark gray clay (Fig. 2). Two black layers are observed at 29-30 cm and at 289 cm sediment depths. Core MD08-3214 from Beta Mound consists of brown clay in the top 20 cm followed by successional blueish-gray to dark gray layers of homogeneous, unlithified clay (Fig. 2). Core MD08-3221 from Gamma Mound mainly comprises brown, brownish-gray and dark to light-gray layers of homogeneous to compact clay. Core MD08-3231 from the same mound is characterized by a top layer of 10 cm consisting of brown homogenous clay followed by a transition to gray clay below (Fig. 2). Cores from Gamma Mound show a higher abundance of *L. pertusa*, *M. oculata* and a lower abundance of dendrophylliid species than the cores from Alpha and Beta Mound where *L. pertusa* and *M. oculata* is mostly constrained to the top 50 and 25 cm, respectively while mostly dendrophylliid corals are found below (Fig. 2; Van Rooij et al., in review). Comparison of the preservation state of the buried corals reveals that the best state of preservation is found at Gamma Mound in contrast to intermediate conditions at Alpha and Beta Mound and strong corrosion of the corals at Alpha Mound below a depth of 300 cm. Detailed core analyses of cores from the same mounds including results of XRD analyses, magnetic susceptibility and CT-scans can be found in Van Rooij et al. (in review).

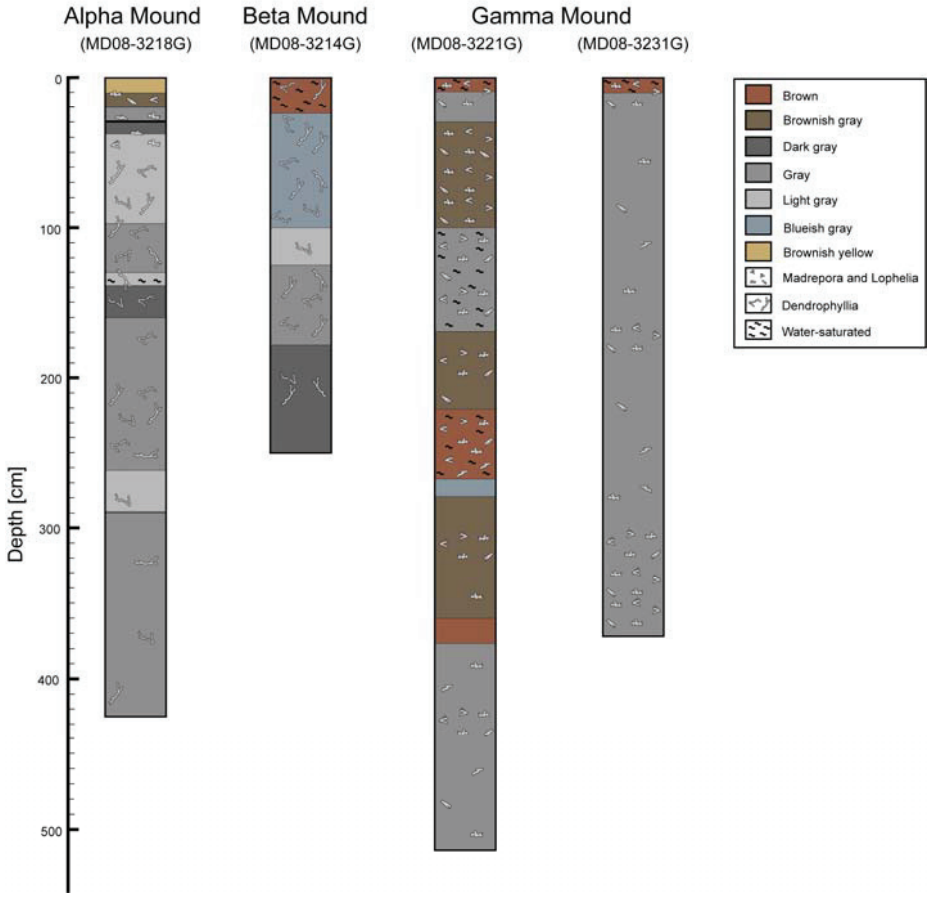

Figure 2: Lithological description of the four cores retrieved at Alpha, Beta and Gamma Mound.

4.2 Methane concentration

Methane concentration profiles from Alpha, Beta and Gamma Mound are displayed in Figure 3. In the core from Alpha Mound, methane concentrations of ~0.08 mM were detected below 320 cm sediment depth. The Beta Mound core showed increasing methane concentrations below 110 cm with a concentration peak of 0.2 mM at 150 cm and slightly decreasing values at greater depth. A sample from the core catcher showed elevated values again (~0.2 mM; data not shown). In core MD08-3221 from Gamma Mound methane concentration were below detection limit. In Core MD08-3231 from the same mound methane concentrations of 0.07 and 0.08 mM were detected at 270 cm and 310 cm sediment depth.

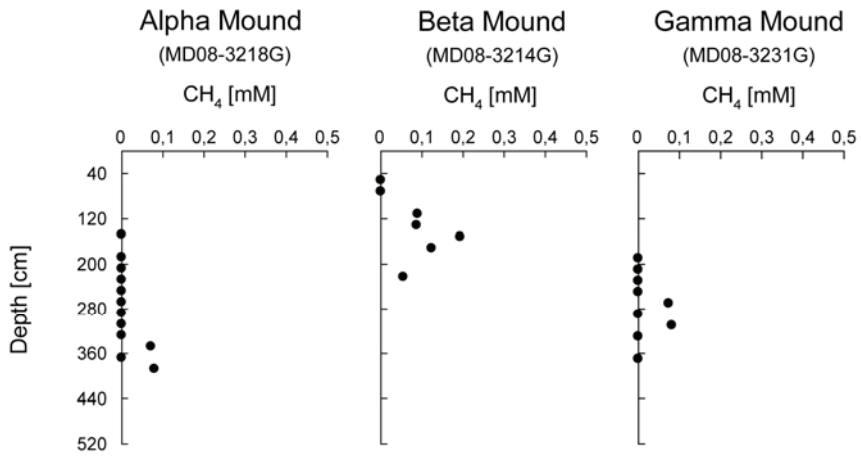

Figure 3: Methane concentrations in cores MD08-3218 (Alpha Mound), MD08-3214 (Beta Mound) and MD08-3231 (Gamma Mound).

4.3 Solid-phase composition

4.3.1 Total inorganic carbon, $CaCO_3$, total organic carbon concentrations and carbonate minerology

An overview of the average total inorganic carbon (TIC), corresponding $CaCO_3$ and total organic carbon concentrations (TOC) for all cores as well as the average carbonate mineralogy is presented in Table 2. Distributions of TIC and TOC with depth are shown in Fig. 4a. In all cores, TIC concentrations were uniform or slightly increased with depth. An exception to this trend was found at Gamma Mound core MD08-3231 were the TIC content was moderately elevated in a discrete layer (65-110 cm). TOC concentrations were in a similar range for all cores (in average 0.4-0.5 wt.%); only Gamma Mound core MD08-3231 exhibited slightly elevated TOC values of 0.7 wt.%. Mound sediments consisted of a large fraction of calcite (26.1-40.8 wt.%) with minor contributions of aragonite (2.1-4.6 wt.%) and dolomite (2.8-6 wt.%) and varying fractions of high Mg-calcite (Fig. 4b). All measured high Mg-calcite fractions contained between 32-45 mol% $MgCO_3$ (2.94 to 2.90 Å). The cores from Beta Mound and Gamma Mound MD08-3221 showed only small contributions of high-Mg calcite (averages values <5 wt.%). A layer of elevated high-Mg calcite concentrations was found between 105-130 cm sediment depth in Gamma Mound core MD08-3231. Three zones can be delineated in Alpha Mound core MD08-3218. Elevated high-Mg calcite concentrations were found throughout the top 215 cm (Zone I) and below 300 cm sediment depth (Zone III) while in between high-Mg calcite concentrations were low

(Zone II). Elevated high-Mg calcite concentrations can be attributed the formation of authigenic carbonate minerals at these depths (Fig. 4b).

Table 2. Average total inorganic carbon (TIC), $CaCO_3$ and total organic carbon (TOC) concentrations and average carbonate mineralogy [wt.%] including standard deviation (1 σ) of the four cores.

Location	Core	TIC [wt. %]	$CaCO_3$ [wt. %]	TOC [wt. %]	Aragonite [wt. %]	Calcite [wt. %]	High-Mg calcite [wt. %]	Dolomite [wt. %]
Alpha Mound	MD08-3218	6.5 (± 0.8)	54.3 (± 6.9)	0.4 (± 0.2)	4.6 (± 2.6)	29.5 (± 7.6)	14.3 (± 9.7)	6.0 (± 1.4)
Beta Mound	MD08-3214	4.8 (± 0.9)	39.6 (± 7.6)	0.5 (± 0.3)	4.4 (± 2.4)	26.1 (± 4.5)	4.1 (± 1.8)	5.0 (± 1.1)
Gamma Mound	MD08-3221	5.1 (± 0.7)	42.3 (± 5.8)	0.4 (± 0.2)	2.1 (± 0.9)	36.1 (± 5.6)	1.2 (± 1.5)	2.8 (± 1.1)
Gamma Mound	MD08-3231	6.1 (± 0.7)	50.6 (± 5.5)	0.7 (± 0.3)	3.1 (± 2.4)	40.8 (± 6.0)	3.4 (± 4.9)	3.3 (± 0.5)

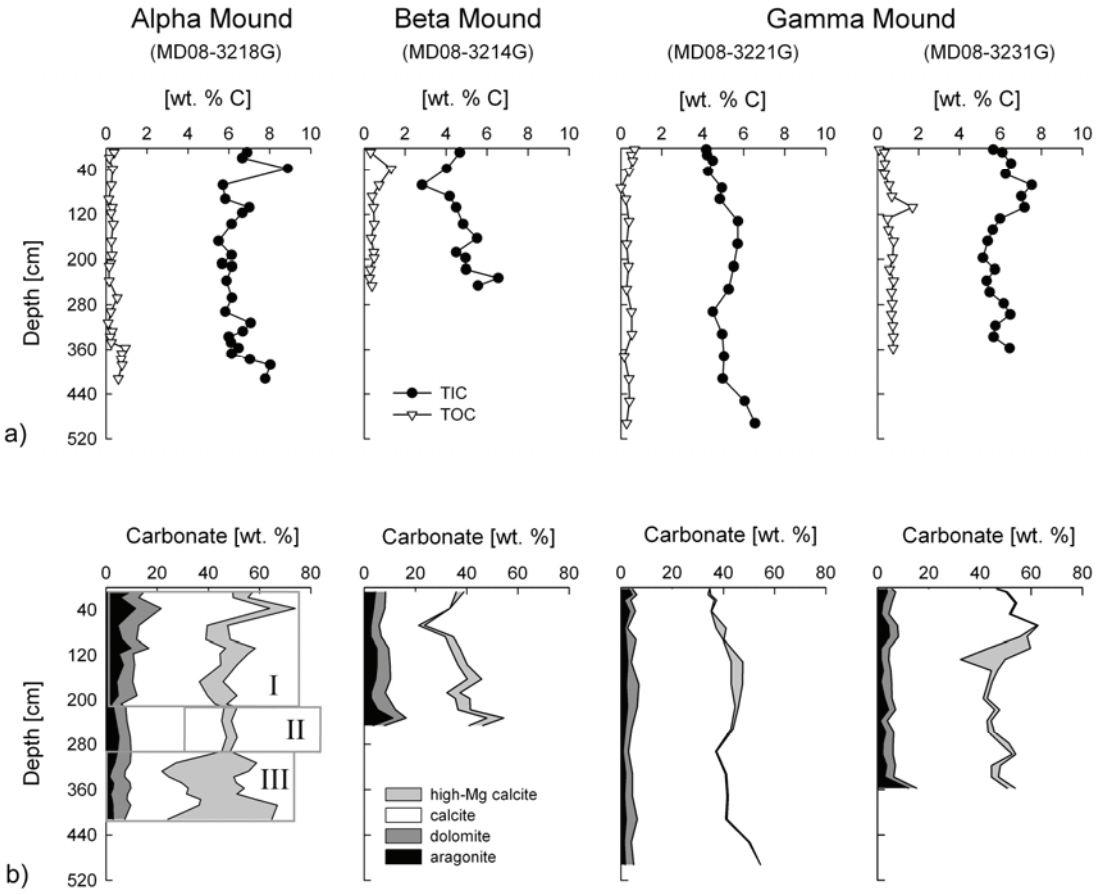

Figure 4: a) Total inorganic carbon (TIC), total organic carbon (TOC) and **b)** carbonate mineralogy with depth. Boxes I-III delineate the three characteristic zones in Alpha Mound.

4.3.2 Sequentially extracted iron phases and chromium reducible sulfur concentrations and degree-of-pyritization

Table 3 summarizes the average concentrations of the sequentially extracted Fe fractions, CRS and the average DOP. Gamma Mound cores were characterized by elevated $Fe_{ads+carb}$ and high (easily) reducible Fe-(oxyhydr)oxides contents as well as low pyrite concentrations and a low DOP. Alpha and Beta Mound displayed large differences in composition between the top 30 cm and the remaining part of the cores. The top 30 cm of the cores were characterized by elevated (easily) reducible Fe-(oxyhydr)oxides contents. Below 30 cm a strong decrease in Fe-(oxyhydr)oxides and a concomitant increase in pyrite concentrations and high DOP values were detected. Figure 5a-c shows the extracted Fe phases and Figure 6a the CRS content with depth. FeS (AVS) concentrations in all cores were below detection.

Table 3. Average concentrations of the sequentially extracted Fe fractions [wt.%], chromium reducible sulfur (CRS) content [wt.% S] including standard deviation (1 σ) and degree-of-pyritization (DOP) of the four cores.

Location	Core	$Fe_{ads+carb}$ [wt. %]	Fe_{ox1} [wt. %]	Fe_{ox2} [wt. %]	Fe_{PRS} [wt. %]	CRS [wt. % S]	DOP
Alpha Mound, top	MD08-3218 0-30 cm	0.07 (± 0.03)	0.2 (±0.05)	0.4 (± 0.3)	1.0 (± 0.3)	0.10 (± 0.14)	0.2
Beta Mound, top	MD08-3214 0-30 cm	0.06 (± 0.03)	0.2 (0.08)	0.6 (± 0.24)	0.9 (± 0.07)	<0.07	< 0.1
Alpha Mound, bottom	MD08-3218 > 30 cm	< 0.04	0.07 (± 0.03)	< 0.02	0.6 (± 0.1)	0.74 (± 0.19)	0.8
Beta Mound, bottom	MD08-3214 > 30 cm	< 0.05	0.10 (± 0.02)	< 0.03	0.6 (± 0.1)	0.84 (± 0.20)	0.8
Gamma Mound	MD08-3221	0.1 (± 0.03)	0.3 (± 0.06)	0.4 (± 0.08)	0.8 (± 0.16)	0.12 (± 0.08)	0.1
Gamma Mound	MD08-3231	0.1 (± 0.05)	0.4 (± 0.06)	0.5 (± 0.08)	0.9 (± 0.11)	0.10 (± 0.06)	0.1

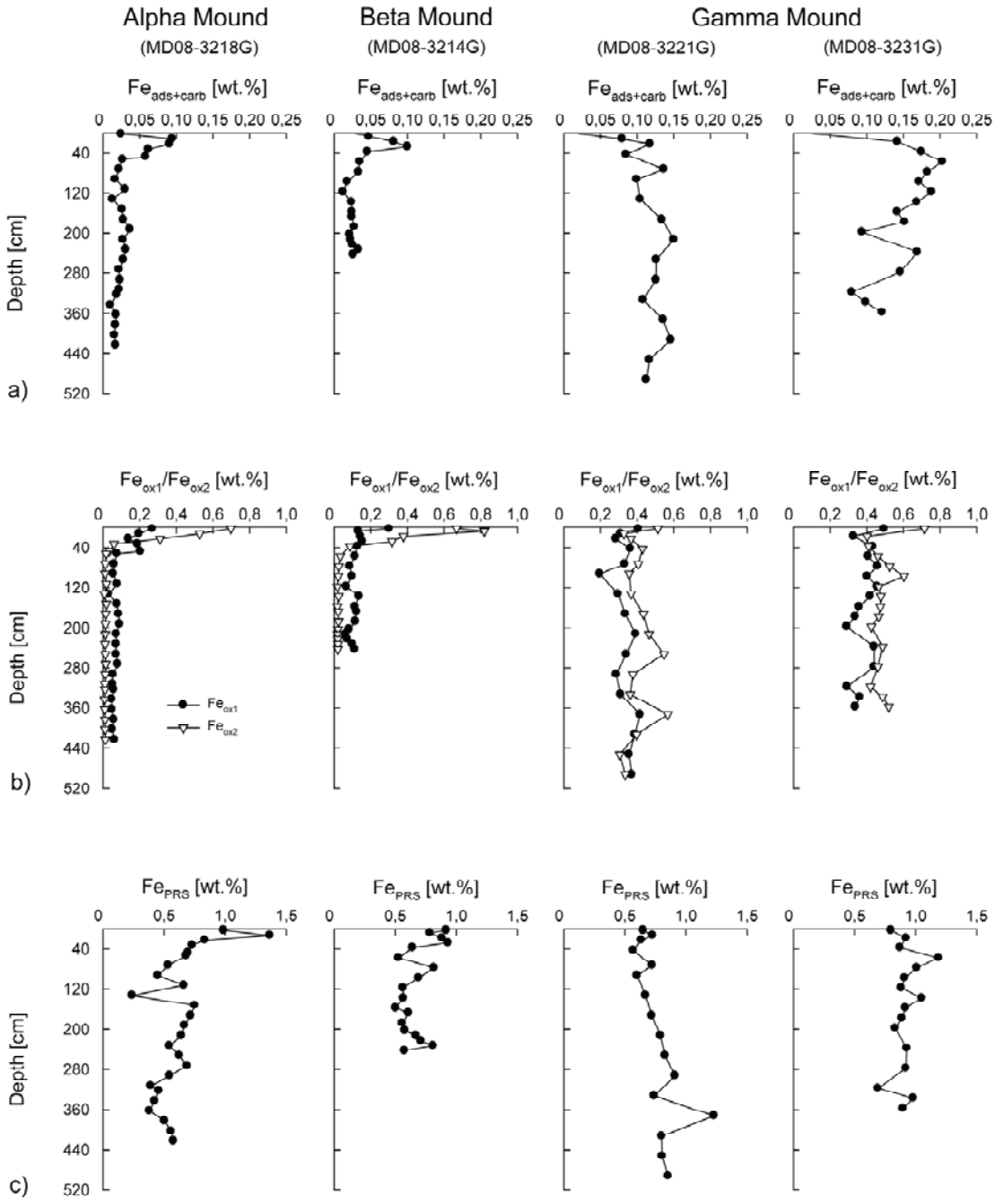

Figure 5: a) Results of sequential Fe-extraction procedure including adsorbed and carbonate-bound Fe ($Fe_{ads+carb}$), **b)** easily reducible and reducible Fe-oxy(hydr)oxides (Fe_{ox1} and Fe_{ox2}) and **c)** poorly reactive sheet silicate Fe (Fe_{PRS}) with depth.

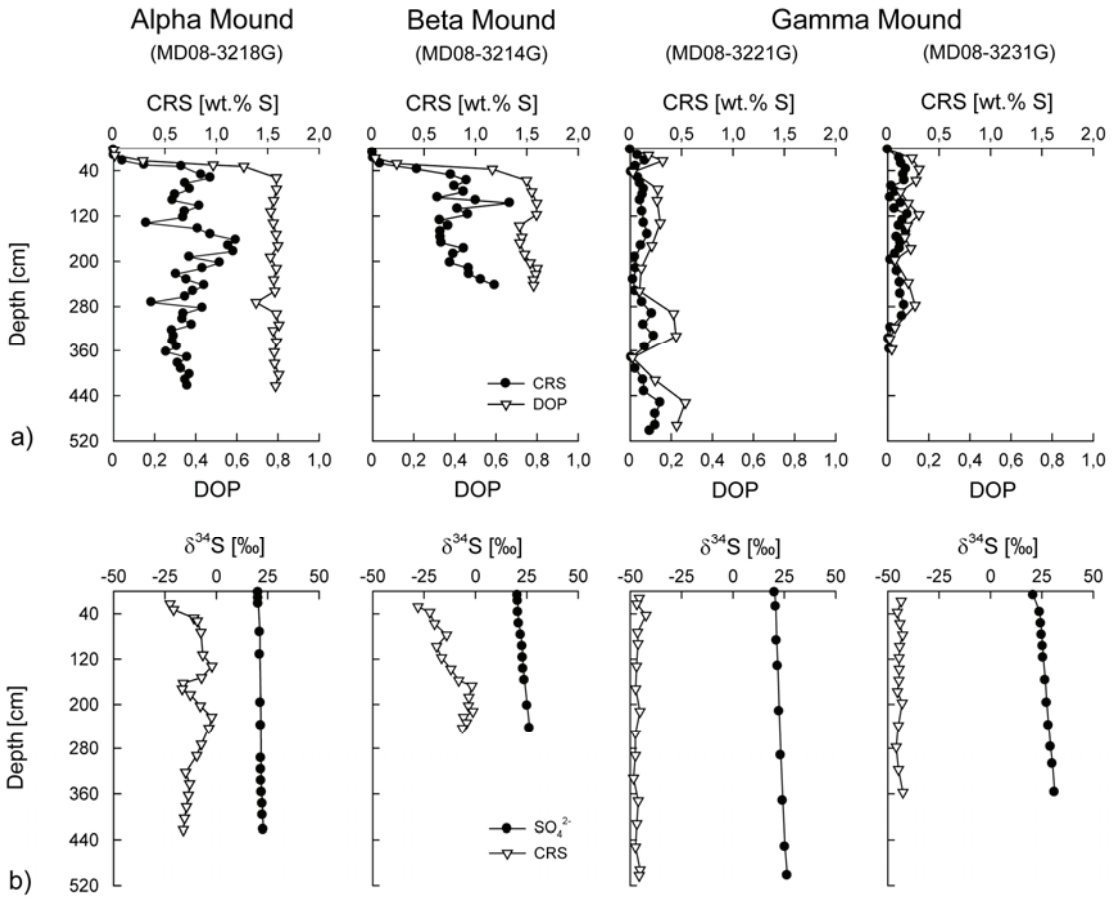

Figure 6: a) Chromium reducible sulfur (CRS), degree-of-pyritization (DOP) and **b)** $\delta^{34}S$ composition of solid-phase CRS and pore-water sulfate with depth.

4.4 Pore-water geochemistry

4.4.1 Sulfate, chloride and sodium concentrations

The pore-water distributions of SO_4^{2-}, Cl^- and Na^+ are shown in Figure 7a. In the core retrieved from Alpha Mound, Cl^- and Na^+ concentrations exhibited only minor changes with depth and SO_4^{2-} concentrations decreased to a minimum of 23.6 mM below 300 cm. In the core from Beta Mound, SO_4^{2-} decreased linearly from seawater concentrations to a minimum value of 17.2 mM. Cl^- and Na^+ concentrations in this core showed a reverse behavior with near-seawater concentrations at the sediment surface and maximum values of 795 mM (Cl^-) and 746 mM (Na^+) in the deepest layer. The cores from Gamma Mound exhibited only slight decreases in SO_4^{2-} concentration to minimum values of 22 mM (MD08-3221) and 18.7 mM (MD08-3231), respectively, while Cl^- and Na^+ concentrations remained unchanged throughout the cores.

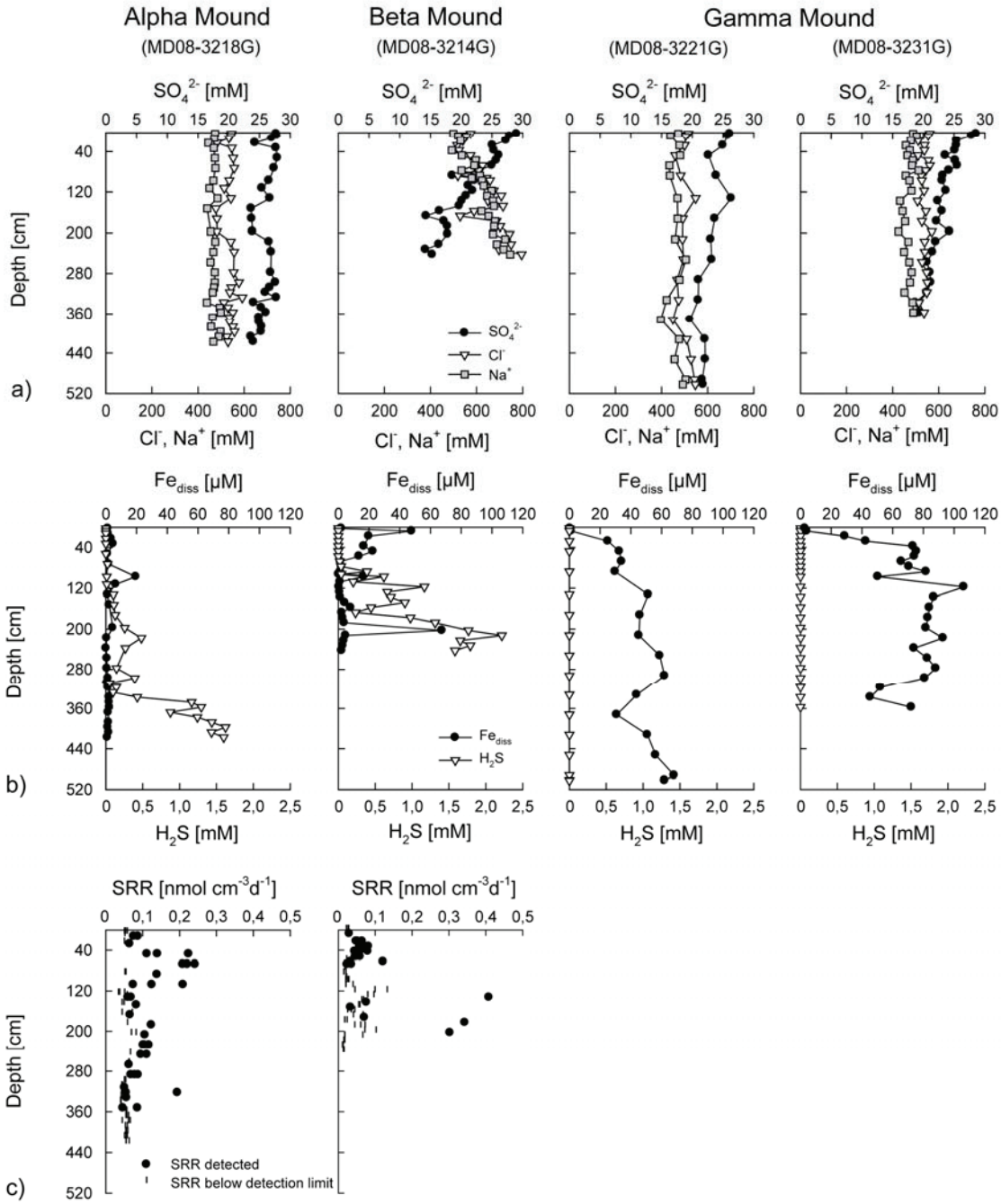

Figure 7: a) Pore-water SO_4^{2-}, Cl^-, Na^+ distribution and **b)** H_2S and dissolved Fe (Fe_{diss}) concentrations of all investigated cores with depth as well as **c)** sulfate reduction rates (SRR) including values below calculated minimum detection limit of cores MD08-3218 (Alpha Mound) and MD08-3214 (Beta Mound).

4.4.2 Hydrogen sulfide and dissolved iron concentrations

Pore-water H_2S and Fe_{diss} distributions with depth are shown in Fig. 7b. Within the top 35 cm of Alpha Mound no H_2S was detected. In an intermediate zone from 35 to 340 cm sediment depth H_2S concentration was < 0.5 mM but increased to maximum

values around 1.6 mM in the deepest part of the core (390-425 cm sediment depth). Fe_{diss} concentrations in this core remained below 6 µM except for a peak of 20 µM at 97.5 cm. In the core from Beta Mound no H_2S was detected in the top 60 cm while below, H_2S concentration showed an overall trend to increasing values with maximum concentrations of 2.2 mM at 212.5 cm depth. Fe_{diss} concentration in the top 60 cm of this core reached a maximum value of 50 µM at 7.5 cm depth. In contrast to Alpha and Beta Mound, no H_2S was detected in sediments recovered from Gamma Mound, while the concentrations of Fe_{diss} were high in both cores from this mound with values up to 106 µM.

4.4.3 Calcium, magnesium, strontium and lithium concentrations

In Fig. 8a and b pore-water concentrations of Ca^{2+}, Mg^{2+}, Sr^{2+} and Li^{+} are displayed. In the cores from Alpha and Gamma Mound Ca^{2+} and Mg^{2+} distributions exhibited only minor changes with average concentrations around seawater values of 10.8 mM and 52.8 mM. At Beta Mound, Ca^{2+} concentration showed a subtle increase to maximum values around 12.5 mM, while Mg^{2+} concentration decreased from the surface (52 mM) to a minimum concentration of 41 mM at the bottom of the core. Pore-water Sr^{2+} and Li^{+} concentrations increased with depth in all cores. At Alpha Mound, these increases were least pronounced. Gamma Mound cores showed intermediate increases and the strongest Sr^{2+} and Li^{+} increases were measured in the core from Beta Mound. A more than three-fold linear increase in Sr^{2+} concentration from 93 µM to 360 µM and a two-fold increase Li^{+} concentration from 28 µM to 58 µM was found in a narrow zone (37.5-92.5 cm sediment depth) of this core. Maximum concentrations at Beta Mound reached 616 µM of Sr^{2+} and 96 µM of Li^{+}.

4.4.4 Dissolved inorganic carbon and total alkalinity concentrations

Pore-water profiles of dissolved inorganic carbon (DIC) and total alkalinity (TA) are displayed in Figure 8c. TA and DIC concentrations in the cores from Alpha and Beta Mound increased to maximum values of 3.8 mM (DIC) and 4.7 mM (TA) in the first core and 4.9 mM (DIC) and 6.5 mM (TA) in the latter core. Only minor increases to values of 2.6 mM and 3.1 mM for DIC and TA and 3.5 mM (DIC) and 4.0 mM (TA) were measured for Gamma Mound cores MD08-3221 and MD08-3231, respectively.

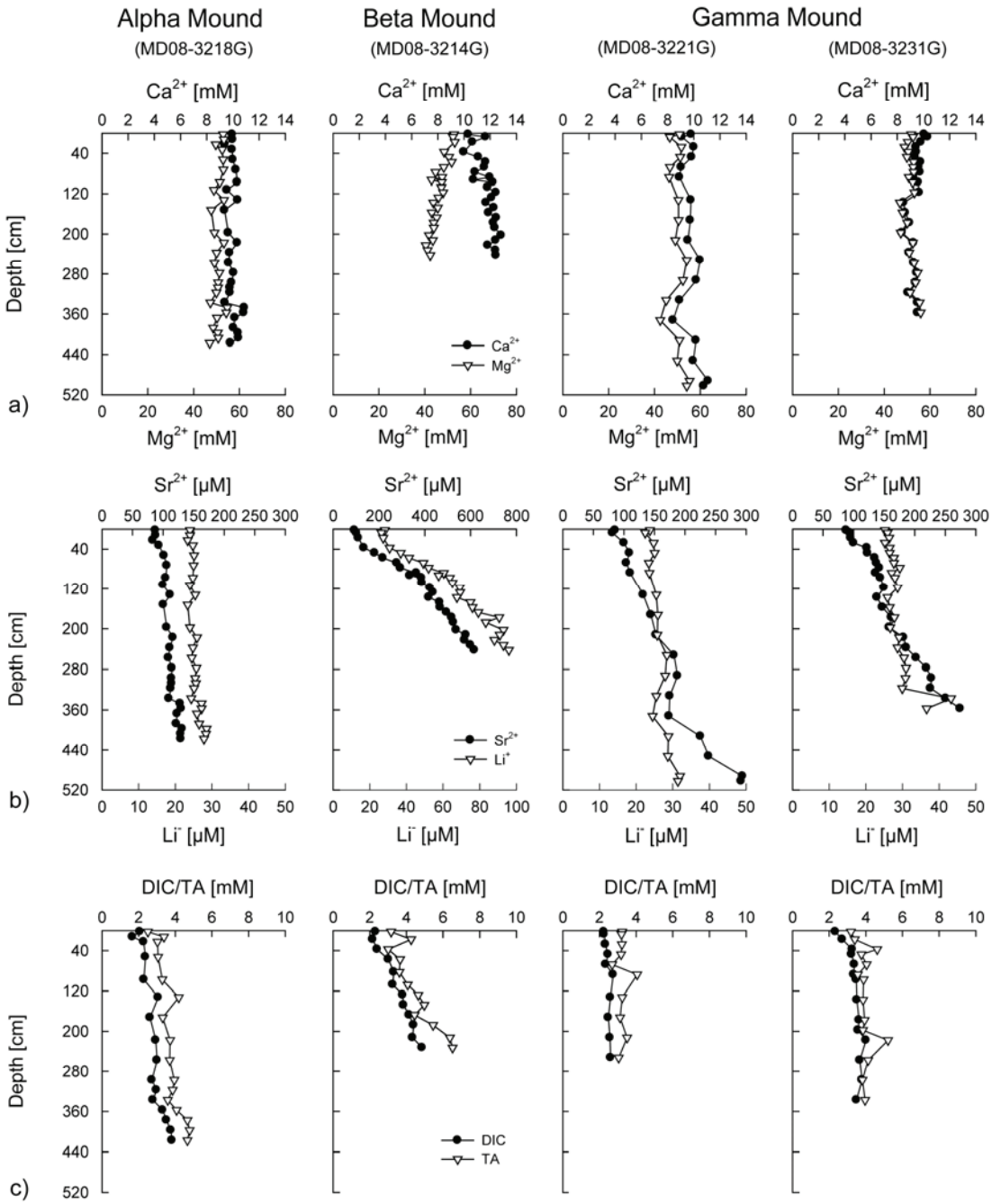

Figure 8: a) Pore-water Ca^{2+}, Mg^{2+} concentrations as well as **b)** Sr^{2+} and Li^{+} distribution with depth **c)** and dissolved inorganic carbon (DIC) and total alkalinity (TA).

4.5 Sulfate reduction rate measurements

Results of sulfate reduction rate (SRR) measurements are shown in Fig. 7c. No sulfate reduction was detectable in the cores from Gamma Mound. At Alpha Mound an upper sulfate reduction zone (10-110 cm) with average rates of 0.14 nmol cm^{-3} d^{-1} was detected. Below this zone, rates decreased and showed a scattered behavior with

multiple samples below detection limit and no detectable sulfate reduction below 355 cm. Sulfate reduction in Beta Mound core displayed a pronounced zone with rates averaging 0.06 nmol cm^{-3} d^{-1} at 20-70 cm sediment depth and only few scattered values below this zone.

4.6 Stable isotope analyses

4.6.1 Sulfur isotope composition of solid-phase pyrite and sulfur and oxygen isotope composition of pore-water sulfate

Sulfur isotope compositions of solid-phase pyrite (δ^{34}S-CRS) and pore-water sulfate ($\delta^{34}S\text{-}SO_4^{2-}$) are shown in Fig. 6b. δ^{34}S-CRS values in Alpha Mound showed a progressive enrichment in the heavier isotope with depth from -23 ‰ at 25 cm to -2 ‰ at 135 cm. This trend was interrupted by an abrupt change to light values of up to -17 ‰ at 175 cm. Below this depth δ^{34}S-CRS approached -2 ‰ at 225 cm before it showed a gradual enrichment in the lighter isotope to a value of -16 ‰ in the deepest layer. $\delta^{34}S\text{-}SO_4^{2-}$ composition of the same core showed only a minor enrichment in the heavier isotope from 20 ‰ at the sediment surface to 23 ‰ at 425 cm sediment depth. The core from Beta Mound displayed ^{34}S-enrichment of δ^{34}S-CRS with values starting at -28 ‰ at 25 cm to around -3 ‰ below 190 cm. In the deepest part of this core SO_4^{2-} was enriched in ^{34}S by 4 ‰ compared to the core top. δ^{34}S-CRS values from Gamma Mound were nearly uniform averaging -46 ‰ and -44 ‰, respectively. In the Gamma Mound core MD08-3221, SO_4^{2-} became slightly enriched in the heavier isotope ranging from 20 ‰ in the top of the core to 26 ‰ at bottom. This trend was more pronounced in the Gamma Mound core MD08-3231 with surface values of 21 ‰ and a value 31 ‰ in the deepest part of the core.

Oxygen isotope composition of pore-water sulfate ($\delta^{18}O\text{-}SO_4^{2-}$; Fig. 10) in the cores from Alpha and Beta Mound showed progressive enrichment with depth approaching values of 12 ‰ in both cores. A prominent enrichment trend was observed in the cores from Gamma Mound with values of 18 ‰ (MD08-3221) and 22 ‰ (MD08-3231).

4.6.2 Carbon and oxygen composition of the bulk sedimentary carbonate

δ^{13}C and δ^{18}O values of the bulk sedimentary carbonate ($\delta^{13}C\text{-}CaCO_3$ and $\delta^{18}O\text{-}CaCO_3$) are displayed in Fig. 9a. $\delta^{13}C\text{-}CaCO_3$ and $\delta^{18}O\text{-}CaCO_3$ compositions from Alpha Mound core showed the strongest variability. In this core, three zones can be

distinguished characterized by specific carbon and oxygen isotope compositions which reflect the zones delineated from the carbonate mineralogy in the same core (section 4.3.1). In a top zone from 0-210 cm (Zone I), δ^{13}C-$CaCO_3$ values showed depletion in the heavier isotope with depth to a maximum value of -17 ‰ at around 140 cm sediment depth. In an intermediate zone below (Zone II), δ^{13}C-$CaCO_3$ values were in the range of -5 ‰ to -2 ‰. Below 300 cm in Zone III, δ^{13}C-$CaCO_3$ showed a strong depletion in ^{13}C again with average values of -19 ‰. The oxygen isotope composition of the bulk carbonate in this core exhibited the opposite distribution. In Zone I δ^{18}O-$CaCO_3$ values showed enrichment in ^{18}O from around 29 ‰ at the sediment surface to values of 33-34 ‰ at the bottom of this zone. Below values average 32 ‰ (Zone II) and in Zone III ^{18}O-enrichment with average δ^{18}O-$CaCO_3$ values of 35.5 ‰ was measured. In Beta Mound δ^{18}O-$CaCO_3$ showed only minor variation and δ^{13}C-$CaCO_3$ values in this core were only slightly depleted in the heavy isotope with a minimum value of 4.1 ‰ at around 37.5 cm depth. The cores from Gamma Mound showed almost uniform δ^{13}C-$CaCO_3$ and δ^{18}O-$CaCO_3$ distributions with values around 29.2 ‰ and 29.1 ‰, for the carbon and -1 ‰ for the oxygen isotope composition of the carbonate. Core MD08-3231 showed slightly scattered δ^{18}O-$CaCO_3$ values below 105 cm sediment depth in the range of 27.4-31 ‰.

4.6.3 Carbon isotope composition of dissolved inorganic carbon

δ^{13}C values of pore-water dissolved inorganic carbon (δ^{13}C-DIC) from the cores retrieved at Alpha, Beta and Gamma Mound core MD08-3231 are displayed in Fig. 9b. δ^{13}C-DIC from Alpha and Beta Mound cores showed increasing depletion in ^{13}C with depth from surface sediment (5-10 cm depth) values of -0.8 ‰ and -1.4 ‰, respectively to values of -13.5 ‰ and -15.6 ‰ in the deepest part of the cores. Pore-water δ^{13}C-DIC values from Gamma Mound showed depletion in ^{13}C in the top ~75 cm of the core from -1.4 ‰ to -7.3 ‰. Below changes in the δ^{13}C-DIC value were minimal with the lowest value of -9.1 ‰ determined at 320 cm sediment depth.

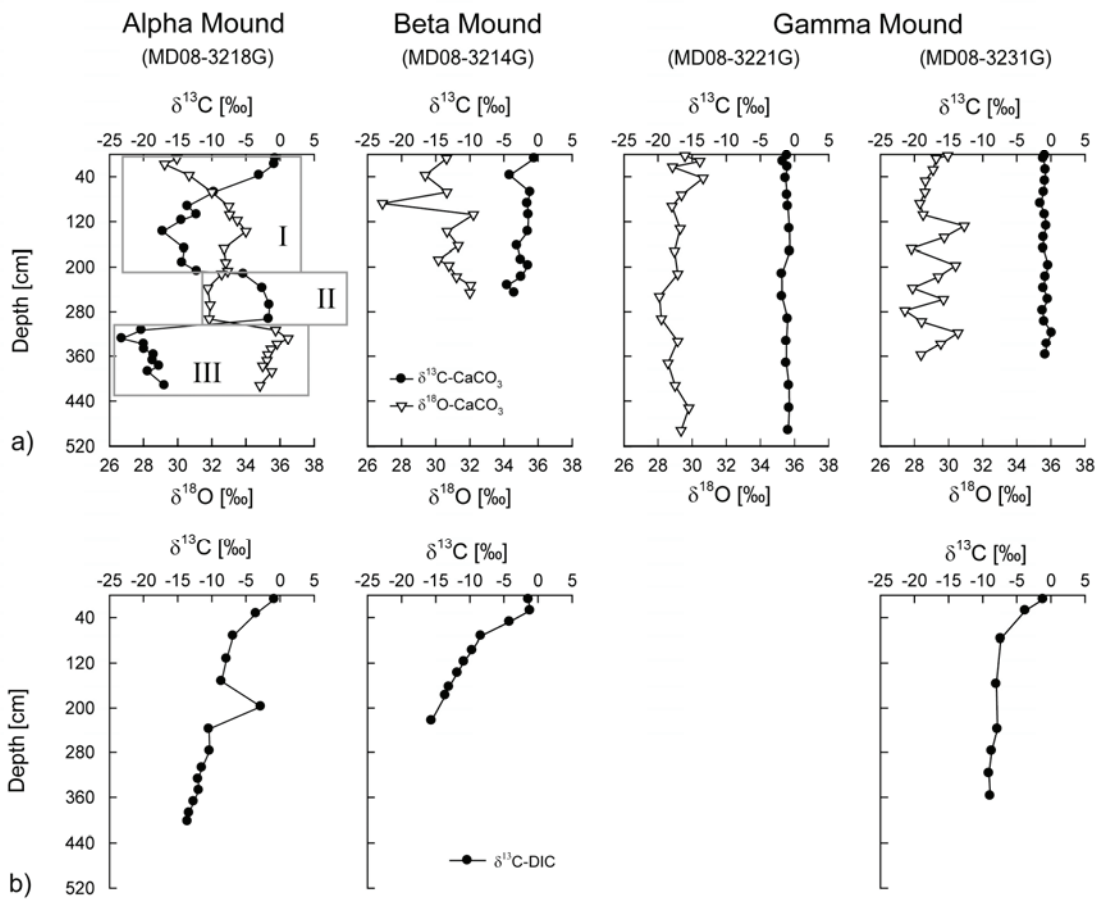

Figure 9: $\delta^{13}C$ and $\delta^{18}O$ composition of bulk carbonate ($\delta^{13}C$-$CaCO_3$ and $\delta^{18}O$-$CaCO_3$) with depth. Boxes I-III in the graph from Alpha Mound (MD08-3218) delineate three different zones of characteristic isotope composition. Also shown is the $\delta^{13}C$ composition of dissolved inorganic carbon ($\delta^{13}C$-DIC) from cores MD08-3218 (Alpha Mound), MD08-3214 (Beta Mound) and MD08-3231 (Gamma Mound).

5. Discussion

In the following, we examine the diagenetic history and geochemical processes with regard to the sulfur and iron cycle and carbonate dynamics in sediments at two of the mounds, Alpha and Beta Mound, that are affected by AOM and have a shallow sulfate methane transition zone (SMTZ). We compare these to Gamma Mound, which shows no apparent influence of shallow AOM. Due to the close proximity of the three mounds we assume that the oceanographic drivers of early diagenetic change are the same across all three mounds. That is, all structures receive similar depositional input of Fe-mineral phases including Fe-(oxyhydr)oxides and organic matter. The similar range of TOC concentrations (Tab. 2) and total Fe concentrations (Fe-mineral phases and CRS fraction; Figs. 5 and 6a) supports this assumption. The retrieved cores also show similarities in coral content. Despite these similarities in sediment input, the

investigated mounds show large discrepancies in pore-water and solid-phase geochemistry and lithology. The diagenetic history of Gamma Mound contrasts with Alpha and Beta Mound by differences in Fe speciation (Figs. 5a and b, 6a), concentration profiles of H_2S and Fe_{diss} (Fig. 7b) as well as sulfur isotope composition of pyrite (Fig. 6b). We hypothesize that these differences are caused by a varying influence of ascending hydrocarbon-bearing fluids from underlying strata rather than by differences in sediment input. While diagenetic processes in Gamma Mound can be attributed to mineralization of deposited organic matter at low rates, Alpha and Beta Mound show intrinsic signals of AOM influence in the solid-phase iron and sulfur geochemistry and the sulfur isotope composition of associated mineral phases. The latter two mounds are, however, also distinct from each other by differences in carbonate phases (Fig. 4b) and profiles for dissolved sulfate (Fig. 7a). We first discuss the diagenetic processes in the sediments from Gamma Mound. We then discuss the diagenetic history of Alpha and Beta Mound and give an interpretation of the past and present geochemical processes in Alpha Mound. We conclude with an explanation of the origin of the migrating fluids.

5.1 Diagenetic processes in non-methane influenced mound systems: Gamma Mound

Our results indicate that the major electron donating process in Gamma Mound is the mineralization of deposited organic matter. Methane was not detected except at very low concentration in the deepest part of core MD08-3231 (Fig. 3). Moreover, the δ^{13}C-DIC signal of this core (Fig. 9b) shows a trend typical for mineralization of marine-derived organic matter (Bickert, 2006). Pore-water profiles from the cores from Gamma Mound show high Fe_{diss} concentrations and the absence of H_2S (Fig. 7b). This suggests that Fe-(oxyhydr)oxides serve as terminal electron acceptor for the oxidation of organic carbon during dissimilatory Fe reduction (DIR) (Lovley, 1991,1997; Nealson and Saffarini, 1994; Weber et al., 2006) and/or that Fe_{diss} is produced by reaction of H_2S with the reactive Fe pool and Fe-containing minerals (Afonso and Stumm, 1992; Canfield, 1989, Yao and Millero, 1996). Sulfate reduction rates below detection limit, subtle decreases in pore-water sulfate (Fig. 7a) and slight increases in pyrite content with depth (Fig. 6a) indicate that sulfate reduction is proceeding at very low rates.

The dominance of microbial Fe reduction as described by Lovley (1991, 1997) has previously been reported from sites exhibiting high reactive Fe contents, e.g. the

Kattegat (Jensen et al., 2003) and Skagerrak (Canfield et al., 1993). Sediments from Gamma Mound are characterized by very high contents of Fe-(oxyhydr)oxides (Fe_{ox1} and Fe_{ox2}) that probably allow the microbial Fe-reducing community to largely out-compete sulfate reducers during anaerobic carbon mineralization. The presumed dominance of DIR over sulfate reduction results in a well-buffered pore-water carbonate system because this proton consuming process induces a strong rise in pore-water pH (Soetaert et al., 2007). Consistent with these findings is the occurrence of very well preserved coral fragments in Gamma Mound and elevated $Fe_{ads+carb}$ values. $Fe_{ads+carb}$ represents dissolved Fe adsorbed on mineral phases but probably also comprises siderite, a Fe-carbonate mineral that is regarded to be thermodynamically unstable in the presence of H_2S (Coleman et al., 1993). Siderite can precipitate in Fe-rich sediments as a consequence of Fe^{2+} and HCO_3^- production during DIR (Canfield, 1989).

There is evidence from sulfur and oxygen isotope data of dissolved sulfate and of sulfide minerals that sulfate reduction in Gamma Mound is either overprinted by oxidative sulfur cycling, i.e. disproportionation of elemental sulfur or that sulfate reduction is strongly reversible. Slight ^{34}S-enrichments with depth were found in the sulfur isotope profiles of sulfate ($\delta^{34}S\text{-}SO_4^{2-}$) in the cores from Gamma Mound (Fig. 6b). The sulfur isotopic composition of pyrite ($\delta^{34}S$-CRS) from the same cores, which are a good approximation of the average composition of the pore-water H_2S source from which it formed (Böttcher et al., 1998; Butler et al., 2004; Price and Shieh, 1979), were depleted in ^{34}S by approximately 70 ‰ relative to $\delta^{34}S\text{-}SO_4^{2-}$. Sulfur isotope fractionations larger than 50 ‰ by sulfate reducers have not been observed in laboratory experiments yet (e.g. Canfield and Thamdrup, 1994; Brunner and Bernasconi, 2005; Farquhar et al., 2008). However, such isotopic differences are often found in the marine environment and are commonly attributed to sulfide reoxidation by reactive Fe and bacterial disproportionation of sulfur intermediates (Bak and Cypionka, 1987; Böttcher et al., 2001, Jørgensen, 1990; Jørgensen and Bak, 1991; Canfield and Thamdrup, 1994). Alternatively, it is hypothesized that dissimilatory sulfate reduction could cause isotope fractionations exceeding 70 ‰ in cases where the enzymatic steps during sulfate reduction become fully reversible (Brunner and Bernasconi, 2005; Kaplan and Rittenberg, 1964). Both processes can be evoked for the large sulfur isotopic offset between pore-water sulfate and hydrogen sulfide trapped as pyrite in Gamma Mound.

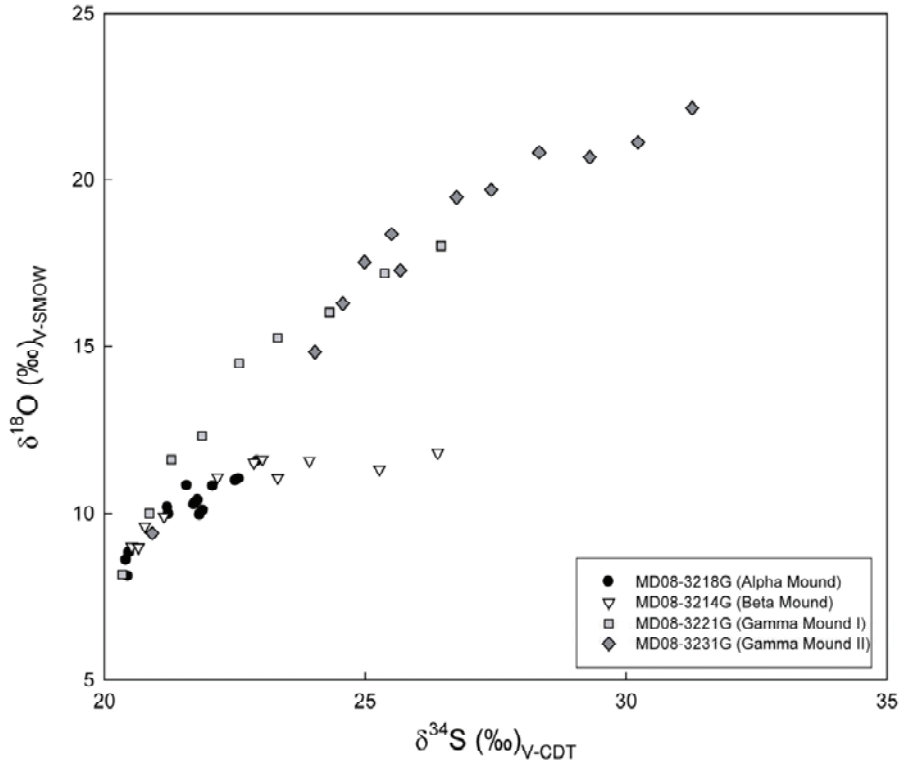

Figure 10: Sulfur versus oxygen isotope composition of pore-water sulfate in all four investigated cores.

This hypothesis is supported by the steep $\delta^{18}O$-$\delta^{34}S$ trend observed in Gamma Mound compared to Alpha and Beta Mound (Figure 10). Enrichment in ^{18}O of sulfate during sulfate reduction is the result of oxygen isotope exchange between water and sulfur intermediates (Brunner et al., 2005). Sulfate produced by disproportionation of sulfur can be enriched in ^{18}O relative to the surrounding water by up to 22 ‰ (Böttcher et al., 2005). While both disproportionation and sulfate reduction cause enrichment in ^{18}O of sulfate, disproportionation can return sulfur depleted in ^{34}S to the sulfate pool. Such a process leads to a stronger enrichment in ^{18}O relative to ^{34}S and superimposes $\delta^{18}O$-$\delta^{34}S$ effects by sulfate reduction. Reversibility of the sulfate reduction pathway also leads to strongly enhanced oxygen isotope exchange between sulfate and water over intermediates in the sulfate reduction pathway, most likely also resulting in a steepening of $\delta^{18}O$- $\delta^{34}S$ trends.

5.2 Diagenetic processes in methane influenced mound systems: Alpha and Beta Mound

In contrast to Gamma Mound, Alpha and Beta Mound show signals of a shallow sulfate methane transition zone (SMTZ). Foubert et al. (2008) and Maignien et al. (in

press) previously suggested the presence of a shallow SMTZ at ~300 cm depth in Alpha Mound. Methane was present at low concentrations in the intermediate and bottom parts of the cores from Alpha and Beta Mound (Fig. 3). Further evidence for a shallow SMTZ is AOM activity at 300-330 cm sediment depth in Alpha Mound (L. Maignien, personal communication) and δ^{13}C-DIC values of < -13 ‰ in the pore-waters of both mounds. The ^{13}C-depleted DIC can be assigned to the occurrence of AOM. This process is known to result in strongly ^{13}C-depleted carbon isotope signals of the produced DIC due to the ^{13}C-depleted isotope composition of the consumed methane compared to organic matter and an additional isotope fractionation during AOM (Alperin et al., 1988; Martens et al., 1999). The linear decrease in pore-water sulfate concentration and increases in DIC and TA in Beta Mound gives further indication for the occurrence of a SMTZ. In the cores from Alpha and Beta Mound hydrogen sulfide concentrations strongly increase at depths where sulfate reduction rates are very low or not detectable (Figs. 7b and 7c). The decoupling of sulfide distribution from the present occurrence of microbial sulfate reduction suggests that sulfide diffuses upward from the SMTZ.

5.2.1 The impact on iron and sulfur geochemistry

The production and upward diffusion of AOM-derived hydrogen sulfide has left a profound imprint on the sedimentary record of Alpha and Beta Mound that is manifested in the solid-phase iron and sulfur geochemistry. High iron-sulfide mineral contents (CRS) and elevated values for degree–of-pyritization (DOP, Fig. 6a) indicate reductive dissolution of Fe-(oxyhydr)oxides and transformation to Fe-sulfide minerals driven by the reaction of hydrogen sulfide with dissolved Fe^{2+}, intermediate iron sulfide species and reactive Fe-oxy(hydr)oxides (see Rickard et al., 1995; Rickard and Luther, 2007; and Schoonen, 2004 for review). The reaction of hydrogen sulfide with Fe-mineral phases is controlled by their reactivity towards sulfide (Canfield et al., 1992; Jørgensen et al., 2004; Poulton et al., 2004). Canfield et al. (1992) and Poulton et al. (2004) show that Fe-oxy(hydr)oxides such as ferrihydrite, lepidocrocite, goethite and hematite are characterized by very short half-lives in the order of hours to years with respect to the reaction with hydrogen sulfide. These mineral phases, extracted as Fe_{ox1} and Fe_{ox2} in the sequential extraction sequence, show a strong depletion below the top 30 cm in the cores from Alpha and Beta Mound, respectively (Fig. 5b). At similar depths, pyrite (CRS) concentrations increase as shown in Figure 6a, while iron-monosulfides (AVS) are not present. This indicates that pyrite constitutes the

predominant sink for produced hydrogen sulfide in these sediments. The extensive transformation of reactive Fe-mineral phases to pyrite is reflected in the values for degree-of-pyritization (DOP). DOP serves as proxy to estimate the remaining fraction of reactive Fe for reaction with H_2S with values approaching 1 indicating complete removal of reactive Fe-mineral phases (Berner, 1970; Lyons and Severmann, 2006; Raiswell et al., 1988; Raiswell and Canfield, 1996; Raiswell and Canfield, 1998). Below the top 30 cm of the cores from Alpha and Beta Mound, DOP averaged 0.7 (Fig. 6a), which suggests the extensive removal of reactive Fe available for reaction with H_2S on early diagenetic timescales. DOP rarely reaches these values because the availability of metabolizable organic matter limits the formation of Fe-sulfide minerals in siliciclastic non-hydrocarbon influenced sediments (Berner and Raiswell, 1984; Morse and Berner, 1995; Morse et al., 2002).

In the topmost 20 cm of the cores from Alpha and Beta Mound, there is no detectable sulfate reduction, whereas Fe_{diss} concentrations rise to 50 μM. This suggests that anaerobic carbon mineralization in the top part of these cores is driven by DIR or sulfur-iron cycling, similar to the processes occurring in Gamma Mound. In this relatively narrow zone, Fe-(oxy)hydroxides probably become continuously replenished by the re-oxidation of upward diffusing Fe_{diss} in the oxic zone (Millero et al., 1987; Stumm and Lee, 1961). The re-oxidation of Fe_{diss} is promoted by bioturbation of benthic organisms inhabiting cold-water coral mounds in large numbers (e.g. De Mol et al., 2007; Jensen and Frederiksen, 1992; Wienberg et al., 2008) that maintains high Fe-(oxyhydr)oxide concentrations in the sediment surface layers (Aller and Rude, 1988; Canfield et al., 1993; Jensen et al., 2003; Rysgaard et al., 1998; Thamdrup, 2000). Below approximately 50 cm sediment depth Alpha and Beta Mound are, however, severely affected by the upward diffusion of H_2S from the SMTZ as this causes the depletion of reactive Fe-(oxyhydr)oxides. Consequently, net Fe reduction, by DIR or oxidation of sulfide to elemental sulfur, does not occur below this depth. Organoclastic sulfate reduction alone, as shown by detectable SRR, is the dominant pathway for degradation of organic matter above the SMTZ in Alpha and Beta Mound (Fig. 7c).

5.2.2 The impact on the sulfur isotope record

The sulfur isotope composition of pyrite (δ^{34}S-CRS) from Alpha and Beta Mound sediments records both (1) the isotopic signal of H_2S produced during organoclastic sulfate reduction, and (2) upwards diffusing H_2S derived from sulfate

reduction coupled to AOM in the SMTZ. Whereas δ^{34}S-CRS values in Gamma Mound are constant at approximately -48 ‰, the δ^{34}S-CRS composition from Alpha and Beta Mound are much more variable showing values between -25 ‰ and -2 ‰ in Alpha Mound and between -25 ‰ and -3 ‰ in Beta Mound (Fig. 6b). This contrasts to the sulfur isotope profiles of sulfate that show similar distributions for all mounds with a slight enrichment in ^{34}S with depth. This pattern implies that the isotope composition of sulfide derived from the SMTZ has overprinted the isotope signature of organoclastic sulfate reduction in Alpha and Beta Mound. Sulfate reduction coupled to AOM can generate H_2S with a sulfur isotope composition close to seawater sulfate, and this isotope composition can be recorded in the pyrite offset in depth from the SMTZ (Jørgensen et al., 2004; Neretin et al., 2004). Similarly, H_2S from the SMTZ in Alpha and Beta Mound is likely to be enriched in ^{34}S compared to sulfide from organoclastic sulfate reduction (Jørgensen et al., 2004). Upward migration of sulfide from the SMTZ is therefore the most likely cause for the observed isotope signatures of pyrite in Alpha and Beta Mound.

5.3 The diagenetic history of Alpha Mound – A case study

Although Alpha and Beta Mound are similarly imprinted by a shallow SMTZ, there are some distinct geochemical features in the core from Alpha Mound. These include sediment lithologies that indicate authigenic carbonate formation as well as coral dissolution and shifts in the isotopic composition of pyrite and carbonate. This suggests that episodic changes in fluid dynamics at Alpha Mound trigger fluctuations in the depth of the SMTZ.

5.3.1 Fluctuating depth of the SMTZ

Alpha Mound shows zones of enhanced formation of authigenic high-Mg calcite (Fig. 4b) with concomitant light carbon isotope composition of bulk carbonate (Zone I and III, Figs. 4b and 9a) as well as multiple shifts from light to heavier δ^{34}S-CRS values. These shifts may have been caused by changes in the depth of the SMTZ. A shallow SMTZ exchanges ^{34}S-enriched sulfate originating from isotope fractionation due to sulfate reduction with sulfate from the overlying water column that has a seawater sulfate isotope composition. The isotope system is “open” as described by Jørgensen (1979) and strong ^{34}S enrichment of the sulfate in the SMTZ is prevented. With deepening of the SMTZ the sulfate exchange between the SMTZ and the overlying

water column becomes smaller resulting in elevated ^{34}S values of the sulfate in the SMTZ (Jørgensen, 1979; Jørgensen et al., 2004). H_2S produced in a shallow SMTZ is thus more depleted in ^{34}S than sulfide derived from a deeper located SMTZ. These changes are recorded in the isotope composition of CRS. Authigenic high-Mg calcite formation is connected to anaerobic oxidation of ^{13}C-depleted methane at depth of the SMTZ. This process is known to result in a strong alkalinity increase and oversaturation of the pore-water with respect to carbonate (Aloisi et al., 2002; Bohrmann et al., 1998; Luff et al., 2005; Peckmann et al., 2001; Ritger et al., 1987).

The variation in the flux of AOM-derived H_2S and contribution of ^{13}C-depleted DIC suggests an up and downward migration of the SMTZ probably caused by changes in the methane flux from below. Similar findings have been described e.g. by Hensen et al. (2003) for the Argentine Basin and by Meister et al. (2007) for the Peru Margin. These changes might be connected to pressure effects at the mounds flanks. Cold-water coral mounds represent elevated features on the seafloor that are subjected to high current speeds which might facilitate the development of high pressure zones at the lows of the slopes and low pressure zones at or near the summit (Depreiter et al., 2005). These pressure effects expedite the migration of fluids from deeper layers to the top of the mounds (Depreiter et al., 2005). Changes in the prevailing hydrodynamic regime and current speeds in the Gulf of Cadiz (Llave et al., 2006; Maldonado and Nelson, 1999) may force alternations of the methane flux and depth of the SMTZ within the mound. The model proposed by Depreiter et al. (2005) also serves as an explanation for the apparent non-steady state conditions in Alpha Mound at present. While several factors provide evidence for a shallow AOM zone the sulfate profile remains rather unchanged (Fig. 7a). This can be explained by the lateral in-flow of seawater at this site as consequence of the build-up of a low pressure zone near the mound summit which superimposes the pore-water signals of the prevailing diagenetic processes. Alternatively, a change in methane flux could be the result of a regional fluctuation in the tectonic activity as suggested by Pinheiro et al. (2003), who report variations in the activity of mud volcanoes due to seismic activity in this tectonically very active area.

5.3.2 Mechanisms of coral dissolution

Below 300 cm sediment depth buried cold-water coral fragments at Alpha Mound are extensively dissolved. Foubert et al. (2008) and Maignien et al. (in press) also observed zones of dissolved corals on cores from the same mound just above or

within the SMTZ. Three mechanisms that may lead to coral dissolution are (1) aerobic methanotrophy, (2) H_2S /pyrite oxidation, and (3) dissolution by H_2S titration. Here we discuss all three mechanisms and conclude that dissolution by H_2S titration is most likely, although we cannot exclude dissolution related to pyrite oxidation.

(1) Foubert et al. (2008) proposed that coral dissolution and carbonate precipitation in Alpha Mound at similar depth was due to aerobic methane oxidation driven by methane fluxes reaching the aerobic zone. Aerobic methanotrophy (MOx) however has a small effect on pH (Soetaert et al., 2007). It is usually constrained to a narrow surface horizon (<1 cm in vertical extension) even at sites of very active methane seepage (e.g. Håkon Mosby Mud Volcano in the Barents Sea, Niemann et al., 2006b) because oxygen penetration depth into the sediment is very limited due to oxygen consumption by processes other than MOx. It is thus unlikely that MOx would have maintained pore-water pH below aragonite saturation on a scale sufficient for substantial coral dissolution.

(2) A second process inducing coral dissolution in Alpha Mound may be the oxidation of pore-water H_2S and probably also the oxidation of solid-phase pyrite. Oxidation of H_2S with oxygen causes a strong decrease in the pH. It is proposed that this process leads to extensive carbonate dissolution in carbonate sediments from the Florida Keys and Bahamas Banks (Walter et al., 1993; Walter and Burton, 1990). In a study by Pirlet et al. (2010), the authors suggest that the lateral inflow of oxidizing seawater fluids resulted in the onset of ample pyrite oxidation in a pyrite-rich layer of Mound Perseverance located in the Porcupine Seabight. Pyrite oxidation induced dissolution of buried cold-water corals and created secondary porosity in this cold-water coral mound (Pirlet et al., 2010). In Alpha Mound, high pyrite concentrations may have supported a similar mechanism and the transient pore-water profiles in this mound support the assumption that it is subjected to the occasional lateral in-flow of oxygenated seawater.

(3) We propose a dissolution mechanism (Fig. 11) that links AOM-driven sulfide production with translocated aragonite dissolution. AOM coupled to sulfate reduction occurs at a shallow depth in Alpha Mound. It produces DIC and H_2S in a 1:1 stoichiometry (Reaction 1). While H_2S increases strongly with depth (Fig. 7b), there was a smaller increase in the DIC profile (Fig. 8c) most likely due to the precipitation of authigenic carbonate. H_2S diffuses upward from the SMTZ to overlying sediments.

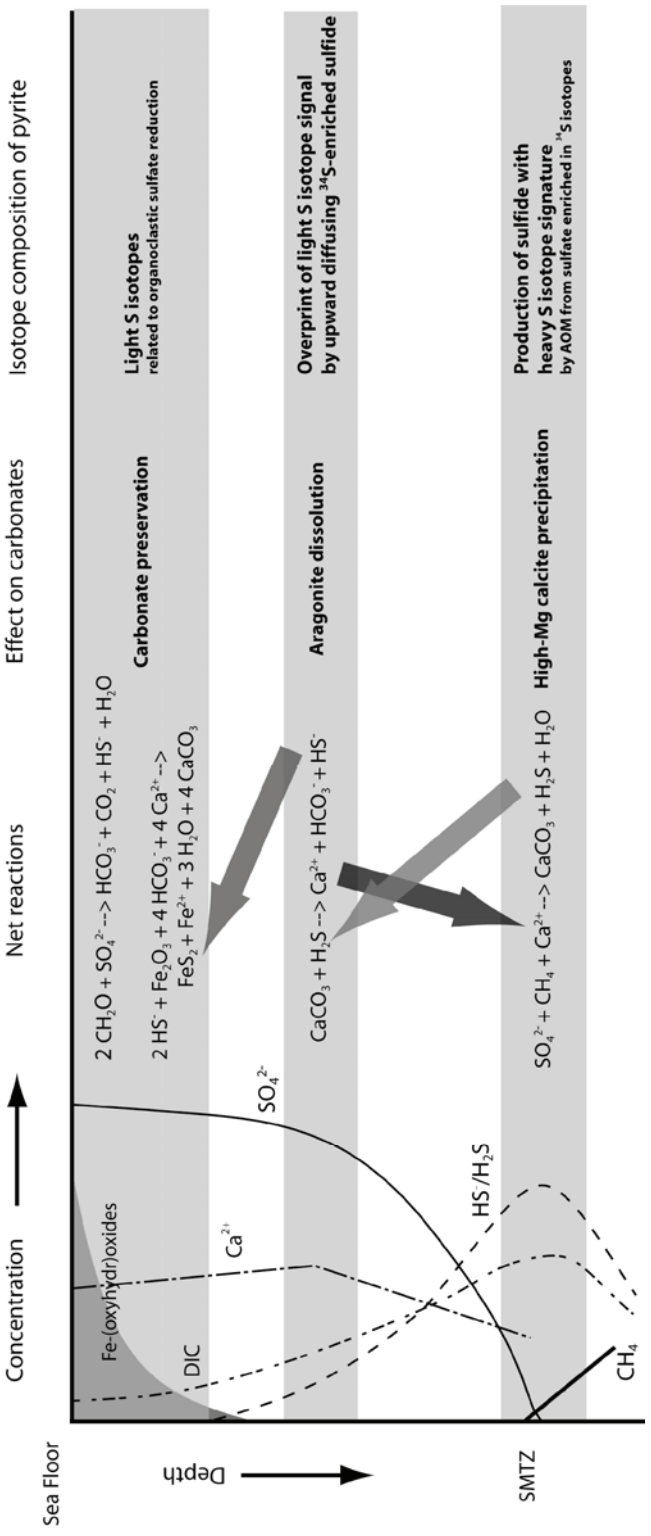

Figure 11: Schematic of profiles and major biogeochemical reactions in Alpha Mound and the effects on carbonate preservation and sulfur isotope composition of pyrite. The grey fields delineate principle reaction zones. Arrows indicate the predominating fluxes of the involved pore-water constituents.

There, H_2S functions as a weak acid and reacts with the carbonate ions (CO_3^{2-}) in the solubility equilibrium of calcium carbonate to form bicarbonate (HCO_3^-) and HS^-. This results in further dissolution of calcium carbonate to sustain the solubility equilibrium, as manifested by strongly corroded corals at this depth. The H_2S produced in the SMTZ essentially titrates the carbonate system in the overlying coral-bearing layers, leading to

coral dissolution. Above the zone of coral dissolution hydrogen sulfide ($H_2S + HS^-$) is consumed by reaction with Fe-(oxyhydr)oxides and consequent pyrite precipitation. This process prevents further coral dissolution and may even contribute to carbonate precipitation. The proposed mechanism for carbonate dissolution underscores the importance of not only delineating biogeochemical processes that occur at a given depth, but also to take into account transport-driven changes in the pore-water chemistry.

5.4 Signals and sources of ascending fluids

Pore-water enrichments in Sr^{2+} and (to a lesser extent) in Li^+ (Fig. 8b) as well as heavy $\delta^{18}O$ values of bulk carbonate in Alpha Mound suggest that the geochemistry of the three mounds is influenced by ascending fluids. In contrast to the surrounding mud volcanoes, the origin of the fluids and hydrocarbons migrating into the coral mounds is still under debate and three sources are discussed: 1) deep Mesozoic reservoirs, 2) gas hydrates and 3) migration of gas from adjacent mud volcano lobes (Foubert et al., 2008; Van Rooij et al., in review). In the following we argue in favor of a deep source linked to clay mineral dehydration within Mesozoic source rocks.

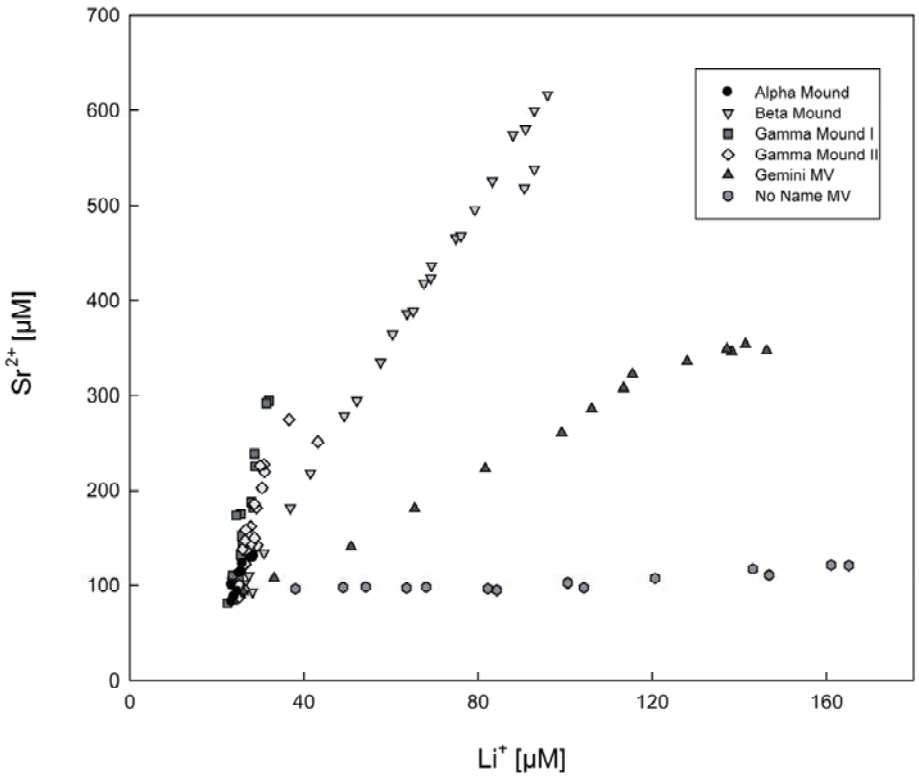

Figure 12: Pore-water Sr^{2+} versus Li^+ concentrations in all four investigated cores. Additionally pore-water Sr^{2+} versus Li^+ distribution in Gemini MV and No Name MV are displayed (data from Hensen et al. 2007).

All three mounds show an increase in Li^+ and Sr^{2+} concentrations with depth which is most pronounced in Beta Mound (Fig. 8b). Good correlation between the Li^+ and Sr^{2+} concentrations argues against coral dissolution as the main source for Sr^{2+}. Li^+ and Sr^{2+} enrichment patterns have been observed by Hensen et al. (2007) and Scholz et al. (2009) in fluids from mud volcanoes in the immediate surrounding of Pen Duick Escarpment. The comparison of the pore-water Sr^{2+} versus Li^+ concentrations from the mounds investigated in the present study to the fluids of two mud volcanoes (Gemini Mud Volcano and No Name Mud Volcano, Hensen et al. 2007) located in close proximity to the cold-water coral mounds (Fig. 1b), however show differences in the ratio of Sr^{2+} to Li^+ between the mounds and the mud volcanoes (Fig. 12). Additionally, data from Gemini MV and No Name MV show depletions in Na^+, Cl^- and K^+ relative to seawater (Hensen et al., 2007), while pore-waters from the cold-water coral mounds show seawater concentrations or enrichments in these elements. These discrepancies argue against the assumption that mud volcano fluids are the direct source for fluids ascending into the mounds as previously suggested by Foubert et al. (2008). Nevertheless, the overall similar trend in enrichment patterns between the mud volcanoes and cold-water coral mounds indicate that analog mechanisms imprint fluids migrating into both edifices. Hensen et al. (2007) and Scholz et al. (2009) attributed excess Sr^{2+} and Li^+ concentrations in near-shore mud volcanoes in the Gulf of Cadiz to intensive clay mineral dehydration in terrigenous sediments and rocks i.e. Mesozoic and Cenozoic marls, shales and limestones at several kilometers depth and at temperatures of up to 150°C. A similar mechanism is likely for the fluids ascending into the cold-water coral mounds in line with the recent work of Van Rooij et al. (in review) who suggested a stratigraphic connection between deep-located Mesozoic reservoirs and the top of Pen Duick Escarpment installed by the uplift of Miocene series during the Pliocene. Further evidence for the occurrence of clay mineral dehydration is given by the $\delta^{18}O$ composition of bulk carbonate in Alpha Mound which indicates the upward flow of ^{18}O-enriched fluids. The oxygen and carbon isotope composition of bulk carbonate from Zone I and Zone III in the core from Alpha Mound shows a strong negative correlation between decreasing $\delta^{13}C$-$CaCO_3$ and increasing $\delta^{18}O$-$CaCO_3$ (Fig. 9a and Fig. 13). It is likely that this pattern is caused by the imprint of the isotope composition of the authigenic high-Mg calcite that formed in close vicinity of a SMTZ. The $\delta^{18}O$ composition of authigenic carbonates is dependent on the temperature, mineralogy and $\delta^{18}O$ composition of the ambient fluid. If assuming equilibrium isotope

fractionation, the $\delta^{18}O$ composition of precipitating high-Mg calcite (12 mol % Mg) in Zone III can be calculated according to (Friedman and O'Neil, 1977; Tarutani et al., 1969):

$$\alpha = \frac{\left({}^{18}O/{}^{16}O_{CaCO_3}\right)}{\left({}^{18}O/{}^{16}O_{Fluid}\right)} \quad (3)$$

$$1000 \ln\alpha = 2.78 \times (10^6 T^{-2}) - 2.89 + 0.72 \quad (4)$$

where α is the carbonate-water fractionation factor expressed as 1000 lnα and T is the bottom water temperature.

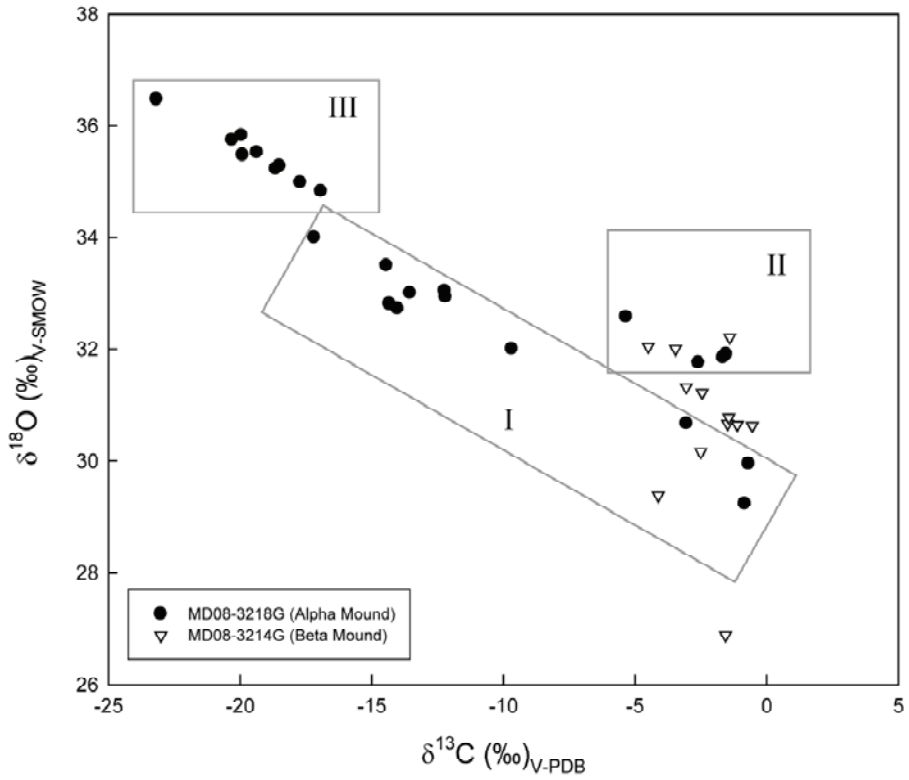

Figure 13: Carbon versus oxygen isotope composition for bulk carbonates in core MD08-3218 (Alpha Mound) and MD08-3214 (Beta Mound). Boxes I-III delineate the three zones of characteristic carbon and oxygen isotope composition for Alpha Mound.

Using ambient temperature values of 10-12°C and $\delta^{18}O_{SMOW}$= 0.94 ‰ for the bottom seawater composition (Craig and Gordon, 1965) this calculation gives a $\delta^{18}O$ isotopic value of 33.5–34.0 ‰ for the authigenic high-Mg calcite. The $\delta^{18}O$-$CaCO_3$ values (34.8-36.5 ‰) in this zone are, however, more enriched than these calculated values. At

10-12°C ambient temperature, the carbonate would have precipitated from ^{18}O-enriched fluids with an isotopic composition that is enriched to 3.8 ‰, far above seawater composition. ^{18}O-enrichment of pore-fluids is known to result from the dehydration of clay minerals (e.g. Dahlmann and de Lange, 2003) or the dissociation of gas hydrates releasing hydrate-bound, ^{18}O-enriched water (Aloisi et al., 2000, Bohrmann et al., 1998, Davidson et al., 1983; Maekawa and Imai, 2000). The latter process, however can largely be excluded as the oxygen isotope fractionation factor for gas hydrate formation of 1.0028-1.0032 (Maekawa and Imai, 2000) would not lead to a sufficient enough enrichment of ^{18}O in the carbonates especially if taking into account that ascending fluids undergo dilution with ambient fluids during transport.

The pore-water Sr^{2+} versus Li^{+} concentrations for the three investigated mounds displayed in Figure 12 show that Alpha and Beta Mound cluster close together and differ from Gamma Mound. This is consistent with the finding that methane reaches shallow depth in Alpha and Beta Mound but not in Gamma Mound. A puzzling finding, however, is that the Alpha and Beta Mound, despite their close proximity of 300 m also show distinct differences in pore-water composition as manifested by the strong increases in Na^{+} and Cl^{-} observed in Beta Mound alone (Fig. 7a). The strongly increasing Na^{+} and Cl^{-} concentrations in Beta Mound which display a Na/Cl ratio of close to 1 can be attributed to the addition of NaCl originating from halite dissolution (Bernasconi, 1987). A similar scenario has been evoked for pore-water Na^{+} and Cl^{-} enrichment at the proximate Mercator Mud Volcano (Scholz et al., 2009). The dissimilar geochemistry of pore-fluids migrating into the three cold-water coral mounds suggest that either the source reservoirs of the fluids within the Mesozoic sedimentary sequence are different or that during upward migration the fluids get overprinted by different secondary processes, e.g. halite dissolution in case of Beta Mound.

6. Conclusions

The three investigated cold-water coral mounds located in close proximity to each other on Pen Duick Escarpment in the Gulf of Cadiz are affected by ascending methane-bearing fluids. Based on geochemical signatures and active processes the mounds can be grouped in two categories, one that is affected by a shallow SMTZ (Alpha and Beta Mound), and another where there is no evidence for the presence of a shallow SMTZ (Gamma Mound). It appears that the methane flux from below is large enough to sustain a shallow SMTZ only at Alpha and Beta Mound. This may be due

either to higher methane concentrations in ascending fluids, higher total fluid advection in Alpha and Beta Mound or different fluid sources. Strong fluctuations in the depth of the SMTZ due to changing fluid dynamics are manifested in the geochemical record of Alpha Mound.

The emplacement of a shallow SMTZ in Alpha and Beta Mound has left a profound imprint on the geological record, in form of diagenetic high-Mg carbonates and high DOP values caused by the production and upward diffusion of hydrogen sulfide during AOM which resulted in the extensive pyritization of Fe-(oxyhydr)oxides. This process overprinted the sulfur isotope composition of sulfides formed during organoclastic sulfate reduction. Furthermore, it facilitated localized coral dissolution in Alpha Mound by a shift of the carbonate solubility equilibrium suggesting a strong coupling between the sulfur cycle and carbonate dynamics.

The sulfide flux related to the occurrence of a shallow SMTZ within the cold-water coral mounds also induced a shift in the organic carbon oxidation pathway and most probably in the sub-seafloor microbial community. Mineralization of organic matter in Gamma Mound is dominated by dissimilatory iron reduction promoted by high reactive Fe-oxy(hydr)oxide concentrations and sulfate reduction coupled to oxidative sulfur cycling via iron reduction (i.e. disproportionation of elemental sulfur). In contrast, reductive iron cycling in Alpha and Beta Mound is confined to the topmost sediments. Below, almost all reactive iron phases have been scavenged by the upward diffusing AOM-derived hydrogen sulfide. Thus, the pathways involving iron reduction are suppressed and the mineralization of organic matter between the surface sediments and the SMTZ is diverted to dissimilatory sulfate reduction.

Alpha and Beta Mound in the Gulf of Cadiz differ from other cold-water coral mounds investigated so far, e.g. Challenger Mound in the Porcupine Seabight, where the SMTZ at present is located below the mound base (Ferdelman et al., 2006). The example of Alpha and Beta Mound shows that these structures are very sensitive recorders of changes in fluid flow regimes. The presence of AOM has consequences not only for the geochemistry and lithology of the SMTZ but for the sulfur and iron biogeochemistry of the entire coral-bearing mound structure.

References

Afonso, M.D. and Stumm, W.: Reductive Dissolution of Iron(III) (Hydr)oxides by Hydrogen Sulfide, Langmuir, 8, 1671-1675, 1992.

Aller, R.C., Rude, P.D.: Complete oxidation of solid-phase sulfides by manganese and bacteria in anoxic marine sediments, Geochim. Cosmochim. Ac., 52, 751-765, 1988.

Aloisi, G., Bouloubassi, I., Heijs, S.K., Pancost, R.C., Pierre, C., Sinninghe Damsté, J.S., Gottschal, J.C., Forney, L.J., Rouchy, J.-M.: CH_4-consuming microorganisms and the formation of carbonate crusts at cold seeps, Earth. Planet. Sc. Lett., 203, 195-203, 2002.

Aloisi, G., Pierre, C., Rouchy, J.M., Foucher, J.P., Woodside, J.: Methane-related authigenic carbonates of eastern Mediterranean Sea mud volcanoes and their possible relation to gas hydrate destabilization, Earth. Planet. Sc. Lett., 184, 321-338, 2000.

Alperin, M.J., Reeburgh, W.S.,Whiticar, M.J.: Carbon and hydrogen isotope fractionation resulting from anaerobic methane oxidation, Global. Biogeochem. Cy., 2, 278-288, 1988.

Bak, F., Cypionka, H.: A novel type of energy metabolism involving fermentation of inorganic sulfur compounds, Nature 326, 891-892, 1987.

Baraza, J., Ercilla, G.: Gas-charged sediments and large pockmark-like features on the Gulf of Cadiz slope (SW Spain), Mar. Petrol. Geol., 13, 253-261, 1996.

Bernasconi, S.M.: Interstitial water chemistry in the western Mediterranean: Results from Leg 161. Proceedings of the Ocean Drilling Program, Scientific Results 161, 423–432, 1987.

Berner, R.A.: Sedimentary Pyrite Formation, Am. J. Sci., 268, 1-23, 1970.

Berner, R.A., Raiswell, R.: C/S Method for distinguishing fresh-water from marine sedimentary rocks, Geology, 12, 365-368, 1984.

Bickert, T.: Influence of geochemical processes on stable isotope distribution in marine sediments, in: Marine Geochemistry, editied by: Schulz, H.D. and Zabel, M., Springer, Berlin Heidelberg, 339-369, 2006.

Boetius, A. Ravenschlag, K., Schubert, C. J., Rickert, D., Widdel, F., Gieseke, A., Amann, R., Jørgensen, B. B., Witte, U., Pfannkuche, O.: A marine microbial consortium apparently mediating anaerobic oxidation of methane, Nature, 407, 623-626, 2000.

Bohrmann, G., Greinert, J., Suess, E., Torres, M.: Authigenic carbonates from the Cascadia subduction zone and their relation to gas hydrate stability, Geology, 26, 647-650, 1998.

Böttcher, M.E., Smock, A.M., Cypionka, H.: Sulfur isotope fractionation during experimental precipitation of iron(II) and manganese (II) sulfide at room temperature, Chem. Geol., 146, 127-134, 1998.

Böttcher, M.E., Thamdrup, B., Gehre, M., Theune, A.: $^{34}S/^{32}S$ and $^{18}O/^{16}O$ fractionation during sulfur disproportionation by *Desulfobulbus propionicus*, Geomicrobiol. J., 22, 219-226, 2005.

Böttcher, M.E., Thamdrup, B., Vennemann, T.W.: Oxygen and sulfur isotope fractionation during anaerobic bacterial disproportionation of elemental sulfur, Geochim. Cosmochim. Ac., 65, 1601-1609, 2001.

Brunner, B., Bernasconi, S.M.: A revised isotope fractionation model for dissimilatory sulfate reduction in sulfate reducing bacteria, Geochim. Cosmochim. Ac., 69, 4759-4771, 2005.

Brunner, B., Bernasconi, S.M., Kleikemper, J., Schroth, M.H.: A model for oxygen and sulfur isotope fractionation in sulfate during bacterial sulfate reduction processes, Geochim. Cosmochim. Ac., 69, 4773-4785, 2005.

Butler, I.B., Bottcher, M.E., Rickard, D., Oldroyd, A.: Sulfur isotope partitioning during experimental formation of pyrite via the polysulfide and hydrogen sulfide pathways: implications for the interpretation of sedimentary and hydrothermal pyrite isotope records, Earth. Planet. Sc. Lett., 495-509, 2004.

Canfield, D.E.: Reactive iron in marine sediments, Geochim. Cosmochim. Ac., 53, 619-632, 1989.

Canfield, D.E., Raiswell, R., Bottrell, S.: The reactivity of sedimentary iron minerals toward sulfide, Am. J. Sci., 292, 659-683, 1992.

Canfield, D.E., Thamdrup, B., Hansen, J.W.: The anaerobic degradation of organic matter in Danish coastal sediments - Iron reduction, manganese reduction, and sulfate reduction, Geochim. Cosmochim. Ac., 57, 3867-3883, 1993.

Canfield, D.E., Thamdrup, B.: The Production of ^{34}S-Depleted Sulfide During Bacterial Disproportionation of Elemental Sulfur, Science 266, 1973-1975, 1994.

Cline, J.D.: Spectrophotometric Determination of Hydrogen Sulfide in Natural Waters, Limnol. Oceanogr., 14, 454-458, 1969.

Coleman, M.L., Hedrick, D.B., Lovley, D.R., White, D.C., Pye, K.: Reduction of Fe(III) in Sediments by Sulfate-Reducing Bacteria, Nature, 361, 436-438, 1993.

Craig, H., Gordon, L.I.: Isotopic oceanography: Deuterium and oxygen-18 variations in the ocean and the marine atmosphere, in: Stable Isotopes in Oceanographic Studies and Paleotemperatures, editied by Tongiorgi, E., Cons. Naz. di Rech., Spoleto, Italy, 9-130, 1965.

Dahlmann, A. and de Lange, G.J.: Fluid-sediment interactions at Eastern Mediterranean mud volcanoes: a stable isotope study from ODP Leg 160, Earth. Planet. Sc. Lett., 212, 377-391, 2003.

Davidson, D.W., Leaist, D.G., Hesse, R.: ^{18}O-Enrichment in the water of a clathrate hydrate, Geochim. Cosmochim. Ac., 47, 2293-2295, 1983.

De Mol, B., Kozachenko, M., Wheeler, A, Alvares, H., Henriet, J. P., Roy, K. O. L.: Therese Mound: a case study of coral bank development in the Belgica Mound Province, Porcupine Seabight, Int. J. Earth Sci., 96, 103-120, 2007.

De Mol, B., Huvenne, V., Canals, M.: Cold-water coral banks and submarine landslides: a review, Int. J. Earth Sci., 98, 885-899, 2009.

Depreiter, D., Foubert, A., Henriet, J.-P.: Geofluid pumping in carbonate mound systems: A factor for growth and stabilization ? IOC UNESCO Workshop Report 197, pp.16, 2005.

Díaz-del-Río, V., Somoza, L., Martinez-Frias, J., Mata, M.P., Delgado, A., Hernandez-Molina, F.J., Lunar, R., Martín-Rubí, J.A., Maestro, A., Fernández-Puga, M.C., Léon, R., Llave, E., Medialdea, T., Vázquez, J.T.: Vast fields of hydrocarbon-derived carbonate chimneys related to the accretionary wedge/olistostrome of the Gulf of Cádiz. Mar. Geol., 195, 177-200, 2003.

Dorschel, B., Hebbeln, D., Rüggeberg, A., Dullo, C.: Carbonate budget of a cold-water coral carbonate mound: Propeller Mound, Porcupine Seabight, Int. J. Earth Sci., 96, 73-83, 2007.

Eisele, M., Hebbeln, D., Wienberg, C.: Growth history of a cold-water coral covered carbonate mound - Galway Mound, Porcupine Seabight, NE-Atlantic, Mar. Geol., 253, 160-169, 2008.

Farquhar, J., Canfield, D.E., Masterson, A., Bao, H., Johnston, D.: Sulfur and oxygen isotope study of sulfate reduction in experiments with natural populations from Faellestrand, Denmark, Geochim. Cosmochim. Ac., 72, 2805-2821, 2008.

Ferdelman, T.G., Kano, A., Williams, T., Henriet, J.-P. and the Expedition 307 Scientists, 2006. Proc. IODP, 307: Washington, DC (Integrated Ocean Drilling Program Management International, Inc.). doi:10.2204/iodp.proc.307.102.2006

Fernández-Puga, M. C., Vazquez, J. T., Somoza, L., Díaz-del-Río, V., Medialdea, T., Mata, M. P., Léon, R.: Gas-related morphologies and diapirism in the Gulf of Cádiz, Geo.-Mar. Lett., 23, 300-310, 2007.

Fossing, H., Jørgensen, B.B.: Measurement of Bacterial Sulfate Reduction in Sediments - Evaluation of a Single-Step Chromium Reduction Method, Biogeochemistry 8, 205-222, 1989.

Foubert, A., Depreiter, D., Beck, T., Maignien, L., Pannemans, B., Frank, N., Blamart, D., Henriet, J.P.: Carbonate mounds in a mud volcano province off north-west Morocco: Key to processes and controls, Mar. Geol., 248, 74-96, 2008.

Freiwald, A.: Reef-forming cold-water corals, in: Ocean Margin Systems, edited by: Wefer, G., Billett, D., Hebbeln, D., Jørgensen, B.B., Schlüter, M. and van Weering, T.C.E., Springer, Heidelberg, 365-385, 2002.

Friedman, I., O'Neil, J.R.: Compilation of stable isotope fractionation factors of geochemical interest, U.S.G.S. Professional Paper, 1977.

Gardner, J.M.: Mud volcanoes revealed and sampled on the Western Moroccan continental margin, Geophys. Res. Lett., 28, 339-342, 2001.

Gieskes, J. M., Rogers, W. C.: Alkalinity Determination in Interstitial Waters of Marine Sediments, J. Sediment. Petrol., 43, 272–277, 1973.

Gutscher, M. A., Malod, J., Rehault, J. P., Contrucci, I., Klingelhoefer, F., Mendes-Victor, L., Spakman, W.: Evidence for active subduction beneath Gibraltar, Geology 30, 1071-1074, 2002.

Hall, P. O., Aller, R. C.: Rapid, small-volume, flow injection analysis for ΣCO2 and NH_4^+ in marine and freshwaters, Limnol. Oceanogr., 37, 1113–1119, 1992.

Hardy, R., Tucker, M.: X-ray powder diffraction of sediments, in: Techniques in Sedimentology, editied by Tucker, M., Blackwell Scientific Publications, 191-228, 1988.

Hensen, C., Zabel, M., Pfeifer, K., Schwenk, T., Kasten, S., Riedinger, N., Schulz, H.D., Boetius, A.: Control of sulfate pore-water profiles by sedimentary events and the significance of anaerobic oxidation of methane for the burial of sulfur in marine sediments, Geochim. Cosmochim. Ac., 67, 2631-2647, 2003.

Hensen, C., Nuzzo, M., Hornibrook, E., Pinheiro, L.M., Bock, B., Magalhães, V.H., Brückmann, W.: Sources of mud volcano fluids in the Gulf of Cadiz - indications for hydrothermal imprint, Geochim. Cosmochim. Ac., 71, 232-1248, 2007.

Hinrichs, K.U., Hayes, J.M., Sylva, S.P., Brewer, P.G., DeLong, E.F.: Methane-consuming archaebacteria in marine sediments, Nature 398, 802-805, 1999.

Huvenne, V.A.I., De Mol, B., Henriet, J.P.: A 3D seismic study of the morphology and spatial distribution of buried coral banks in the Porcupine Basin, SW of Ireland, Mar. Geol., 198, 5-25, 2003.

Jensen, A., Frederiksen, R.: The fauna associated with the bank-forming deep-water coral Lophelia-pertusa (scleractinaria) on the Faroe Shelf, Sarsia 77, 53-69, 1992.

Jensen, M.M., Thamdrup, B., Rysgaard, S., Holmer, M., Fossing, H.: Rates and regulation of microbial iron reduction in sediments of the Baltic-North Sea transition, Biogeochemistry 65, 295-317, 2003.

Jørgensen, B.B.:. Comparison of methods for the quantification of bacterial sulfate reduction in coastal marine-sediments .1. Measurement with radiotracer techniques, Geomicrobiol. J., 1, 11-27, 1978.

Jørgensen, B.B.: Theoretical model of the stable sulfur isotope distribution in marine sediments, Geochim. Cosmochim. Ac., 43, 363-374, 1979.

Jørgensen, B.B.: A Thiosulfate Shunt in the Sulfur Cycle of Marine Sediments, Science, 249, 152-154, 1990.

Jørgensen, B.B. and Bak, F.: Pathways and Microbiology of Thiosulfate Transformations and Sulfate Reduction in a Marine Sediment (Kattegat, Denmark). Appl. Environ. Microb., 57, 847-856, 1991.

Jørgensen, B.B., Böttcher, M.E., Luschen, H., Neretin, L.N., Volkov, II: Anaerobic methane oxidation and a deep H_2S sink generate isotopically heavy sulfides in Black Sea sediments, Geochim. Cosmochim. Ac., 68, 2095-2118, 2004.

Jørgensen, B.B., Kasten, S.: Sulfur Cycling and Methane Oxidation, in: Marine Geochemistry, editied by Schulz, H.D. and Zabel, M., Springer, Berlin Heidelberg, 271-310, 2006.

Kallmeyer, J., Ferdelman, T.G., Weber, A., Fossing, H,. Jørgensen, B.B.: A cold chromium distillation procedure for radiolabeled sulfide applied to sulfate reduction measurements. Limnol. Oceanogr.-Meth., 2, 171-180, 2004.

Kaplan, I.R., Rittenberg, S.C.: Microbiological Fractionation of Sulphur Isotopes, J. Gen. Microbiol., 34, 195-212, 1964.

Knittel, K., Boetius, A., Lemke, A., Eilers, H., Lochte, K., Pfannkuche, O., Linke, P., Amann, R.: Activity, distribution, and diversity of sulfate reducers and other bacteria in sediments above gas hydrate (Cascadia margin, Oregon), Geomicrobiol. J., 20, 269-294, 2003.

Knittel, K., Losekann, T., Boetius, A., Kort, R., Amann, R.: Diversity and distribution of methanotrophic archaea at cold seeps, Appl. Environ. Microb., 71, 467-479, 2005.

León, R., Somoza, L., Medialdea, T., Maestro, A., Díaz-del-Río, V, Fernández-Puga, M.d.: Classification of sea-floor features associated with methane seeps along the Gulf of Cádiz continental margin, Deep-Sea Research II, 53, 1464-1481, 2006.

Lindberg, B., Mienert, J.: Postglacial carbonate production by cold-water corals on the Norwegian Shelf and their role in the global carbonate budget, Geology, 33, 537-540, 2005.

Llave, E., Schönfeld, J., Hernández-Molina, F.J., Mulder, T., Somoza, L., Díaz del Río, V., Sánchez-Almazo, I.: High-resolution stratigraphy of the Mediterranean outflow contourite system in the Gulf of Cadiz during the late Pleistocene: The impact of Heinrich events, Mar. Geol., 227, 241-262, 2006.

Lovley, D.R.: Dissimilatory Fe(III) and Mn(IV) Reduction, Microbiol. Rev., 55, 259-287, 1991.

Lovley, D.R.: Microbial Fe(III) reduction in subsurface environments, FEMS Microbiol. Rev., 20, 305-313, 1997.

Luff, R., Greinert, J., Wallmann, K., Klaucke, I., Suess, E.: Simulation of long-term feedbacks from authigenic carbonate crust formation at cold vent sites, Chem. Geol., 216, 157-174, 2005.

Lumsden, D.N.: Discrepancy between Thin-Section and X-Ray Estimates of Dolomite in Limestone, J. Sediment. Petrol., 49, 429-436, 1979.

Lyons, T.W., Severmann, S.: A critical look at iron paleoredox proxies: New insights from modern euxinic marine basins, Geochim. Cosmochim. Ac., 70, 5698-5722, 2006.

Maekawa, T., Imai, N.: Hydrogen and oxygen isotope fractionation in water during gas hydrate formation. Gas Hydrates: Challenges for the Future, 912, 452-459, 2000.

Maldonado, A., Nelson, C.H.: Interaction of tectonic and depositional processes that control the evolution of the Iberian Gulf of Cadiz margin, Mar. Geol., 155, 217-242, 1999.

Maignien, L., Depreiter, D., Foubert, A., Reveillaud, J., De Mol, L., Boeckx, P., Blamart, D., Henriet, J.-P., Boon, N., Anoxic methane oxidation in a cold-water coral carbonate mound from the Gulf of Cadiz, Int. J. Earth Sci., in press.

Martens, C.S., Albert, D.B., Alperin, M.J.: Stable isotope tracing of anaerobic methane oxidation in the gassy sediments of Eckernforde Bay, German Baltic Sea, Am. J. Sci., 299, 589-610, 1999.

März, C., Hoffmann, J., Bleil, U., De Lange, G.J., Kasten, S.: Diagenetic changes of magnetic and geochemical signals by anaerobic methane oxidation in sediments of the Zambezi deep-sea fan (SW Indian Ocean), Mar. Geol., 255, 118-130, 2008.

Medialdea, T., Somoza, L., Pinheiro, L.M., Fernández-Puga, M.C., Vázquez, J.T., León, R., Ivanov, M.K., Magalhães, V., Díaz-del-Río, V., Vegas, R.: Tectonics and mud volcano development in the Gulf of Cádiz, Mar. Geol., 261, 48-63, 2008.

Medialdea, T., Vegas, R., Somoza, L., Vázquez, J. T., Maldonado, A., Díaz-del-Río, V., Maestro, A., Córdoba, D., Fernández-Puga, M. C.: Structure and evolution of the "Olistostrome" complex of the Gibraltar Arc in the Gulf of Cadiz (eastern Central Atlantic): evidence from two long seismic cross-sections, Mar. Geol., 209, 173-198, 2004.

Meister, P., McKenzie, J.A., Vasconcelos, C., Bernasconi, S., Frank, M., Gutjahr, M., Schrag, D.P.: Dolomite formation in the dynamic deep biosphere: results from the Peru Margin, Sedimentology, 54, 1007-1031, 2007.

Michaelis, W., Seifert, R., Nauhaus, K., Treude, T., Thiel, V., Blumenberg, M., Knittel, K., Gieseke, A., Peterknecht, K., Pape, T., Boetius, A., Amann, R., Jørgensen, B.B., Widdel, F., Peckmann, J.R., Pimenov, N.V., Gulin, M.B.: Microbial reefs in the Black Sea fueled by anaerobic oxidation of methane, Science, 297, 1013-1015, 2002.

Mienis, F., de Stigter, H.C., White, M., Duineveld, G., de Haas, H., van Weering, T.C.E.: Hydrodynamic controls on cold-water coral growth and carbonate-mound development at the SW and SE Rockall Trough Margin, NE Atlantic Ocean, Deep-Sea Res. Pt. I ,54, 1655-1674, 2007.

Millero, F.J., Sotolongo, S., Izaguirre, M.: The Oxidation-Kinetics of Fe(II) in Seawater, Geochim. Cosmochim. Ac., 51, 793-801, 1987.

Morse, J.W., Berner, R.A.: What Determines Sedimentary C-S Ratios, Geochim. Cosmochim. Ac., 59, 1073-1077, 1995.

Morse, J.W., Gledhill, D.K., Sell, K.S., Arvidson, R.S.: Pyritization of iron in sediments from the continental slope of the Northern Gulf of Mexico, Aquat. Geochem., 8, 3-13, 2002.

Naehr, T.H., Eichhubl, P., Orphan, V. J., Hovland, M., Paull, C. K., Ussler, W., Lorenson, T. D., Greene, H. G.: Authigenic carbonate formation at hydrocarbon seeps in continental margin sediments: A comparative study, Deep-Sea Res. Pt. II, 54, 1268-1291, 2007.

Nauhaus, Boetius, A., Krüger, M., Widdel, F.: In vitro demonstration of anaerobic oxidation of methane coupled to sulphate reduction in sediment from a marine gas hydrate area, Environ. Microbiol., 4, 296-305, 2002.

Nealson, K.H., Saffarini, D.: Iron and Manganese in Anaerobic Respiration - Environmental Significance, Physiology, and Regulation, Annu. Rev. Microbiol., 48, 311-343, 1994.

Neretin, L.N., Böttcher, M.E., Jørgensen, B.B., Volkov, I.I., Lüschen, H., Hilgenfeldt, K.: Pyritization processes and greigite formation in the advancing sulfidization front in the Upper Pleistocene sediments of the Black Sea, Geochim. Cosmochim. Ac., 68, 2081-2093, 2004.

Niemann, H. Duarte, J., Hensen, C., Omoregie, E., Magalhães, V., Elvert, M., Pinheiro, L.M., Kopf, A., Boetius, A.: Microbial methane turnover at mud volcanoes of the Gulf of Cadiz, Geochim. Cosmochim. Ac., 70, 5336-5355, 2006a.

Niemann, H., Lösekann, T., de Beer, D., Elvert, M., Nadalig, T., Knittel, K., Amann, R., Sauter, E. J., Schlüter, M., Klages, M., Foucher, J.P., Boetius, A.: Novel microbial communities of the Haakon Mosby mud volcano and their role as a methane sink, Nature, 443, 854-858, 2006b.

Nuzzo, M., Hornibrook, E. R. C., Gill, F., Hensen, C., Pancost, R. D., Haeckel, M., Reitz, A., Scholz, F., Magalhães, V. H., Bruckmann, W., Pinheiro, L. M.: Origin of light volatile hydrocarbon gases in mud volcano fluids, Gulf of Cadiz – Evidence for multiple sources and transport mechanisms in active sedimentary wedges, Chem. Geol., 266, 350-363, 2009.

Orphan, V.J., House, C.H., Hinrichs, K.U., McKeegan, K.D., DeLong, E.F.: Methane-consuming archaea revealed by directly coupled isotopic and phylogenetic analysis, Science, 293, 484-487, 2001.

Passier, H.F., Dekkers, M.J., de Lange, G.J.: Sediment chemistry and magnetic properties in an anomalously reducing core from the eastern Mediterranean Sea, Chem. Geol., 152, 287-306, 1998.

Peckmann, J., Reimer, A., Luth, U., Luth, C., Hansen, B.T., Heinicke, C., Hoefs, J., Reitner, J.: Methane-derived carbonates and authigenic pyrite from the northwestern Black Sea, Mar. Geol., 177, 129-150, 2001.

Pinheiro, L.M., Ivanov, M.K., Sautkin, A., Akhmanov, G., Magalhães, V.H., Volkonskaya, A., Monteiro, J.H., Somoza, L., Gardner, J.V., Hamouni, N., Cunha, M.R.: Mud volcanism in the Gulf of Cadiz: results from the TTR-10 cruise, Mar. Geol., 195, 131-151, 2003.

Pirlet, H., Wehrmann, L.M., Brunner, B., Frank, N., Dewanckele, J., Van Rooij, D., Foubert, A., Swennen, R., Naudts, L., Boone, M., Cnudde, V., Henriet, J.-P.: Diagenetic formation of gypsum and dolomite in a cold-water coral mound in the Porcupine Seabight, off Ireland, Sedimentology, 57, 786-805, 2010.

Poulton, S.W., Canfield, D. E.: Development of a sequential extraction procedure for iron: implications for iron partitioning in continentally derived particulates, Chem. Geol., 214, 209–221, 2005.

Poulton, S.W., Krom, M.D., Raiswell, R.: A revised scheme for the reactivity of iron (oxyhydr)oxide minerals towards dissolved sulfide, Geochim. Cosmochim. Ac., 68, 3703-3715, 2004.

Price, F.T., Shieh, Y.N.: Fractionation of sulfur isotopes during laboratory synthesis of pyrite at low temperatures, Chem. Geol., 27, 245-253, 1979.

Raiswell, R., Buckley, F., Berner, R.A., Anderson, T.F.: Degree of pyritization of iron as a paleoenvironmental indicator of bottom water oxygenation, J. Sediment. Petrol., 58, 812-819, 1988.

Raiswell, R., Canfield, D.E.: Rates of reaction between silicate iron and dissolved sulfide in Peru Margin sediments, Geochim. Cosmochim. Ac., 60, 2777-2787, 1996.

Raiswell, R., Canfield, D.E.: Sources of iron for pyrite formation in marine sediments, Am. J. Sci., 298, 219-245, 1998.

Rickard, D., Luther, G.W.: Chemistry of Iron Sulfides, Chem. Rev., 107, 514-562, 2007.

Rickard, D., Schoonen, M.A.A., Luther, G.W.: Chemistry of iron sulfides in sedimentary environments, in: Geochemical Transformations of Sedimentary Sulfur, editied by: Vairavamurthy, M.A., Schoonen, M.A.A., ACS Symposium Series 612, Washington DC, 168-193, 1995.

Riedinger, N., Pfeifer, K., Kasten, S., Garming, J.F.L., Vogt, C., Hensen, C.: Diagenetic alteration of magnetic signals by anaerobic oxidation of methane related to a change in sedimentation rate, Geochim. Cosmochim. Ac., 69, 4117-4126, 2005.

Ritger, S., Carson, B., Suess, E.: Methane-Derived Authigenic Carbonates Formed by Subduction Induced Pore-Water Expulsion Along the Oregon Washington Margin, Geol. Soc. Am. Bull., 98, 147-156, 1987.

Roberts, J.M., Wheeler, A.J., Freiwald, A.: Reefs of the deep: The biology and geology of cold-water coral ecosystems, Science, 312, 543-547, 2006.

Rosenbaum, J., Sheppard, S.M.F.: An isotopic study of siderites, dolomites and ankerites at high temperatures, Geochim. Cosmochim. Ac., 50, 1147-1150, 1986.

Rüggeberg, A., Dullo, C., Dorschel, B. and Hebbeln, D.: Environmental changes and growth history of a cold-water carbonate mound (Propeller Mound, Porcupine Seabight), Int. J. Earth Sci., 96, 57-72, 2007.

Rysgaard, S., Thamdrup, B. Risgaard-Petersen, N., Fossing, H., Berg, P., Christensen, P.B., Dalsgaard, T.: Seasonal carbon and nutrient mineralization in a high-Arctic coastal marine sediment, Young Sound, Northeast Greenland, Mar. Ecol. Prog. Ser., 175, 261-276, 1998.

Scholz, F., Hensen, C., Reitz, A., Romer, R.L., Liebetrau, V., Meixner, A., Weise, S.M., Haeckel, M.: Isoptopic evidence ($^{87}Sr/^{86}Sr$, $\delta^{7}Li$) for alteration of the oceanic crust at deep-rooted mud volcanoes in the Gulf of Cadiz, NE Atlantic Ocean, Geochim. Cosmochim. Ac., 73, 5444-5459, 2009.

Schoonen, M.A.A.: Mechanisms of sedimentary pyrite formation, in: Sulfur Biogeochemistry - Past and Present, editied by: Amend, J.P., Edwards, K.J., Lyons, T.W., Geol. S. Am. S., 117-134, 2004.

Seeberg-Elverfeldt, J., Schlüter, M., Feseker, T. and Kölling, M.: Rhizon sampling of porewaters near the sediment-water interface of aquatic systems, Limnol. Oceanogr.-Meth., 3, 361-371, 2005.

Soetaert, K., Hofmann, A.F., Middelburg, J.J., Meysman, F.J.R. and Greenwood, J.: The effect of biogeochemical processes on pH, Mar. Chem., 106, 380-401, 2007.

Somoza, L., Díaz-del-Río, V., León, R., Ivanov, M., Fernández-Puga, M. C., Gardner, J. M., Hernández-Molina, F. J., Pinheiro, L. M., Rodero, J., Lobato, A., Maestro, A., Vázquez, J. T., Medialdea, T., Fernández-Salas, L. M.: Seabed morphology and hydrocarbon seepage in the Gulf of Cadiz mud volcano area: Acoustic imagery, multibeam and ultra-high resolution seismic data, Mar. Geol., 195, 153-176, 2003.

Stadnitskaia, A., Ivanov, M.K., Blinova V., Kreulen R., van Weering, T.C.E.: Molecular and carbon isotopic variability of hydrocarbon gases from mud volcanoes in the Gulf of Cadiz, NE Atlantic, Mar. Petrol. Geol., 23, 281-296, 2006.

Stadnitskaia, A., Ivanov, M.K., Sinninghe Damsté, J.S.: Application of lipid biomarkers to detect sources of organic matter in mud volcano deposits and post-eruptional methanotrophic processes in the Gulf of Cadiz, NE Atlantic, Mar. Geol., 255, 1-14, 2008.

Stookey, L.L.: Ferrozine: a new spectrophotometric re-agent for iron, Anal. Chem., 42, 779-781, 1970.

Stumm, W., Lee, G.F.: Oxygenation of Ferrous Iron, Ind. Eng. Chem., 53, 143-146, 1961.

Tarutani, T., Clayton, R.N., Mayeda, T.K.: Effect of Polymorphism and Magnesium Substitution on Oxygen Isotope Fractionation between Calcium Carbonate and Water, Geochim. Cosmochim. Ac., 33, 987-996, 1969.

Thamdrup, B.: Bacterial manganese and iron reduction in aquatic sediments, Advances in Microbial Ecology, Vol 16, 41-84, 2000.

Titschack, J., Thierens, M., Dorschel, B., Schulbert, C., Freiwald, A., Kano, A., Takashima, C., Kawagoe, N., Li, X., IODP Expedition 307 scientific party: Carbonate budget of a cold-water coral mound (Challenger Mound, IODP Exp. 307), Mar. Geol. 259, 36-46, 2009.

Treude, T., Boetius, A., Knittel, K., Wallmann, K., Jørgensen, B.B.: Anaerobic oxidation of methane above gas hydrates at Hydrate Ridge, NE Pacific Ocean, Mar. Ecol. Prog. Ser., 264, 1-14, 2003.

Valentine, D.L., Reeburgh, W.S.: New perspectives on anaerobic methane oxidation, Environ. Microbiol., 2, 477-484, 2000.

Van Rensbergen, P. Depreiter, D., Pannemans, B., Moerkerke, G., VanRooij, D., Marsset, B., Akhmanov, G., Blinova, V., Ivanov, M., Rachidi, M., Magalhaes, V., Pinheiro, L., Cunha, M., Henriet, J.P.: The El arraiche mud volcano field at the Moroccan Atlantic slope, Gulf of Cadiz, Mar. Geol., 219, 1-17, 2005.

Van Rooij, D., Depreiter, D., Bouimetarhan, I., Boever, E.D., Rycker, D., Foubert, A., Huvenne, V., Reveillaud, J., Staelens, P., Vercruysse, J., Versteeg, W., Henriet, J.P.: First sighting of active fluid venting in the Gulf of Cadiz. Eos Transactions AGU, 86, 509-520, 2005.

Van Rooij, D., Blamart,, De Mol, L., Mienis, F., Pirlet, H., Wehrmann, L.M., Barbieri, R., Maignien, L., Templer, S.P., de Haas, H., Hebbeln, D., Frank, N., Larmagnat, S., Stadnitskaia, A., Stivaletta, N., van Weering, T., Zhang, Y., Hamoumi, N., Cnudde, V., Duyck, P., Henriet, J.-P. & the MiCROSYSTEMS MD 169 shipboard party. Cold-water coral mounds on the Pen Duick Escarpment, Gulf of Cadiz: the MiCROSYSTEMS approach, Mar. Geol., in review.

van Weering, T.C.E., de Haas, H., de Stigter, H.C., Lykke-Andersen, H., Kouvaev, I.: Structure and development of giant carbonate mounds at the SW and SE Rockall Trough margins, NE Atlantic Ocean, Mar. Geol., 198, 67-81, 2003.

Walter, L.M., Bischof, S.A., Patterson, W.P. and Lyons, T.W.: Dissolution and recrystallization in modern shelf carbonates: evidence from pore water and solid phase chemistry, Philos. T. Roy. Soc. Lond. A, 344, 27-36, 1993.

Walter, L.M. and Burton, E.A.: Dissolution of Recent Platform Carbonate Sediments in Marine Pore Fluids, Am. J. Sci., 290, 601-643, 1990.

Weaver, P.P.E., Billett, D.S.M., Boetius, A., Danovaro, R., Freiwald, A., Sibuet, M.: Hot-spot ecosystem research on Europe's deep-ocean margins, Oceanography 17, 123-143, 2004.

Weber, K.A., Achenbach, L.A., Coates, J.D.: Microorganisms pumping iron: anaerobic microbial iron oxidation and reduction, Nature Rev. Microbiol., 4, 752-764, 2006.

Webster, G., Blazejak, A., Cragg, B.A., Schippers, A., Sass, H., Rinna, J., Tang, X., Mathes, F., Ferdelman, T.G., Fry, C., Weightmann, A.J., Parkes, J.R.: Subsurface microbiology and

biogeochemistry of a deep, cold-water carbonate mound from the Porcupine Seabight (IODP Expedition 307), Environ. Microbiol., 11, 239-257, 2009.

Wehrmann, L.M., Knab, N.J., Pirlet, H., Unnithan, V., Wild, C., Ferdelman, T.G.: Carbon mineralization and carbonate preservation in modern cold-water coral reef sediments on the Norwegian shelf, Biogeosciences, 6, 663-680, 2009.

Wheeler, A.J., Beyer, A., Freiwald, A., de Haas, H., Huvenne, V. A. I., Kozachenko, M., Roy, K. O. L., Opderbecke, J.: Morphology and environment of cold-water coral carbonate mounds on the NW European margin, Int. J. Earth Sci., 96, 37-56, 2007.

Wienberg, C., Beuck, L., Heidkamp, S., Hebbeln, D., Freiwald, A., Pfannkuche, O., Moteys, W.: Franken Mound: facies and biocoenoses on a newly-discovered "carbonate mound" on the western Rockall Bank, NE Atlantic, Facies 54, 1-24, 2008.

Wienberg, C., Hebbeln, D., Fink, H.G., Mienis, F., Dorschel, B., Vertino, A., López Correa, M., Freiwald, A.: Scleractinian cold-water corals in the Gulf of Cádiz-First clues about their spatial and temporal distribution, Deep-Sea Res. Pt. I, 56, 1873-1893, 2009.

Yao, W.S., Millero, F.J.: Oxidation of hydrogen sulfide by hydrous Fe(III) oxides in seawater, Mar. Chem. 52, 1-16, 1996.

Zitellini, N., Gracia, E., Matias, L., Terrinha, P., Abreu, M. A., DeAlteriis, G., Henriet, J. P., Danobeitia, J. J., Masson, D. G., Mulder, T., Ramella, R., Somoza, L., Diez, S.: The quest for the Africa-Eurasia plate boundary west of the Strait of Gibraltar, Earth. Planet. Sc. Lett., 280, 13-50, 2009.

CHAPTER 7:

DIAGENETIC FORMATION OF GYPSUM AND DOLOMITE IN A COLD-WATER CORAL MOUND IN THE PORCUPINE SEABIGHT, OFF IRELAND.

Hans Pirlet[1], Laura M. Wehrmann[2,3], Benjamin Brunner[2], Norbert Frank[4], Jan Dewanckele[5,6], David Van Rooij[1], Anneleen Foubert[7], Rudy Swennen[7], Lieven Naudts[1], Matthieu Boone[6], Veerle Cnudde[5,6] and Jean-Pierre Henriet[1].

[1]Renard Centre of Marine Geology, Department of Geology and Soil Science, Ghent University, Krijgslaan 281 s8, B-9000 Gent, Belgium.

[2]Biogeochemistry Research Group, Max Planck Institute for Marine Microbiology, Celsiusstrasse 1, D-28359 Bremen, Germany.

[3]Coral Reef Ecology Work Group, GeoBio-Center, Ludwig-Maximilians Universität, Richard-Wagner-Strasse 10, D-80333 München, Germany.

[4]Laboratoire des Sciences du Climat et de L'Environnement (LSCE), Unité Mixte CEA/CNRS/UVSQ, Bat 12, Avenue de la Terrasse, F- 91190 Gif-sur-Yvette, France.

[5]Department of Geology and Soil Science, Ghent University, Krijgslaan 281 s8, B-9000 Gent, Belgium.

[6]Department of Subatomic and Radiation Physics, Ghent Univeristy, B-9000 Gent, Belgium.

[7]Department of Earth and Environmental Sciences, Geology, K.U. Leuven, Celestijnenlaan 200E, 3001 Heverlee, Belgium.

***Sedimentology,* 57, 786-805, 2010**

Abstract

Authigenic gypsum was found in a gravity core, retrieved from the top of Mound Perseverance, a giant cold-water coral mound in the Porcupine Basin, off Ireland. The occurrence of gypsum in such an environment is intriguing, since gypsum, a classic evaporitic mineral, is undersaturated with respect to sea water. Sedimentological, petrographic and isotopic evidence point to diagenetic formation of the gypsum, tied to oxidation of sedimentary sulphide minerals (i.e. pyrite). This oxidation is attributed to a phase of increased bottom currents which caused erosion and enhanced inflow of oxidizing fluids into the mound sediments. The oxidation of pyrite produced acidity, causing carbonate dissolution and subsequently leading to pore-water oversaturation with respect to gypsum and dolomite. Calculations based on the isotopic compositions of gypsum and pyrite reveal that between 21.6 % and 28.6 % of the sulphate incorporated into the gypsum derived from pyrite oxidation. The dissolution of carbonate increased the porosity in the affected sediment layer but promoted lithification of the sediments at the sediment-water interface. Thus, authigenic gypsum can serve as a signature for diagenetic oxidation events in carbonate-rich sediments. These observations demonstrate that fluid flow, steered by environmental factors, has an important effect on the diagenesis of coral mounds.

1. Introduction

The occurrence of cold-water corals has been reported all along the Atlantic European margin over a wide bathymetric and hydrographical range (Freiwald & Roberts, 2005; Roberts et al., 2006). The framework-building cold-water corals, *Lophelia pertusa* and *Madrepora oculata* are found from northern Norway, where they form elongated reefs (Lindberg et al., 2007; Wheeler et al., 2007), to the Gulf of Cadiz where they occur in the vicinity of mud volcanoes (Foubert et al., 2008). In the Porcupine Seabight, located south-west of Ireland, Lophelia and Madrepora have built mounds up to 200 m high (De Mol et al., 2002; Henriet et al., 1998; Huvenne et al., 2002). In the latter area, the mounds occur in three well-delineated provinces (Fig. 1): the Belgica mound province, on the eastern slope of the Porcupine Seabight, the Hovland mound province, on the northern slope of the basin and the Magellan mound province which flanks the Hovland mounds to the north. The mounds in each of these provinces feature distinct morphologies (De Mol et al., 2002; Van Rooij et al., 2003).

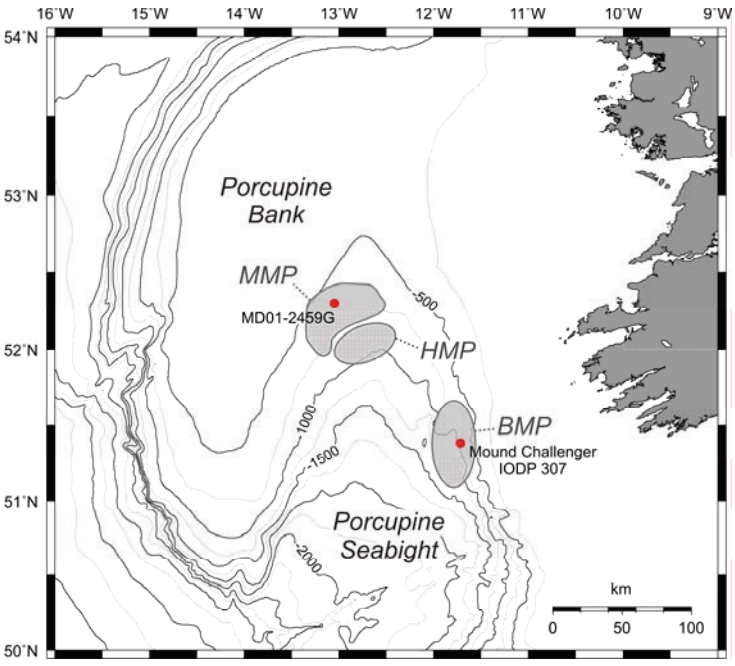

Figure 1: Overview map of the Porcupine Seabight, SW of Ireland, including main morphological features and localization of core MD01-2459G. The three mound provinces: Belgica Mound Province (BMP), Hovland Mound Province (HMP) and Magellan Mound Province (MMP) are indicated.

Until now, little attention has been paid to the diagenetic processes that occur within these cold-water coral mounds (Noé et al., 2006). This paper focuses on the diagenetic changes observed within a gravity core (MD01-2459G) which was retrieved close to the top of Mound Perseverance (Magellan mound province, northern slope of the Porcupine Seabight). The aim of this study is to explore the process that led to the alteration of the corals and the formation of gypsum and dolomite crystals in the sediment. It is proposed

that the presence of authigenic gypsum in carbonate-dominated sediments serves as an indicator for early diagenetic oxidation events.

1.1 Regional setting

Mound Perseverance is situated in the Magellan mound province, where more than 1000 mounds occur with a spatial density of approximately 1 mound/km² (Fig. 2) (Huvenne et al., 2007). The growth of these mounds was influenced and shaped by north-south oscillating palaeocurrents. All mounds root on one seismic horizon, indicating a sudden start-up event (Huvenne et al., 2007). According to the results of the Integrated Ocean Drilling Program (IODP) Expedition 307, the start-up event of Challenger Mound, located in the Belgica mound province, is dated at 2.7 Ma (Kano et al., 2007).

In contrast to the Belgica mounds, which have a broad base, most Magellan mounds have an ovoid shape, suggesting growth in competition with concurrent sedimentation (De Mol et al., 2002; Huvenne et al., 2007). Nowadays, most mounds in the Magellan mound province are buried. Based on the coccolith assemblage and the stratigraphy of a core taken on top of one of the buried mounds, it was concluded that the mounds were buried before Marine Isotope Stage (MIS) 6 (Foubert et al., 2007). Unfortunately, this core did not penetrate the buried mound, so no exact timing of the burial is known. Mound Perseverance is one of few Magellan mounds which are still outcropping at the sea bed (Fig. 2). The top of this mound is situated at a water depth of 610 m and its height above the actual mound base is ca. 160 m. The mound is elevated 50 m above the present-day sea bed and shows a NNE-SSW elongation. Video footage that was taken during the Caracole cruise in 2001 with ROV Victor 6000 showed the presence of living corals on the flanks of Mound Perseverance (Huvenne et al., 2007).

The water-mass stratification within the Porcupine Seabight has been reviewed by Hargreaves (1984), Rice et al. (1991) and White (2001). The depth range of the mounds in this area (600 to 1000 m) marks the upper boundary of the Mediterranean Outflow Water (MOW) which is overlain by the Eastern North Atlantic Water (ENAW). Both water masses are carried northwards by the eastern boundary slope current (White, 2007). At the northern end of the seabight, where the Magellan mounds are located, currents are relatively weaker with some evidence of topographic steering of the mean flow cyclonically around the slope of the Porcupine Basin (Huvenne et al., 2002; White, 2001, 2007).

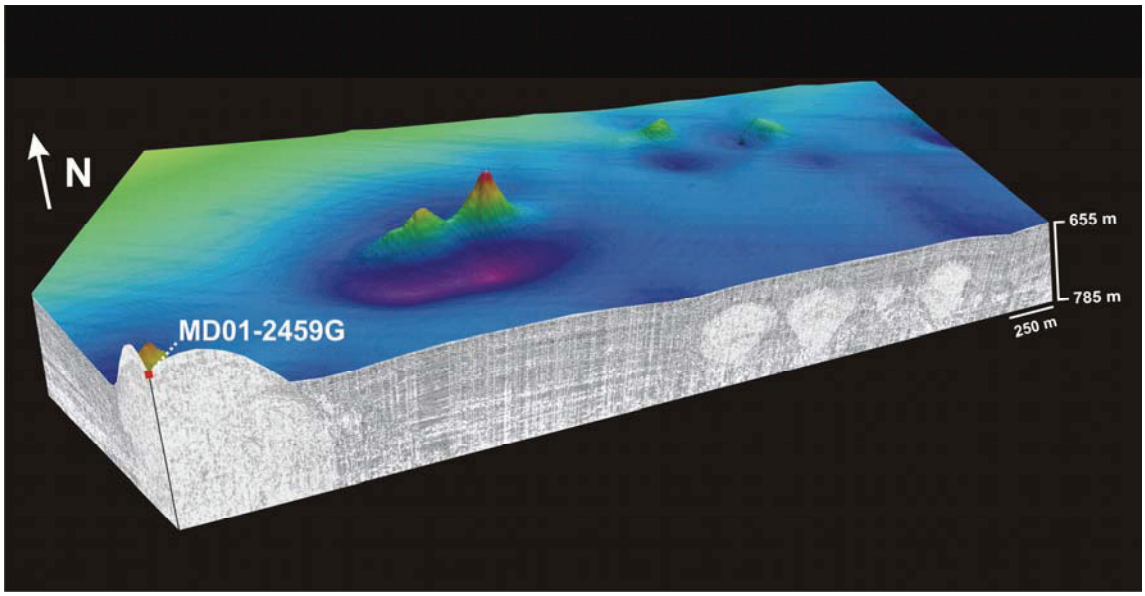

Figure 2: Location of core MD01-2459G, close to the top of mound Perseverance. The bathymetry, derived from 3D seismic data, is used in combination with single channel reflection seismic profiles. East of Perseverance, buried mounds are observed on the seismic line.

1.2 Diagenesis in cold-water coral mounds

It is important to understand how early diagenetic processes alter the original sedimentary record of mound sediments in order to decipher their geological history. The imprint on the sediment thereby provides information about the microbial and geochemical processes that occur within cold-water coral mounds.

Until recently, limited attention has been paid to these diagenetic processes. The most prominent diagenetic feature in cold-water coral mounds is the dissolution of the aragonitic corals (Foubert et al., 2007). The latter authors described the dissolution of coral fragments and precipitation of carbonate in mounds in the Porcupine Seabight. They attributed the coral alteration to oxidation of organic matter, affecting the saturation state of aragonite. Geochemical processes controlling the preservation of corals in cold-water coral mounds have been described in detail by Ferdelman et al. (2006) and Wehrmann et al. (2009). Both studies suggest a coupling between microbially-mediated organic matter degradation and carbonate-mineral diagenesis and link sediment composition and coral skeleton preservation by showing that the availability of reactive iron leads to an effective buffering of the pore-water carbonate system.

2. Material and Methods

2.1 Sedimentological data

Core MD01-2459G was obtained with a gravity corer during the MD123-Geosciences campaign with R/V Marion Dufresne in September 2001. The core was retrieved close to the top of Mound Perseverance at a water depth of 610 m with a recovery of 1079 cm (52°18'00.60"N 13°02'51.00"W) (Fig. 2). After retrieval, the core was analyzed on board with the GEOTEK Multi Sensor Core Logger with a resolution of 2 cm, measuring magnetic susceptibility, gamma-ray density and P-wave velocity (Foubert et al., 2007; Van Rooij et al., 2001). X-ray images were obtained using the SCOPIX X-ray equipment (DGO, Université Bordeaux I), described by Foubert et al. (2007).

The major chemical element composition was analyzed using an AVAATECH XRF core scanner installed at the Royal Netherlands Institute for Sea Research (Royal NIOZ). X-ray fluorescence is a semi-quantitative, non-destructive method which provides high-resolution records of chemical composition on split sediment cores (Richter et al., 2006). The principle of X-ray fluorescence is explained in detail by Jenkins and De Vries (1970).

Element intensities were measured in two runs with a resolution of 1 cm. In the first run, element intensities were measured for the elements ranging from aluminum to cobalt using a computer controlled forced air cooled Oxford 50 Watt X-ray source operating at a current of 0.15 mA and 10 kV. In the second run the element intensities for the elements ranging from zinc to zirconium were determined with the X-ray source operating at a current of 0.8 mA and 30 kV. In both runs the count time was 30 sec (Foubert & Henriet, 2009).

The different mineralogical phases of the sediment matrix of 14 samples were identified and quantified using X-ray diffraction (XRD) at the department of Earth and Environmental Sciences, Geology, K.U. Leuven. A representative amount of sediment was dried (around 30 g) before crushing the sample by hand and passing it through a 500 μm sieve. Subsequently, 10% ZnO was added to the sample as an internal standard and the sample was powdered in a McCrone Micronizing mill using 4 ml of methanol as lubricating agent. X-ray data were collected on a Philips PW1830 diffractometer (Bragg-Bretano geometry). An angular range of 5 to 70° 2θ was measured with a step size of 0.02° and 2 sec counting time, each step. For quantitative phase analysis the Rietveld refinement program Topas academic was used.

2.2 Micro-CT scan

Computer tomography (CT) investigates the external and internal structure of objects in 3D, in a non-destructive way (Kak & Slaney, 1988). These CT-scans were carried out at the Centre for X-ray CT at Ghent University (UGCT). The set-up of the micro-CT scanner was described in detail by Masschaele et al. (2007). For this study, the high power directional head was used as an X-ray source. The samples were scanned at 130 kV with a thin Cu-filter, to minimize beam hardening effects. A total of 800 projections were taken, each projection averaging 2 frames of 400 millisec exposure time. A Varian 2520V Paxscan was used as an X-ray detector. This detector consists of 1880 x 1496 pixels, with a pixel size of 127 µm by 127 µm. To enhance image statistics, a pixel averaging of 2 x 2 pixels was used which reduced the resolution.

The CT data were processed with the reconstruction software Octopus (UGCT). 3D morphological analysis was performed using Morpho+ (UGCT). This software enables the volume to be segmented using advanced thresholding techniques (Vlassenbroeck et al., 2007). Furthermore it allows different objects to be labelled, classified and separated in the volume. VGStudioMax 1.2 from Volume Graphics (64 bit version) was used for 3D volume rendering.

2.3 Petrography

Standard thin sections were studied using conventional transmitted, reflected and UV light microscopy. For further investigation of diagenetic features, cold cathode luminescence (CL) was used. Cold CL allows the differentiation of primary biogenic carbonates from diagenetic carbonates and the discrimination of different cement sequences which formed under changing diagenetic conditions. It is generally accepted that Mn^{2+} and trivalent rare earth element ions are the most important activators of extrinsic CL in carbonate minerals, while ferrous iron (Fe^{2+}) functions as quencher of CL (Richter et al., 2003). Biogenic carbonate fragments are usually non-luminescent unless they undergo (partial) recrystallization. Diagenetic calcite is typically yellow-orange luminescent, while dolomite appear in yellow-red colours.

Individual gypsum crystals were embedded in epoxy. After polishing and carbon-coating they were studied with a JSM 6400 scanning electron microscope (SEM) at Ghent University. Bulk sediment associated with the gypsum was dissolved in distilled water and treated in an ultrasonic bath for 20 sec. Subsequently, the solution was filtered and dried. The filter was gold-coated and studied with a SEM. The

composition of several points was measured using Energy Dispersive Spectroscopy (EDS).

2.4 Isotope measurements

The oxygen and sulphur isotopic composition of gypsum-bound sulphate was measured on hand-picked gypsum crystals at the Max Planck Institute for Marine Microbiology Bremen and the Swiss Federal Institute of Technology (ETH) Zurich. The crystals were digested in a $NaCl_2$/ascorbic acid solution and subsequently precipitated in the form of $BaSO_4$ by addition of $BaCl_2$. To determine the sulphur isotopic composition of pyrite, sediment sub-samples were subjected to a two-step chromium-II reduction method (Fossing & Jørgensen, 1989). This method separately traps acid volatile sulphide (AVS) and chromium reducible sulphur (CRS) as ZnS. The CRS fraction, which mainly consists of sulphur bound as pyrite, was converted into Ag_2S by treatment with $AgNO_3$. Precipitates were washed several times with deionized water and dried.

Sulphur isotope ratios were measured by adding 0.4 to 0.6 mg of $BaSO_4$ or 0.2 to 0.4 mg Ag_2S to 1 mg of V_2O_5 in a tin capsule and combusted at 1060ºC in an elemental analyzer (EURO EA Elemental Analyzer®) to produce SO_2. The evolved SO_2 was carried by a helium stream through a GC column, Finnigan Conflo III®, and into a Finnigan Delta V® stable isotope ratio mass spectrometer to determine $\delta^{34}S$. The sulphur isotope measurements were calibrated with reference materials National Bureau Standards (NBS) 127 ($\delta^{34}S$ = +20.3 ‰) and IAEA-SO-6 ($\delta^{34}S$ = –34.1 ‰). The standard errors ($\sigma 1$) of the measurements were less than 0.2 ‰ for $\delta^{34}S$.

For oxygen isotope analysis, approximately 0.16 mg of $BaSO_4$ was transferred to a silver capsule and thermochemically reduced at 1450ºC in the presence of graphite and glassy carbon in the Finnigan Thermal Conversion/Elemental Analyzer (TC/EA®) to produce CO. The evolved CO was carried by a helium stream through a GC column, Finnigan Conflo III®, and into a Thermo Scientific MAT 253® stable isotope ratio mass spectrometer to measure $\delta^{18}O$. The oxygen isotope measurements were calibrated with NBS 127 ($\delta^{18}O$ = +8.6 ‰; Boschetti & Iacumin, 2005), IAEA-SO-5 ($\delta^{18}O$ = +12.0 ‰) and IAEA-SO-6 ($\delta^{18}O$ = -11.3 ‰; Halas et al., 2007). The standard errors ($\sigma 1$) of the measurements were less than 0.3 ‰ for $\delta^{18}O$.

The isotope measurements are reported with respect to the standards, Vienna Standard Mean Oceanic Water (VSMOW) and Vienna Canyon Diablo Troilite (VCDT).

3. Results

3.1 Core stratigraphy

Based on the magnetic susceptibility, gamma ray density, XRF, XRD and X-ray imagery, core MD01-2459G was subdivided into two units. Unit A comprises the top 535 cm of the core and unit B comprises the lower 544 cm (Fig. 3) (Foubert & Henriet, 2009). Unit A is composed of olive-gray medium grained silt (5Y 4/2) and contains large coral fragments. In general, the calcium and strontium values are high, but lower than those of unit B. Except for a peak in the top 50 cm, the magnetic susceptibility values of this unit are rather low, averaging around 5 SI. The XRF iron intensities are high compared to unit B, averaging around 12K counts/sec. XRD analysis shows that the sediment matrix of unit A is dominated by quartz (25.6%), calcite (26.7%) and clay minerals (23.7%). Feldspar (7.3%) and aragonite (2.7%) appear in minor quantities (Fig. 4). The age of the corals in unit A have been dated to correspond to the Holocene (Frank et al., in press).

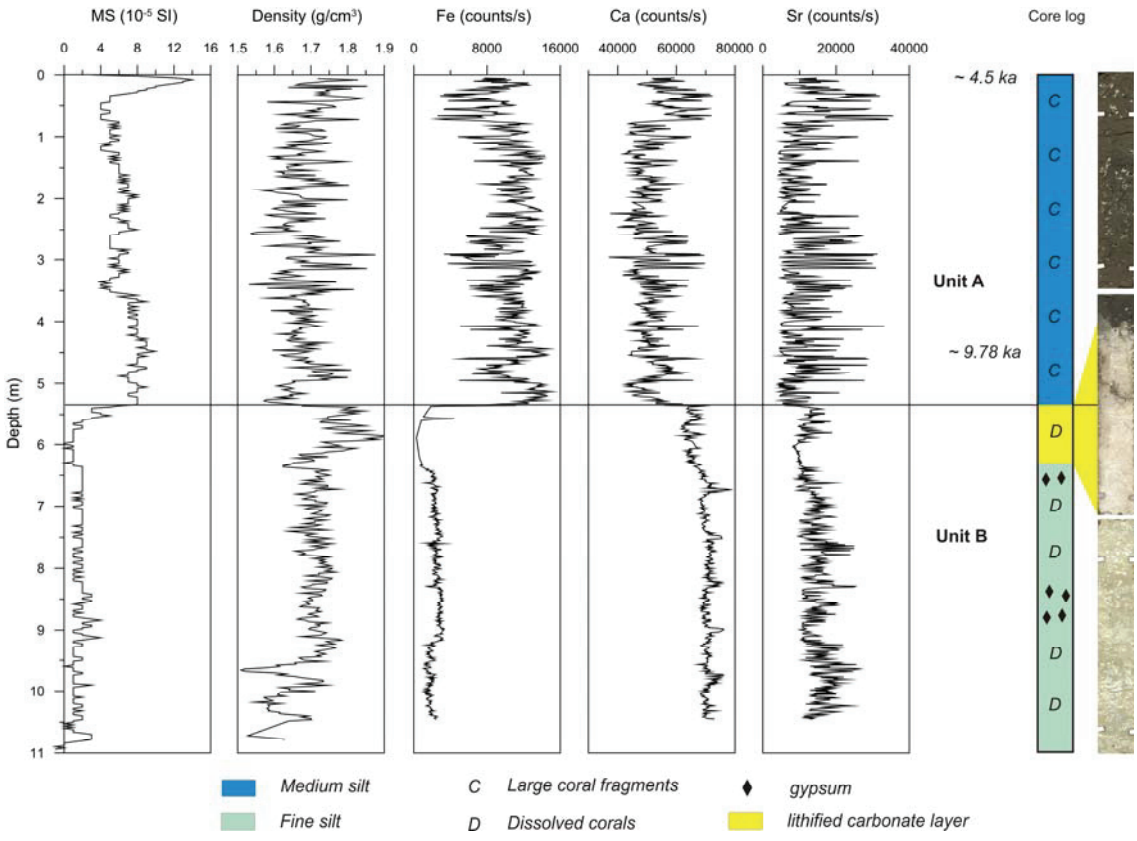

Figure 3: Overview of the stratigraphy of core MD01-2459G featuring the Magnetic Susceptibility (MS), Density, X-Ray Fluorescence (XRF), a basic core log. Images of core sections 300-375, 525-600 & 750-825 cm are given. U-Th dating of the corals of unit A are also noted (Frank et al., submitted). Gypsum crystals were discovered in two intervals in unit B: i.e. at a depth of 658-671 and 840-891 cm (modified after Foubert and Henriet, 2009).

Unit B consists of light-gray fine grained silt (7.5Y 6/1) rich in diagenetically altered corals which are characterized by fragile skeleton walls. The corals are hardly recognizable on X-ray images, indicating little density contrast between the corals and the surrounding sediment. The alteration of the corals prevented uranium-thorium dating in unit B. The magnetic susceptibility records extremely low values for unit B which can be explained by the presence of carbonate-rich sediments. This is also reflected in the high XRF calcium values, averaging around 70K counts/sec. The strontium values increase in unit B compared to unit A, while there is a significant decrease in the iron intensities. A remarkable feature in unit B is a lithified carbonate layer between 535 and 630 cm, which is reflected in the high density values. The coral fragments in this layer are (almost) completely dissolved. Between 555 and 560 cm, a horizon of dark, siliciclastic sediment occurs, characterized by a peak in the XRF iron counts. Some lithified carbonate fragments are embedded in the siliciclastic sediment. At 630 cm, there is a sharp boundary to the unlithified sediment below.

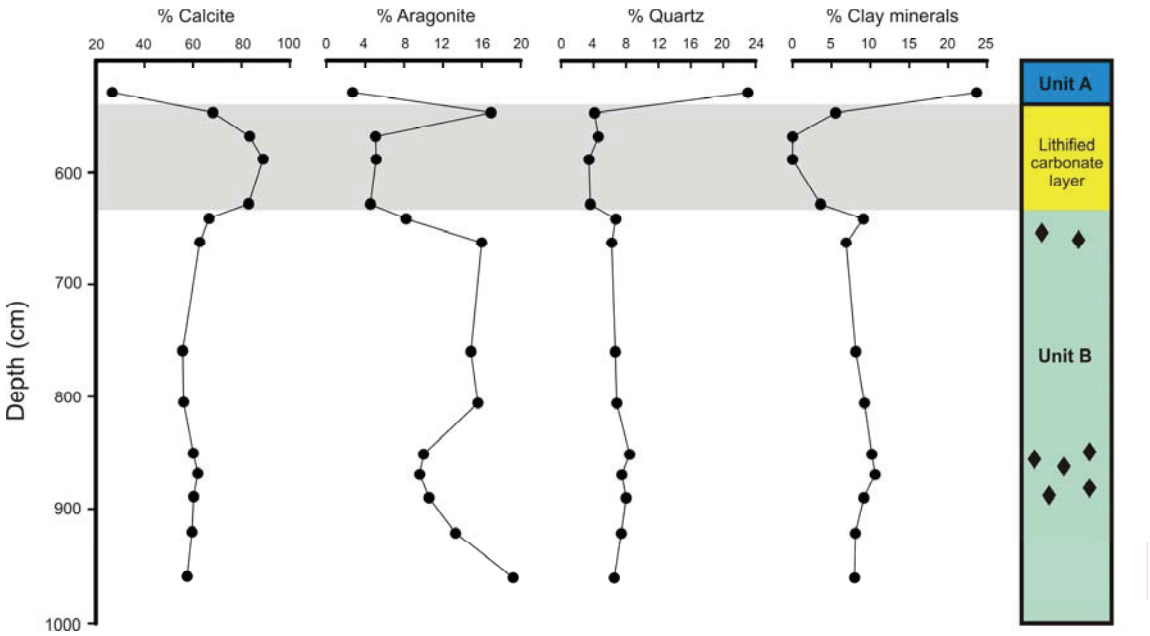

Figure 4: XRD-data of the bulk sediment. The percentages of calcite, aragonite, quartz and clay minerals are presented.

XRD analysis shows significantly more calcite in unit B than in unit A (Fig. 4). The lithified carbonate layer contains between 68 and 90% calcite with an average of 81%. The sediments of unit B below the lithified layer show lower percentages of calcite, ranging between 55 and 66% (average: 60.1%). The aragonite content of unit B fluctuates strongly. The lithified carbonate layer contains approximately 5% aragonite

while the lower part of unit B contains 8 to 19% aragonite. Quartz (3 to 8%) and clay minerals (3 to 10%) occur in minor abundances. Gypsum, pyrite and dolomite were detected in some samples in very low quantities at the limit of the resolution of XRD analysis (< 2%). Gypsum crystals were discovered in two intervals in unit B: at a depth of 658 to 671 cm and 840 to 891 cm. The gypsum occurs as euhedral, tabular crystals with a size between 1.5 and 4 mm, in a matrix of fine grained silt. The crystals are transparent white to beige and often twinned (Fig. 5).

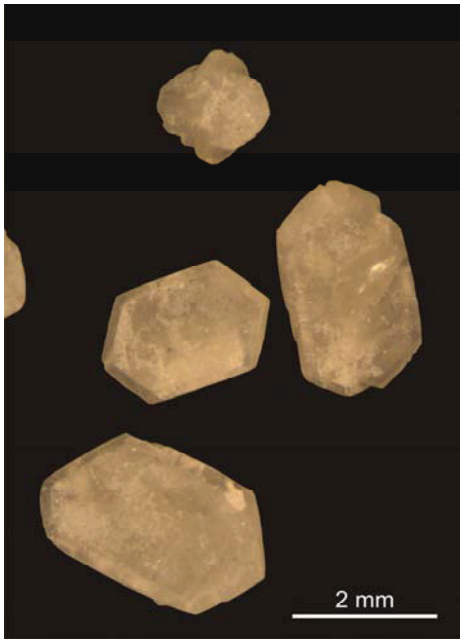

Figure 5: Euhedral, tabular gypsum crystals with a size between 1.5 and 4 mm. Often, the crystals occur as twins.

3.2 Micro-CT-scan of unit B

The micro-CT-scans enable visualization and quantification of diagenetic features (Fig. 6). Scans of corals from unit B show signs of strong dissolution which created a secondary moldic porosity (Fig. 6A). Only the most robust parts of the corals, where the septae meet the outer rim of the calyx, are preserved. The scanned sections have a porosity up to 0.43 % pores which is almost entirely related to the dissolution of the corals. Micropores could not be visualized in this sample using micro-CT, because the scans were performed with a resolution of 20 µm.

The visualization of the gypsum crystals in unit B clearly shows that the crystals have no preferential orientation and are randomly scattered in the sediment (Fig. 6B). Quantification of the scans indicates that the samples contain between 0.18 and 0.34 volume % gypsum. There is no apparent spatial correlation between the gypsum crystals and the occurrence of coral relics (Fig. 6C).

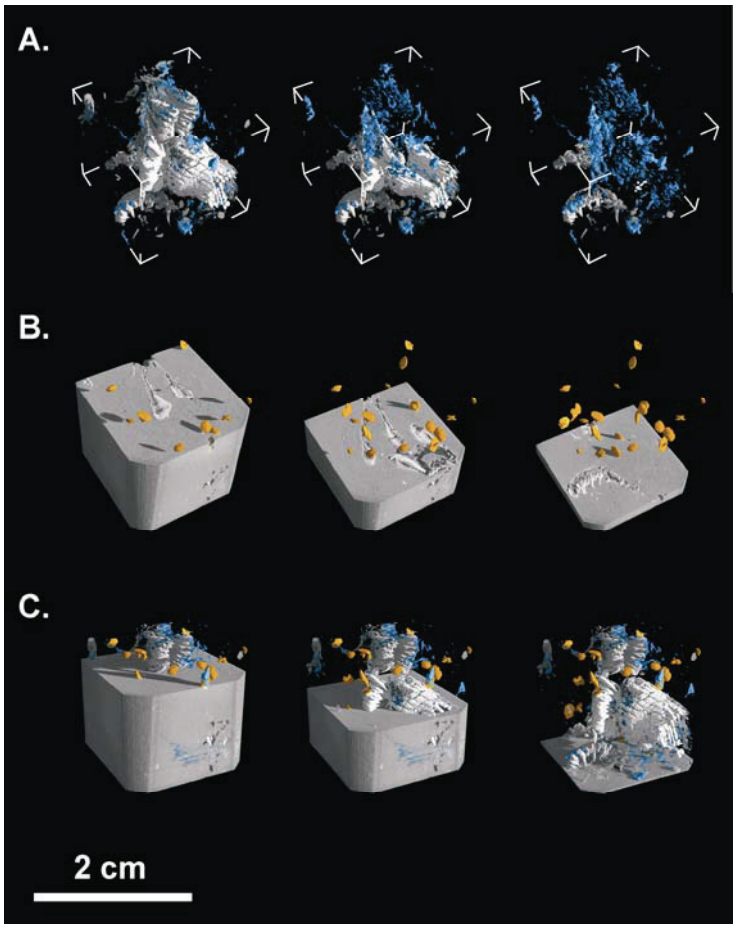

Figure 6: Micro-CT-scans of sediment that was sampled at a depth of 889-891 cm. A. Micro-CT scans visualizing the dissolution of the corals (white) and subsequent creation of a secondary porosity (blue). B. Micro-CT scans showing the occurrence of gypsum crystals (yellow) in the sediment. C. Overview of the combined occurrence of gypsum (yellow), coral (white) and porosity (blue) in the sediment.

3.3 Petrography of intervals containing gypsum crystals

The gypsum crystals are embedded in a fine matrix of micritic mud with many biogenic fragments (i.e. corals, foraminifera, bivalve shells, etc.) (Fig. 7A and B). Framboidal pyrite is scattered in the matrix (Fig. 7C). The corals show obvious signs of dissolution whereas the foraminifera are better preserved. Some foraminifera are (partially) filled with the embedding sediment and a few foraminifera contain framboidal pyrite (Fig. 7D). In two thin sections, faecal pellets were observed in the vicinity of the gypsum crystals, indicating the presence of benthic feeders. There are clusters of framboidal pyrite on the outer rim of the pellets (Fig. 7E). The gypsum crystals are lens-shaped (Fig. 7A) and often twinned. All crystals contain biogenic fragments such as foraminifera, corals (Fig. 7F) and shell-fragments. Some of the investigated gypsum crystals revealed the presence of framboidal pyrite inside the gypsum (Fig. 7G). A few crystals encase foraminifera containing intraparticular

framboidal pyrite (Fig. 7H). These findings were confirmed with SEM-EDS by which calcitic and siliceous biogenic fragments and iron sulphide crystals were indentified within the gypsum crystals (Fig. 7I and J). Sometimes, the inclusions in the gypsum are aligned according to the cleavage of the crystals but in most cases, they appear randomly. A striking feature is the occurrence of broken and even displaced crystals, with displacement occurring along different crystallographic orientations (Fig. 7K). However, it is unclear if this is the result of sample preparation (i.e. sediment sampling, thin section preparation) or a genuine feature. With the exception of some inclusions, the gypsum crystals are non-luminescent in cold cathode CL. The biogenic fragments are also non-luminescent.

The matrix contains some bright yellow-red luminescent, rhombohedral crystals up to 50 μm with clear zonation (Fig. 7L). These crystals were identified using SEM-EDS as dolomite ($CaMg(CO_3)_2$). The SEM-images reveal the incorporation of coccoliths in the dolomite crystals (Fig. 7M and N).

3.4 Isotope measurements

The sulphur isotopic composition of gypsum ($\delta^{34}S$), found at a depth of 890 cm in this core, is +11.0 ‰ VCDT, the oxygen isotopic composition ($\delta^{18}O$) is +8.9 ‰ VSMOW. The $\delta^{34}S$ values for pyrite, sampled at different depths, are reported in Table 1.

Table 1. Sulphur isotope composition of pyrite occurring adjacent to the gypsum crystals except sample 910 which was sampled in a zone 9 cm below the interval containing gypsum crystals.

Sample-depth (cm)	$\delta^{34}S_{pyrite}$ [‰]
870 cm	-22.88
880 cm	-18.89
890 cm	-21.14
900 cm	-17.59
910* cm	-12.30

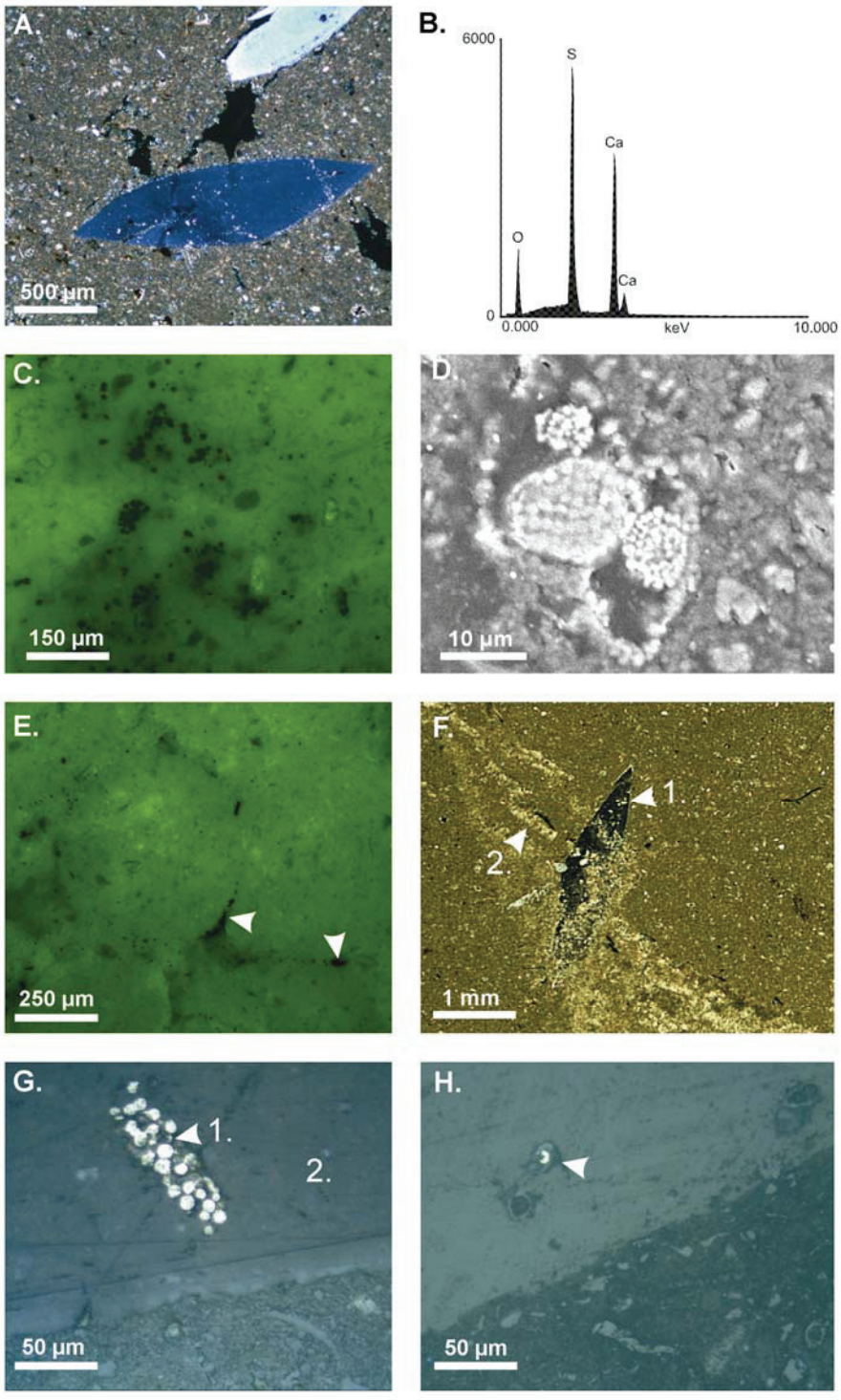

Figure 7: A. The occurrence of gypsum crystals in a micritic matrix containing some biogenic fragments (Plane-polarized light). B. An EDS-profile of one of the gypsum crystals. C. Framboidal pyrite (black spheres) in the sediment associated with the gypsum crystals (UV-light). D. A detail of a foraminifera containing intraparticular framboidal pyrite (SEM). E. Clusters of framboidal pyrite on the outer rim of the fecal pellets (UV-light). F. The incorporation of an altered coral (1.) in a gypsum crystal (2.) (Plane-polarized light). G. The occurrence of framboidal pyrite (1.) incorporated in a gypsum crystal (2.) (reflected light). H. A foraminifera containing intraparticular framboidal pyrite incorporated in a gypsum crystal (reflected light).

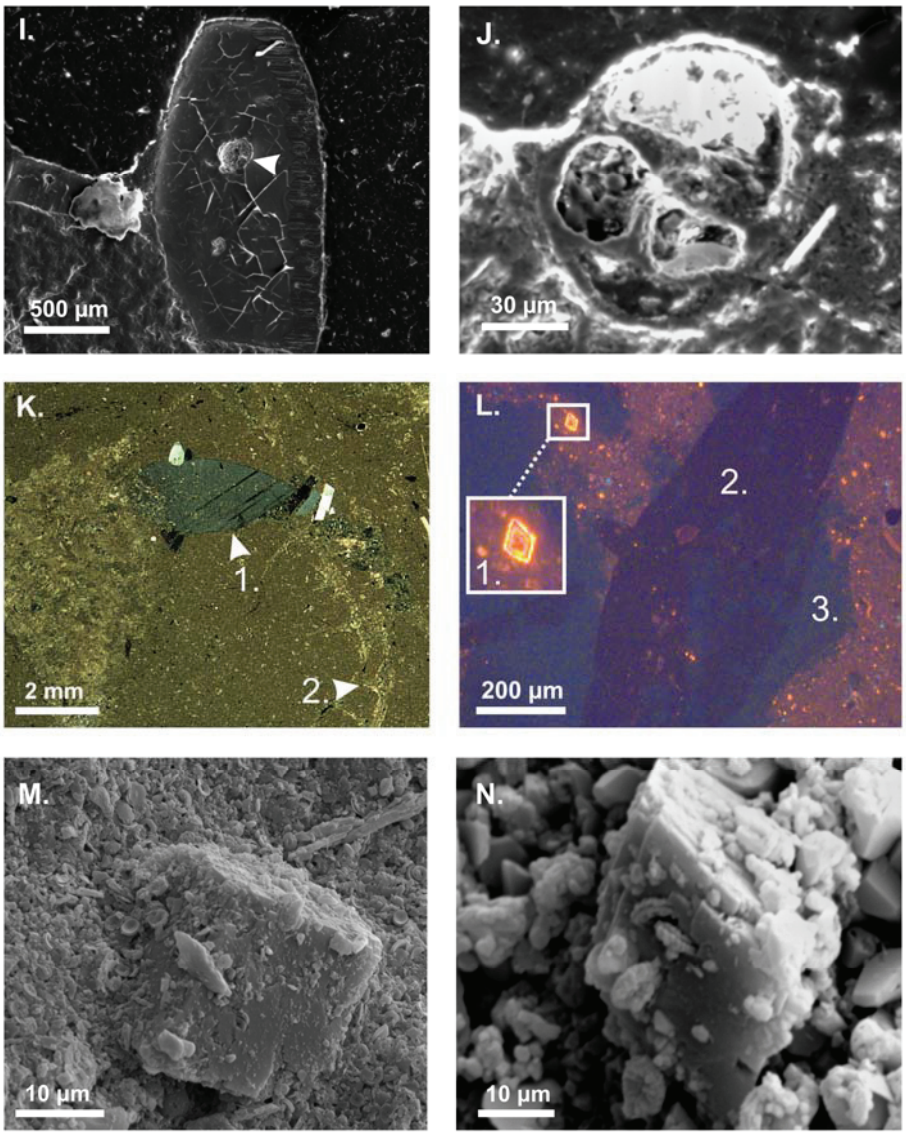

Figure 7: I.-J. SEM images of foraminifera incorporated in gypsum crystals. K. A twinned gypsum crystal (1.) that was broken and displaced in different crystallographic orientations (Plane-polarized light). Strongly dissolved coral (2.) L. Cold Cathode Luminescence (CL) of a luminescent dolomite crystal (1.) in association with a non-luminescent gypsum crystal (2.) and non-luminescent coral (3.). M.-N. SEM images of dolomite crystals associated with the gypsum crystals. Note the incorporation of coccoliths into the dolomite crystals in picture N.

4. Discussion

Gypsum and its dehydrated form anhydrite are relatively common in sedimentary deposits throughout the world and throughout the geologic record (Bain, 1990). In general, the formation of these gypsum crystals is attributed to evaporation processes, i.e. in hypersaline basins, sabkhas and playas.

An evaporative nature, however, can be excluded for the gypsum crystals in Mound Perseverance. The fact that biogenic fragments and even coral pieces (Fig. 7F) are incorporated into the gypsum indicates that the crystals precipitated *in situ*, due to a diagenetic process. Gypsum occurs only if extraordinary high sulphate and calcium concentrations cause oversaturation of this mineral. Therefore, reports of non-evaporitic gypsum are limited as this mineral is strongly undersaturated with respect to sea water. Gontharet et al. (2007) attributed the precipitation of gypsum in carbonate crusts associated with mud volcanoes to the presence of rising sulphate-rich fluids originating from the dissolution of underlying Messinian evaporites. Gypsum precipitation associated with the formation of sulphate-rich brines in the Bannock Basin was reported by Corselli and Aghib (1987). Bain (1990) attributed the formation of non-evaporitic gypsum to oxidizing calcium-rich groundwater. Similarly, Siesser and Rogers (1976) described gypsum crystals in calcareous plankton-rich sediments on the South West African continental slope in association with authigenic pyrite. The authors propose that pyrite first formed due to the production of sulphide during microbial sulphate reduction which reacted with sedimentary iron phases. Subsequently, a drop in the pH induced the dissolution of calcareous organisms, liberating high concentrations of calcium. Briskin and Schreiber (1978) attributed the occurrence of gypsum in carbonate deep-sea ooze to the influx of oxygen-rich, undersaturated Antarctic Bottom Water, which actively dissolved the foraminiferal ooze, supplying the necessary calcium for gypsum precipitation at the sediment/water interface. Xavier and Klemm (1979) described the occurrence of authigenic gypsum in deep-sea manganese nodules in the Central Pacific Ocean. (Wang et al., 2004) reported the occurrence of authigenic gypsum crystals associated with gas hydrates at Hydrate Ridge in the Eastern North Pacific. They propose that the crystals precipitated at the interface between downward advecting sulphate-rich sea water and gas hydrates, where calcium concentrations are high due to hydrate formation. Similarly, Zhong et al. (2007) described the formation of gypsum and pyrite in association with gas venting in the Nansha Trough.

Gypsum crystals are also sometimes observed on the surface of cores due to the pore-water drying-out after core retrieval. In the present study, CT-scans allowed the amount of gypsum crystals in the matrix to be quantified. Based on a mean value of 0.26 vol%, it was calculated that 33.8 g of gypsum is present in the core in the interval between 840 to 891 cm, using a gypsum-density of 2.3 g/cm³. Gypsum solubility in sea water is up to 3.8 g/l (Kopittke et al., 2004). Consequently, 8.9 l of sea water would

need to evaporate completely in order to obtain this amount of gypsum. The volume of this core-section is only 8.5 l, therefore, it is impossible to create this quantity of gypsum after coring. Moreover the core was stored under stable conditions (6°C), showing no signs of drying out.

In order to assess the exact timing of gypsum precipitation, uranium-thorium dating was applied to the gypsum crystals. However, the uranium (0.035 ppm) and thorium (0.028 ppm) concentrations in the gypsum are extremely low. Given these low concentrations and the small amount of sample material (0.2 g), the uranium and thorium isotopic values were impossible to determine with sufficient precision. Therefore, the dating of the crystals was not successful.

In this study, the oxygen and sulphur isotopic composition of gypsum and the sulphur isotopic composition of pyrite are used to reconstruct the diagenetic setting during gypsum formation and elucidate the mechanism for the formation of the authigenic gypsum crystals. Based on these findings, a mechanism is proposed that links the formation of gypsum to a phase of increased bottom currents which caused erosion and enhanced inflow of oxidizing fluids into previously anoxic sediments. This induced the oxidation of pyrite, carbonate dissolution and subsequent gypsum precipitation.

4.1 Potential sources of the sulphate in gypsum

The oxygen and sulphur isotopic composition of gypsum can be used to estimate the isotopic composition of the pore-water sulphate from which the gypsum originated. In an open system and at chemical equilibrium, gypsum is enriched in ^{34}S by +1.65 ‰ and in ^{18}O by +3.5 ‰ compared to dissolved sulphate (Holser and Kaplan, 1966; Thode and Monster, 1965). However, rapid precipitation of gypsum (i.e. precipitation in disequilibrium) or closed system conditions could suppress this isotope effect. Consequently, the isotopic composition of dissolved pore-water sulphate likely fell between +9.3 and +11.0 ‰ VCDT for sulphur and +5.4 and +8.9 ‰ VSMOW for oxygen (Fig. 8, Area B). Compared to sea-water sulphate with a sulphur isotopic composition of +20.3 ‰ (Longinelli, 1989), the pore-water sulphate from which the gypsum originated was depleted in ^{34}S. Depending on the assumed oxygen isotope fractionation for gypsum precipitation (0 to 3.5 ‰), the pore-water sulphate had the same oxygen isotopic composition as sea water (8.6 ‰ VSMOW; Boschetti and Iacumin, 2005) or was depleted in ^{18}O.

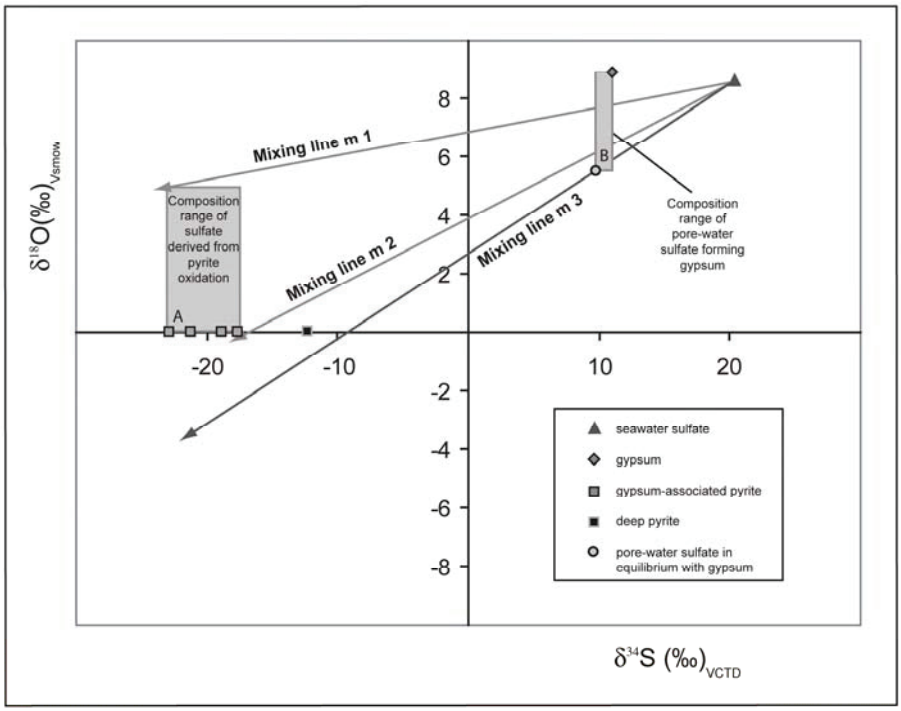

Figure 8: $\delta^{18}O$ versus $\delta^{34}S$ isotope plot showing the composition for seawater sulphate, gypsum and pyrite.

These observations indicate that apart from sea-water sulphate, which is a very likely sulphate source for gypsum in marine sediment, another source depleted in ^{34}S relative to sea-water sulphate must have contributed to the pore-water sulphate. A potential sulphate source is the oxidation of hydrogen sulphide-rich fluids. At Mound Perseverance, this process is most likely of minor importance. Pore-water profiles from Challenger Mound (IODP expedition 307) located in the close vicinity of Mound Perseverance show no accumulation of hydrogen sulphide within the mound sequence (Ferdelman et al., 2006). Low sulphide concentrations are the result of extremely low rates of anaerobic carbon mineralization (organoclastic sulphate reduction) in cold-water coral bearing sediments (Wehrmann et al., 2009) and a large pool of reactive iron (oxyhydr)oxides that traps sulphide. The oxidation of such accumulated iron sulphide minerals (i.e. pyrite) is the more likely source of sulphate depleted in ^{34}S. Eventually, a mixture of sea-water sulphate and sulphate derived from the oxidation of pyrite precipitated as gypsum. This hypothesis is supported by the occurrence of framboidal pyrite within the gypsum crystals in some thin sections which indicates that gypsum precipitated after pyrite formation (Fig. 7G and H).

4.2 Estimation of the $\delta^{18}O$ and $\delta^{34}S$ of sulphate derived from pyrite oxidation

Sulphate derived from pyrite oxidation has almost the same sulphur isotopic composition as the original sulphide because sulphur isotope fractionation during this process is smaller than 1 ‰ (Balci et al., 2007). The sulphur isotopic composition of pyrite within the zone where gypsum was formed varies between - 22.9 to -17.9 ‰. Therefore it can be assumed that sulphate, derived from partial oxidation of these pyrites, would possess a sulphur isotopic composition covering the same range. The oxygen isotopic composition of sulphate derived from pyrite oxidation depends on the oxygen source (i.e. water and dissolved oxygen) and the oxidation mechanism (Balci et al., 2007; Brunner et al., 2008; Taylor et al., 1984; Toran & Harris, 1989). According to (Balci et al., 2007), water-derived oxygen accounts for around 90 % of oxygen incorporated into sulphate during pyrite oxidation while 10 % is derived from dissolved oxygen. Both sources are characterized by very different isotopic compositions: $\delta^{18}O_{H2O} \cong \delta^{18}O_{VSMOW} = 0$ ‰ for sea water and $\delta^{18}O_{O2} = +23.5$ ‰ for oxygen (Kroopnick & Craig, 1972). In aquatic environments, oxidation of pyrite with oxygen derived from water is associated with a positive oxygen isotope fractionation effect of roughly 0 to 4 ‰ (Balci et al., 2007; Brunner et al., 2008; Taylor et al., 1984). Oxidation of pyrite with oxygen derived from dissolved oxygen is associated with a negative oxygen isotope fractionation effect of around -10 ‰ (Balci et al., 2007; Kroopnick & Craig, 1972). Consequently, it can be expected that sulphate derived from pyrite oxidation would have a sulphur isotopic composition of - 22.9 to -17.9 ‰ and an oxygen isotopic composition of 0 to 5 ‰ (Fig. 8, Area A).

4.3 Estimation of the relative contribution of sulphate from pyrite oxidation versus sea-water sulphate

Mixing of sulphate from pyrite oxidation with sea-water sulphate could have produced the pore-water sulphate the gypsum precipitated from (Fig. 8). Based on this hypothesis, a sulphur isotope mass balance can be used to assess the contribution of sulphate derived from pyrite oxidation relative to the contribution of sea-water sulphate:

$$a*\delta^{34}S_{pyrite} + b*\delta^{34}S_{sea\text{-}water} = (a+b) * (\delta^{34}S_{gypsum} - \Delta^{34}S_{pore\text{-}water\_gypsum}) \quad (1)$$

The parameters a and b denote the contribution of sulphate from pyrite oxidation and sea-water sulphate, respectively. $\delta^{34}S_{pyrite}$ denotes the sulphur isotopic composition of

sulphate derived from pyrite oxidation and $\delta^{34}S_{sea\text{-}water}$ denotes the sulphur isotopic composition of sea-water sulphate. $\delta^{34}S_{gypsum}$ denotes the sulphur isotopic composition of gypsum, and $\Delta^{34}S_{pore\text{-}water\_gypsum}$ the sulphur isotope fractionation for the precipitation of gypsum from pore-water sulphate.

The rearrangement of equation (1) allows the introduction of the relative ratio (x), the contribution of sulphate from pyrite oxidation and sulphate from sea water.

$$a/b^* \delta^{34}S_{pyrite} + \delta^{34}S_{sea\text{-}water} = [(a+b)/b]^* (\delta^{34}S_{gypsum} - \Delta^{34}S_{pore\text{-}water\_gypsum})$$
$$x^* \delta^{34}S_{pyrite} + \delta^{34}S_{sea\text{-}water} = [x+1]^* (\delta^{34}S_{gypsum} - \Delta^{34}S_{pore\text{-}water\_gypsum}) \quad (2)$$
$$x^*(\delta^{34}S_{pyrite}-(\delta^{34}S_{gypsum} - \Delta^{34}S_{pore\text{-}water\_gypsum})) = \delta^{34}S_{gypsum} - \Delta^{34}S_{pore\text{-}water\_gypsum} - \delta^{34}S_{sea\text{-}water}$$
$$x = (\delta^{34}S_{sea\text{-}water} - \delta^{34}S_{gypsum} + \Delta^{34}S_{pore\text{-}water\_gypsum}) / (\delta^{34}S_{gypsum} - \Delta^{34}S_{pore\text{-}water\_gypsum} - \delta^{34}S_{pyrite})$$

The estimates for $\delta^{34}S_{sea\text{-}water}$ (+20.3 ‰), $\delta^{34}S_{gypsum}$ (+11.0 ‰), $\Delta^{34}S_{pore\text{-}water\_gypsum}$ (0 to +1.65 ‰), and $\delta^{34}S_{pyrite}$ (-17.9 to -22.9 ‰) can be used to calculate the contribution of sulphate from pyrite oxidation relative to the contribution of sea-water sulphate. The calculations show that about 22 % to 29 % of sulphate in gypsum could have been derived from pyrite oxidation. Using the graphical combination of sulphur and oxygen isotope mixing, the relative contribution from pyrite oxidation can be even better constrained. About 23 % to 26 % of sulphate in gypsum was derived from pyrite oxidation (Fig. 8, mixing line m 1 and m 2). Assuming that the concentration of sea-water sulphate was 28 mM, the calculated values would correspond to a sulphate contribution from sulphide oxidation to the pore-water sulphate pool of 7.7 to 11.2 mM sulphate. To produce the latter amount of sulphate, an oxidation of around 0.1 to 0.2 wt. % wet weight pyrite would have been required. Given the amount of pyrite that was observed in the thin-sections (Fig. 7C), this estimate is reasonable.

4.4 Two pyrite generations?

The mixing lines in the oxygen-sulphur isotope plot in Figure 8 do not only allow the calculation of the contribution of sulphate from pyrite oxidation to gypsum (lines m 1 and m 2), but also provide information about the isotope fractionation related to gypsum precipitation. The intercepts between m 1, respectively m 2 and the composition range of pore-water sulphate forming gypsum (Fig. 8, Area B) indicate that the isotope fractionation (1.2 to 2.8 ‰ for $\Delta^{34}S_{pore\text{-}water\_gypsum}$ and 0.6 to 1.2 ‰ for $\Delta^{18}O_{pore\text{-}water\_gypsum}$) is smaller than the reported equilibrium isotope fractionation (1.65

‰ for sulphur and 3.5 ‰ for oxygen (Holser & Kaplan, 1966; Thode & Monster, 1965). Such a suppression of the isotope fractionation effect could be due to closed-system or non-equilibrium conditions, e.g. rapid precipitation of gypsum. However, the alternative hypothesis that gypsum formed under isotopic equilibrium, can also be tested. In this case, the sulphur isotopic composition of sulphate derived from pyrite oxidation is estimated using a mixing line through the isotopic composition of sea-water sulphate and pore-water sulphate at isotopic equilibrium (Fig. 8, mixing line m 3). It is assumed that the lowest oxygen isotopic composition of sulphate derived from pyrite oxidation is equal to the oxygen isotopic composition of sea water, thus 0 ‰ VSMOW. Therefore, the sulphur composition of the pyrite that was oxidized would be around -9 ‰ (intercept of m 3 with $\delta^{18}O_{SMOW}$ = 0 ‰). This scenario is possible under the assumption that the pyrite associated with gypsum, featuring sulphur isotope values around -20 ‰ VCDT, formed after gypsum precipitation. In the latter case, an earlier pyrite generation, with sulphur isotope values around -9 ‰ VCDT, was to a great extent removed by pyrite oxidation. A sulphur isotopic composition of -12.3 ‰ VCDT of pyrite found in the layer 10 cm below the zone of gypsum formation supports this hypothesis. Under this assumption (i.e. oxidation of pyrite with $\delta^{34}S$ around -9 ‰ VCDT), the relative contribution of sulphate from pyrite oxidation would be around 34 % (Fig. 8, mixing line m 3).

4.5 Proposed mechanism of gypsum and dolomite formation

Initial setting

In marine sediments, oxic to sub-oxic conditions are usually restricted to the top few centimetres while sediments below are anoxic. In cold-water coral bearing sediments anaerobic carbon mineralization is extremely slow (Wehrmann et al., 2009). Sulphate profiles from Challenger Mound suggest decomposition of organic matter by sulphate reduction within the top 50 m of the mound sequence while sulphate reduction coupled to anaerobic oxidation of methane is constrained to the underlying Miocene sediments (Ferdelman et al., 2006). Sulphide produced during sulphate reduction in the mound sediments reacts with ferric iron minerals in the siliciclastic fraction and precipitates as framboidal pyrite (Berner, 1970).

The oxidation event

The oxygen and sulphur isotope values of the gypsum crystals indicate oxidation of pyrite as driver of the diagenetic alterations in the sediment of Mound Perseverance. It is proposed that oxidizing fluids enter previously anoxic sediments and induce the oxidation of pyrite. Pyrite oxidation with oxygen or ferric iron (Fe^{3+}) as oxidants produces sulphate and protons (H^+) (reaction R1, R2). To maintain reaction R2 the produced ferrous iron (Fe^{2+}) needs to be oxidized to ferric iron, most likely by oxygen (reaction R3).

$$FeS_2 + 15/4\ O_2 + 1/2\ H_2O \rightarrow Fe^{3+} + 2\ SO_4^{2-} + H^+ \quad (R1)$$

$$FeS_2 + 14\ Fe^{3+} + 8\ H_2O \rightarrow 15\ Fe^{2+} + 2\ SO_4^{2-} + 16\ H^+ \quad (R2)$$

$$15\ Fe^{2+} + 15\ H^+ + 15/4\ O_2 \rightarrow 15\ Fe^{3+} + 15/2\ H_2O \quad (R3)$$

Dissolved ferric iron also reacts with H_2O to form iron (oxyhdydr)oxides (reaction R4).

$$Fe^{3+} + 2\ H_2O \rightarrow FeOOH + 3\ H^+ \quad (R4)$$

The oxidation event may have been initiated by increasing bottom currents. Van Rooij et al. (2007) describe significant variations of bottom currents in the Porcupine Seabight throughout glacial-interglacial cycles. The intensification of the bottom currents enhances the pore-water transport from the bottom water into the sediment, bringing oxidizing fluids into intervals where pyrite previously formed (Fig. 9).

This hypothesis is supported by the occurrence of framboidal pyrite within the gypsum (Fig. 7G and H). Increasing currents can induce sediment erosion of a cold-water coral mound (Dorschel et al., 2005), lowering the redox zones in the sediment column. The alternation of reducing and oxidizing conditions might be recorded in the zonation of the dolomites associated with the gypsum crystals (Fig. 7L). The appearance of bright luminescent and non-luminescent layers in the dolomite, points toward crystallization under changing pore-water chemistry conditions (Richter et al., 2003).

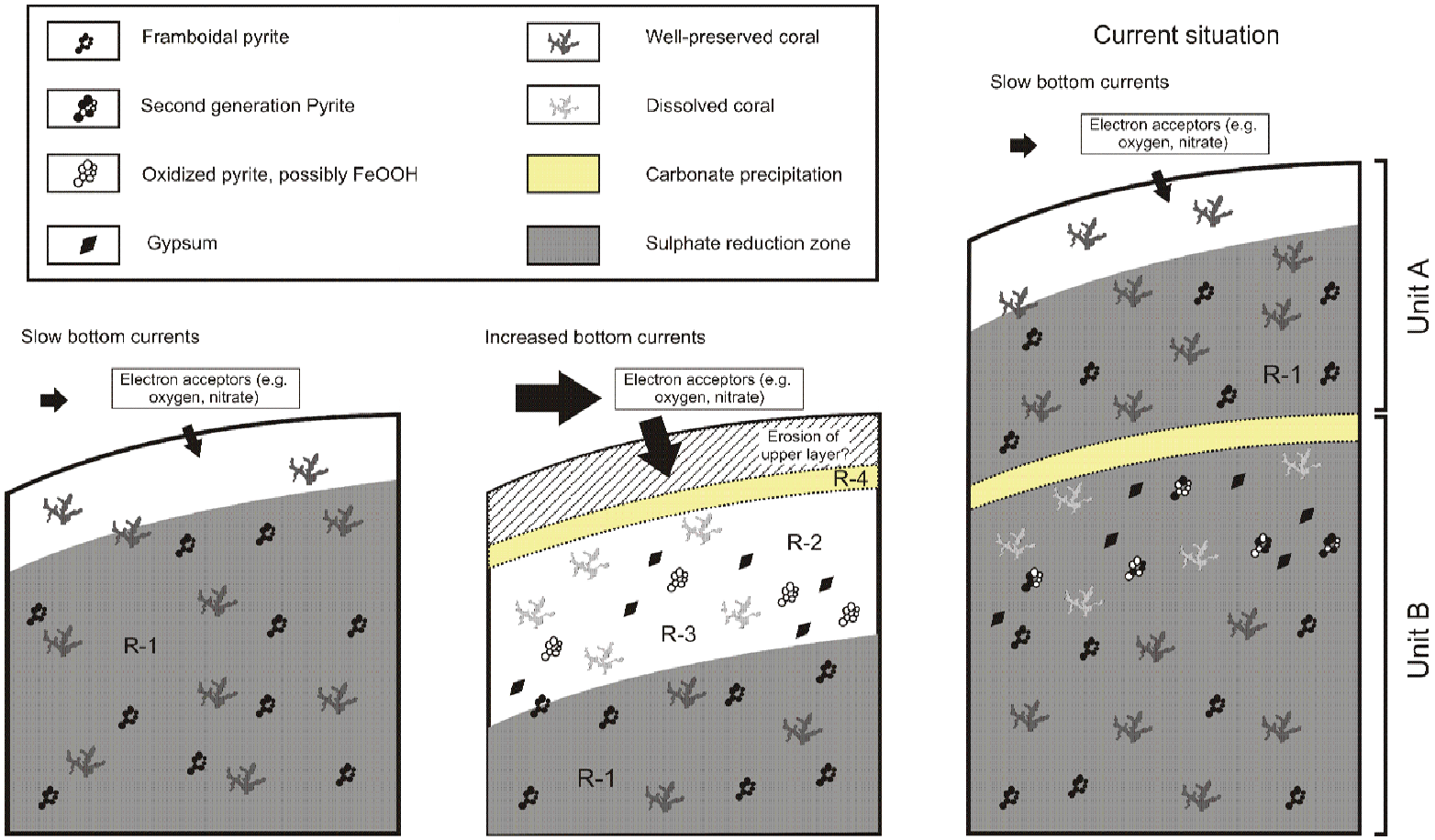

Figure 9: Schematic representation showing the increase of bottom current enhances the (sideward) inflow of electron acceptors in the upper layer of the sediment, oxidizing framboidal pyrite. The oxidation of pyrite produces sulphate and acidity, which induces dissolution of aragonitic corals. Subsequently the produced sulphate and calcium precipitate as gypsum. Erosion of the upper sediment layers, due to the increase of the bottom currents, might have triggered this oxidation process. R-1: formation of framboidal pyrite, R-2: sulphide oxidation

The influx of electron acceptors into the upper part of the sediment is favoured by the shape of a mound. This elevated structure promotes lateral inflow of oxidizing fluids. The presence of a coral framework in the mound potentially yields a higher hydraulic conductivity which allows oxidizing sea water to penetrate deep into the sediment. (Depreiter, 2009) modeled that increased bottom currents will push down the sulphate methane transition zone (SMTZ) significantly in an elevated structure on the sea bed, due to the strong lateral inflow of fluids advecting sulphate. Moreover, the organic matter turnover in cold-water coral reef sediments is low because the organic matter is already altered by aerobic and anaerobic microbially-mediated oxidation, leaving very refractory organic material (Wehrmann et al., 2009). This also allows a deeper penetration of oxidizing fluids into the mound sediments compared to other surface sediments as oxygen consumption by aerobic carbon mineralization is lower.

Buffering of pyrite oxidation by carbonate dissolution

Pyrite oxidation strongly decreases the pore-water pH. Both oxidation pathways (R1 and R2) produce a similar amount of protons. The production of H^+ (drop in pH) leads to a decrease in the pore-water saturation state for carbonate phases (e.g. high-Mg calcite and aragonite) and hence induces dissolution of these minerals (reaction R5) (Ku et al., 1999). This process is enhanced by the precipitation of iron oxyhydroxides (R4).

$$4\ CaCO_3 + 4\ H^+ \rightarrow 4\ Ca^{2+} + 4\ HCO_3^- \qquad \text{(R5)}$$

This acidification process explains why the coral fragments in unit B are significantly altered, resulting in a secondary porosity (Fig. 6A). In conjunction, XRD-data indicates the preferential dissolution of aragonite in the sediment containing gypsum. The zones of gypsum crystal occurrence are characterized by a decrease of aragonite in the sediment matrix (9.6%) compared to other zones in unit B (below the lithified layer) (average 15.7%) while the calcite content remains stable around 60% (Fig. 4). Brachert and Dullo (2000) and James et al. (2005) already discussed the preferential dissolution of aragonite during early marine diagenesis in cool-water carbonates.

Gypsum formation

The described mechanism of carbonate-buffered pyrite oxidation leads to the addition of dissolved sulphate and calcium. This results in oversaturation of the pore water with respect to gypsum and subsequent gypsum precipitation (reaction R6):

$$2\ SO_4^{2-} + 2\ Ca^{2+} + 4H_2O \rightarrow 2\ CaSO_4.2H_2O \qquad (R6)$$

The net total reaction of carbonate-buffered pyrite oxidation can be written as follows:

$$FeS_2 + 15/4\ O_2 + 9/2\ H_2O + 4\ CaCO_3 \rightarrow\ 4\ Ca^{2+} + 4\ HCO_3^- + 2\ SO_4^{2-} + FeOOH + 2\ H_2O$$
$$\rightarrow\ 2\ CaSO_4.2H_2O\ (s) + 2\ Ca^{2+} + 4\ HCO_3^- + FeOOH$$
(R7)

In the following, the mass balance calculation (equation 2) will be used to test the proposed mechanism under the assumed conditions. The mass balance shows that 23% to 26% (or even 34%) of sulphate in the gypsum crystals derived from pyrite oxidation. For further calculations, a mean value of 25% is used. Assuming a sea-water sulphate concentration of 28 mM, pyrite oxidation contributed 7 mM sulphate. Consequently, the pore-water sulphate concentration during gypsum precipitation is approximately 35 mM. In order to produce 7 mM sulphate, an equivalent of 3.5 mM pyrite is oxidized. Oxidation of 3.5 mM pyrite (R1, R2) and subsequent precipitation of iron oxyhydroxides (R4) result in the production of 14 mM H^+. This reaction is buffered by the dissolution of carbonates (R4) which produces an equivalent of 14 mM Ca^{2+}. Given that sea water contains 10 mM calcium, the pore-water concentration of calcium during the oxidation event reaches approximately 24 mM. A sulphate concentration of 35 mM and a calcium concentration of 24 mM results in an ion product of:

$$35*10^{-3} * 24*10^{-3} = 8.4*10^{-4}\ mol^2/l \qquad (3)$$

The gypsum solubility product in sea water is in the order of $1.52*10^{-3}$ mol^2/l (assuming a sea-water density of 1030 kg/m^3) (Shaffer, 1967) and $4.88*10^{-4}$ mol^2/l (Kopittke et al., 2004). The calculated value of the ion product of calcium and sulphate is within the range of these values. Thus, gypsum precipitation related to oxidation of

pyrite is a feasible process. Gypsum precipitation is even more likely if the possibility is considered that up to 35% of the gypsum may have been derived from pyrite oxidation, which corresponds to an ion product of $1.1*10^{-3}$ mol^2/l ($37.8*10^{-3}$ * $29.6*10^{-3}$).

The calculations show that the concentrations of sulphate and calcium in the pore water must be considerably higher than sea water in order to reach saturation with respect to gypsum. A semi-closed system is required to allow for the accumulation of calcium and sulphate. Consequently, the oxidant for sulphide oxidation may have been predominantely supplied by diffusive and not advective fluxes.

Dolomite precipitation

Pyrite oxidation and subsequent precipitation of gypsum favours the formation of dolomite (Fig. 7L). The incorporation of coccoliths in the dolomite crystals clearly indicates that these crystals have a diagenetic origin (Fig. 7M and N). Moreira et al. (2004) highlighted the role of sulphide oxidation in dolomitization in a lagoon system. The oxidation of sulphide provides acid that decreases the pore-water saturation state for high-magnesium calcite and aragonite, favouring the precipitation of dolomite. Carbonate phases such as calcite and high-magnesium calcite have been found to precipitate competitively with dolomite (Arvidson & Mackenzie, 1999). If auxiliary carbonate phases are prevented from precipitating, dolomite may be the preferred phase. Moreover, the formation of gypsum contributes significantly to dolomitization via incorporation of calcium ions into the gypsum crystals, resulting in an increase of the magnesium/calcium ratio in the associated fluids (Moore, 2001). This process has been described in evaporative marine diagenetic environments (Moore, 2001; Moreira et al., 2004). There are however no reports of a similar process under deep-sea conditions.

Formation of the lithified carbonate layer

In core MD01-2459G, the layer containing gypsum is overlain by a lithified carbonate layer. This suggests a link between the formation of this layer and gypsum precipitation. Most likely, excess calcium and bicarbonate produced during carbonate dissolution diffuse upwards from sites where pyrite oxidation occurs. Close to the sea bed, the pH increases and saturation of the pore-water with respect to carbonate occurred which resulted in the precipitation of calcite. The formation of calcite led to the lithification of the sediment at the top of unit B. Usually, the appearance of lithified carbonate layers at the sea bed is associated with increased currents and a reduced

sedimentation rate or even erosion (Allouc, 1990; Mutti & Bernoulli, 2003; Noé et al., 2006). This supports the hypothesis that erosion or reduced sedimentation due to increased bottom currents is responsible for the influx of electron acceptors and subsequent pyrite oxidation in Mound Perseverance.

Return to initial conditions

During the Holocene, unit A is deposited which causes a return to anoxic conditions in the sediments of unit B (Fig. 9). Microbial sulphate reduction recommences, leading to the formation of a second pyrite generation and the removal of the iron oxyhydroxides. The presence of two pyrite generations was already hypothesized, based on the sulphur isotopes composition of pyrite in unit B (Table 1).

5. Conclusions

In this study sedimentological, mineralogical and geochemical evidence is presented for a major diagenetic oxidation event in sediments from a cold-water coral mound. It is hypothesized that increased currents caused partial erosion and enhanced inflow of sea water in the mound. This led to penetration of oxygenated fluids into formerly anoxic sediments. Oxidation of sulphide minerals caused dissolution of aragonite and increased sulphate and calcium concentration, triggering the precipitation of gypsum and dolomite. Near the surface, upward diffusing bicarbonate was reprecipitated as carbonate, leading to a lithification of the sediment. This lithified carbonate layer was buried by Holocene sediments (Fig. 9).

If the hypothesis that increased currents led to an oxidation of anoxic sediments in Mound Perseverance is correct, it can be expected that other cold-water coral mounds in the same region might have undergone similar events of pyrite oxidation. However, layers containing gypsum, that would be diagnostic for such oxidation events, have not been reported in other coral mounds as yet. One possibility is that the oxidation in Perseverance was a local process. The other possibility is that, so far, gypsum crystals went undetected in previous studies. This scenario is not unlikely given that the maximum amount of gypsum found in the gravity core from Mound Perseverance was 0.34 vol%. This quantity is not detectable by XRD analysis and is easily overlooked in visual core description. Therefore, it is concluded that the detection of diagenetic gypsum needs to be a target in studies investigating the diagenesis of coral mounds and carbonate sediments in general.

This study demonstrates the importance of environmental factors that affect fluid flow in cold-water coral mounds. It shows how changes in the flow regime impact the (early) diagenesis of these structures. In the future, the occurrence gypsum in marine sediments could be a powerful tool to indentify oxidation processes in carbonate sediments.

References

Allouc, J.: Quaternary crusts on slopes of the Mediterranean Sea - A tentative explanation for their genesis, Mar. Geol., 94, 205-238,1990.

Arvidson, R.S. and Mackenzie, F.T.: The dolomite problem: Control of precipitation kinetics by temperature and saturation state, Am. J. Sci., 299, 257-288,1999.

Bain, R.J.: Diagenetic, nonevaporative origin for gypsum, Geology, 18, 447-450,1990.

Balci, N., Shanks, W.C., Mayer, B. and Mandernack, K.W.: Oxygen and sulfur isotope systematics of sulfate produced by bacterial and abiotic oxidation of pyrite, Geochim. Cosmochim. Ac., 71, 3796-3811, 2007.

Berner, R.A.: Sedimentary pyrite formation, Am. J. Sci., 268, 1-23, 1970.

Boschetti, T. and Iacumin, P.: Continuous-flow delta O-18 measurements: new approach to standardization, high-temperature thermodynamic and sulfate analysis, Rapid. Commun. Mass. Sp., 19, 3007-3014, 2005.

Brachert, T.C. and Dullo, W.C.: Shallow burial diagenesis of skeletal carbonates: selective loss of aragonite shell material (Miocene to Recent, Queensland Plateau and Queensland Trough, NE Australia) - implications for shallow cool-water carbonates, Sediment. Geol., 136, 169-187, 2000.

Briskin, M. and Schreiber, B.C.: Authigenic gypsum in marine sediments, Mar. Geol., 28, 37-49, 1978.

Brunner, B., Yu, J.Y., Mielke, R.E., MacAskill, J.A., Madzunkov, S., McGenity, T.J. and Coleman, M.: Different isotope and chemical patterns of pyrite oxidation related to lag and exponential growth phases of Acidithiobacillus ferrooxidans reveal a microbial growth strategy, Earth. Planet. Sc. Lett., 270, 63-72, 2008.

Corselli, C. and Aghib, F.S., Brine formation and gypsum precipitation in the Bannock Basin, Eastern Mediterranean, Mar. Geol., 75, 185-199, 1987.

De Mol, B., Van Rensbergen, P., Pillen, S., Van Herreweghe, K., Van Rooij, D., McDonnell, A., Huvenne, V., Ivanov, M., Swennen, R. and Henriet, J.-P.: Large deep-water coral banks in the Porcupine Basin, southwest of Ireland, Mar. Geol., 188, 193-231, 2000.

Depreiter, D.: Sources, modes and effects of seabed fluid flow, PhD, Ghent University, Ghent, 207 pp, 2009.

Dorschel, B., Hebbeln, D., Rüggeberg, A., Dullo, C. and Freiwald, A.: Growth and erosion of a cold-water coral covered carbonate mound in the Northeast Atlantic during the Late Pleistocene and Holocene, Earth. Planet. Sc. Lett., 233, 33-44, 2005.

Ferdelman, T.G., Kano, A., Williams, T., Henriet, J.-P. and the Expedition 307 Scientists. Proc. IODP, 307: Washington, DC (Integrated Ocean Drilling Program Management International, Inc.). doi:10.2204/iodp.proc.307.102.2006

Fossing, H. and Jørgensen, B.B.: Measurement of Bacterial Sulfate Reduction in Sediments - Evaluation of a Single-Step Chromium Reduction Method, Biogeochemistry, 8, 205-222, 1989.

Foubert, A., Depreiter, D., Beck, T., Maignien, L., Pannemans, B., Frank, N., Blamart, D. and Henriet, J.-P.: Carbonate mounds in a mud volcano province off north-west Morocco: Key to processes and controls, Mar. Geol., 248, 74-96, 2008.

Foubert, A. and Henriet, J.P.: Nature and significance of the recent carbonate mound record: the Mound Challenger Code, Springer-Verlag, Heidelberg, 350 pp, 2009.

Foubert, A., Van Rooij, D., Blamart, D. and Henriet, J.-P.: X-ray imagery and physical core logging as a proxy of the content sediment cores in cold-water coral mound provinces: a case study from Porcupine Seabight, SW of Ireland, Int. J. Earth Sci., 96, 141-158, 2007.

Frank, N., Ricard, E., Paque, A., van der Land, C., Colin, C., Blamart, D., Foubert, A., Van Rooij, D., Henriet, J.P., De Haas, H. and Van Weering, T.: Carbonate mound evolution on Rockall Bank and in Porcupine Seabight derived from ^{230}Th/U dating of deep-water corals, Mar. Geol., in press.

Freiwald, A. and Roberts, J.M., Cold-water corals and ecosystems - Preface. Cold-Water Corals and Ecosystems, 7-12, 2005.

Gontharet, S., Pierre, C., Blanc-Valleron, M.M., Rouchy, J.M., Fouquet, Y., Bayon, G., Foucher, J.P., Woodside, J. and Mascle, J.: Nature and origin of diagenetic carbonate crusts and concretions from mud volcanoes and pockmarks of the Nile deep-sea fan (eastern Mediterranean Sea), Deep-Sea Res. Pt. II, 54, 1292-1311, 2007.

Halas, S., Szaran, J., Czarnacki, M. and Tanweer, A.: Refinements in BaSO4 to CO2 preparation and delta O-18 calibration of the sulfate reference materials NBS-127, IAEA SO-5 and IAEA SO-6, Geostand. Geoanal. Res., 31, 61-68, 2007.

Hargreaves, P.M.: The Distribution of Decapoda (Crustacea) in the open ocean and near-bottom over an adjacent slope in the northern North-East Atlantic Ocean during Autumn 1979, J. Mar. Biol. Assoc. UK, 64, 829-857, 1984.

Henriet, J.-P., De Mol, B., Pillen, S., Vanneste, M., Van Rooij, D., Versteeg, W., Croker, P.F., Shannon, P.M., Unnithan, V., Bouriak, S., Chachkine, P. and The Porcupine-Belgica 97 Shipboard Party: Gas hydrate crystals may help build reefs, Nature, 391, 648-649, 1998.

Holser, W.T. and Kaplan, I.R.: Isotope geochemistry of sedimentary sulfates, Chem. Geol., 1, 93-135, 1966.

Huvenne, V.A.I., Bailey, W.R., Shannon, P.M., Naeth, J., di Primio, R., Henriet, J.-P., Horsfield, B., de Haas, H., Wheeler, A.J. and Olu-Le Roy, K.: The Magellan mound province in the Porcupine Basin, Int. J. Earth Sci., 96, 85-101, 2007.

Huvenne, V.A.I., Blondel, P. and Henriet, J.-P., Textural analyses of sidescan sonar imagery from two mound provinces in the Porcupine Seabight, Mar. Geol., 189, 323-341, 2002.

James, N.P., Bone, Y. and Kyser, T.K.: Where has all the aragonite gone? - Mineralogy of holocene neritic cool-water carbonates, southern Australia, J. Sediment. Res., 75, 454-463, 2005.

Jenkins, R. and De Vries, J.L.: Practical X-ray Spectrometry, MacMillan, London, 190 pp, 1970.

Kak, A.C. and Slaney, M.: Principles of computerized tomographic imaging. IEEE press, 1988.

Kano, A., Ferdelman, T.G., Williams, T., Henriet, J.P., Ishikawa, T., Kawagoe, N., Takashima, C., Kakizaki, Y., Abe, K., Sakai, S., Browning, E., Li, X. and the IODP Expedition 307 Scientists: Age constraints on the origin and growth history of a deep-water coral mound in northeast Atlantic drilled during Integrated Ocean Drilling Program Expedition 307, Geology, 35, 1051-1054, 2007.

Kopittke, P.M., Menzies, N.W. and Fulton, I.M.: Gypsum solubility in seawater, and its application to bauxite residue amelioration, Aust. J. Soil. Res., 42, 953-960, 2004.

Kroopnick, P. and Craig, H.: Atmospheric oxygen - isotopic composition and solubility fractionation, Science, 175, 54-55, 1972.

Ku, T.C.W., Walter, L.M., Coleman, M.L., Blake, R.E. and Martini, A.M.: Coupling between sulfur recycling and syndepositional carbonate dissolution: Evidence from oxygen and sulfur isotope composition of pore-water sulfate, South Florida Platform, USA, Geochim. Cosmochim. Ac., 63, 2529-2546, 1999.

Lindberg, B., Berndt, C. and Mienert, J.: The Fugloy Reef at 70°N; acoustic signature, geologic, geomorphologic and oceanographic setting, Int. J. Earth Sci., 96, 201-213, 2007.

Longinelli, A. Oxygen-18 and sulphur-34 in dissolved oceanic sulphate and phosphate, In: Handbook of Environmental Isotope Geochemistry, edited by Fritz, P. and Fontes, J.C., 3, pp. 219-255, 1989, Elsevier, Amsterdam.

Masschaele, B.C., Cnudde, V., Dierick, M., Jacobs, P., Van Hoorebeke, L. and Vlassenbroeck, J.: UGCT: New x-ray radiography and tomography facility, Nuclear Instruments & Methods in Physics Research Section a-Accelerators Spectrometers Detectors and Associated Equipment, 580, 266-269, 2007.

Moore, C.H.: Carbonate Reservoirs: Porosity evolution and diagenesis in a sequence stratigraphic framework, Elsevier, 2001.

Moreira, N.F., Walter, L.M., Vasconcelos, C., McKenzie, J.A. and McCall, P.J., Role of sulfide oxidation in dolomitization: Sediment and pore-water geochemistry of a modern hypersaline lagoon system, Geology, 32, 701-704, 2004.

Mutti, M. and Bernoulli, D.: Early marine lithification and hardground development on a Miocene ramp (Maiella, Italy): Key surfaces to track changes in trophic resources in nontropical carbonate settings, J. Sediment. Res., 73, 296-308, 2003.

Noé, S., Titschack, J., Freiwald, A. and Dullo, W.C.: From sediment to rock: diagenetic processes of hardground formation in deep-water carbonate mounds of the NE Atlantic, Facies, 52, 183-208, 2006.

Rice, A.L., Billet, D.S.M., Thurston, M.H. and Lampitt, R.S.: The Institute of Oceanographic Sciences Biology programme in the Porcupine Seabight: background and general introduction, J. Mar. Biol. Assoc. UK, 71, 281-310, 1991.

Richter, D.K., Gotte, T., Gotze, J. and Neuser, R.D.: Progress in application of cathodoluminescence (CL) in sedimentary petrology, Miner. Petrol., 79, 127-166, 2003.

Richter, T.O., van der Gaast, S., Koster, B., Vaars, A., Gieles, R., de Stigter, H.C., De Haas, H. and van Weering, T.C.E.: The Avaatech XRF Core Scanner: technical description and applications to NE Atlantic sediments, In: New techniques in Sediment Core Analysis (Ed R.G. Rothwell), Special Publications, 267, pp. 39-50, 2006 Geological Society, London.

Roberts, J.M., Wheeler, A.J. and Freiwald, A.: Reefs of the deep: The biology and geology of cold-water coral ecosystems, Science, 312, 543-547, 2006.

Shaffer, L.H.: Solubility of gypsum in sea water and sea-water concentrates at temperatures from ambient to 65 degrees C, J. Chem. Eng. Data, 12, 183-189, 1967.

Siesser, W.G. and Rogers, J.: Authigenic pyrite and gypsum in South West African continental slope sediments, Sedimentology, 23, 567-577, 1976.

Taylor, B.E., Wheeler, M.C. and Nordstrom, D.K.: Stable isotope geochemistry of acid mine drainage: Experimental oxidation of pyrite, Geochim. Cosmochim. Ac., 48, 2669-2678, 1984.

Thode, H.G. and Monster, J.: Sulfur-isotopes geochemistry of petroleum, evaporates and ancient seas, In: Fluids in subsurface environments: American Association of Petroleum Geologists Memoir 4 (Eds A. Young and J.S. Galley), pp. 367-377, 1965.

Toran, L. and Harris, R.F.: Interpretation of sulfur and oxygen isotopes in biological and abiological sulfide oxidation, Geochim. Cosmochim. Ac., 53, 2341-2348, 1989.

Van Rooij, D., Blamart, D., Richter, T.O., Wheeler, A.J., Kozachenko, M. and Henriet, J.-P.: Quaternary sediment dynamics in the Belgica mounds province, Porcupine Seabight: Ice rafting events and contour current processes, Int. J. Earth Sci., 96, 121-140, 2007.

Van Rooij, D., Blamart, D. and Unnithan, V.: Cruise report MD123-Géosciences: Leg 2, part GEOMOUND, RCMG, Gent, 2001.

Van Rooij, D., De Mol, B., Huvenne, V., Ivanov, M.K. and Henriet, J.-P.: Seismic evidence of current-controlled sedimentation in the Belgica mound province, upper Porcupine slope, southwest of Ireland, Mar. Geol., 195, 31-53, 2003.

Vlassenbroeck, J., Dierick, M., Masschaele, B., Cnudde, V., Hoorebeke, L. and Jacobs, P.: Software tools for quantification of X-ray microtomography, Nuclear Instruments & Methods in Physics Research Section a-Accelerators Spectrometers Detectors and Associated Equipment, 580, 442-445, 2007.

Wang, J.S., Suess, E. and Rickert, D.: Authigenic gypsum found in gas hydrate-associated sediments from Hydrate Ridge, the eastern North Pacific, Science in China Series D-Earth Sciences, 47, 280-288, 2004.

Wehrmann, L.M., Knab, N.J., Pirlet, H., Unnithan, V., Wild, C. and Ferdelman, T.G.: Carbon mineralization and carbonate preservation in modern cold-water coral reef sediments on the Norwegian shelf, Biogeosciences, 6, 663-680, 2009.

Wheeler, A.J., Beyer, A., Freiwald, A., de Haas, H., Huvenne, V.A.I., Kozachenko, M., Olu-Le Roy, K. and Opderbecke, J.: Morphology and environment of cold-water coral carbonate mounds on the NW European margin, Int. J. Earth Sci., 96, 37-56, 2007.

White, M.: Hydrography and physical dynamics at the NE Atlantic margin that influence the deep water cold reef ecosystem, Dept. of Oceanography, NUI, Galway, Ireland, Galway, 2001.

White, M.: Benthic dynamics at the carbonate mound regions of the Porcupine Sea Bight continental margin, Int. J. Earth Sci., 96, 1-9, 2007.

Xavier, A. and Klemm, D.D.: Authigenic gypsum in deep-sea manganese nodules, Sedimentology, 26, 307-310, 1979.

Zhong, C., Wen, Y., Mu-hong, C., Jun, L. and Sen-chang, G.: Formation of authigenic gypsum and pyrite assemblage and its significance to gas ventings in Nansha Trough, South Chine Sea, Marine Geology & Quaternary Geology, 27, 90-100, 2007.

CHAPTER 8:

COLD-WATER CORAL MOUNDS ON THE PEN DUICK ESCARPMENT, GULF OF CADIZ: THE MiCROSYSTEMS APPROACH

Van Rooij, D.[1], Blamart, D.[2], De Mol, L.[1], Mienis, F.[3], Pirlet, H.[1], Wehrmann, L.M.[4], Barbieri, R.[5], Maignien, L.[6], Templer, S.P.[7], de Haas, H.[3], Hebbeln, D.[8], Frank, N.[2], Larmagnat, S.[9], Stadnitskaia, A.[10], Stivaletta, N.[5], van Weering, T.[3], Zhang, Y.[6], Hamoumi, N.[11], Cnudde, V.[12], Duyck, P.[13], Henriet, J.-P.[1] & the MiCROSYSTEMS MD 169 shipboard party.

[1] Renard Centre of Marine Geology, Department of Geology & Soil Science, Ghent University, Krijgslaan 281 S8, B-9000 Gent, Belgium

[2] LSCE-IPSL-UVSQ, Laboratoire mixte CEA/CNRS, Avenue de la Terrasse, bâtiment 12, F-91198 Gif-sur-Yvette, France

[3] Department of Marine Geology, Royal NIOZ, P.O. Box 59, NL-1790 AB Den Burg, The Netherlands

[4] Biogeochemistry Research Group, Max Planck Institute for Marine Microbiology, Celciusstrasse 1, D-28359 Bremen, Germany

[5] Dipartemento di Scienza della Terra e Geologica-Ambientali, Universita di Bologna, Italy

[6] Laboratory of Microbial Ecology and Technology, Faculty of bioengineering, Ghent University, Coupure Links 653, B-9000 Gent, Belgium

[7] Swiss Federal Institute of Technology (ETH) Zurich, Geological Institute, Sonneggstrasse 5, 8092 Zürich, Switzerland

[8] MARUM, Leobener Strasse, D-28359 Bremen, Germany

[9] Département de Géologie & Génie Géologique, Université de Laval, Québec, Canada

[10] Department of Marine Biogeochemistry, Royal NIOZ, P.O. Box 59, NL-1790 AB Den Burg, The Netherlands

[11] Department of Earth Sciences, Mohammed V-Agdal University, Rabat, Morocco

[12] Centre for X-ray Tomography (UGCT), Department of Geology & Soil Science, Ghent University, Krijgslaan 281 S8, B-9000 Gent, Belgium

[13] Department of Radiology and Medical Imagery, Ghent University Hospital, De Pintelaan 185, B-9000 Gent, Belgium

***Marine Geology,* in review**

Abstract

The last decade, many NE Atlantic cold-water coral mound provinces have been discovered and studied. A common point of discussion, surpassing the broad range of regional and morphological variability of these mounds, concerns the driving forces regarding the initiation of these complex deep-water systems. Both oceanographic and geological processes have been proposed to play a significant role in the mound nucleation, growth and decline. During Integrated Ocean Drilling Program (IODP) Expedition 307, the importance of biogeochemical processes was elucidated. Here we present a case study of three cold-water coral mounds in a juvenile growth stage on top of the Pen Duick Escarpment (PDE) in the Gulf of Cadiz. Although cold-water corals are a common feature on the adjacent cliffs, mud volcanoes and seafloor, no actual living reef has been observed. This multidisciplinary study aims to present a comprehensive and holistic view on the local dynamic geological and oceanographic environment. Both data from cores as from seismic profiles illustrate active methane seepage and sources; (1) a direct connection with Mesozoic reservoirs is possible through uplifted Miocene series, (2) migration from the lobes of adjacent mud volcanoes, and (3) destabilization of gas hydrates which are located at the foot of PDE. The dominant morphology of PDE has influenced the local hydrodynamics within the course of the Pliocene, as documented by the emplacement of a sediment drift. Predominantly during post-Middle Pleistocene glacial episodes, favourable conditions were present for mound growth. An additional advantage for mound nucleation near the top of PDE is offered through seepage-related carbonate crusts which might offer elevated positions to the corals. Present-day seabed observations and coring revealed the architectural importance of open coral rubble frameworks in the role of mound building. These graveyards not only act as sediment trap but also as micro-habitat for a wide range of organisms. The presence of a fluctuating Sulphate-Methane Transition Zone (SMTZ) is responsible for diagenesis, affecting both geochemical as physical characteristics, transforming the buried reef into a solid mound. Nevertheless, the responsible seepage fluxes seem to be locally variable. As such, the origin and evolution of the cold-water coral mounds on top of the Pen Duick Escarpment is, probably more than any other NE Atlantic cold-water coral mound province, located on the crossroads of environmental (hydrodynamic) and geological (seepage) pathways.

4. CONCLUDING REMARKS & PERSPECTIVES

Biogeochemical processes in sediments associated to cold-water coral ecosystems were investigated in this thesis. The first part of this work aimed to elucidate early diagenetic processes in sediments associated with living cold-water coral reefs on the Norwegian margin. By using a variety of biogeochemical tools, such as high-resolution pore-water and solid-phase analyses at several reef sites, the focus was to understand the prevailing microbially mediated processes in the sediments. The attempt was made to not only unravel the subseafloor diagenesis but also to integrate the findings into a comprehensive understanding of the ecosystem including pelagic, benthic and sedimentary processes. The second part of this thesis focused on diagenetic processes in ancient cold-water coral mounds. The effect of a major diagenetic oxidation event was investigated at Mound Perseverance in the Porcupine Seabight. The impact of hydrocarbon-rich fluids on geochemical processes and the sedimentary record of Pen Duick cold-water coral mounds in the Gulf of Cadiz was explored. This study linked biogeochemical observations with the geological setting of the mounds in this region. In the following, the most important findings of both parts of this thesis are summarized and interlinked, and an outlook on future research questions for specific aspects is given.

4.1.1 Carbon cycling in cold-water coral reef ecosystems and biogeochemical processes in reef-associated sediments

Cold-water coral ecosystems represent distinctive habitats with respect to carbon and nutrient cycling among the different ecosystem compartments and the members of the coral reef-associated food web (Chapters 1-4; Van Oevelen et al. 2009). This habitat strongly differs from its warm-water counterpart, as well as other habitats on continental shelves. Organic matter is transported down from productive surface waters by a variety of hydrodynamic mechanisms (e.g. downwelling events and internal tidal waves; De Mol et al., 2002; Dorschel et al., 2007a; Frederiksen et al., 1992; White et al., 2005). Within the reef the organic matter is efficiently mineralized by the benthic reef-associated fauna which ranges from large mobile animals to foraminifera living mainly on dead coral thickets and coral rubble, and the microbial communities living in the reef-adjacent waters and associated with living corals and the coral rubble layer (Chapters 1-3). The living and dead coral thickets and coral rubble effectively decouple the reef sediments from the thriving productive reef ecosystem. Stoichiometric

calculations based on modelling of major pore-water constituents reveal an oxidation state of the organic matter more reduced than carbohydrate stoichiometries classically employed in geochemical diagenetic models (Chapter 1). Consistently, a variety of biogeochemical indicators for the degree of organic matter decomposition demonstrated low concentrations of organic matter that reach the underlying sediments and an elevated degradation state of the sedimentary organic matter (Chapter 2). Rates of anaerobic carbon mineralization primarily driven by microbial sulfate reduction in the reef-associated sediments are extremely low. Nonetheless, there is spatial variability in the rates and pathways of carbon mineralization at cold-water coral ecosystems. For example, at Røst Reef a distinct facies zonation was discovered. The different zones (i.e. the reef top, the coral rubble zone and the clay zone), are characterized by different microbially driven diagenetic processes. At the reef top the suboxic zone is extended to greater depth and nitrate reduction and manganese oxide reduction are likely the dominating processes. Within the coral rubble and the clay zone, microbial sulfate reduction prevails, but turnover rates are higher in the coral rubble zone compared to the clay zone (Chapter 1).

The interplay of low rates of sulfate reduction and a large pool of (easily) reducible Fe-(oxyhydr)oxides in the siliciclastic sediments results in a well-buffered carbonate system. Authigenic carbonate precipitation driven by the production of bicarbonate during sulfate reduction is likely to occur rather than coral dissolution. Thus, the reef associated sediments are characterized by a high preservation potential for the buried cold-water coral fragments (Chapter 1).

4.1.2 Future research questions for the study of living cold-water coral reefs

Further research is needed to complement our understanding of the carbon and nutrient cycling at living cold-water coral reefs. Little is known about annual variability in carbon cycling. Initial results indicate that especially at those reefs that are dependent on organic matter supply from a local surface phytoplankton bloom, such as Tisler Reef in the Skagerrak, the retention of carbon in the ecosystem during the winter and early spring time might be of great importance (Chapter 4). So far, we can only speculate about the controlling factors for the spatial variability in biogeochemical processes among the different reef facies zones. Factors such as the distance to the living reef top, sedimentation rates and/or the burial of remains of the reef-associated fauna can be evoked. An extended study including geochemical measurements as well as molecular

tools such as microbial cell counts and community composition analyses at multiple sites of one reef would give new insights into these aspects. Such a study would also further decipher the degradation status of organic matter in the reef ecosystem if combined with analyses of particulate organic matter in the reef water column and sediment trap samples deployed at the different zones and at different heights above the reef. Organic matter in marine sediments is predominately associated with inorganic mineral phases (Hedges and Keil 1995). Thus, analyses of organic matter associated to different grain size fractions and different mineral components would advance our understanding of the degradation characteristics of the sedimentary organic matter. The carbonate-rich siliciclastic sediments at cold-water coral reefs offer the unique opportunity to study the partitioning of organic matter components among clay minerals and carbonate phases as well as the role of intracrystalline organic matter.

The role of cold-water coral ecosystems in the carbon cycle on a local, regional as well as global scale is poorly understood. They might contribute up to 1 % to the global carbonate budget and thus represent a long-term sink for inorganic carbon. Yet, they might also function as an important source for dissolved organic carbon (DOC). DOC in reef-adjacent surface waters reaches concentrations > 50 mM (Chapter 4). These values exceed DOC concentrations reported from the deep sea by three orders of magnitude (Hansell and Carlson 1998). Large cold-water coral reefs on continental margins such as Røst Reef, which reach several km in diameter, thus might strongly influence the DOC budget of the surrounding waters on a regional scale. A study on the annual dynamics of DOC concentrations in reef-associated waters and the fluxes of DOC against the background of the local current regime would help to interpret the role of cold-water coral reef derived DOC.

4.2.1 Diagenetic processes in cold-water coral mounds

Cold-water coral mound sediments have undergone extensive diagenesis, driven by microbially mediated carbon mineralization, and non-steady state, diagenetic processes that result from the distinct character of a mound as an elevated feature rising from the surrounding seafloor (Chapter 6-8). At this stage cold-water coral mounds influence the local hydrodynamic regime and simultaneously are exposed to changes of the oceanographic setting which in extreme cases can cause mound erosion or burial. We have described such a process for Mound Perseverance located in the Porcupine Seabight off Ireland (Chapter 7). At Mound Perseverance, increased bottom currents

caused sediment erosion and the inflow of oxidizing fluids into previously anoxic mound sediments. Biogeochemical processes sequentially facilitated the oxidation of sedimentary pyrite, intensive coral dissolution, and the formation of gypsum and dolomite once the sediments turned anoxic again.

Cold-water coral mounds located in Pen Duick Mound Province in the Gulf of Cadiz at present have to be considered as the exception rather than the rule in terms of the biogeochemical processes within the mound sequences. Several of these mounds are influenced by hydrocarbon-rich deep fluids presumably originating from Mesozoic source rocks which are migrating to shallow sediment depth. The geochemical imprint of these fluids as well as processes related to the installation of a shallow sulfate-methane transition zone (SMTZ) delineates the Pen Duick Mounds from other mounds investigated so far (e.g. Challenger Mound drilled during the Integrated Ocean Drilling Program (IODP) Expedition 307). Within the hydrocarbon-influenced mounds, the production of hydrogen sulfide by microbial sulfate reduction coupled to the anaerobic oxidation of methane (AOM), caused extensive pyritization of reactive Fe-(oxyhydr)oxides, while the production of bicarbonate during AOM resulted in the formation of authigenic high-Mg calcite. Due to the lack of reactive Fe-mineral phases at Alpha Mound, hydrogen sulfide diffused out of the SMTZ resulting in a shift of the carbonate solubility equilibrium and coral dissolution (Chapter 6, Fig. 11).

Biogeochemical processes in non-methane influenced cold-water coral mounds such as Gamma Mound in the Gulf of Cadiz, similar to the Norwegian reefs, are driven by extremely low rates of carbon mineralization which is proceeding via microbial sulfate reduction but most likely also involves oxidative sulfur cycling (i.e. disproportionation of elemental sulfur). Cold-water corals in these sediments are well-preserved. As suggested for the sediments underlying living cold-water coral reefs, the coupling of the sulfur and iron cycle and carbonate dynamics functions as a buffer for the pore-water carbonate system.

4.2.2 Future research questions for the study of cold-water coral mounds

At almost all cold-water coral mounds investigated so far, there is evidence that non-steady state diagenetic processes play a central role. Further research is needed to study a) the driving-forces for these processes and b) the immediate and long-term impact of shifts of the prevailing biogeochemical processes on the sedimentary record. It is assumed that changes in the oceanographic setting of a mound region influence the

depth and succession of geochemical processes within the mound sequences (Chapter 7, 8). This might proceed by a weakening or an intensification of the local currents which results in changes of the pressure effects imposed on a coral mound and drives increased sediment deposition or erosion, respectively (Depreiter, 2009). Eustatic sea level changes and concomitant variations of the hydrostatic conditions might further trigger shifts in mound geochemistry (Depreiter, 2009). Cold-water coral mounds in the Gulf of Cadiz are also subject to the migration of hydrocarbon-rich fluids. Changes of the flux of these fluids, for example, due to seismic activity or gas hydrate dissociation, represent an additional factor for non-steady state diagenetic processes. The aftermath of non-steady state processes in the mounds lays in the potential to cause diagenetic extremes, such as the oversaturation of gypsum and dolomite (Chapters 7-9). No attempts have been made to date, which integrate distinct geochemical features related to non-steady state diagenetic processes and the regional oceanographic history due to difficulties in putting good age constraints on mound sequences. The combination of biogeochemical tools, age reconstruction and the application of numerical modeling, however, offers great potential for a holistic understanding of the geochemistry of cold-water coral mounds over time.

4.3 Concluding remarks

The studies conducted in the framework of this thesis revealed intriguing aspects on biogeochemical processes in living cold-water coral reef associated sediments and ancient cold-water coral mounds. The study of microbially driven diagenetic processes against the background of the ecosystem functioning of cold-water coral reefs represented one of the highlights of this work. Similarly, the integrated study of biogeochemical and geological characteristics of cold-water coral mounds in the Porcupine Seabight and the Gulf of Cadiz provided new insight into their diagenetic history. It became evident that non-methane influenced cold-water coral mounds can be regarded as analogs for low activity “deep biosphere” sediments in continental margin settings. Nonetheless, this work has to be regarded as a starting point of comprehensive cold-water coral ecosystem research. The complexity and dynamics of these ecosystems can only be fully understood by interlinking new discoveries made in the fields of microbiological, geochemical, geological, and oceanographic cold-water coral research. If these interrelations are made, cold-water coral ecosystems in many aspects represent

unique model systems that offer great potential to extend our understanding of the development, burial and fate of marine biodiversity hot-spots over geological timescales.

References

Depreiter, D.: Sources, modes and effects of seabed fluid flow, PhD thesis, Ghent University, 2009.

De Mol, B., Van Rensbergen, P., Pillen, S., Van Herreweghe, K., Van Rooij, D., McDonnell, A., Huvenne, V., Ivanov, M., Swennen, R. and Henriet, J.-P.: Large deep-water coral banks in the Porcupine Basin, southwest of Ireland, Mar. Geol., 188, 193-231, 2000.

Dorschel, B., Hebbeln, D., Foubert, A., White, M. and Wheeler, A.J.: Hydrodynamics and cold-water coral facies distribution related to recent sedimentary processes at Galway Mound west of Ireland, Mar. Geol., 244, 184-195, 2007a.

Frederiksen, R., Jensen, A. and Westerberg, H.: The distribution of the scleractinian coral Lophelia pertusa around the Faroe Islands and the relation to internal tidal mixing, Sarsia, 77, 157-171, 1992.

Hansell, D.A., and Carlson C.A.: Deep-ocean gradients in the concentration of dissolved organic carbon, Nature, 395, 263-266, 1998.

Hedges, J.I., and Keil, R.G.: Sedimentary Organic-Matter Preservation - an Assessment and Speculative Synthesis, Marine Chemistry 49, 81-115, 1995.

van Oevelen, D., Duineveld, G., Lavaleye, M., Mienis, F., Soetaert, K. and Heip, C.H.R.: The cold-water coral community as a hot spot for carbon cycling on continental margins: A food-web analysis from Rockall Bank (northeast Atlantic), Limnology and Oceanography 54, 1829-1844, 2009.

White, M., Mohn, C., de Stigter, H. and Mottram, G.: Deep-water coral development as a function of hydrodynamics and surface productivity around the submarine banks of the Rockall Trough, NE Atlantic, in: Cold-water corals and ecosystems, edited by: Freiwald, A. and Roberts, J.M., Springer, Heidelberg, 503-514, 2005.

DANKSAGUNG

Mein Dank gilt den beiden Gutachtern meiner Arbeit Prof. Dr. Bo Barker Jørgensen und PD Dr. Matthias Zabel sowie meinem Thesis Committee um Dr. Tim Ferdelman, PD Dr. Christian Wild, Dr. Dirk de Beer und Prof. Dr. Dieter Wolf-Gladrow.
Tim Ferdelman und Christian Wild gilt mein aller herzlichster Dank für die Betreuung meiner Doktorarbeit, die großartige Zusammenarbeit, das Vertrauen und die immerwährende Unterstützung.

Ich möchte mich herzlich bei meinen beiden „großen Brüdern“ Ben Brunner und Mike Formolo bedanken, ohne deren Hilfe ich wohl manchmal im wissenschaftlichen Chaos versunken wäre. Meine beiden Kaltwasserkorallenriffdoktorandenkollegen Sandra Schöttner und Hans Pirlet möchte ich ganz besonders für ihre großartige Unterstützung unterwegs und immerzu danken.

Auch der restlichen „belgischen Connection“ besonders David Van Rooij, Lois Maignien und Jean-Pierre Henriet gebührt mein besonderer Dank. Ausserdem möchte ich Prof. Dr. Antje Boetius und Dr. Friederike Hoffmann, Prof. Dr. Vikram Unnithan sowie Dr. Olaf Dellwig und Dr. Bernhard Schnetger für ihre Unterstützung im Rahmen dieses Projektes danken.

Ich möchte mich ausserdem ganz herzlich bei der gesamten Arbeitsgruppe Biogeochemie am Max Planck Institut, besonders Patrick Meister, Natascha Riedinger, Nina Knab, Gail Lee Arnold, Alberto Robador, Casey Hubert sowie allen Technikern für ihre großartige Unterstützung und Zusammenarbeit bedanken. Des weiteren gilt mein Dank Ulrike Tietjen, Helge Niemann, Katharina Kohls, Thomas Wilkop, Sergio Contreras, Elke Allers und allen anderen Kollegen am MPI die zum Gelingen dieser Arbeit beigetragen haben. Gail Lee Arnold und Roy Price möchte ich ausserdem für die Hilfe bei der Anfertigung dieser Arbeit danken.

Ich danke meinen Freundinnen und Kolleginnen Jana Miluçka und Caroline Verna für ihr offenes Ohr, ihre großartige Unterstützung und Fürsorge.

Mein ganz besonderer Dank gilt meinen Eltern und meinen Geschwistern für ihre, z.T. auch fachliche, Unterstützung und den Rückhalt den sie mir gegeben haben.

ERKLÄRUNG

Hiermit versichere ich, dass ich die vorliegende Arbeit

1. ohne unerlaubte, fremde Hilfe angefertigt habe

2. keine anderen, als die von mir im Text angegebenen Quellen und Hilfsmittel benutzt habe,

3. die den benutzten Werken wörtlich oder inhaltlich entnommenen Stellen als solche kenntlich gemacht habe.

Bremen, den 15.01.2010

Laura Mariana Wehrmann